

## INFORMATION TO USERS

This manuscript has been reproduced from the microfilm master. UMI films the text directly from the original or copy submitted. Thus, some thesis and dissertation copies are in typewriter face, while others may be from any type of computer printer.

**The quality of this reproduction is dependent upon the quality of the copy submitted.** Broken or indistinct print, colored or poor quality illustrations and photographs, print bleedthrough, substandard margins, and improper alignment can adversely affect reproduction.

In the unlikely event that the author did not send UMI a complete manuscript and there are missing pages, these will be noted. Also, if unauthorized copyright material had to be removed, a note will indicate the deletion.

Oversize materials (e.g., maps, drawings, charts) are reproduced by sectioning the original, beginning at the upper left-hand corner and continuing from left to right in equal sections with small overlaps.

Photographs included in the original manuscript have been reproduced xerographically in this copy. Higher quality 6" x 9" black and white photographic prints are available for any photographs or illustrations appearing in this copy for an additional charge. Contact UMI directly to order.

ProQuest Information and Learning  
300 North Zeeb Road, Ann Arbor, MI 48106-1346 USA  
800-521-0600

UMI<sup>®</sup>



**University of Alberta**

**A fluid inclusion and stable isotopic examination of the Boston, greenstone belt hosted, Archean lode-gold deposit, Hope Bay volcanic belt, Nunavut, Canada.**

by



James Uwe Stemler

A thesis submitted to the Faculty of Graduate Studies and Research in partial fulfillment of the requirements for the degree of Master of Science

Department of Earth and Atmospheric Sciences

Edmonton, Alberta

Fall, 2000



National Library  
of Canada

Acquisitions and  
Bibliographic Services

395 Wellington Street  
Ottawa ON K1A 0N4  
Canada

Bibliothèque nationale  
du Canada

Acquisitions et  
services bibliographiques

395, rue Wellington  
Ottawa ON K1A 0N4  
Canada

*Your file Votre référence*

*Our file Notre référence*

The author has granted a non-exclusive licence allowing the National Library of Canada to reproduce, loan, distribute or sell copies of this thesis in microform, paper or electronic formats.

The author retains ownership of the copyright in this thesis. Neither the thesis nor substantial extracts from it may be printed or otherwise reproduced without the author's permission.

L'auteur a accordé une licence non exclusive permettant à la Bibliothèque nationale du Canada de reproduire, prêter, distribuer ou vendre des copies de cette thèse sous la forme de microfiche/film, de reproduction sur papier ou sur format électronique.

L'auteur conserve la propriété du droit d'auteur qui protège cette thèse. Ni la thèse ni des extraits substantiels de celle-ci ne doivent être imprimés ou autrement reproduits sans son autorisation.

0-612-59883-7

Canada

**University of Alberta**

**Library Release Form**

**Name of Author:** James Uwe Stemler


**Title of Thesis:** A fluid inclusion and stable isotopic examination of the  
Boston, greenstone belt hosted, Archean lode-gold deposit,  
Hope Bay volcanic belt, Nunavut, Canada.

**Degree:** Master of Science

**Year this Degree Granted:** 2000

Permission is hereby granted to the University of Alberta Library to reproduce single copies of the thesis and to lend or sell such copies for private, scholarly or scientific research purposes only.

The author reserves all other publications and other rights in association with the copyright in the thesis, and except as herein before provided, neither the thesis nor any substantial portion thereof may be printed or otherwise reproduced in any material form whatever without the author's prior written permission.



2643-137 Street  
Surrey, British Columbia  
V4P 1S6

Date: 09/27/00

## **Abstract**

Primary liquid-rich H<sub>2</sub>O-CO<sub>2</sub> fluid inclusions associated with gold mineralization in the Boston Archean lode-gold deposit are of low salinity ( $4.4 \pm 1.6$  eq. wt.% NaCl, n = 91) and contain pure CO<sub>2</sub> ( $T_{mCO_2} = -56.8 \pm 0.2^\circ\text{C}$ , n = 75). Homogenization temperatures averaging  $272 \pm 34^\circ\text{C}$  (n = 81) and pressures averaging  $2.5 \pm 0.5$  kilobars (n = 51) are interpreted to approximate trapping conditions because of coexistence of primary CO<sub>2</sub> gas-rich and liquid-rich inclusions.

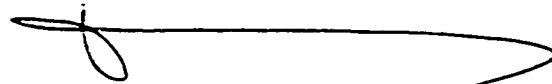
Carbonates from the mineralised zones vary by 1.5‰ in  $\delta^{13}\text{C}$  (-4.6 to -3.1‰, n = 15) and 1.6‰ in  $\delta^{18}\text{O}$  (11.2 to 12.8‰, n = 15); quartz varies by 2.1‰ in  $\delta^{18}\text{O}$  (12.9 to 14.8‰, n = 12); and pyrite varies by 1.4‰ in  $\delta^{34}\text{S}$  (2.1 to 3.5‰, n = 8). The  $\delta^{18}\text{O}_{\text{H}_2\text{O}}$ ,  $\delta^{13}\text{C}_{\text{CO}_2}$ , and  $\delta^{34}\text{S}_{\text{H}_2\text{S}}$  values of the fluid calculated from these minerals at  $272^\circ\text{C}$  are intermediate between a metamorphic and magmatic source for water, sulphur and carbon.

Petrographic and geochemical data for the Boston deposit is consistent with data from Archean lode-gold deposits world wide, implying that the Boston deposit formed in a similar environment from similar gold-bearing fluids.

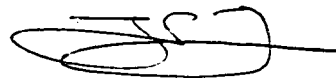
**University of Alberta**

**Faculty of Graduate Studies and Research**


The undersigned certify that they have read, and recommend to the Faculty of Graduate Studies and Research for acceptance, a thesis entitled A fluid inclusion and stable isotopic examination of the Boston, greenstone belt hosted, Archean lode-gold deposit, Hope Bay volcanic belt, Nunavut, Canada submitted by James Uwe Stemler in partial fulfillment of the requirements for the degree of Master of Science.



Dr. Karlis Muehlenbachs (chair and examiner)



Dr. Jeremy P. Richards (supervisor)



Dr. Qi Liu (committee member)

Date: 26/9/00

*for my father*  
*Uwe Louis Stemler*



## **Acknowledgements**

The author wishes to acknowledge the numerous individuals and organizations that offered support, in various forms, throughout the course of this study.

I would like to thank Bruce Nesbitt for his original suggestion for this study and for seeing its potential, even in the early days. I would like to thank Jeremy Richards for agreeing to supervise this project, for giving me access to his laboratory and facilities, and for his insight into problems that came up along the way. I would also like to thank Karlis Muehlenbachs for access to his laboratory, without which the stable isotopic analysis would have been impossible. I also wish to thank Karlis for always having the time to answer my questions, address my concerns, and to offer good advice when it was really needed.

I would like to thank the Broken Hill Proprietary Company Limited of Canada (BHP) for the permission to conduct this study and for financial support. I would especially like to thank Dave Clark, Ross McElroy, and Greg MacMaster for sticking by BHP's commitment to me even when the future of the Boston deposit was uncertain. I would also like to thank the people I worked with at the Boston deposit for the interest and support they showed for this project. Discussions with the individuals mentioned above, as well as Andrew Locock, Peter Kleespies, and the rest of the BHP staff were enlightening and their suggestions were quite helpful in the progression of this study. I wish to thank the Hope Bay joint venture for supplying samples from the South Patch and Discovery areas and for showing continued interest in this project. I would also like to thank the Society of Economic Geologists, the University of Alberta, and Karlis Muehlenbachs for supporting this project financially.

I also wish to thank all of my fellow graduate students for their interest, encouragement, and friendship over the last three years. Several of the technical staff of the Department of Earth and Atmospheric Sciences at the University of Alberta were also of great help in the completion of this study. These people include Don Resultay and Mark Labbe for the making of thin and polished sections, Dianne Caird for X-ray diffraction analyses, Olga Levner for oxygen isotope analysis, Lang Shi for microprobe analyses, and Randy Pakan for hand sample photography.

Finally, I would like to thank my family Carol, Uwe, and Owen for the support and encouragement they have given me throughout my education. I would also like to thank my family and friends for their generosity and support especially in the final days of this study. Rod Potter deserves special thanks for using his vast computer knowledge to get me out of a tough situation more than once. Most of all, I would like to thank Sandra Jasinowski for being there for me in both the good times and the bad, and for her help, encouragement, and support over the past two years.

## Table of Contents

	Page
<b>1. Introduction</b> .....	1
<b>2. Regional Geology</b> .....	5
<b>2.1. Slave Structural Province</b> .....	5
<b>2.2. Bathurst Block</b> .....	7
<b>2.3. Hope Bay Volcanic Belt</b> .....	8
<b>2.3.1. Hope Bay Volcanic Belt - Structural Geology</b> .....	15
<b>2.3.2. Hope Bay Volcanic Belt - Exploration History</b> .....	18
<b>3. Deposit Geology</b> .....	19
<b>3.1. The Boston Lode-Gold Deposit</b> .....	19
<b>3.1.1. Structural Setting</b> .....	20
<b>3.1.2. Host Lithologies</b> .....	23
<b>3.1.3. Hydrothermal Alteration</b> .....	34
<b>3.1.4. Boston Mineralized Zones</b> .....	42
<b>3.1.5. Vein Paragenesis</b> .....	49
<b>3.2. The South Patch Occurrence</b> .....	58
<b>4. Sample Selection and Analytical Methods</b> .....	59
<b>4.1. Petrography, XRD, and XRF Whole Rock Analysis</b> .....	60
<b>4.2. Fluid Inclusion Analysis</b> .....	61
<b>4.3. Stable Isotopic Analysis</b> .....	62
<b>5. Results</b> .....	67
<b>5.1. XRF Whole Rock Analysis</b> .....	67

<b>5.2. Fluid Inclusions</b> .....	<b>67</b>
<b>5.2.1. Fluid Inclusion Types</b> .....	<b>67</b>
<b>5.2.2. Microthermometry</b> .....	<b>72</b>
<b>5.3. Stable Isotopes</b> .....	<b>86</b>
<b>5.3.1. Carbonate and Quartz (Mineralized Veins)</b> .....	<b>86</b>
<b>5.3.2. Carbonate (Country Rocks)</b> .....	<b>92</b>
<b>5.3.3. Carbonate and Quartz (Regional Veins)</b> .....	<b>109</b>
<b>5.3.4. Pyrite</b> .....	<b>114</b>
<b>5.3.5. Graphite</b> .....	<b>124</b>
<b>5.4. Stable Isotopes from the South Patch Occurrence</b> .....	<b>124</b>
<b>5.4.1. Carbonate and Quartz (Mineralized Veins)</b> .....	<b>124</b>
<b>5.4.2. Carbonate (Country Rocks)</b> .....	<b>125</b>
<b>6. Discussion</b> .....	<b>128</b>
<b>6.1. Fluid Types and Paragenesis</b> .....	<b>128</b>
<b>6.1.1. Auriferous Fluid</b> .....	<b>129</b>
<b>6.1.2. Barren Fluids</b> .....	<b>132</b>
<b>6.2. Stable Isotopes</b> .....	<b>134</b>
<b>6.2.1. The <math>\delta^{18}\text{O}_{\text{H}_2\text{O}}</math> Composition of the Auriferous Fluid</b> .....	<b>134</b>
<b>6.2.2. The <math>\delta^{13}\text{C}_{\text{CO}_2}</math> Composition of the Auriferous Fluid</b> .....	<b>135</b>
<b>6.2.3. The <math>\delta^{34}\text{S}_{\text{H}_2\text{S}}</math> Composition of the Auriferous Fluid</b> .....	<b>138</b>
<b>6.2.4. The <math>\delta^{13}\text{C}</math> and <math>\delta^{18}\text{O}</math> Composition of Secondary Carbonate in the Country rocks</b> .....	<b>140</b>
<b>6.2.5. The <math>\delta^{13}\text{C}</math> and <math>\delta^{18}\text{O}</math> Composition of Quartz and Carbonate in Regional Veins</b> .....	<b>142</b>

<b>6.3. Deposition of Gold</b> .....	<b>143</b>
<b>6.4. The South Patch Occurrence</b> .....	<b>145</b>
<b>6.5. Similarity to Other Archean Lode-Gold Deposits</b> .....	<b>146</b>
<b>6.5.1. Mineralization and Wallrock Alteration</b> .....	<b>147</b>
<b>6.5.2. Nature of the Mineralizing Fluids</b> .....	<b>150</b>
<b>7. Conclusions</b> .....	<b>152</b>
<b>8. References</b> .....	<b>155</b>
<b>Appendix A.</b> .....	<b>172</b>
<b>Appendix B.</b> .....	<b>188</b>
<b>Appendix C</b> .....	<b>189</b>
<b>Appendix D</b> .....	<b>203</b>
<b>Appendix E</b> .....	<b>209</b>
<b>Appendix F</b> .....	<b>211</b>
<b>Appendix G</b> .....	<b>212</b>

## List of Tables

<b>Table</b>		<b>Page</b>
<b>5.1</b>	Summary of the results of microthermometric analysis of quartz-carbonate veins in the Boston deposit. ....	<b>74</b>
<b>5.2</b>	Summary of the results of the stable isotopic analysis of calcite, ankerite, and ferroan dolomite separated from mineralized and barren veins, and wallrocks associated with the Boston deposit. ....	<b>87</b>
<b>5.3</b>	Summary of the results of the stable isotopic analysis of quartz separated from mineralized and barren veins in the Boston deposit. ....	<b>90</b>
<b>5.4</b>	Summary of the results of the stable isotopic analysis of pyrite adjacent to mineralized and barren veins and pyrite vugs and bands within turbiditic and graphitic sediments associated with the Boston deposit. ....	<b>121</b>
<b>5.5</b>	Summary of the results of the stable isotopic analysis of calcite, ankerite, and ferroan dolomite separated from mineralized and barren veins, and wallrocks associated with the South Patch occurrence. ....	<b>125</b>
<b>6.1</b>	Wallrock alteration associated with the Boston deposit and typical basalt hosted Archean lode-gold deposits: Archean lode-gold information adapted from Groves and Foster (1991). ....	<b>149</b>
<b>6.2</b>	Fluid characteristics and selected stable isotopic values for the Boston deposit, the South Patch occurrence, and Archean lode-gold deposits in general: Archean lode gold deposit data modified after Groves and Foster (1991) and de Ronde et al. (1997). NA = Not Available .....	<b>151</b>

## List of Figures

<b>Figure</b>		<b>Page</b>
<b>1.1</b>	The geology of the Slave Structural Province showing the location of the Hope Bay volcanic belt (HBVB): modified from the Hope Bay Project - Exploration Overview, 1999 (published with permission from the Hope Bay joint venture), originally simplified from Fyson et al. (1993). .....	<b>2</b>
<b>1.2</b>	Hope Bay Volcanic belt geology: modified from the Hope Bay Project - Exploration Overview, 1999 (published with permission from the Hope Bay joint venture). .....	<b>4</b>
<b>2.1</b>	Generalized stratigraphy and deformational history of the Hope Bay volcanic belt (HBVB). Constructed using information in the Hope Bay Project - Exploration Overview, 1999, and Hebel 1999 .....	<b>10</b>
<b>3.1</b>	The geology of the Boston area; modified from the Hope Bay Project - Exploration Overview, 1999 (published with permission from the Hope Bay joint venture). .....	<b>21</b>
<b>3.2</b>	A generalized cross section of the Boston deposit looking north, from the Hope Bay Project - Exploration Overview, 1999, (published with permission from the Hope Bay joint venture). .....	<b>43</b>
<b>5.1</b>	Salinity (eq. wt.% NaCl) vs homogenization temperature plots for mineralized and barren crosscutting veins in (a) the B2 zone, and (b) the B3 zone (MSQC vein = main stage quartz carbonate vein). .....	<b>76</b>
<b>5.2</b>	The homogenization temperature of primary and secondary type 2 fluid inclusions from (a) the B2 zone, (b) the B3 zone, and (c) the B4 zone, and secondary type 2, 3, and 4 inclusions within crosscutting veins in (d) the B2 zone, and (e) the B3 zone, (MSQC vein = main stage quartz-carbonate vein). .....	<b>77</b>

<b>Figure</b>	<b>Page</b>
5.3	The salinity of primary and secondary type 2 fluid inclusions from (a) the B2 zone, (b) the B3 zone, and (c) the B4 zone, and secondary type 2, 3, and 4 fluid inclusions within cross-cutting veins in (d) the B2 zone, and (e) the B3 zone. .... 78
5.4	Minimum pressure calculated from the homogenization temperature of primary and secondary type 2 fluid inclusions within (a) the B2 zone, (b) the B3 zone, and (e) the B4 zone; secondary type 2 fluid inclusions within ladder veins in (c) the B2 zone, and (d) the B3 zone. .... 79
5.5	The (a) carbon and (b) oxygen stable isotopic composition of carbonate separated from gold-bearing veins within the B2, B3, and B4 zones; (c) the oxygen stable isotopic composition of quartz separated from gold-bearing and flat veins in the B2, B3, and B4 zones. .... 89
5.6	The stable isotopic composition of carbonate minerals separated from gold-bearing veins and (a) disseminated throughout the country rocks distal to the Boston deposit; and (b) and (c) wallrocks directly adjacent to the mineralized veins within the Boston deposit. .... 94
5.7	The (a) carbon, and (b) oxygen stable isotopic composition of secondary carbonate minerals disseminated throughout metamorphically altered basaltic rocks, turbiditic sediments, and strongly deformed rocks associated with the Boston deposit. .... 100
5.8	The carbon stable isotopic composition of secondary carbonate minerals within (a) gold-bearing veins and altered basaltic rocks in the Boston area and (b) the carbon stable isotopic composition of secondary carbonate minerals from within basaltic rocks with respect to distance from mineralized veins in the Boston area (all distances are measured from 7505000N and 441150E, approximately halfway between the B2 and B3 zones). .... 101

- 5.9** The oxygen stable isotopic composition of secondary carbonate minerals within (a) gold-bearing veins and altered basaltic rocks in the Boston area and (b) the oxygen stable isotopic composition of secondary carbonate minerals from within basaltic rocks with respect to distance from mineralized veins in the Boston area (all distances are measured from 7505000N and 441150E, approximately halfway between the B2 and B3 zones). ..... **102**
- 5.10** The carbon stable isotopic composition of secondary carbonate minerals within (a) gold-bearing veins and altered gabbroic rocks in the Boston area and (b) the carbon stable isotopic composition of secondary carbonate minerals from within gabbroic rocks with respect to distance from mineralized veins in the Boston area (all distances are measured from 7505000N and 441150E, approximately halfway between the B2 and B3 zones). ..... **103**
- 5.11** The oxygen stable isotopic composition of secondary carbonate minerals within (a) gold-bearing veins and altered gabbroic rocks in the Boston area and (b) the oxygen stable isotopic composition of secondary carbonate minerals from within gabbroic rocks with respect to distance from mineralized veins in the Boston area (all distances are measured from 7505000N and 441150E, approximately halfway between the B2 and B3 zones). ..... **104**
- 5.12** The carbon stable isotopic composition of secondary carbonate minerals within (a) gold-bearing veins and altered turbiditic sediments in the Boston area and (b) the carbon stable isotopic composition of secondary carbonate minerals from within turbiditic sediments with respect to distance from mineralized veins in the Boston area (all distances are measured from 7505000N and 441150E, approximately halfway between the B2 and B3 zones). ..... **105**



<b>Figure</b>		<b>Page</b>
<b>5.13</b>	The oxygen stable isotopic composition of secondary carbonate minerals within (a) gold-bearing veins and altered turbiditic sediments in the Boston area and (b) the oxygen stable isotopic composition of secondary carbonate minerals from within turbiditic sediments with respect to distance from mineralized veins in the Boston area (all distances are measured from 7505000N and 441150E, approximately halfway between the B2 and B3 zones). .....	<b>106</b>
<b>5.14</b>	The carbon stable isotopic composition of secondary carbonate minerals within (a) gold-bearing veins and altered graphitic argillites in the Boston area and (b) the carbon stable isotopic composition of secondary carbonate minerals from within graphitic argillites with respect to distance from mineralized veins in the Boston area (all distances are measured from 7505000N and 441150E, approximately halfway between the B2 and B3 zones). .....	<b>107</b>
<b>5.15</b>	The oxygen stable isotopic composition of secondary carbonate minerals within (a) gold-bearing veins and altered graphitic argillites in the Boston area and (b) the oxygen stable isotopic composition of secondary carbonate minerals from within graphitic argillites with respect to distance from mineralized veins in the Boston area (all distances are measured from 7505000N and 441150E, approximately halfway between the B2 and B3 zones). .....	<b>108</b>
<b>5.16</b>	(a) The stable isotopic composition of carbonate minerals separated from gold-bearing and regional veins associated with the Boston deposit; and (b) the oxygen stable isotopic composition of quartz separated from gold-bearing and regional veins in the Boston area. ....	<b>110</b>
<b>5.17</b>	The carbon stable isotopic composition of carbonate minerals separated from (a) gold-bearing veins and regional veins hosted by basalts in the Boston area and (b) the carbon stable isotopic composition of carbonate minerals separated from regional veins hosted by basalts with respect to distance from mineralized veins in the Boston area (all distances measured from 7505000N and 441150E, approximately halfway between the B2 and B3 zones). .....	<b>115</b>

<b>5.18</b>	The oxygen stable isotopic composition of carbonate minerals separated from (a) gold-bearing veins and regional veins hosted by basalts in the Boston area and (b) the oxygen stable isotopic composition of carbonate minerals separated from regional veins hosted by basalts with respect to distance from mineralized veins in the Boston area (all distances measured from 7505000N and 441150E, approximately halfway between the B2 and B3 zones). .....	<b>116</b>
<b>5.19</b>	The oxygen stable isotopic composition of quartz separated from (a) gold-bearing veins and regional veins hosted by basalts in the Boston area and (b) the oxygen stable isotopic composition of quartz separated from regional veins hosted by basalt with respect to distance from mineralized veins in the Boston area (all distances measured from 7505000N and 441150E, approximately halfway between the B2 and B3 zones). .....	<b>117</b>
<b>5.20</b>	The oxygen stable isotopic composition of quartz separated from (a) gold-bearing veins and regional veins hosted by gabbros in the Boston area and (b) the oxygen stable isotopic composition of quartz separated from regional veins hosted by basalt with respect to distance from mineralized veins in the Boston area (all distances measured from 7505000N and 441150E, approximately halfway between the B2 and B3 zones). .....	<b>118</b>
<b>5.21</b>	The carbon stable isotopic composition of carbonate minerals separated from (a) gold-bearing veins and regional veins hosted by turbiditic sediments in the Boston area and (b) the carbon stable isotopic composition of carbonate minerals separated from regional veins hosted by turbiditic sediments with respect to distance from mineralized veins in the Boston area (all distances measured from 7505000N and 441150E, approximately halfway between the B2 and B3 zones). .....	<b>119</b>

<b>Figure</b>		<b>Page</b>
<b>5.22</b>	The oxygen stable isotopic composition of carbonate minerals separated from (a) gold bearing veins and regional veins hosted by turbiditic sediments in the Boston area and (b) the oxygen stable isotopic composition of carbonate minerals separated from regional veins hosted by turbiditic sediments with respect to distance from mineralized veins in the Boston area (all distances measured from 7505000N and 4411150E, approximately halfway between the B2 and B3 zones). .....	<b>120</b>
<b>5.23</b>	The sulphur stable isotopic composition of pyrite separated from the sulphidation halo around mineralized and barren veins, and from clots within graphitic argillite and vugs within turbidites in the Boston area. ....	<b>122</b>
<b>5.24</b>	The stable isotopic composition of secondary carbonate minerals within gold-bearing veins and metamorphically altered country rocks associated with the South Patch occurrence. ....	<b>126</b>

## List of Plates

<b>Plate</b>		<b>Page</b>
<b>2.1</b>	(a) mafic volcanic rocks approximately 33 kilometers north of the Boston deposit. Note the dark weathering pillow selvages (photo provided by BHP); (b) turbiditic sediments in the Hope Bay volcanic belt (photographs published with permission from the Hope Bay joint venture). .....	<b>11</b>
<b>3.1</b>	(a) Photomicrograph exposed in transmitted plane polarized light of a typical greenschist facies basalt from the Boston area consisting of 55% clinocllore, 20% plagioclase, 15% calcite, 7% quartz, 3% rutile, and trace pyrite and chalcopyrite. Relict igneous textures are also present in this sample; (b) Sample of basalt from diamond drill core, irregular calcite-filled fractures occur throughout this sample. ....	<b>25</b>
<b>3.2</b>	Photomicrographs (a) exposed in transmitted plane polarized light and (b) under crossed nicols of a foliated gabbro consisting predominantly of dark olive green clinocllore (50%), and coarse grained laths of plagioclase (30%). Calcite (10%), sericite (paragonite, 5%), quartz, (3%), rutile (2%), and trace pyrite are also typically present in this rock type; (c) a sample of gabbro from diamond drill core. ....	<b>27</b>
<b>3.3</b>	(a) a photomicrograph exposed in transmitted plane polarized light of a well foliated, hydrothermally altered, ultramafic picrite (B3 gabbro) consisting of wispy bands of sericite (paragonite/muscovite) and clinocllore (50%), alternating with grey bands of dolomite (30%), and quartz (12%). Pyrite, arsenopyrite, and chalcopyrite (5%) are also typically present along with minor amounts of rutile (3%); (b) two samples of the B3 gabbro from diamond drill core, note the distinctive bands of bright green paragonite + sericite alteration. ....	<b>28</b>

<b>Plate</b>	<b>Page</b>
<p><b>3.4</b> Photomicrographs (a) exposed in transmitted plane polarized light and (b) under crossed nicols of a massive graywacky consisting of large rounded clasts of quartz (20%) and plagioclase (18%) in a finer grained matrix of sericite (28%), quartz (17%), carbonate (15%), rutile (2%) and trace sulphides. Photomicrograph (c) and diamond drill core sample (d, scale bar in cm) of typical bedded turbiditic sediment consisting of calcite (30%), quartz (24%), graphite (20%), muscovite (12%), clinocllore (8%), and sulphides (pyrite, chalcopyrite, arsenopyrite, and pyrrhotite; 6%). .....</p>	<b>30</b>
<p><b>3.5</b> Photomicrographs (a) and (b) exposed in transmitted plane polarized light and (c) diamond drill core sample of well foliated graphitic argillite consisting of bands of fine grained graphite (50%), and clots and foliation parallel stringers of fine to moderately coarse grained calcite (18%) and quartz (15%). Paragonite (15%) occurs intergrown with graphite in most samples. Irregular clots of pyrite (Py), sphalerite (Sph), chalcopyrite, and pyrrhotite are also common (b and c). .....</p>	<b>31</b>
<p><b>3.6</b> Strongly folded argillic sediment. Photomicrographs (a) exposed in transmitted plane polarized light; (b) exposed under crossed nicols; and (c) photograph of strongly folded graphitic argillite from diamond drill core (scale in cm). .....</p>	<b>32</b>
<p><b>3.7</b> Hydrothermally altered andesitic dyke from between the B2 and B3 zones. The dyke consists of fine-grained carbonate (50%), sericite (muscovite/paragonite) and clinocllore (25%), quartz (15%), and residual plagioclase (5%). Magnetite and course pyrite (Py) clots also occur throughout this unit. Photomicrograph (a) exposed under crossed nicols; photograph from diamond drill core; note the presence of irregular pyrite clots in this sample. ....</p>	<b>33</b>

<b>Plate</b>	<b>Page</b>
<p><b>3.8</b></p> <p>Basalt that has experienced relatively weak hydrothermal alteration in the within the Boston fault zone. The sample is well foliated and consists of fine grained calcite (35%), paragonite (25%), clinochlore (18%), plagioclase (15%), quartz (5%), and rutile (2%). Plagioclase laths are oriented roughly parallel to foliation and in most cases have been at least partially replaced by calcite and sericite. (a) Photomicrograph exposed in transmitted plane polarized light and (b) photograph from diamond drill core. ....</p>	<p><b>36</b></p>
<p><b>3.9</b></p> <p>Basalt that has experienced moderate levels of hydrothermal alteration and deformation within the Boston fault zone. Moderately altered basalt is generally fine grained and well foliated and consists of mm- to cm-scale wispy bands of paragonite (40%), clinochlore (13%), and rutile (7%) that alternate with slightly thicker bands of carbonate (22%) and quartz (18%). Trace pyrite, chalcopyrite, and arsenopyrite also occur in most samples. Photomicrographs (a) exposed in transmitted plane polarized light and (b) under crossed nicols; (c) photograph of moderately altered basalt from diamond drill core. ....</p>	<p><b>38</b></p>
<p><b>3.10</b></p> <p>Basalt that has experienced high levels of hydrothermal alteration and deformation within the Boston fault zone. Millimeter-scale bands of paragonite (50%), clinochlore (13%), and rutile (2%) define a strongly developed foliation in this unit. Deformed bands and lenses of carbonate (20%) and quartz (15%) occur within and between the paragonite/clinochlore bands. This sample has retained no primary textures and is difficult to tell apart from strongly deformed gabbros, and sediments that also occur within the Boston fault zone. (a)Photomicrograph exposed in transmitted plane polarized light and (b) photograph from diamond drill core. ....</p>	<p><b>39</b></p>
<p><b>3.11</b></p> <p>The sulphidation halo around main stage quartz carbonate veining in the B2 zone. Note the thick foliation parallel clots of coarse grained, gold-bearing pyrite in the wallrock immediately adjacent to the quartz-carbonate vein (lens cap in photo is approximately 6cm in diameter). ....</p>	<p><b>41</b></p>

- 3.12** The sequence of events that led to the development of the main stage quartz-carbonate veins, ladder veins, and flat veins in the Boston deposit (modified after Hodgson, 1989, and Hurst, 1935, for mineralized veining in the Hollinger mine, Timmins, Ontario); (a) several stages of main stage quartz-carbonate vein formation (1a, 1b, 1c, etc.) by crack seal processes; (b) ladder veins (2) form within the main stage quartz-carbonate veins in response to compression-related deformation directed perpendicular to the walls of the main stage veins; (c) as compression-related deformation continues under brittle conditions flat veins (3) form which crosscut the main stage quartz-carbonate veins; (d) continued deformation results in folding of the flat veins and boudinage of the main stage veins; (e) deformed main stage quartz-carbonate fissure vein and associated flat veins typically observed in the B2 zone (hammer is approximately 40cm long). ..... 45
- 3.13** (a) gold (Au) inclusions within pyrite (Py, B3 zone); (b) gold inclusions within arsenopyrite (Aspy, B3 zone); (c) a gold inclusion within chalcopyrite (Cpy, B3 zone); (d) gold and chalcopyrite inclusions within large pyrite-arsenopyrite grain (B3 zone); (e) visible gold associated with a stringer of strongly altered wallrock within main stage quartz-carbonate vein (B2 zone, scale in mm); (f) visible gold associated with pyrite and arsenopyrite in wallrock stringer within a main stage quartz-carbonate vein (B2 zone); (g) visible gold within a main stage quartz-carbonate vein (B2 zone). (a-b), (f), and (g) reflected light photomicrographs, (e) handsample ..... 46
- 3.14** Main stage quartz-carbonate veining (1) in the B3 zone. Numerous crosscutting extension-related ladder veins (2) give the B3 zone an overall brittle, stockwork-like appearance (lens cap is approximately 6cm in diameter). ..... 48

<b>3.15</b>	(a) Photomicrograph of deformed and recrystallized quartz typically present in unsheltered quartz-carbonate veins within the Boston deposit (exposed under crossed nicols); (d) ladder veins hosted by a main stage quartz-carbonate vein (B2 zone); photomicrographs (c) exposed in transmitted plane polarized light and (d) under crossed nicols of several thin ladder veins hosted by a recrystallized main stage quartz-carbonate vein in the B2 zone. ....	<b>51</b>
<b>3.16</b>	(a) Flat vein in the B2 zone crosscutting a subvertical quartz-carbonate vein; weathering has highlighted quartz (white) and carbonate (brown) crystals growing into the vein, perpendicular to the vein walls (perpendicular to the maximum compressive stress in the Boston fault zone; lens cap is approximately 6cm in diameter); (b) a photomicrograph exposed under crossed nicols of elongate quartz and carbonate grains similar to in (a) growing into the flat vein at roughly right angles to the vein walls (vein wall is at the bottom of the photomicrograph); (c) a bridge of strongly altered wallrock that became incorporated into the flat vein as it opened (B2 zone). ....	<b>55</b>
<b>3.17</b>	Photomicrographs (a) exposed in transmitted plane polarized light and (b) under crossed nicols of phantom veinlets hosted by a main stage quartz-carbonate vein in the B2 zone. The phantom veinlets and the quartz that hosts them have been extensively recrystallized and deformed. All that indicates the existence of these veinlets is a difference in fluid inclusion density between quartz within and outside of the veinlets. (c) crosscutting late brittle veinlets within the B2 zone (scale is in centimetres). ....	<b>57</b>



<b>5.1</b>	<p>(a) Primary type 1, two phase CO<sub>2</sub> fluid inclusion in quartz; (b) primary type 2, three-phase H<sub>2</sub>O-CO<sub>2</sub> fluid inclusion in quartz; (c) undeformed quartz grains included within a larger carbonate grain in a gabbro-hosted quartz-carbonate vein outside of the Boston deposit; the quartz grain depicted in (d) is circled; (d) primary type 1 and 2 fluid inclusions within an undeformed quartz grain hosted by carbonate, the approximate location of the fluid inclusions depicted in (a) and (b) is circled; (e) undeformed quartz grains included within a larger pyrite grain, the quartz grain depicted in (g) is circled; (f) and (g) primary type 1 and 2 fluid inclusions within undeformed quartz grains hosted by pyrite in the B2 zone. ....</p>	<b>69</b>
<b>5.2</b>	<p>(a) Secondary type 2 fluid inclusions within a main stage quartz-carbonate vein in the B2 zone, the approximate location of the fluid inclusions depicted in (a) is circled; (b) close up of the secondary type 2 fluid inclusions depicted in (a), these fluid inclusions have negative crystal shapes and uniform fill volumes. (c), (b), and (e) show evidence for phase separation within main stage quartz-carbonate veins in the Boston area: (c) coexisting type 1 and type 2 fluid inclusions within a sheltered part of a main stage quartz-carbonate vein hosted by hydrothermally altered sediments within the Boston fault zone; (d) coexisting primary type 1 and type 2 fluid inclusions within an undeformed quartz grain that was protected from deformation by a larger carbonate grain in a gabbro hosted quartz-carbonate vein (close up of Plate 5.1d); (e) coexisting primary type 1 and 2 fluid inclusions within an undeformed quartz grain that was protected from deformation by a larger pyrite grain in the B2 zone (close up of Plate 5.1f). ....</p>	<b>71</b>
<b>5.3</b>	<p>(a) Secondary type 3, two phase H<sub>2</sub>O fluid inclusion in quartz; (b) secondary type 4, two phase H<sub>2</sub>O fluid inclusion in quartz; (c) type 3 fluid inclusions within a crosscutting quartz filled brittle veinlet in the B2 zone, the approximate location of the fluid inclusion depicted in (a) is circled; (d) type 4 fluid inclusions occurring as trails of secondaries along healed microfractures in the B2 zone, the approximate location of the fluid inclusion depicted in (b) is circled. ....</p>	<b>73</b>








## **1. Introduction**

Lode-gold deposits occur within Archean greenstone belts throughout the world. Deposits of this type are among the largest and most lucrative sources of gold on the planet. For example, lode-gold deposits in the Superior Province of the Canadian Shield have produced more than 4500 tonnes of gold alone (Groves and Foster, 1991). In general, several hundred to several thousand individual lode-gold deposits or prospects may occur within a single greenstone belt in highly mineralized Archean cratons.

This study focuses on the Boston mesothermal quartz-carbonate vein lode-gold deposit. The Boston deposit is located in the Slave Structural Province, approximately 700 kilometres northeast of Yellowknife and 170 kilometres southwest of Cambridge Bay, in the southern portion of the Hope Bay volcanic belt (NTS map sheet 76 O/9; Figure 1.1). The Boston deposit represents the first major quartz-carbonate vein lode-gold deposit to be discovered in the Hope Bay volcanic belt since it was initially mapped by the Geological Survey of Canada in 1962. Prior to the 2000 drill program an inferred resource of at least 2.3 million ounces of gold was estimated for the Boston deposit. The apparent isolation of the Boston deposit within the southern portion of the Hope Bay volcanic belt coupled with the tendency for deposits of this type to occur in clusters or districts (for example; the Abitibi belt, Quebec; the Timmins (Porcupine) district, Ontario; and the Kalgoorlie area, western Australia; Groves and Foster, 1991; Robert, 1995) makes understanding the conditions that led to its formation critical.

The purpose of this study is to evaluate the nature of the fluids responsible for lode-gold mineralization and hydrothermal alteration in the Boston deposit using fluid

## Geology of the Slave Structural Province

-  Granitoid rocks  
Gneissic granitoids
-  Migmatites and gneisses
-  Metasedimentary rocks
-  Felsic/Intermediate volcanic rocks
-  Mafic volcanic rocks
-  Synvolcanic rocks
-  Pre-2.8 Ga Basement rocks

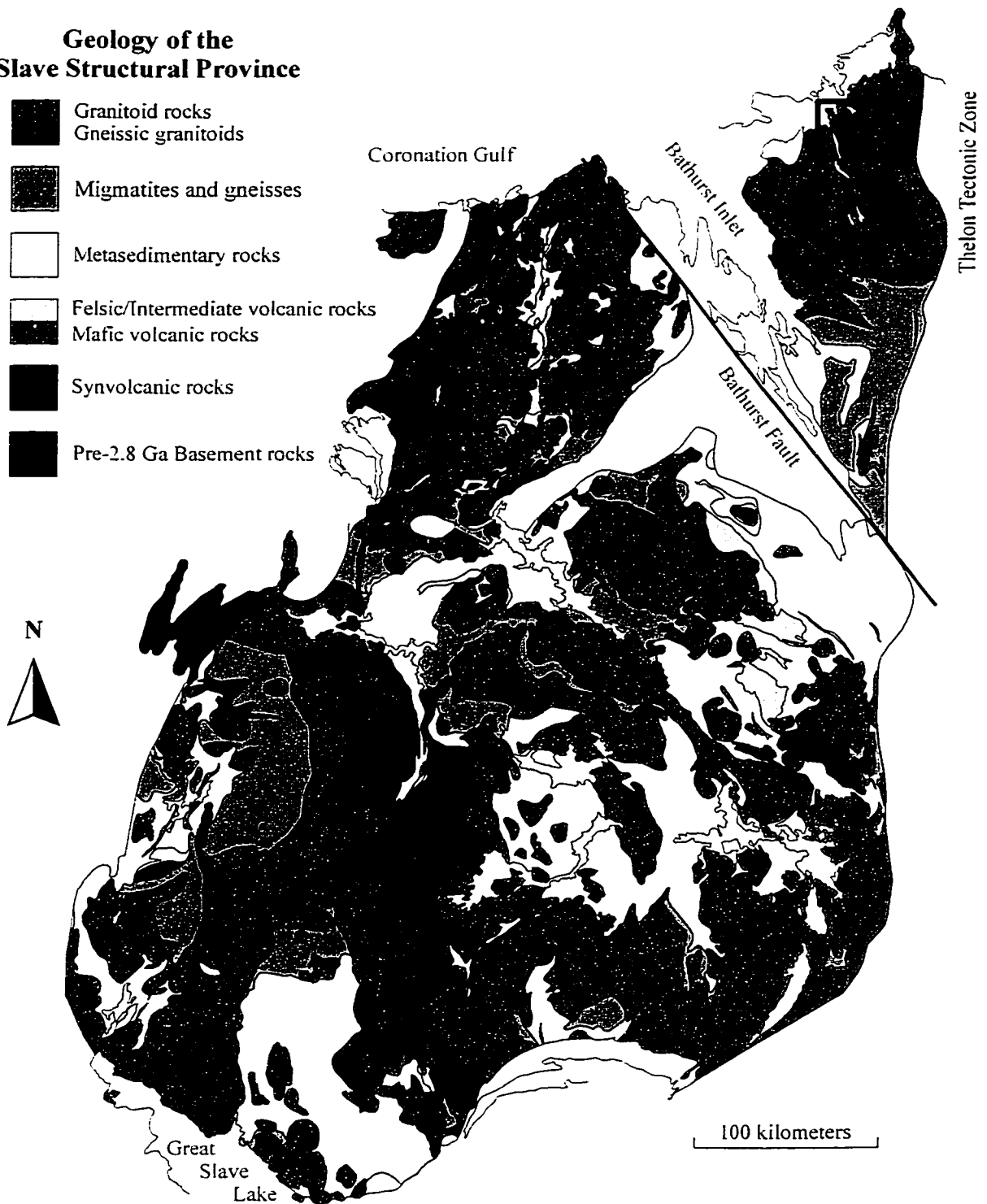


**Figure 1.1.** The geology of the Slave Structural Province showing the location of the Hope Bay volcanic belt (HBVB); modified from the Hope Bay Project - Exploration Overview, 1999 (published with permission from the Hope Bay joint venture), originally from Fyson et al. (1993).

inclusions and stable isotopic analysis. The structure, composition, and paragenesis of the Boston deposit are also described in detail. The results of this study are then compared to the results of a reconnaissance petrographic and stable isotopic study of the South Patch gold prospect, located approximately 45 kilometres to the north of the Boston deposit, near the northern end of the Hope Bay volcanic belt (Figure 1.2). The Boston deposit and the South Patch occurrence will then be compared to what has been observed in Archean lode-gold deposits throughout the world and any similarities will be discussed. Finally, the potential for the discovery of additional lode-gold resources within the Hope Bay volcanic belt will be evaluated.

The author conducted fieldwork at the Boston deposit during the summers of 1997 and 1998, with logistical support from BHP. Fluid inclusion microthermometry, carbonate stable isotopic analyses, and thin section and hand sample petrography was completed at the University of Alberta by the author. Oxygen was extracted from prepared quartz separates by Olga Levenner and Karlis Muehlenbachs at the University of Alberta. Pyrite and graphite separates were sent to the University of Calgary for stable isotopic analysis. Electron microprobe and XRD analyses were done at the University of Alberta by Lang Shi and Dianne Caird, respectively. Samples were sent to XRAL Laboratories in Ontario for XRD whole rock analysis. Thin and doubly polished sections were prepared at the University of Alberta by Don Resultay and Mark Labbe. Several samples were also sent to Petrographic International for sectioning. Hand sample photographs were taken by Randy Pakan at the University of Alberta.

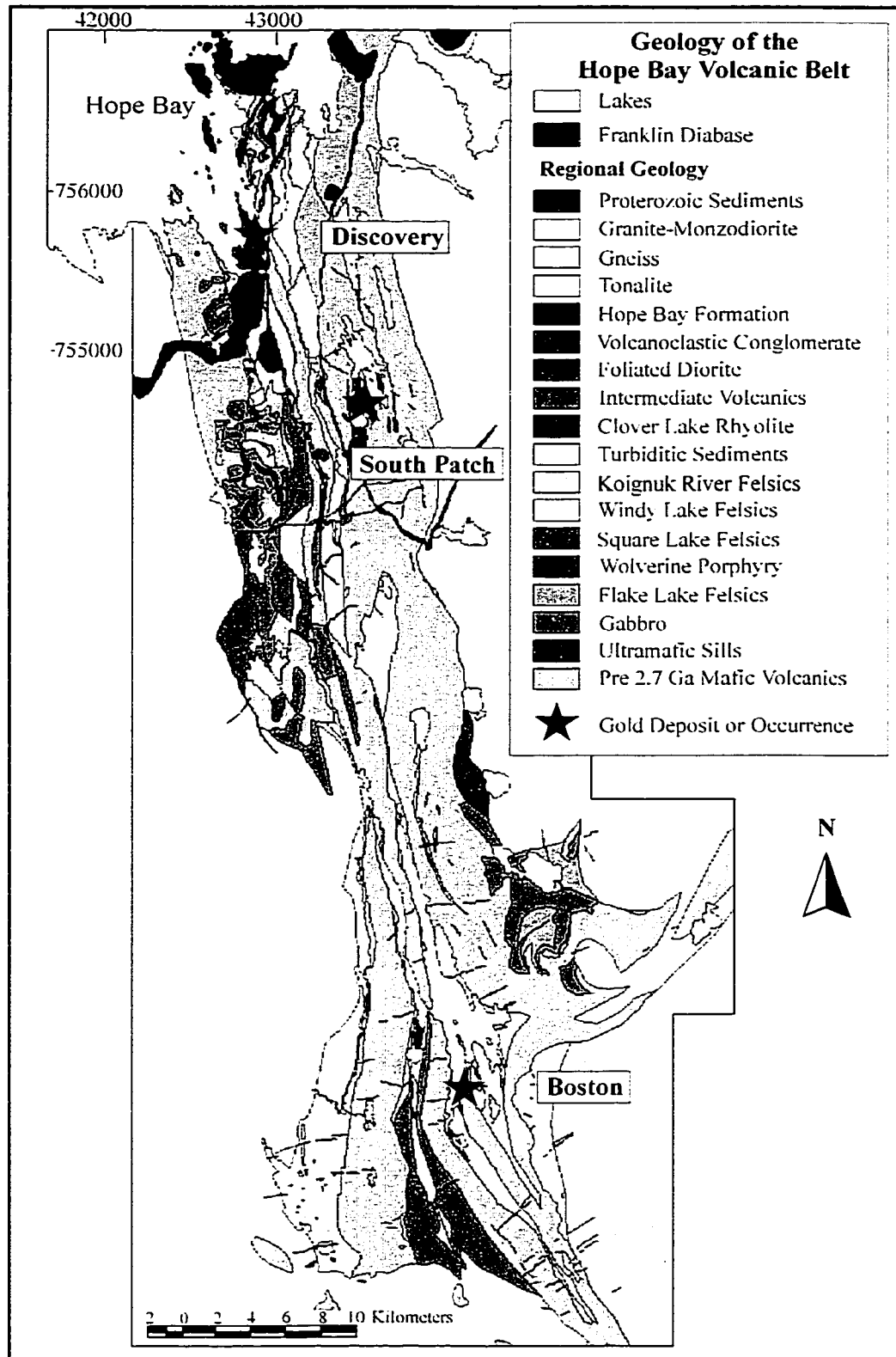


**Figure 1.2.** Hope Bay Volcanic belt geology: modified from the Hope Bay Project - Exploration Overview, 1999 (published with permission from the Hope Bay joint venture).

## **2. Regional Geology**

### ***2.1. Slave Structural Province***

The Slave Structural Province is a well-exposed 2.7 to 2.5 Ga old granite-greenstone terrain in the northwestern portion of the Canadian Shield. The Slave craton is bordered to the east by the 2.0 to 1.9 Ga Thelon orogen, and to the west by the 1.9 to 1.8 Wopmay orogen (Hoffman, 1989). In the south, southwest, and northeast the Slave Structural Province dips beneath younger sedimentary cover (Hoffman, 1989). The absence of komatiitic and alkalic lavas and the high proportion of turbidites relative to volcanic rocks distinguish the Slave craton from other Archean provinces (Padgham, 1985; Padgham and Fyson, 1992). All supracrustal rocks of the Slave craton were subjected to greenschist to lower amphibolite facies metamorphism at approximately 2.63 to 2.58 Ga (Isachsen et al., 1991).

Approximately 60% of the Slave Structural Province is made up of granitoid rocks. Tightly folded metasediments, typically turbidites, make up 32% of the rocks in the craton. The remaining 8% of the Slave structural province consists of metavolcanic rocks (Gebert, 1993; Figure 1.1). The rocks of the Slave craton can be divided into three broad lithological assemblages: the basement assemblage, the Yellowknife Supergroup, and the plutonic assemblage (Davis et al., 1996). The basement assemblage includes all rocks older than 2.75 Ga, including the 3.96 Ga Acasta gneiss (Bowring et al., 1989a). Crust falling into this category has only been recognized in the western part of the craton. The Slave Structural Province is commonly subdivided into western and eastern regions

based largely on the presence of pre-2.7 Ga crust in the west and younger 2.55 to 2.7 Ga crust in the east (Bowring et al., 1989a; Davis and Hegner, 1992; Davis et al., 1996). The basement assemblage is made up of volcanic and metasedimentary sequences, banded amphibolic-tonalitic gneisses, and massive granitoids (Kusky, 1989; Bowring et al., 1989b).

All supracrustal rocks in the Slave Structural Province were originally assigned to the Yellowknife Supergroup (Henderson, 1970). Approximately half of the outcrop exposed in the craton is part of this assemblage. The Yellowknife Supergroup has since been subdivided into a main volcanic-turbidite succession, the Yellowknife Supergroup, and an earlier sequence of orthoquartzites, conglomerates, iron formation, rhyolite, siltstone, and carbonate rocks of the pre-Yellowknife Supergroup (Padgham, 1990). The majority of the Yellowknife Supergroup was formed between 2.7 and 2.59 Ga (Davis et al., 1996). There has been considerable debate as to whether the supracrustal rocks of the Yellowknife Supergroup were deposited directly on top of the basement assemblage, or if they were structurally juxtaposed with the basement assemblage at a later time (Isachsen and Bowring, 1994; Davis et al., 1994). In most cases the contacts between the older and younger rocks are faulted, making their relationship difficult to establish (Davis et al., 1994).

The volcanic belts that make up the Yellowknife Supergroup succession have been divided into two groups based mainly on lithology: the Yellowknife and Hackett River types (Padgham, 1985). Yellowknife-type volcanic belts consist of the lower mafic volcanic Kam Group and the upper intermediate-to-felsic Banting Group. Hackett River

type volcanic belts consist mainly of felsic and intermediate volcanic rocks of calc-alkaline affinity (Padgham, 1985). Mafic Yellowknife-type volcanic belts tend to be more common in the western Slave, whereas the felsic-dominated Hackett River-type volcanic belts are more typical in the central and eastern Slave.

All supracrustal rocks in the Slave craton were deformed at approximately 2.63 to 2.58 Ga resulting in multiple sets of isoclinal folds, foliations, and faults that were later refolded by regional, open cross-folds (Isachsen et al., 1991; van Breemen et al., 1992; Relf, 1992; Davis et al., 1994).

The emplacement of a large volume of late Archean plutonic rocks into the supracrustal succession was the final event leading to stabilization of the Slave craton (Davis et al., 1994). Granitoid rocks predominate over much of the craton between 2.62 and 2.58 Ga, syn- to post-peak deformation and metamorphism (Padgham and Fyson, 1992; van Breemen et al., 1992). These granitoids are the result of widespread late-stage plutonism, which has obscured many of the primary relationships among the supracrustal rocks in the Slave province. The compositions of the plutonic rocks evolved with time from diorite-tonalite suites to younger granites (Davis et al., 1994). The younger granitic suites form two dominant lithologies: alkali-feldspar porphyritic biotite granite, and muscovite-biotite granite (Davis et al., 1996).

## ***2.2. Bathurst Block***

Located in the northeast corner of the Slave structural province, the Bathurst Block is bound to the southwest by the Bathurst fault and to the northwest by the Thelon



tectonic zone (Figure 1.1). The Bathurst Block formed as the result of collision between the Slave and Rae provinces 1.97 to 1.92 Ga ago (Hoffman, 1989). The Bathurst fault developed to accommodate postcollisional indentation through strike slip motion along its length (Hoffman, 1989).

Granitoids make up over 60% of the Archean rocks exposed in the Bathurst Block (Thompson, 1997). The northern parts of the Bathurst Block consist mainly of volcanic rocks, granite to granodiorite plutons, and a heterogeneous gneiss containing remnants of the Yellowknife Supergroup succession (Gebert, 1993). The southern portion of the Block has been divided into two terrains: the Bathurst Terrain, consisting predominantly of sedimentary rocks and their migmatized equivalents, and the Ellice River Terrain, made up predominantly of pink gneiss, migmatite, and granitoids (Gebert, 1990).

### ***2.3. Hope Bay Volcanic Belt***

Within the northern portion of the Bathurst Block lies the Hope Bay volcanic belt, a 90 km-long by 15 to 20 km-wide north-trending greenstone belt (Figure 1.2). The Hope Bay volcanic belt represents a package of Archean supracrustal rocks considered to be more similar to Yellowknife type volcanic belts of the western Slave structural province than the Hackett river type belts of the eastern Slave (Bevier and Gebert, 1991; Gebert, 1993; Clark, 1996). The geology of the Hope Bay volcanic belt was first outlined by Fraser (1964) as part of a government sponsored mapping project. The geology of the Hope Bay belt has since been described in detail by Gebert (1989a,b, 1990a,b, 1992,

1993), LeClair (1990a,b, 1991, 1992), and Clark (1996). It has also been described in numerous unpublished BHP company reports, the most comprehensive being the “Hope Bay Project – Exploration Overview, 1999”. Thompson (1996, 1997) also described the geology of the granitoid rocks that border the belt. U-Pb zircon ages for most of the major rock types in the belt have been determined by Bevier and Gebert (1991) and Hebel (1999). A simplified stratigraphic column and deformational history for the Hope Bay volcanic belt has been constructed in Figure 2.1.

The Hope Bay volcanic belt is made up of 70% mafic volcanic rocks with interfingered intermediate-to-felsic igneous rocks, and sedimentary rocks (Gebert, 1993). The entire Archean assemblage has experienced regional metamorphism to lower greenschist facies. Only a narrow zone, immediately adjacent to the granitoid rocks that mark the eastern limit of the belt, reached amphibolite facies (Thompson, 1997). It should be noted that in the following discussion the prefix “meta” has been dropped when describing the Archean lithological assemblage even though all of these rocks have been metamorphosed.

Pillowed tholeiitic basalts are the most common mafic rocks in the belt (Plate 2.1a), however basaltic-andesites and iron-rich tholeiites are also present. Along the medial axis of the belt the pillowed basalts are commonly variolitic (Gebert, 1990a). Where primary textures are preserved, massive mafic flows can be seen grading into pillowed flow tops, which in turn give way to thin, discontinuous flow top breccias. A thin layer of oxide-facies iron formation commonly caps the flow top breccias, filling in depressions (Gebert, 1993). The entire suite of mafic volcanic rocks in the Hope Bay

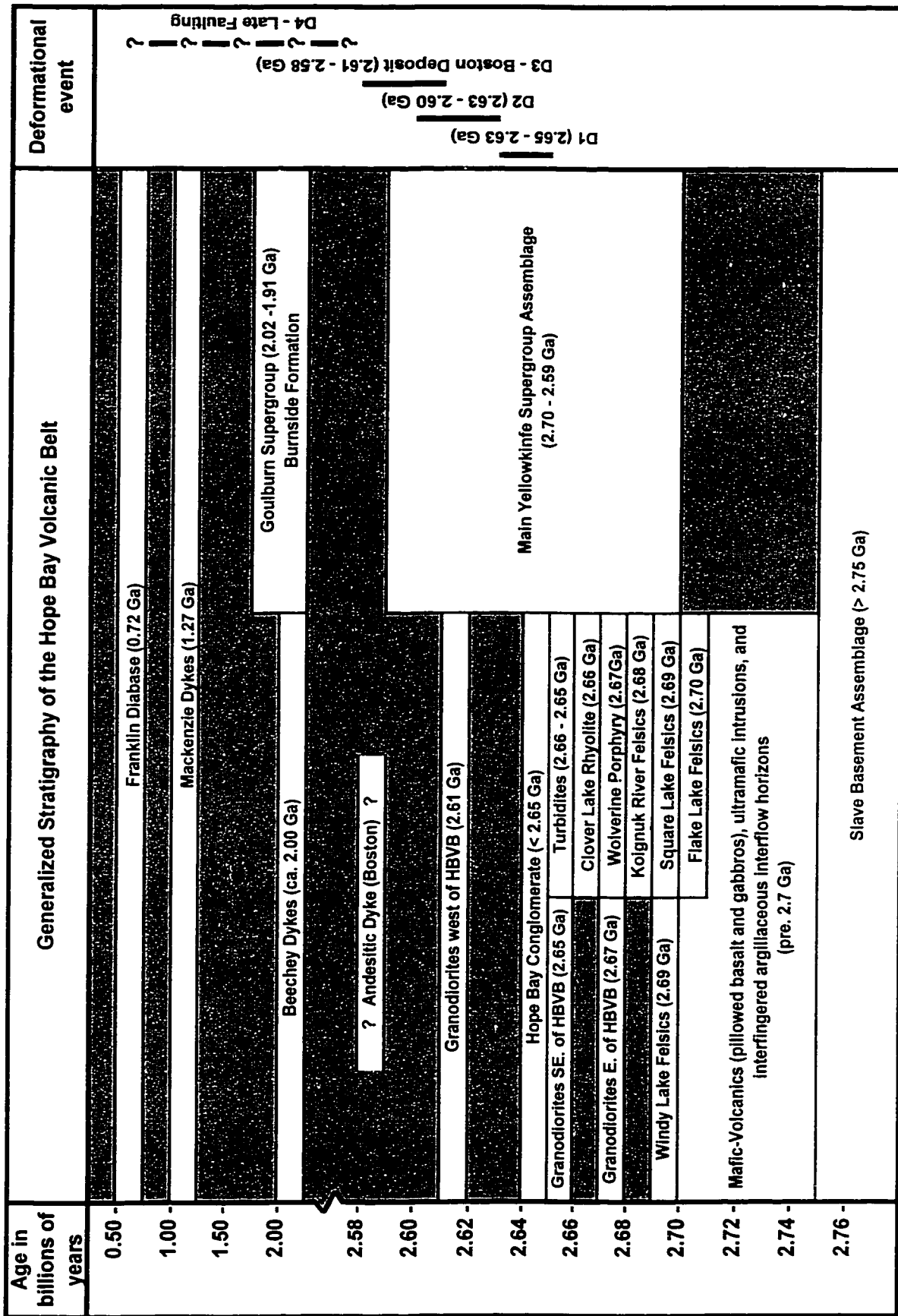


**Figure 2.3.** Generalized stratigraphy and deformational history of the Hope Bay volcanic belt (HBVB). Constructed using information in the Hope Bay Project - Exploration Overview, 1999, and Hebel, 1999.

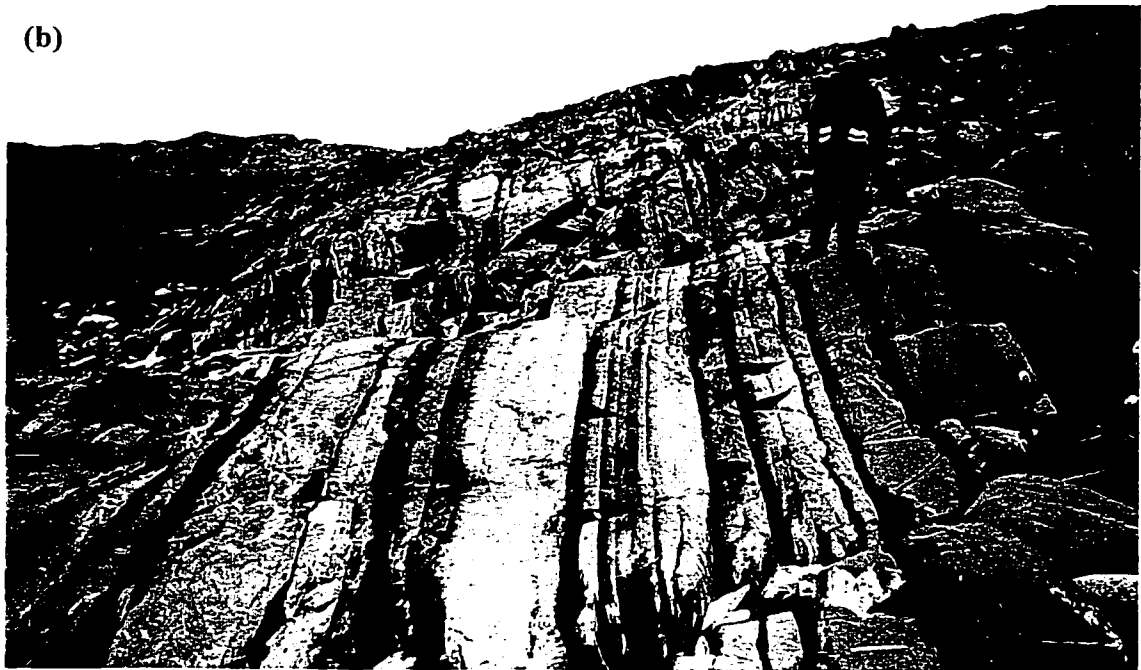
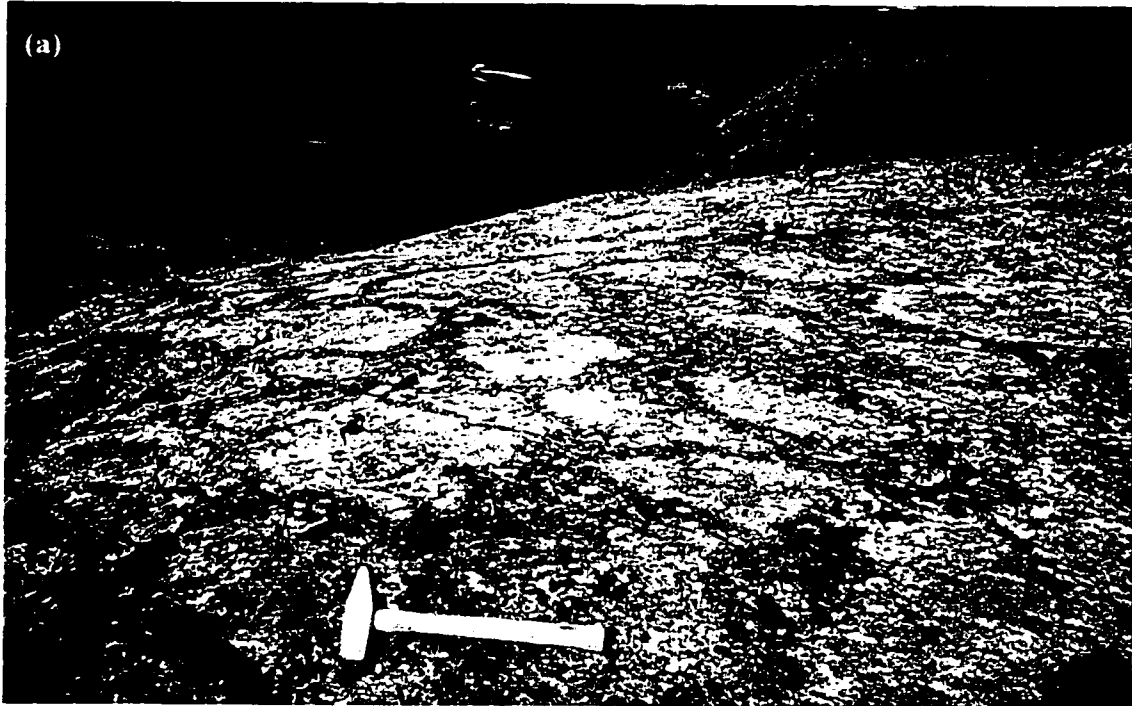


**Plate 2.1.** (a) mafic volcanic rocks approximately 33 kilometers north of the Boston deposit, note the dark weathering pillow selvages: (b) turbiditic sediments in the Hope Bay volcanic belt (photographs published with permission from the Hope Bay joint venture).

Volcanic belt appears to belong to a single pre-2.7 Ga event that has been cut locally by ultramafic intrusions that form sills up to 200 metres thick (BHP internal report, 1999).

Rocks of intermediate composition occur throughout the Hope Bay volcanic belt, although they are more common in the southern portions of the belt. Intermediate rocks typically occur as fragmentals, such as tuffs and lapilli tuffs, although flows have also been observed (Gebert, 1993). Five major suites of felsic volcanic rocks (Figure 1.2) occur in the belt, all of which were formed between 2716 and 2663 Ma (Hebel, 1999). These felsic units include the Windy Lake felsic suite (2686  $\pm$ 3.3/-1.9 Ma), the western Koignuk River felsic suite (2677  $\pm$ 3/-1 Ma), the Wolverine Porphyry (2699  $\pm$ 6.1/-3.7 Ma), the Square Lake felsic suite (2690  $\pm$ 1.4/-1.2 Ma), and the Flake Lake felsic suite (2716  $\pm$ 4.3/-3.4 Ma). Of these, only the Wolverine Porphyry, located in the northern part of the belt, is an intrusive unit, whereas the other four units are made up of fragmental extrusive rocks.

Sedimentary rocks overlie and are interbedded with both mafic and felsic volcanic rocks throughout the Hope Bay volcanic belt (Gebert, 1993). In the northern portions of the belt, coarse-grained conglomerates, wackes, siltstones, and mudstones are common, and have been reported forming successions up to 500 metres thick (Plate 2.1b). In the southern portion of the belt more thinly bedded siltstones and mudstones occur as part of a distal turbidite sequence (Gebert, 1993).

Locally, graphite-rich, argillaceous interflow horizons occur within felsic or mafic volcanic sequences, forming irregular lenses within the volcanic pile (Clark, 1996; Gebert, 1993). Felsic volcanic rocks have also been observed forming thin layers within successions of sedimentary rocks. One of the felsic layers, the Clover Lake rhyolite, has

been dated at  $2663 \pm 6/-5$  Ma (Hebel, 1999). This date suggests that these sediments formed at the same time as typical Slave turbidites deposited throughout the craton at 2.6 Ga.

A conglomeratic unit, containing clasts of rounded granitoid and supracrustal rock, extends for over 12 km in the northern part of the belt. In addition to granitoid clasts, the conglomerate contains clasts of all belt lithologies including rounded clasts of vein quartz (Gebert, 1993). This conglomerate, called the Hope Bay Formation, represents the youngest Archean sequence in the belt having a maximum age of  $2648 \pm 2.8/-2.8$  Ma as defined by the U-Pb age of detrital zircons (Hebel, 1999).

The Hope Bay volcanic belt is bound to the east by a series of granodiorites, tonalites, and gabbros, which separate it from a similar volcanic belt 50 kilometres to the east, the Elu Inlet volcanic belt. Locally enriched in sodium, some of these rocks appear to be trondhjemitic in composition. A granodiorite included within this suite has a U-Pb zircon age of  $2672 \pm 4/-1$  Ma (Bevier and Gebert, 1991).

The eastern margin of the Hope Bay volcanic belt appears to have been consumed by the adjacent plutonic suite. A narrow strip of amphibolite facies volcanic rocks occurs within the intrusive terrain approximately half way between the Hope Bay volcanic belt and the Elu Inlet volcanic belt. The presence of these volcanic rocks suggests that the approximately 2672 Ma plutonic suite intruded the core of a much larger volcanic terrain, dividing it into two distinct volcanic belts (Gebert, 1993).

A heterogeneous gneissic terrain, possibly turbiditic in nature, and several granitoid intrusions define the southeastern margin of the belt. The intrusive rocks have a

U-Pb zircon age of  $2650 \pm 3$  Ma, and U-Pb titanite analysis indicates a  $2589 \pm 2$  Ma age for metamorphism of the gneissic rocks (Hebel, 1999).

To the west, the Hope Bay volcanic belt is bound by granodioritic to granitic rocks with a U-Pb zircon age of  $2608 \pm 5$  Ma (Bevier and Gebert, 1991). These rocks contain xenoliths of foliated mafic volcanic rocks and provide a minimum age for the peak of regional metamorphism in the Hope Bay volcanic belt (Bevier and Gebert, 1991).

Faulted contacts are common along the northwestern border of the Hope Bay volcanic belt. Boundary faults are intensely hematized. Hematization of plutonic rocks along the belt margins is also common and may be the result of Proterozoic weathering (Gebert, 1993).

Along the Arctic coast the Aphebian Burnside Formation of the Goulburn Supergroup (2.02 to 1.91 Ga) unconformably overlies the Archean basement (Gebert, 1993). This formation is made up of red sandstones, pebbly sandstones, and quartz-pebble conglomerates of fluvial origin (Gebert, 1993). Granitoid rocks beneath this Proterozoic cover are bright red as a result of weathering before the deposition of the sedimentary cover.

Three swarms of post-Archean diabase dykes have intruded into the Hope Bay area: the ca. 2000 Ma Beechey dykes, the  $1267 \pm 2$  Ma Mackenzie dykes, and the  $723 \pm 4$  Ma Franklin Diabase. Along the Arctic coast the Franklin Diabase intruded near the unconformity between Archean basement and Proterozoic cover to form sill-like sheets. Further south, the Franklin Diabase forms dipping sheets. The Franklin magma also erupted as volcanic flows high in the Proterozoic cover in the northern portion of the belt (Gebert, 1993).

The entire region has experienced several episodes of glaciation, the last ending around 9000 years ago. Surficial deposits consist of glacial till, glaciomarine sediments, glaciofluvial deposits, lacustrine deposits, and alluvial deposits (Gebert, 1993).

### ***2.3.1. Hope Bay Volcanic Belt - Structural Geology***

The Hope Bay volcanic belt, like most Archean greenstone belts, is structurally complex and a detailed structural study of the Hope Bay volcanic belt has not yet been conducted. At present the only structural information available is from small-scale studies conducted by BHP geologists on individual gold showings throughout the belt. The following discussion is based largely on observations that were made by these geologists and later summarised in the “Hope Bay Project – Exploration Overview, 1999”.

Archean greenstone belts are typically defined as combinations of rocks that formed in different tectonic environments, and which later became juxtaposed during tectonic thrusting and imbrication (Sylvester et al., 1997). The different lithological assemblages that make up the Hope Bay volcanic belt tend to form narrow strips that extend for several kilometres parallel to the strike of the belt. The contacts between these units are generally straight even if the rocks themselves are deformed. For this reason, contacts between different lithological assemblages in the Hope Bay volcanic belt have been treated as structural unless proven to be otherwise.

Several episodes of deformation have affected the Hope Bay volcanic belt since it formed (Figure 2.1). The first phase occurred sometime following the deposition of turbidites ca 2.66 Ga, but before the peak of regional metamorphism and the onset of



regional plutonism at 2.63 Ga in the Slave Structural Province (Davis and Bleeker, 1997). This early stage of deformation (D1) did not produce a penetrative fabric in the belt and its effects are therefore hard to recognise. In other Archean greenstone belts this first stage of deformation was responsible for the formation of large recumbent folds, nappes, and the thrust stacking of the stratigraphy (Kusky and Vearncombe, 1997). It is entirely possible that the D1 phase of deformation had similar control over the distribution of rocks throughout the Hope Bay greenstone belt.

The second episode of deformation (D2) corresponds with the peak of regional metamorphism in the Hope Bay greenstone belt and the peak of compressional deformation in the Slave Structural Province, between 2.63 to 2.60 Ma (van Breemen et al., 1992; Relf, 1992; Davis et al., 1994). Compressional deformation resulted in flattening of rock units, tight folding, and the development of a regionally extensive generally north-trending and sub-vertically dipping foliation that appears to be parallel to the edges of the belt (Gebert, 1993). Pillowed basalt selvages throughout the belt were flattened with their long axes oriented parallel to foliation. In the sedimentary rocks, compression resulted in the development of a penetrative foliation oriented parallel to bedding (Gebert, 1993). A group of granitic rocks to the west of the Hope Bay volcanic belt with a U-Pb zircon age of 2.61 Ga contain inclusions of strongly foliated volcanic rock (Bevier and Gebert, 1991). The granitic suite also appears to have been folded by subsequent episodes of deformation. These rocks must therefore have been emplaced into the volcanic assemblage shortly after the peak of regional metamorphism but before the onset of the next period of deformation.

The third episode of deformation (D3) is associated with retrograde metamorphism that accompanied the emplacement of granitic plutons to the west of the Hope Bay volcanic belt between 2.61 to 2.58 Ga (Padgham and Fyson, 1992; Bleeker and Villeneuve, 1995). During this time there was a shift from pure compressive deformation to oblique compression and regional shearing. Deformation is marked locally by the development of crenulation cleavage and regionally by the development of belt scale, northerly trending folds (Gebert, 1993). In the vicinity of shear zones, foliation that developed in response to shearing is the most strongly developed fabric and overprints the more regionally extensive compression related fabric. However, both fabrics strike roughly north-south and dip subvertically, and in many cases it is difficult to determine whether the observed fabric was the result of localised shearing or belt wide compression. Gold mineralization within the Hope Bay volcanic belt post-dates regional greenschist facies metamorphism and was most likely associated with shearing that developed during D3 deformation.

Brittle faulting (D4) followed late shearing in the Hope Bay volcanic belt. Some of the northwest and north-northwest trending valleys and lakes that occur throughout the belt have been attributed to late faulting. However the nature of these faults is poorly understood due to the lack of marker units that can be used to determine sense of motion. Several deflections occur along the borders of the Hope Bay volcanic belt, some of which appear to be related to this late faulting event (Gebert, 1993). All lithologies including the auriferous veining associated with lode-gold mineralization in the Boston deposit have been subjected to various amounts of offset by these late faults.

### ***2.3.2. Hope Bay Volcanic - Belt Exploration History***

The Hope Bay volcanic belt was first mapped in 1962 by the Geological Survey of Canada as part of a 1:506 880 scale reconnaissance mapping project called “Operation Bathurst”. During the sixties and seventies a number of gold and silver showings were discovered in the belt by Roberts Mining Company, Radiore Uranium Mines, Hope Bay Mining Company, and Perry River Nickel Mines. A small, high-grade silver mine was operated by Hope Bay Mining Company in the northern portion of the Belt during the summers of 1973 and 1974, with a total production in excess of 100 000 ounces of silver.

Between 1977 and 1983, Noranda Ltd. conducted a base-metal exploration program over the entire belt. As part of this exploration, Noranda Ltd. flew 2809 line kilometres of airborne input EM and magnetic surveys. This was followed by geological mapping and ground magnetic/HLEM surveys over anomalies. In 1983 several holes were drilled to test the best EM anomalies, but no areas of economic mineralization were discovered.

In 1987, Abermin Corporation restaked all the known gold showings in the belt. In 1988 Abermin conducted several traverses and staked the Spyder claims over a large carbonate-altered shear zone in the southern portion of the belt. This shear zone was later restaked by the Broken Hill Proprietary Company Limited of Canada (BHP) as part of the Boston claim group in May of 1991.

In 1988, BHP began ground exploration in the Hope Bay volcanic belt and commenced drilling on the Boston property in 1992. From 1992 to 1998, the company completed several consecutive diamond-drilling programs and in 1996 and 1997 a

decline was driven between two of the three main mineralized zones at Boston to a depth of 200 metres, allowing for underground drilling and bulk sampling.

In 1999, BHP sold all of its interests in the Hope Bay volcanic belt to a fifty-fifty joint venture between Miramar Mining Corporation and Cambiex Exploration Incorporated. At present, diamond drilling and property evaluation programs are being conducted over several claim groups. A detailed chronology of all exploration activity in the Hope Bay volcanic belt prior to 1999 can be found in the “Hope Bay Project – Exploration Overview, 1999”.

### **3. Deposit Geology**

#### **3.1. The Boston Lode-Gold Deposit**

The Boston lode-gold deposit is located in the southern portion of the Hope Bay volcanic belt (Figure 1.2), approximately 700 km northeast of Yellowknife and 170 km southwest of Cambridge Bay (NTS map sheet 76O/9). The Boston deposit represents the first major quartz-carbonate-vein lode-gold deposit to be discovered in the Hope Bay volcanic belt since it was initially mapped by the Geological Survey of Canada in 1962. The veining, mineralization, and alteration associated with the deposit appear to be typical of volcanic-hosted, lode gold deposits throughout the Canadian Shield. However, Boston is spatially far removed from any of these historic centers and aside from a few less well-understood gold occurrences to the north, appears to be isolated. Outcrop is scarce in the Boston area and as a result the following discussion relies heavily on the

author's observations made while underground at Boston and on the petrographic and geochemical examination of surface and underground drill core. The observations of numerous BHP geologists, summarized in the "Hope Bay Project – Exploration Overview, 1999", were also taken into account in the following discussion.

### ***3.1.1. Structural Setting***

The Boston lode-gold deposit occurs within a major north-south trending fault zone, called the Boston fault zone (Figure 3.1). The Boston fault zone is part of a larger north-south-trending structure, the Hope Bay fault, which runs down the center of the Hope Bay Volcanic Belt. The Boston fault zone also appears to coincide with the fold axis of what has been interpreted to be a large anticline. This anticline folds the package of metasedimentary and metavolcanic rocks that host the Boston deposit.

The structural setting of the Boston area is poorly understood. Strong shearing and hydrothermal alteration in the vicinity of the Boston fault zone has obscured nearly all of the relationships between different lithological units. Most of the evidence suggesting the presence of an anticline in this area comes from way-up indicators within turbiditic sediments and pillow basalts, and the repetition of gabbroic units on either side of the Boston fault. Lithological contacts in other parts of the Hope Bay volcanic belt are, for the most part, in fault contact. Thus, it is likely that the lithological units that host the Boston deposit are also in structural rather than stratigraphic contact. The Boston fault may simply bring together isolated blocks of rock that happen to young in opposite directions.

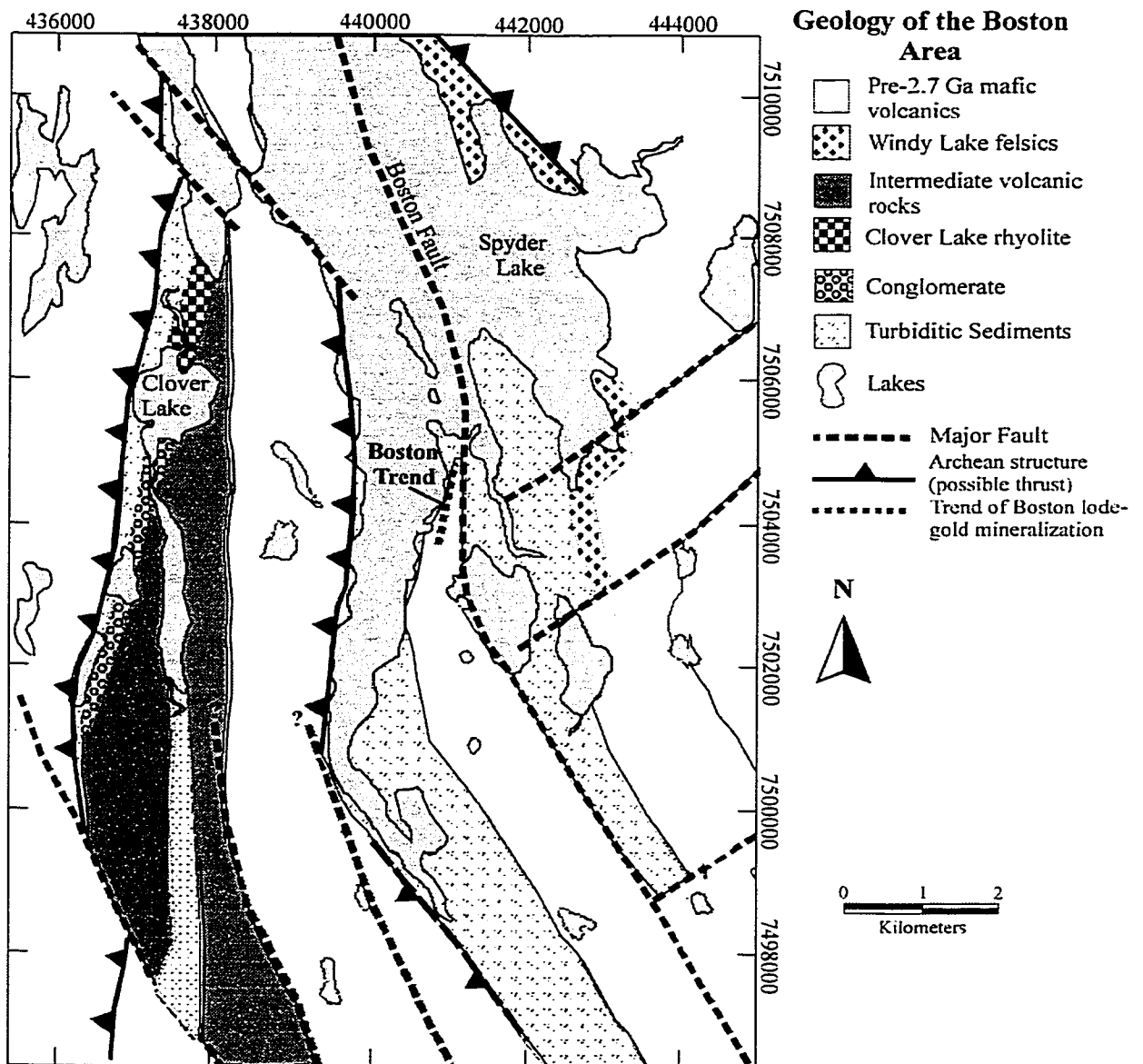


**Figure 3.1.** The geology of the Boston area; modified from the Hope Bay Project - Exploration Overview, 1999 (published with permission from the Hope Bay joint venture).

The rocks that host the Boston deposit were metamorphosed to lower-greenschist facies prior to gold mineralization, hydrothermal alteration, and deformation. Individual mineralized zones occur along the contacts between alternating packages of greenschist facies tholeiitic basalt, gabbro, and sedimentary rocks. The interlayering of ductile sedimentary rocks with more competent mafic-volcanic rocks is an important control on gold mineralization at Boston, with the number of auriferous veins increasing towards the contact between rheologically distinct units.

A major belt-scale flexure occurs in the vicinity of the Boston deposit. This flexure deflects all structures in the southern portion of the Hope Bay volcanic belt and may have created a zone of dilatancy in the Boston area. Hydrothermal fluid flow may have been focused in this area as a result. However, the true nature and origin of this flexure is poorly understood.

Two foliation fabrics occur in association with the Boston deposit. The dominant fabric (S1) has an orientation of  $022^{\circ}/86^{\circ}\text{E}$ . This foliation is parallel to lithological contacts and most likely represents the regional compression-related fabric (D2) that is present throughout the entire Hope Bay volcanic belt. A second fabric (S2), with an orientation of  $052^{\circ}/78^{\circ}\text{E}$ , probably developed in response to localized shearing that accompanied D3 deformation and is most strongly developed in the vicinity of the Boston fault zone. The intersection of these two fabrics defines a strong lineation, trending approximately  $200^{\circ}$  and plunging  $50^{\circ}$  to  $70^{\circ}$  to the south. Mineralized veining within the Boston fault zone appears to have formed parallel to the well-developed intersection lineation. The veins were then folded into sigmoidal shapes and rotated into the Boston fault zone by subsequent movement along the S2 fabric.

The Boston deposit has been affected by at least three generations of post-mineralization faulting (D4). Thrust faults with an orientation of approximately 195°/75°W have been identified that may displace blocks up to 40 metres (hanging wall to the west). Veining is commonly dragged into these faults and they are often associated with a narrow zone of fault gouge.

The second fault set to affect the Boston area has an orientation of approximately 090°/35°S. Veins that crosscut these faults are also dragged into them, but the amount of displacement does not appear to be as great as in the first fault set (<30 cm hanging wall to the west).

A final fault set with an orientation of approximately 070°/87°SE can be seen cutting all veins and lithologies. Movement appears to be dextral strike-slip with an associated displacement of approximately 7-10 metres.

### ***3.1.2. Host Lithologies***

The Boston deposit occurs within a deformed package of igneous and sedimentary rocks centered on the Boston fault zone. In the following discussion, igneous and sedimentary terminology is used when describing the various lithologies in the Boston area. All lithologies were metamorphosed to greenschist facies prior to lode-gold mineralization. For simplicity, in the text the prefix “meta” has been dropped except where the distinction between metamorphic and hydrothermal alteration is necessary.

Mafic Volcanic Rocks: Mafic volcanic rocks are the most common lithology in the Boston area. Massive or pillowed basaltic lava flows are thought to underlie

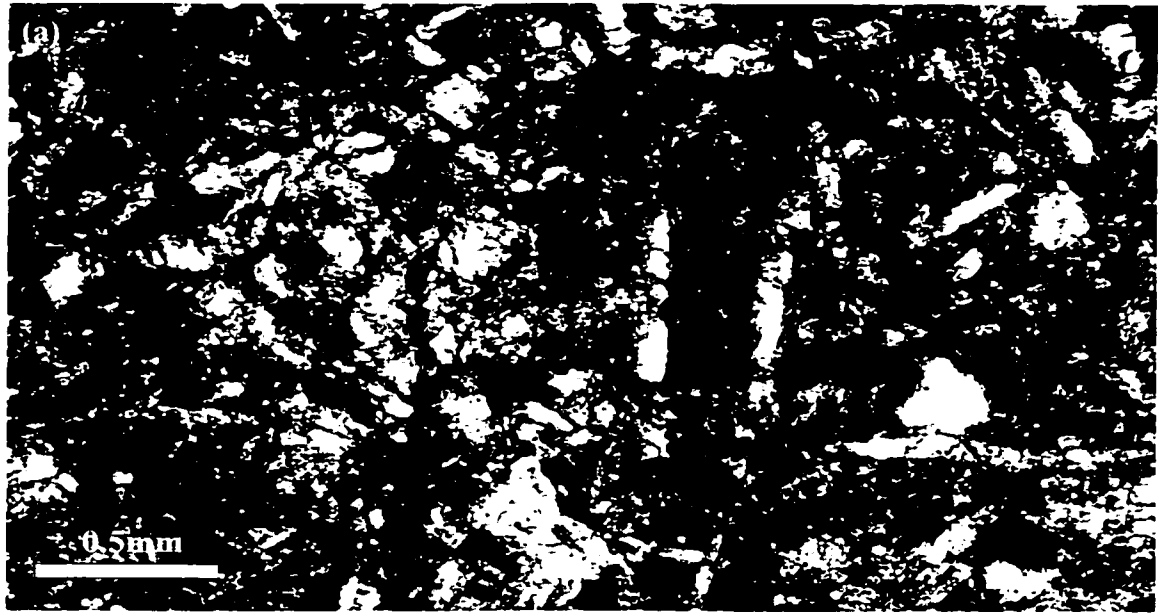


approximately 70% of the Boston claims and make up approximately 90% of the outcrop in the area (Clarke, 1996). Locally, volcanic textures and structures such as flow top breccias and varioles are preserved. Compositionally, these rocks range from tholeiitic basalt to basaltic andesite although iron rich tholeiite has also been reported (Locock, 1998a).

The least hydrothermally altered examples of basalt are found outside of the main fault zone and as an isolated wedge of basalt within the fault zone. Basaltic rocks tend to be massive and fine-grained, resembling a dark, forest-green, chloritic phyllite (Plate 3.1b). This rock type is characterized by a typical lower greenschist facies metamorphic mineral assemblage. Original igneous minerals are rarely observed with the possible exception of plagioclase. The Michel-Levy method was used to determine the relative proportions of albite versus anorthite in the plagioclase in several samples of basalt. In all of the samples examined the plagioclase contained more than 50% anorthite. This is in agreement with the type of feldspar typically present in fresh mafic volcanic rocks (McBirney, 1994).

Magnesian chlorite (clinochlore) is the dominant metamorphic mineral in the basaltic rocks, making up over 60% of most samples. Abundant quartz and small amounts of rutile, epidote, and actinolite are also typically present (Plate 3.1a). A significant amount of fine-grained calcite occurs in most samples. In other samples irregular calcite-filled fractures are common (Plate 3.1b).

Gabbro: Discontinuous gabbroic units up to 200 metres thick are common throughout the mafic volcanic package. There has been some debate as to whether the gabbroic units



(b)



0 5 10 cm

**Plate 3.1.** (a) Photomicrograph exposed in transmitted plane polarized light of a typical greenschist facies basalt from the Boston area consisting of 55% clinocllore, 20% plagioclase, 15% calcite, 7% quartz, 3% rutile, and trace pyrite and chalcopyrite. Relict igneous textures are also present in this sample. (b) Sample of basalt from diamond drill core, irregular calcite-filled fractures occur throughout this sample.

represent distinct intrusions or simply the slowly cooled centers of thicker volcanic flows. The gabbroic units have higher concentrations of potassium, rubidium, and barium than the basaltic units, and are often also richer in iron and titanium (Locock, 1998a). It is therefore likely that the gabbroic units represent a distinct lithological assemblage that intruded into the volcanic pile sometime before the onset of metamorphism and deformation in the belt.

Hydrothermally unaltered samples of gabbro tend to be darker grey-green in colour relative to the dark forest-green basalts (Plate 3.2c). Mineralogically the gabbroic units have the same lower greenschist facies mineral assemblage as the basalts, consisting of clinocllore, quartz, rutile, and coarse-grained plagioclase (Plate 3.2a,b). A significant amount of epidote also occurs in some samples.

Ultramafic Picrite (B3 Gabbro): An ultramafic unit of picritic composition also occurs within the volcanic pile (Locock, 1998a). This unit probably intruded as a sill sometime prior to deformation and mineralization in this area. This unit has been called the B3 gabbro due to the occurrence of the B3 zone along its contact with mafic-volcanic rocks within the Boston fault zone.

In hand sample the ultramafic unit is typically medium to fine-grained and has a distinctive bright turquoise-green colour (Plate 3.3b). The picrite has a slightly different mineral assemblage than the basalts and gabbros due to the higher iron and magnesium content of this rock type. Samples of picrite typically consist of ferroan dolomite and ferroan magnesite, quartz, paragonite, muscovite, clinocllore, and rutile (Plate 3.3a).

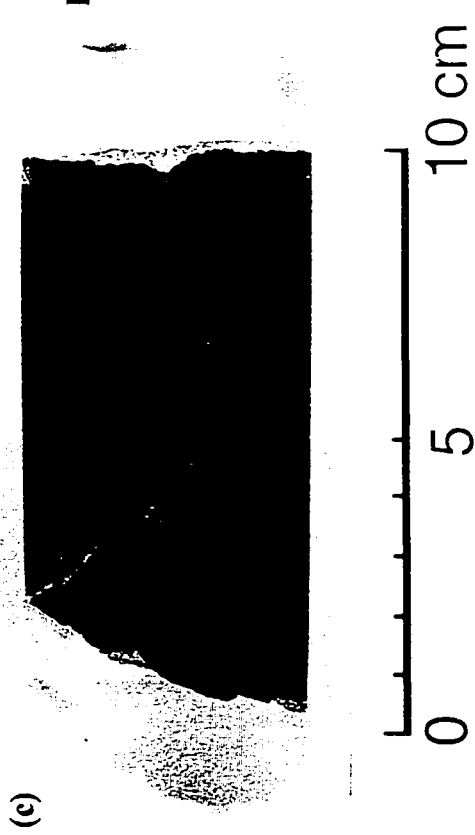
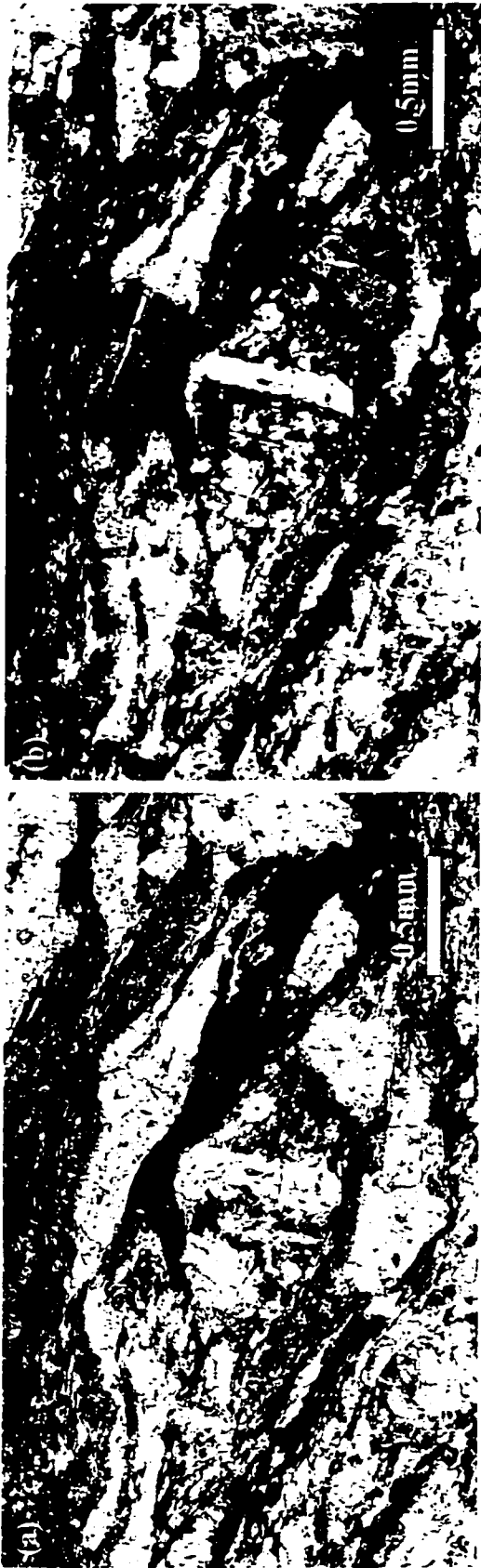
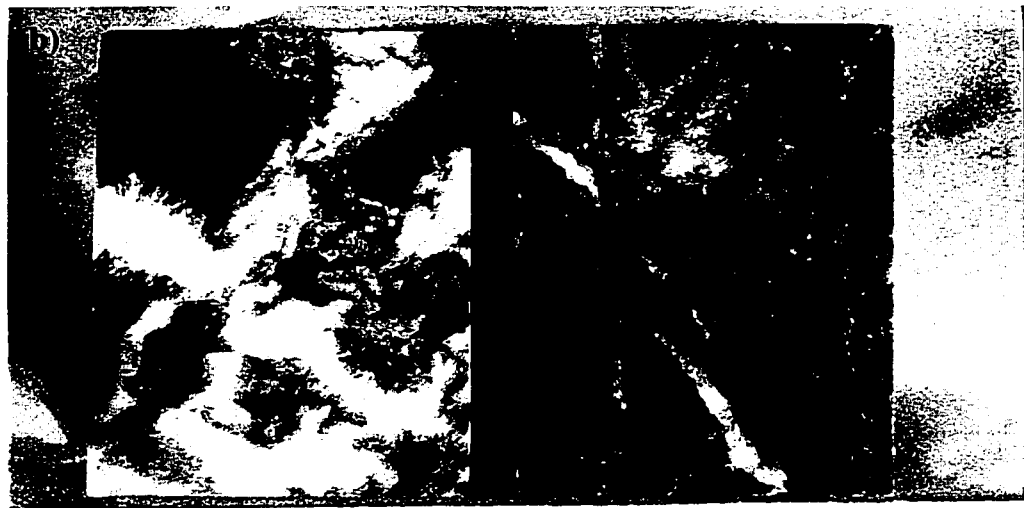
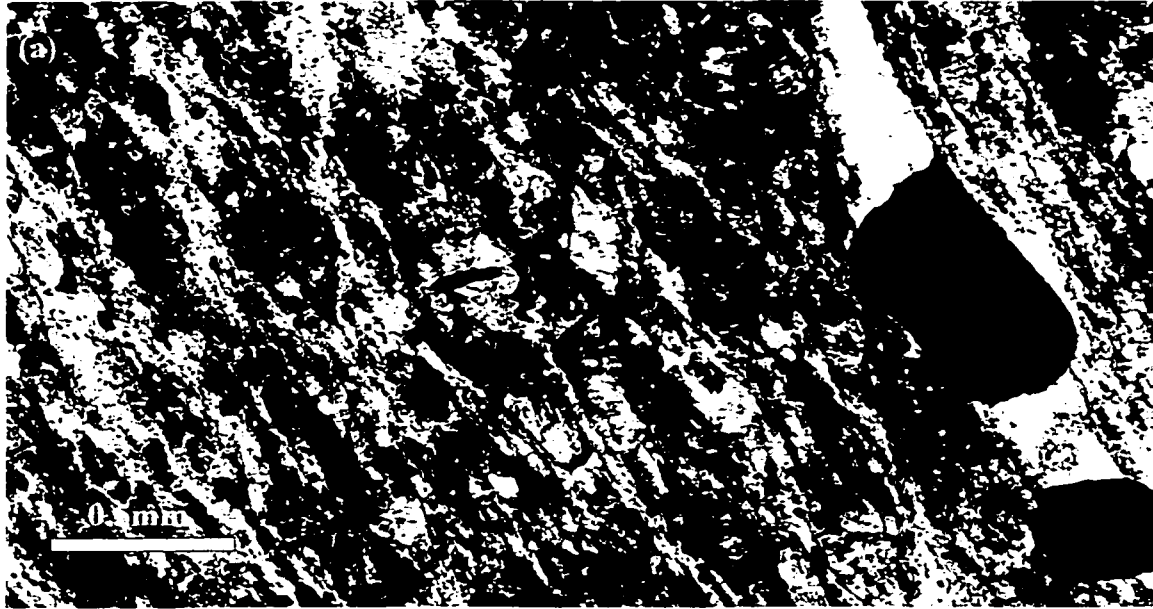


**Plate 3.2.** Photomicrographs (a) exposed in transmitted plane polarized light and (b) under crossed nicols of a foliated gabbro consisting predominantly of dark olive green clinoclase (50%), and coarse grained laths of plagioclase (30%). Calcite (10%), sericite (paragonite, 5%), quartz (3%), rutile (2%), and trace pyrite are also typically present in this rock type; (c) a sample of gabbro from diamond drill core.



0 5 10 cm

**Plate 3.3.** (a) a photomicrograph exposed in transmitted plane polarized light of a well foliated, hydrothermally altered, ultramafic picrite (B3 gabbro) consisting of wispy bands of sericite (paragonite/muscovite) and clinocllore (50%), alternating with grey bands of dolomite (30%), and quartz (12%). Pyrite, arsenopyrite, and chalcopyrite (5%) are also typically present, along with minor amounts of rutile (3%); (b) two samples of the B3 gabbro from diamond drill core; note the distinctive bands of bright green paragonite + sericite alteration.

Sedimentary Rocks: Sedimentary rocks in the Boston area range from massive turbiditic greywackes to fine-grained argillites (Plates 3.4 and 3.5). Unaltered samples of the greywacke are composed of relict quartz and plagioclase grains in a fine-grained matrix of quartz, clinocllore, and muscovite. Minor amounts of paragonite and rutile also occur in most samples (Plate 3.4a,b). Bedding and fining upwards sequences are occasionally preserved in the turbiditic sediments (3.4c,d). Younging directions defined by graded bedding have been used as evidence for an anticline in the Boston area.

Fine-grained argillites occur within both the turbiditic and basaltic units. Argillites are typically dark grey to black in colour and contain interstitial graphite and clots and bands of diagenetic pyrite (Plate 3.5). Pyrite grains are typically associated with inclusions and overgrowths of sphalerite and pyrrhotite (Plate 3.5b). The graphite content of the argillites increases significantly in areas of intense shearing, faulting, and along the sedimentary-volcanic interface. Regional (D2) and shear-related (D3) deformation has also resulted in the development of a crenulation cleavage and tight folding in some samples (Plate 3.6).

Andesitic Dyke: A 0.5 to 3.0-metre wide, beige coloured, fine-grained, andesitic dyke occurs in the vicinity of the Boston deposit (Plate 3.7b). The dyke dips subvertically and runs along the Boston fault zone between the B2 and B3 zones. The dyke is hydrothermally altered in the vicinity of the Boston deposit but is unmineralized. Alteration assemblages consist of quartz, calcite, ferroan dolomite, clinocllore, muscovite, paragonite, and residual Ca-plagioclase (Plate 3.6a). Minor amounts of magnetite also occur in some samples. Fine to medium grained pyrite cubes

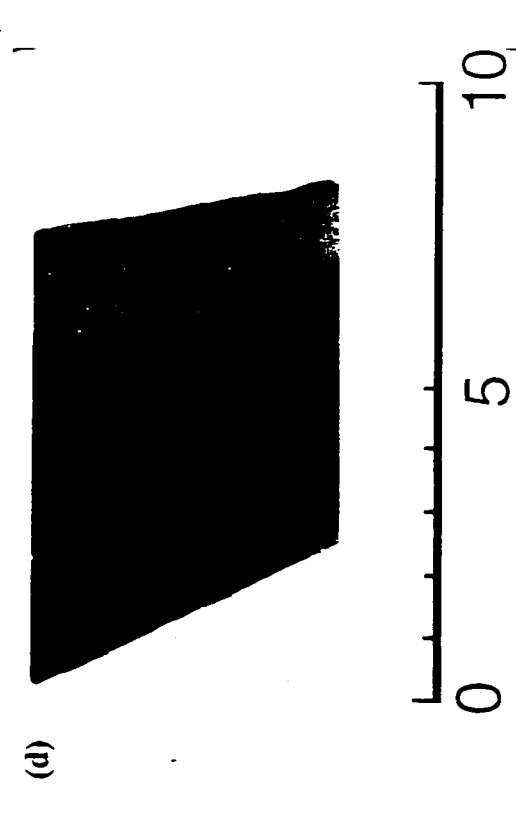


**Plate 3.4.** Photomicrographs (a) exposed in transmitted plane polarized light and (b) under crossed nicols of a massive graywacke consisting of large rounded clasts of quartz (20%) and plagioclase (18%) in a finer grained matrix of sericite (28%), quartz (17%), carbonate (15%), rutile (2%) and trace sulphides. Photomicrograph (c) and diamond drill core sample (d, scale bar in cm) of typical bedded turbiditic sediment consisting of calcite (30%), quartz (24%), graphite (20%), muscovite (12%) clinocllore (8%) and sulphides (pyrite, chalcopyrite, sphalerite, arsenopyrite, and pyrrhotite; 6%).

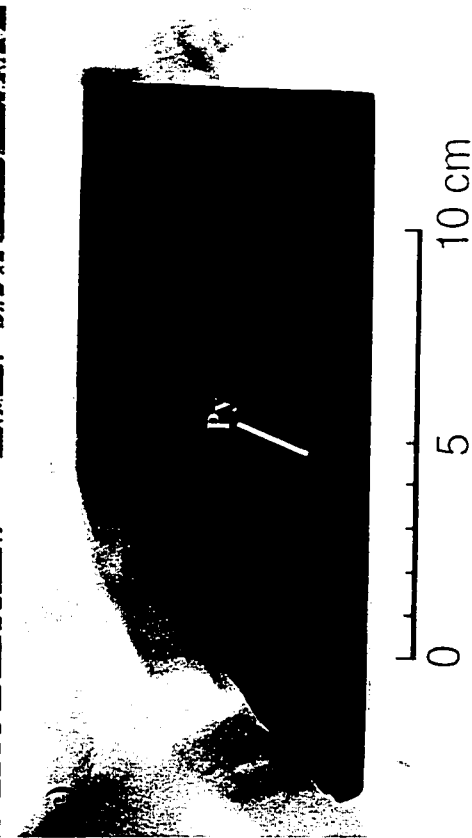
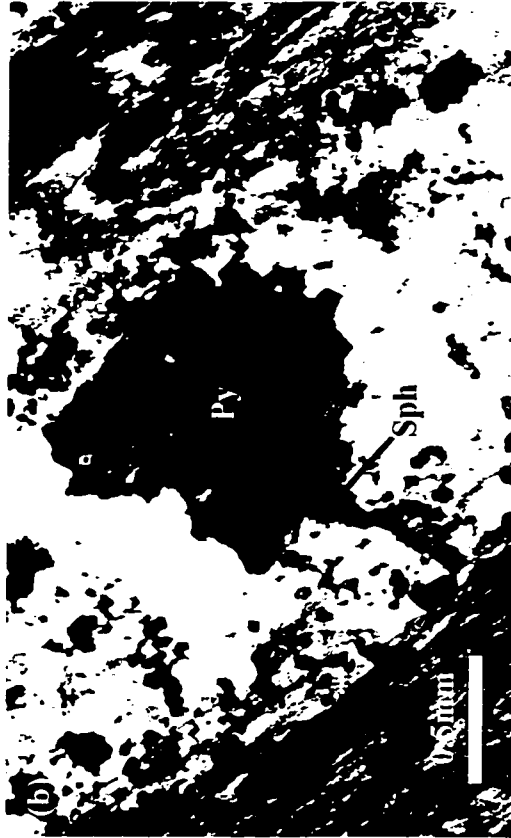


**Plate 3.5.** Photomicrographs (a) and (b) exposed in transmitted plane polarized light and (c) drill core sample of well foliated graphitic argillite consisting of bands of fine grained graphite (50%), and clots and foliation parallel stringers of fine to moderately coarse grained calcite (18%) and quartz (15%). Paragonite (15%) occurs intergrown with graphite. Irregular clots of pyrite (Py), sphalerite (Sph), chalcocopyrite, and pyrrhotite are also common (b and c).



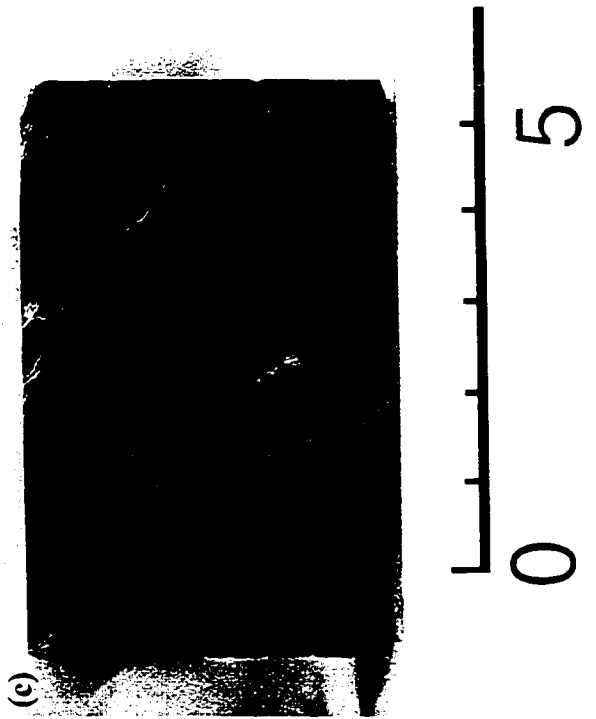


**Plate 3.6.** Strongly folded argillic sediment. Photomicrographs (a) exposed in transmitted plane polarized light; (b) exposed under crossed nicols; and (c) photograph of strongly folded graphitic argillite from diamond drill core (scale in cm).

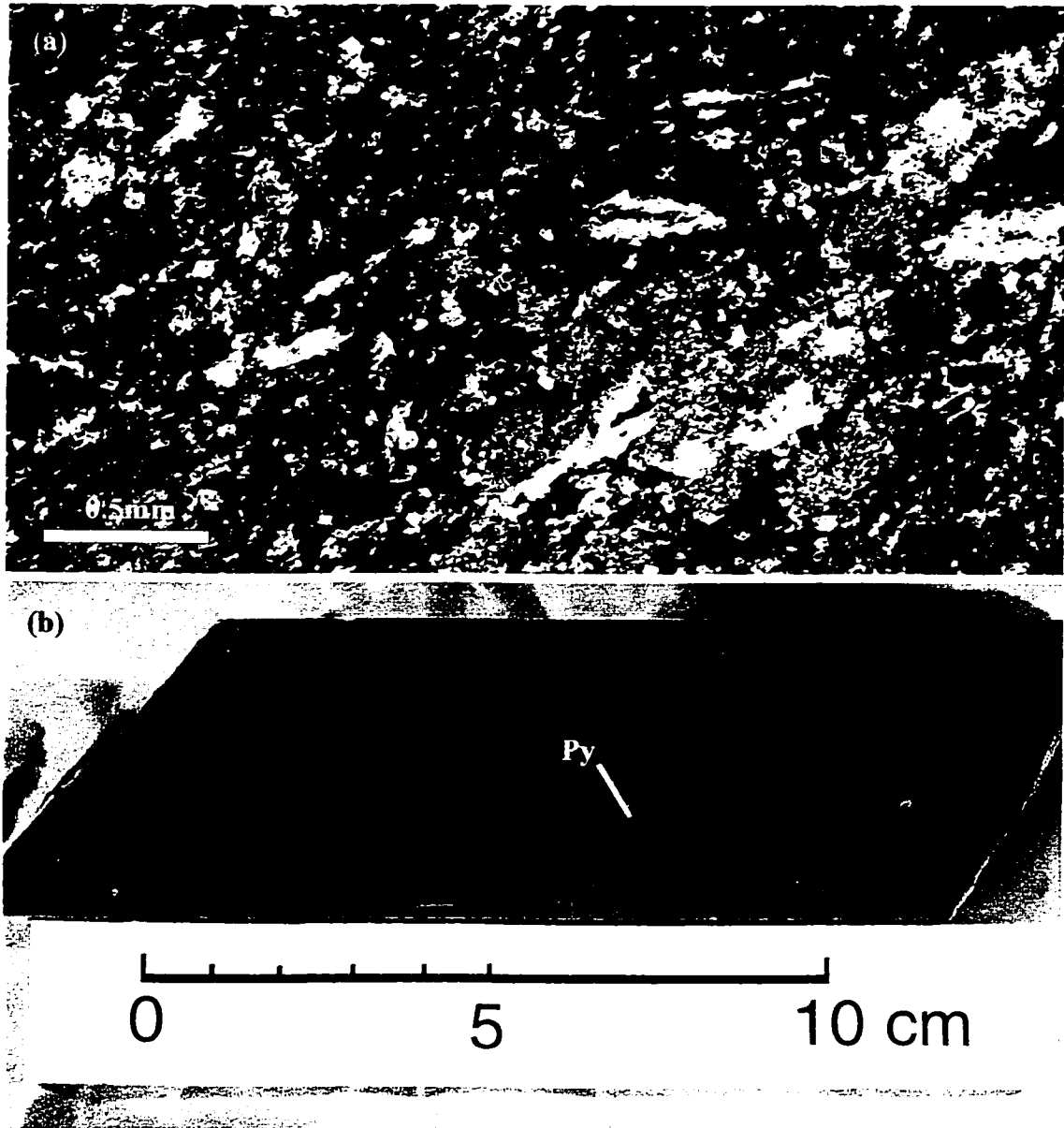


**Plate 3.7.** Hydrothermally altered andesitic dyke from between the B2 and B3 zones. The dyke consists of fine grained carbonate (50%), sericite (muscovite and paragonite) and clinocllore (25%), quartz (15%), and residual plagioclase (5%). Magnetite and coarse pyrite (Py) clots also occur throughout this unit. Photomicrograph (a) exposed under crossed nicols; photograph (b) from diamond drill core; note the presence of irregular pyrite clots in this sample.

occur within the dyke locally (Plate 3.7b).

The dyke appears to post date mineralization and is not as deformed as the surrounding wallrocks or mineralized zones. However, it is hydrothermally altered in the vicinity of the Boston deposit and therefore must have been emplaced before the end of hydrothermal activity in the area. The dyke most likely exploited similar structural weaknesses in the Boston fault zone, as did the hydrothermal fluids. Zircons were separated from the dyke in attempt to date it and thereby constrain the minimum age of mineralization in the Boston area (Locock, 1998b). However, the results were discordant and it was concluded that the zircons were inherited.

### ***3.1.3. Hydrothermal Alteration***

Numerous authors working throughout the world have devoted considerable time and effort to the examination of the wallrock alteration associated with mesothermal lode-gold deposits (Robert and Brown, 1986a; Smith and Kesler, 1985; Kishida and Kerrich, 1987; Phillips and Groves, 1983; Phillips, 1986; Teixeira et al., 1990; Love and Roberts, 1991; Gao and Kwak, 1997). As a result, the thermodynamics and fluid and wallrock chemistry of hydrothermal alteration associated with these deposits is quite well understood. The outcome of this research has been the realization that aside from slight differences in silicate and carbonate mineralogy, and regardless of their age, the hydrothermal alteration associated with lode-gold deposits world wide is quite uniform (Teixeria et al., 1990). These studies have shown that CO<sub>2</sub>, Ca, Na, K, S, B, Cu, As, and Au are typically added to the wallrocks by the hydrothermal fluid and Mg, Fe, Al, and Si are lost to the fluid (Robert and Brown, 1986; Phillips, 1986; Kishida and Kerrich, 1987;

Gao and Kwak, 1997). Petrographically, hydrothermal alteration in the Boston deposit appears to be characterized by similar elemental losses and gains and is described below.

As mentioned previously, all lithologies in the Hope Bay volcanic belt have been affected by regional greenschist facies metamorphism. In the area surrounding the Boston deposit a distinctly zoned hydrothermal alteration mineral assemblage has overprinted the metamorphic mineral assemblage. All lithologies in the vicinity of the Boston deposit have experienced an overall trend to intense carbonation related to the introduction of calcium and significant amounts of CO<sub>2</sub> into the wallrocks from the hydrothermal fluid. A shift from chlorite-dominated to sericite-dominated alteration related to the introduction of sodium and potassium by the hydrothermal fluid is also observed. The effects of hydrothermal alteration can be observed in all of the rock types associated with the Boston deposit but are most obvious in the mafic volcanic and gabbroic rocks directly associated with mineralization in the Boston fault zone. The sequence of hydrothermal alteration described below for mafic volcanic rocks can, therefore, be used as a generalized model for all other rock types in the Boston area.

Mafic Volcanic Rocks: Hydrothermal alteration in the mafic volcanic rocks surrounding the Boston deposit has resulted in a shift from chlorite-dominated rocks to rocks rich in muscovite and paragonite (Plate 3.8a). The proportion of carbonate minerals also increases as the intensity of hydrothermal alteration increases; with a shift from calcite to ferroan dolomite and/or ankerite as the dominant carbonate species. Plagioclase is completely replaced by paragonite and/or muscovite in even weakly altered samples. A

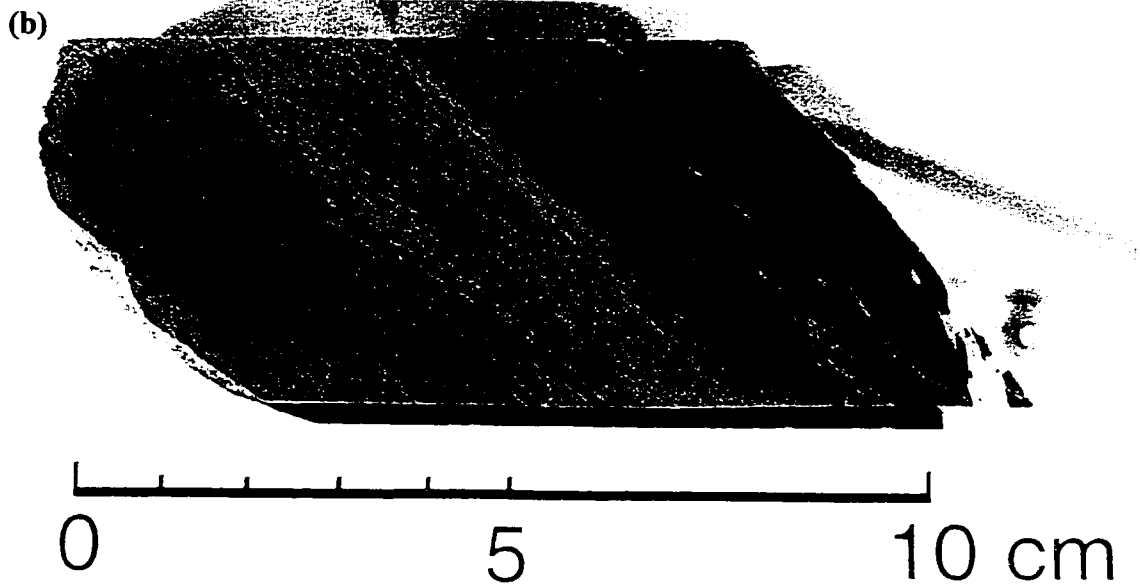
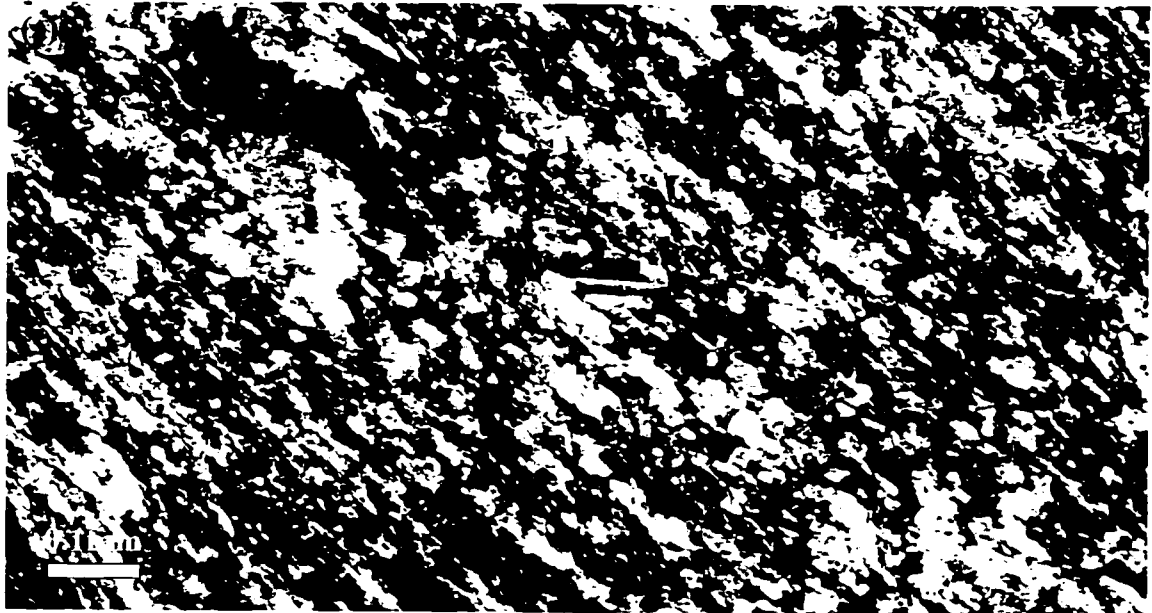


**Plate 3.8.** Basalt that has experienced relatively weak hydrothermal alteration within the Boston fault zone. The sample is well foliated and consists of fine grained calcite (35%), paragonite (25%), clinocllore (18%), plagioclase (15%), quartz (5%) and rutile (2%). Plagioclase laths are oriented roughly parallel to foliation and in most cases have been at least partially replaced by calcite and sericite. (a) Photomicrograph exposed in transmitted plane polarized light and (b) Photograph from diamond drill core.

substantial amount of rutile also occurs in most samples. This new alteration mineral assemblage gives the rock an olive-green to beige colour (Plate 3.8b). Deformation associated with the Boston fault zone has resulted in the development of a strong foliation fabric (S2) in the mafic volcanic rocks. Paragonite, muscovite, chlorite, and rutile tend to be aligned parallel to foliation and define the orientation of this fabric (Plate 3.8a).

Basaltic rocks that have experienced moderate levels of hydrothermal alteration also tend to be strongly deformed and have a banded appearance (Plate 3.9). In addition, all primary igneous textures originally present within the basaltic rocks have been completely obliterated by this stage. The rocks typically consist of millimetre- to centimetre-scale foliation parallel bands of dark grey-brown paragonite, muscovite, chlorite, and rutile that alternate with more massive bands of grey-beige carbonate and quartz (Plate 3.9a,b).

In the areas that have experienced the strongest hydrothermal alteration and deformation in the Boston deposit the rock becomes strongly banded and very dark grey-brown in appearance (Plate 3.10). No remnants of a pre-alteration protolith remain making it difficult to determine rock type in the field. This also makes estimating the exact position of the lithological contacts that host the highest-grade mineralized zones in the Boston deposit difficult. Strongly altered basaltic rocks typically consist of millimetre-scale foliation-parallel bands of paragonite, muscovite, and rutile alternating with centimetre-scale, commonly massive, bands of carbonate and quartz (Plate 3.9a). Dravite is common in the most advanced stages of alteration close to auriferous veins. The presence of dravite indicates that the hydrothermal fluid was slightly acidic and



**Plate 3.9.** Basalt that has experienced moderate levels of hydrothermal alteration and deformation within the Boston fault zone. Moderately altered basalt is generally fine grained and well foliated and consists of mm- to cm-scale wispy bands of paragonite (40%), clinocllore (13%), and rutilite (7%) that alternate with slightly thicker bands of carbonate (22%) and quartz (18%). Trace pyrite, chalcopyrite, and arsenopyrite also occur in most samples. Photomicrographs (a) exposed in transmitted plane polarized light and (b) under crossed nicols; (c) photograph of moderately altered basalt from diamond drill core.



(b)

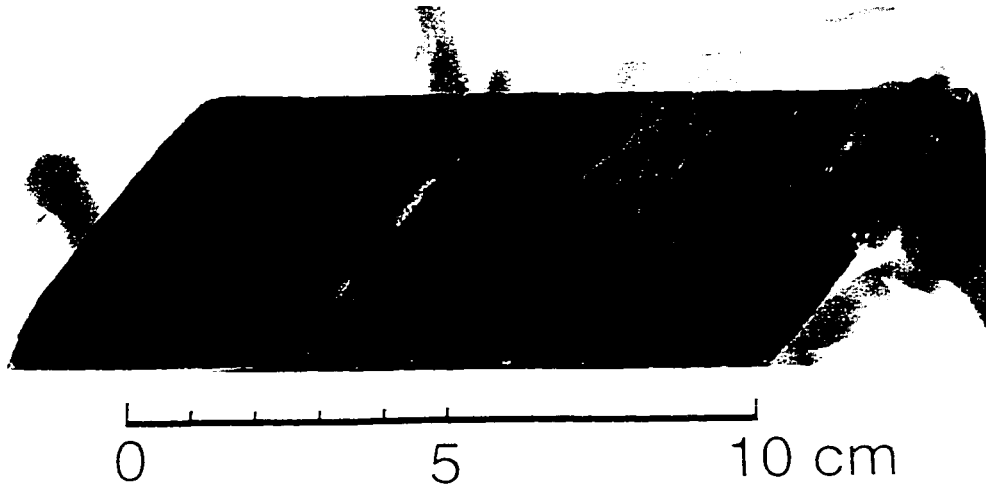


**Plate 3.10.** Basalt that has experienced high levels of hydrothermal alteration and deformation within the Boston fault zone. Millimeter-scale bands of paragonite (50%), clinocllore (13%), and rutile (2%) define a strongly developed foliation in this unit. Deformed bands and lenses of carbonate (20%) and quartz (15%) occur within and between paragonite/clinocllore bands. This sample has retained no primary textures and is difficult to tell apart from strongly deformed gabbros or sediments that also occur within the Boston fault zone. (a) Photomicrograph exposed in transmitted plane polarized light and (b) photograph from diamond drill core.



contained boron and a significant amount of magnesium (London and Manning, 1995). Thicker bands of quartz-carbonate alteration are commonly boudinaged and may contain short quartz-carbonate filled extension related fractures or ladder veins, which are discussed in detail in the next section. In some cases, siderite is also present within very highly altered rocks in the Boston deposit. Minor phlogopite has also been identified in some samples.

The strongly altered rocks adjacent to auriferous quartz-carbonate veins within the Boston fault zone are typically enriched in sulphide minerals. Pyrite, and lesser amounts of arsenopyrite, and chalcopyrite form a halo of sulphide alteration that can extend up to fifteen centimetres into the wallrocks on either side of these veins (Plate 3.11). In some cases sulphide minerals make up over 40% of the wallrock adjacent to mineralized quartz-carbonate veins in the Boston fault zone. A large proportion of the gold resource in the Boston deposit forms as inclusions within, or as fracture fill and thin coatings on the surface of sulphide grains in this halo.

Gabbros: An identical alteration sequence characterized by a shift to more pervasive carbonate- and sericite-rich alteration occurs in gabbroic rocks associated with the Boston deposit as was observed in the basaltic rocks. The two rock types become indistinguishable in both hand sample and thin section in highly altered and deformed samples within the Boston fault zone. In some cases the gabbroic rocks can be distinguished from basaltic rocks by the presence of large quantities of rutile in the form of whitish-pink leucoxene alteration, which gives the rock a speckled appearance. In addition, a higher proportion of arsenopyrite relative to pyrite occurs in the sulphidation



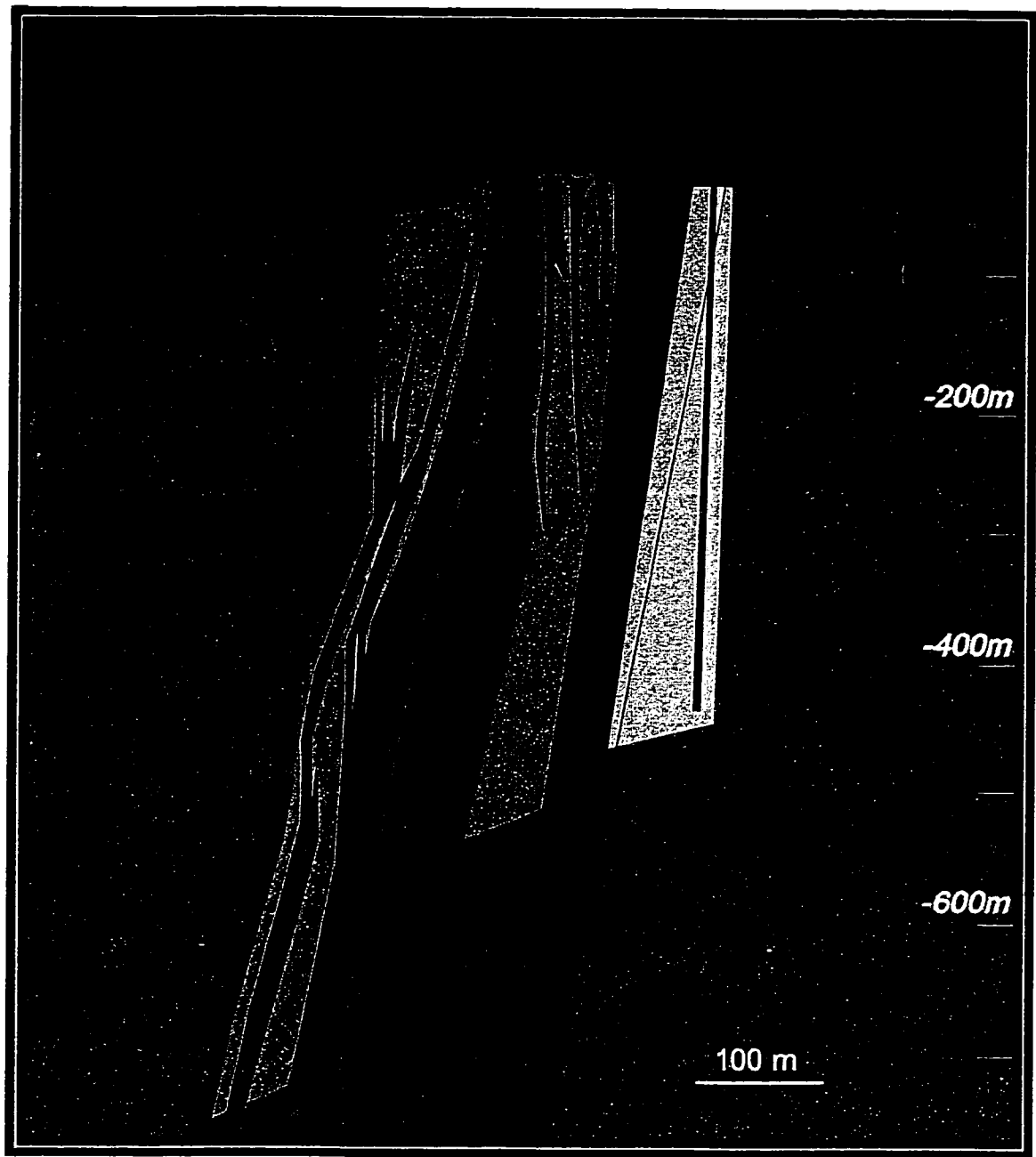
**Plate 3.11.** The sulphidation halo around main stage-quartz carbonate veining in the B2 zone. Note the thick foliation parallel clots of coarse grained, gold-bearing pyrite in the wallrock immediately adjacent to the quartz-carbonate vein (lens cap in photo is approximately 6 cm in diameter).



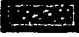






halo around quartz-carbonate veins hosted by gabbroic rocks than is present in the sulphidation halo around basalt-hosted veins.

Sedimentary Rocks: Hydrothermal alteration of the turbiditic sediments and graphitic argillites in the Boston area is also characterized by intense carbonation, sericitization, and deformation. However, the effects of hydrothermal alteration are not as strongly developed in the sedimentary rocks as they are in the mafic and ultramafic igneous rocks in the Boston area. The minerals that make up greywackes and argillites, such as clay and quartz, were originally deposited in a marine environment and as a result are more resistant to further alteration by percolating hydrothermal fluids than the minerals that make up fresh basaltic or gabbroic rocks. As a consequence, the effects of hydrothermal alteration, although still present, are less pronounced in the sedimentary rocks than in the igneous rocks.

#### ***3.1.4. Boston Mineralized Zones***

Gold mineralization in the Boston deposit is restricted to three subparallel zones of auriferous quartz-carbonate veining: the B2, B3, and B4 zones (Figure 3.2). Veining has developed along the contacts between competent mafic rocks and ductile sedimentary units in the Boston fault zone. Vein intensity in each of the mineralized zones increases significantly as the contacts are approached. In fact, most of the differences in the style of veining and grade of mineralization in these three zones stem from differences in the competency of the rocks that host them.



- |   |                    |  |                      |
|---|--------------------|--|----------------------|
|  | B2 Zone            |  | Turbiditic Sediments |
|  | B2 Alteration Halo |  | Mafic Volcanics      |
|  | B3 Zone            |  | Andesitic Dyke       |
|  | B3 Alteration Halo |  |                      |
|  | B4 Zone            |  |                      |
|  | B4 Alteration Halo |  |                      |

**Figure 3.2.** A generalized cross section of the Boston deposit looking north, from the Hope Bay Project - Exploration Overview, 1999 (published with permission from the Hope Bay joint venture).

B2 Zone: The B2 zone has a known strike length of approximately 900 metres and a width of 25 to 50 metres. B2 mineralization occurs within a package of moderate to strongly altered, sheared mafic volcanic rocks at or near the sediment-volcanic contact (Figure 3.2). Veining in the B2 zone consists of quartz-carbonate fissure veins that dip steeply to the west roughly parallel to the sediment-volcanic contact (Plate 3.12). These veins have experienced several episodes of ductile deformation and tension-related fracturing since their formation. As a result, the thickness of mineralized portions of the B2 zone can fluctuate considerably over very short distances. Mineralized veins less than one metre thick to over thirty metres in thickness have been observed underground and in drill core.

A significant proportion of the gold in the B2 zone occurs with pyrite, arsenopyrite, and chalcopyrite (Plate 3.13) in a sulphidation halo that extends up to fifteen centimetres into the wallrocks immediately adjacent to the quartz-carbonate veins (Plate 3.11). Coarse gold and sulphide minerals have also been observed in association with strongly altered wallrock fragments within the quartz-carbonate veins that make up the B2 zone (Plate 3.13e,f). Gold occurring in this form and as free gold within micro- fractures in the B2 veins (Plate 3.13g) is responsible for spectacular, multi-ounce assays characteristic of this zone.

B3 Zone: The B3 zone is situated approximately 10 to 40 metres east of the B2 zone (Figure 3.2), at or near the basalt-gabbro/picrite contact. The B3 zone is approximately parallel to the B2 zone. The B3 zone has a known strike length of 900 metres and an average width of 30 to 50 metres.

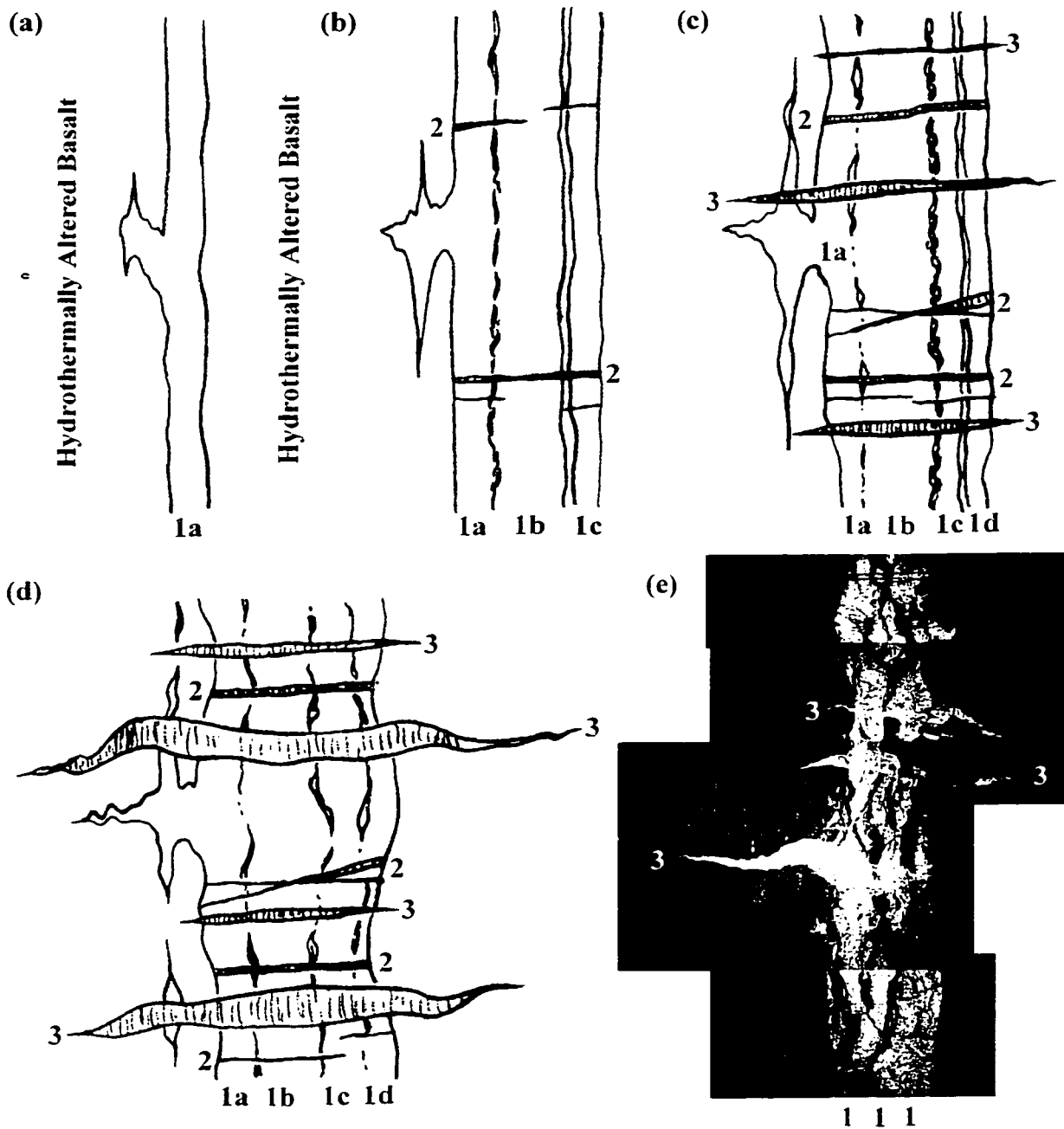


**Plate 3.12.** Sequence of events that led to the development of the main stage quartz-carbonate veins, ladder veins, and flat veins in the Boston deposit (modified after Hodgson, 1989, and Hurst, 1935, for mineralized veining in the Hollinger mine, Timmins, Ontario); (a) several stages of main stage quartz-carbonate vein formation (1a, 1b, 1c, etc) by crack seal processes; (b) ladder veins (2) form within the main stage quartz carbonate veins in response to compression-related deformation directed perpendicular to the walls of the main stage veins; (c) as compression-related deformation continues under brittle conditions flat veins (3) form which crosscut the main stage quartz-carbonate veins; (d) continued deformation results in folding of the flat veins and boudinage of the main stage veins; (e) deformed main stage quartz-carbonate fissure vein and associated flat veins typical of the B2 zone (hammer is approximately 40cm long).

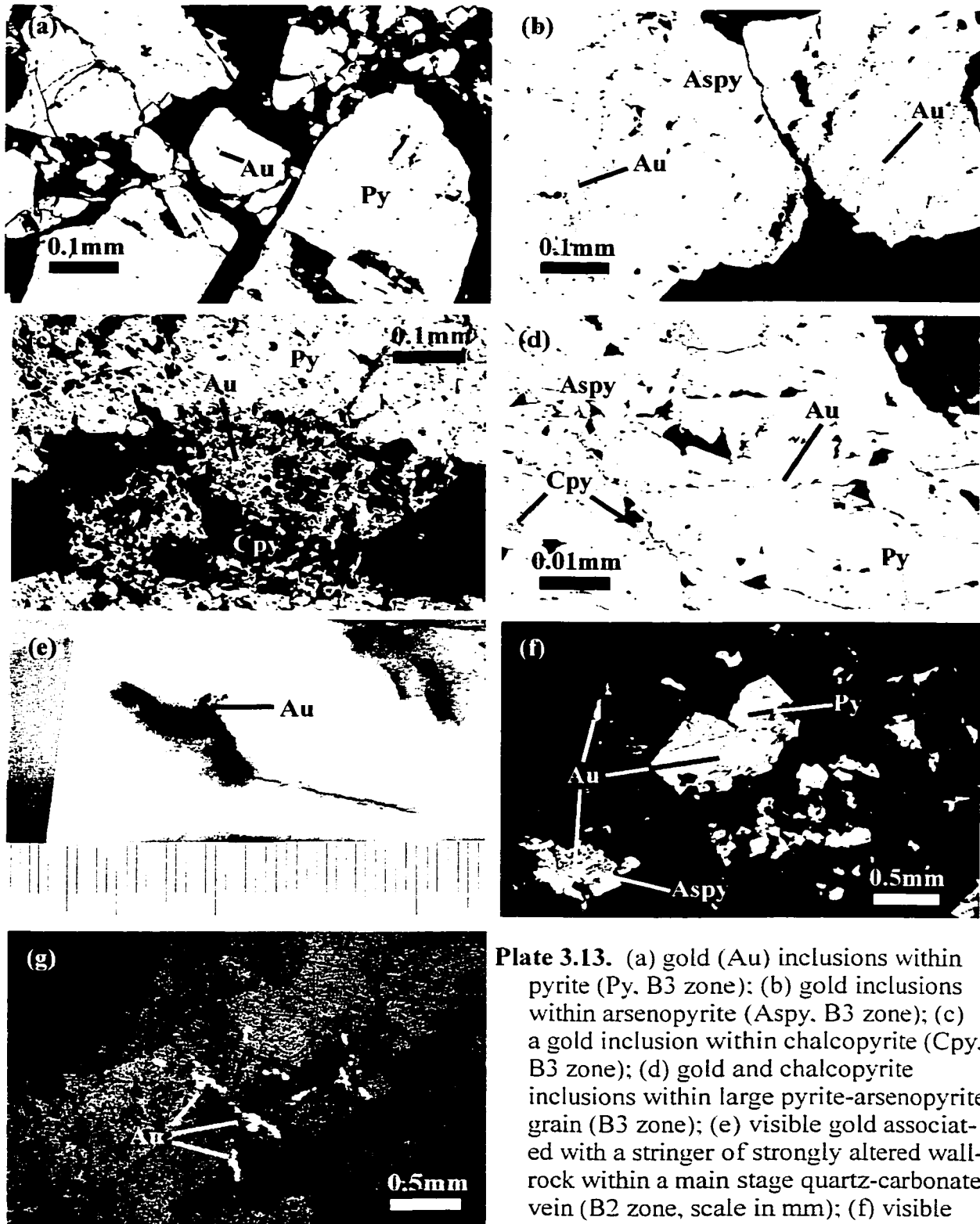


**Plate 3.13.** (a) gold (Au) inclusions within pyrite (Py, B3 zone); (b) gold inclusions within arsenopyrite (Aspy, B3 zone); (c) a gold inclusion within chalcopyrite (Cpy, B3 zone); (d) gold and chalcopyrite inclusions within large pyrite-arsenopyrite grain (B3 zone); (e) visible gold associated with a stringer of strongly altered wallrock within a main stage quartz-carbonate vein (B2 zone, scale in mm); (f) visible gold associated with pyrite and arsenopyrite in wallrock stringer within a main stage quartz-carbonate vein (B2 zone); (g) visible gold within a main stage quartz-carbonate vein (B2 zone); (a-d), (f), and (g) reflected light photomicrographs; (e) handsample photograph.

pyrite in wallrock stringer within a main stage quartz-carbonate vein (B2 zone); (g) visible gold within a main stage quartz-carbonate vein (B2 zone); (a-d), (f), and (g) reflected light photomicrographs; (e) handsample photograph.

Quartz-carbonate veining in the B3 zone tend to be thinner, more irregular, and more discontinuous than veins in the B2 zone due to the resilient nature of the mafic and ultramafic rocks that host them. This gives veining in the B3 zone a brittle or stockwork-like appearance (Plate 3.14). There is evidence of several overprinting sets of foliation parallel and crosscutting veins in the B3 zone that have resulted in intense alteration, sulphidation, and gold deposition in the wallrocks surrounding the quartz-carbonate veins. However, visible gold has not been observed within the auriferous veins in this zone. Numerous extension-related flat veins also occur throughout the B3 zone.

B4 Zone: The B4 zone is not as well understood as the B2 and B3 zones and at the present time has only been intersected a few times in diamond drill core. The B4 zone appears to lie on the contact between graphitic sediments and basalts, much like the B2 zone (Figure 3.2). The B4 zone is located to the east of the B3 zone and is assumed to be parallel to it. Veining in the B4 zone appears to be more discontinuous than the B2 or B3 zones although individual veins can be up to 10 to 25 metres wide locally.

Mineralization within the B4 zone is similar to the B2 zone with significant amounts of wallrock sulphide-gold mineralization occurring around shear-parallel quartz-dolomite veins. Significant amounts of coarse-grained gold have also been observed in micro-fractures within the quartz-dolomite veins.

Due to sampling limitations, the B2 and B3 zones were over represented in this study. The B2 and B3 zones are more easily accessible in outcrop, drill core and underground than the B4 zone. However, the B2 and B4 zones are believed to be similar



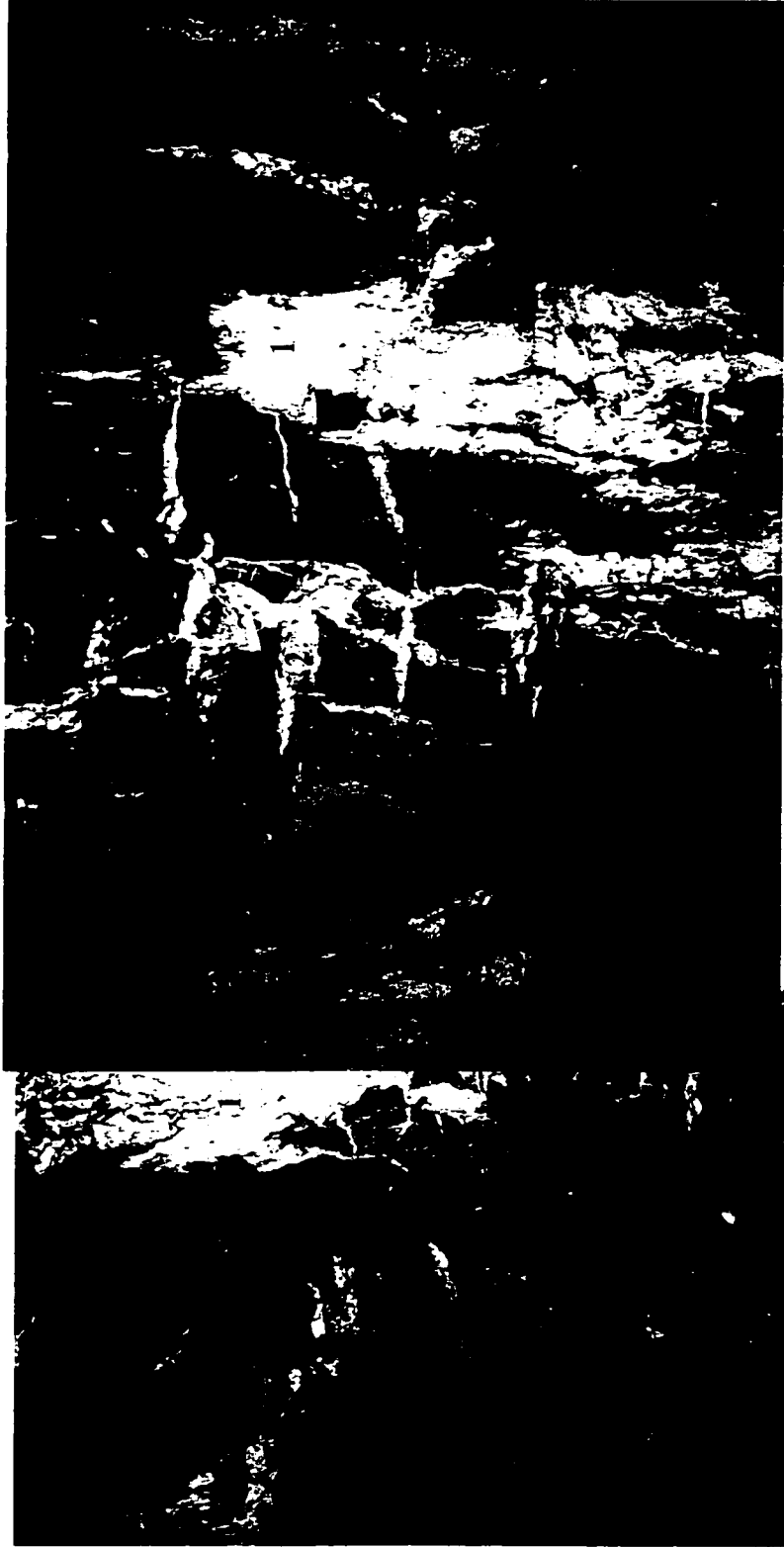


**Plate 3.14.** Main stage quartz-carbonate veining (1) in the B3 zone. Numerous crosscutting extension-related ladder veins (2) give the B3 zone an overall brittle, stockwork-like appearance (lens cap is approximately 6 cm in diameter).

in most respects and what is considered to be true of the B2 zone can be inferred to be true of the B4 zone as well.

### ***3.1.5. Vein Paragenesis***

Several overprinting vein sets occur within the Boston fault zone. Different vein types were identified both underground and from diamond drill core and distinguished on the basis of appearance, mineral assemblage, crosscutting relationships, and intensity of deformation. At least five overprinting episodes of quartz-carbonate veining have been identified in the Boston deposit. The relationship between the three main vein types in the B2 zone is illustrated in Plate 3.12.

Main Stage Quartz-Carbonate Veins: Main stage quartz-carbonate veining in the Boston area has resulted in the formation of fissure or sheeted veins in the B2, B3 and B4 zones (Plates 3.12 and 3.14). These veins are directly related to gold deposition and intense hydrothermal alteration and sulphidation of the wallrocks that host them. On the deposit scale, main stage veins form as north trending, subvertically dipping en-echelon arrays of sigmoidally shaped veins, are aligned parallel to the trend of the Boston fault zone. The main stage quartz-carbonate veins range from several centimetres thick to over thirty metres thick. Ferroan dolomite and/or ankerite are typically deposited adjacent to the vein walls with a mixture of carbonate and quartz filling the center of the veins. Radiating needles and stringers of dravitic tourmaline, coarse pyrite, chalcopyrite, and arsenopyrite, and slivers of strongly altered wallrock also commonly occur within these veins. Gold occurs as inclusions and fracture fillings within pyrite, arsenopyrite, and

chalcopyrite grains associated with strongly altered wallrock stringers in these veins, just as it does in the hydrothermally altered wallrock adjacent to the veins.

The key factor controlling the overall appearance of the main stage quartz-carbonate veins in the B2, B3, and B4 zones is the competency of the surrounding wallrocks. In all three zones main stage veining developed in response to the periodic invasion of hydrothermal fluids along foliation parallel fractures within the Boston fault zone (Hodgson, 1989). Repeated fracturing and resealing at or near the contact between previously formed veins and the wallrock resulted in the incorporation of numerous stringers of strongly altered wallrock into the veins during vein growth (Plate 3.12a, b, c). In the B2 and B4 zones, where veining occurs along the contact between strongly foliated and easily deformed sediments and basalts, the main stage quartz-carbonate veins formed as massive fissure or sheeted veins (Plate 3.12e). The gabbros that host the main stage quartz-carbonate veins in the B3 zone are considerably more competent and difficult to deform than the sediments and basalts that host veining in the B2 and B4 zones. As a result, main stage quartz-carbonate veining in the B3 zone tends to be more irregular, commonly forming discontinuous arrays of thinner veins (Plate 3.14).

Deformation, related to the development of the Boston fault zone, has resulted in both the brittle deformation (brecciation) and ductile deformation (boudinage and tight folding) of all main stage quartz-carbonate veins in the B2, B3, and B4 zones. Quartz and carbonate within the main stage quartz-carbonate veins has been deformed and recrystallized. Quartz also typically displays strong undulose extinction and has sutured grain boundaries (Plate 3.15a). Variable degrees of cataclastic deformation and recrystallization have been observed in sulphide minerals within and surrounding the

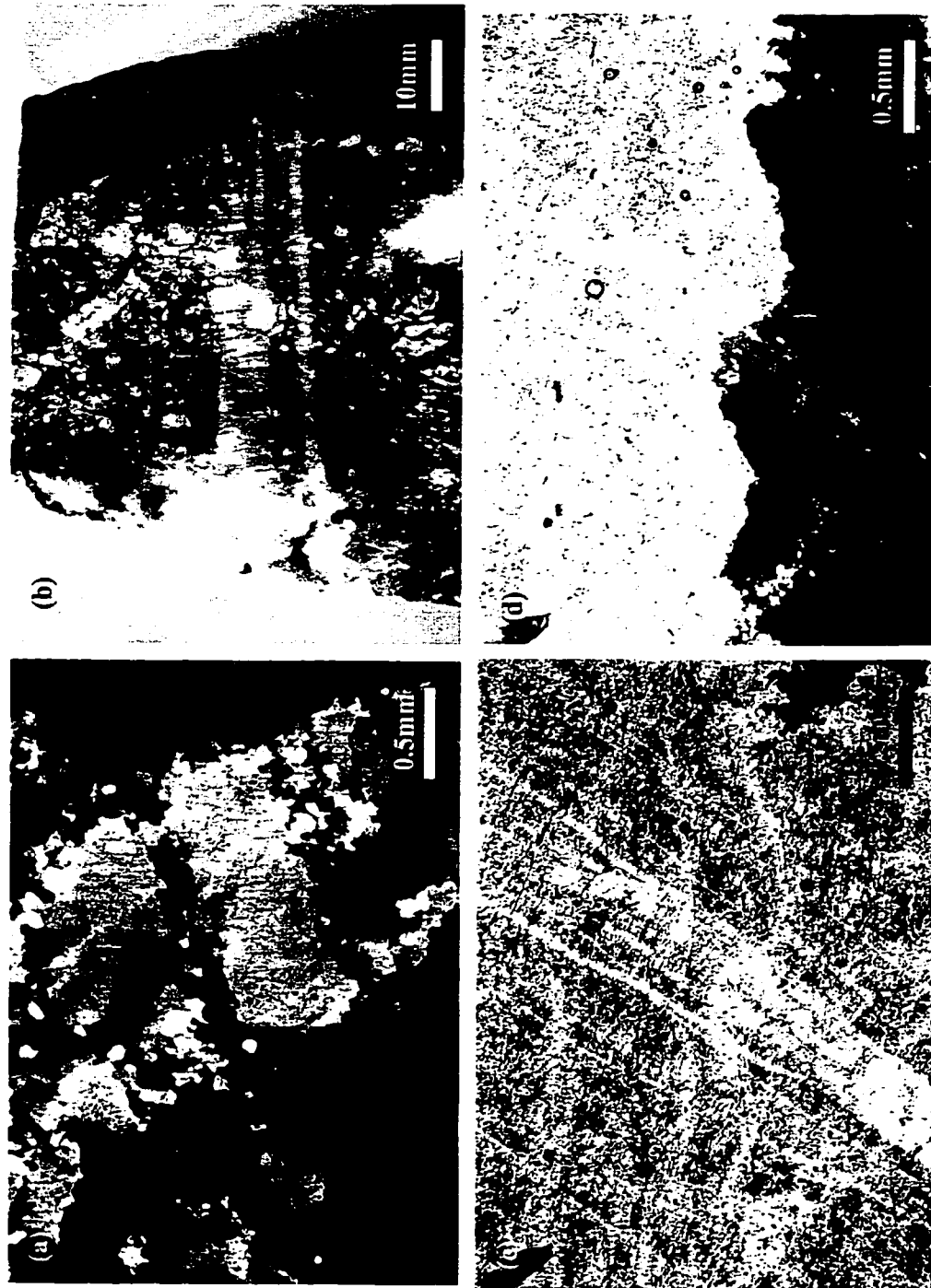


**Plate 3.15.** (a) Photomicrograph of deformed and recrystallized quartz typically present in unsheltered quartz-carbonate veins within the Boston deposit (exposed under crossed nicols); (d) ladder veins hosted by a main stage quartz-carbonate vein (B2 zone); photomicrographs (c) exposed in transmitted plane polarized light and (d) under crossed nicols of several thin ladder veins hosted by a recrystallized main stage quartz-carbonate vein in the B2 zone.

main stage quartz-carbonate veins. The sulphide minerals appear to have been deposited at several different times during D3 deformation, with minerals deposited earlier being more strained than ones deposited later. Localized shearing (D3) resulted in the development of a strong S2 foliation in the vicinity of the Boston fault zone. However, in the most intensely altered wallrocks within and immediately adjacent to the main stage quartz-carbonate veins, the S2 foliation is commonly overprinted by the hydrothermal alteration mineral assemblage. These observations are consistent with the synchronous development of the main stage quartz-carbonate veins and the Boston fault zone (Robert and Poulsen, in press). Furthermore, all of the main stage quartz-carbonate veins in the Boston deposit have been strongly deformed (Plates 3.12e and 3.14). Deformation associated with the Boston fault zone appears to have outlasted the formation of the main stage veins and it is likely that the main stage quartz-carbonate veins were emplaced relatively early in the evolution of this structure.

Ladder Veins (Early Extensional Veins): En-echelon arrays of extensional or ladder veins are common in the Boston deposit and have been observed within competent rock bodies in shear zone hosted lode-gold deposits throughout the world (Groves and Foster, 1991). Ladder veins are typically only a few millimetres to centimetres thick and up to half a metre long and form perpendicular to the minimum compressive stress associated with shear-related deformation (Twiss and Moores, 1973). In the Boston deposit, ladder vein arrays form at right angles to foliation and are roughly horizontal (Plates 3.12c and 3.14). In other Archean lode-gold deposits extension related veins, such as ladder veins, are commonly mineralized. For example, a significant portion of the lode-gold resource in

the Hollinger-McIntyre deposit, Ontario (Burrows et al., 1993), and the Sigma mine Quebec (Robert and Brown, 1986b; Robert and Kelly, 1987) is hosted by extensional veins. However, the ladder veins in the Boston deposit tend to be sub-economic.

Numerous short ladder veins occur within the B2, B3, and B4 zones. In the B2 and B4 zones, the ladder veins occur entirely within the main stage quartz-carbonate veins and strongly dolomitized portions of wallrock, terminating abruptly at unit boundaries (Plate 3.15b). Extension associated with compression in the less competent sediments and basalts outside of these units was accommodated by ductile deformation alone, and as a result, ladder veins did not develop there. Conversely, in the B3 zone, the ladder veins commonly continue into the more competent gabbros and basalts that host the main stage quartz-carbonate veins (Plate 3.14). This gives veining in the B3 zone an overall stockwork-like appearance that is quite different from veining in the B2 and B4 zones.

The ladder veins are typically composed of highly elongate quartz and carbonate grains that grew into the veins as they opened and, as a result, have a preferred orientation perpendicular to the vein walls (Plate 3.15b). The quartz and carbonate within the ladder veins has been deformed and recrystallized along with the main stage quartz-carbonate veins that host them. Most quartz grain boundaries crosscut the ladder veins and display strong undulose extinction (Plate 3.15c,d). In the B3 zone, ladder veins have commonly been buckled by D3 deformation that occurred after they were formed (Plate 3.14). However, in all cases, S2 foliation remains at high angles to the vein walls indicating that they were deformed under conditions compatible with those that led to their formation within the Boston fault zone. Furthermore, the overall geometry and

configuration of both the main stage quartz-carbonate veins and the ladder veins in the B2, B3, and B4 zones appears to be consistent with the kinematics of the Boston fault zone. These observations suggest that the ladder veins were emplaced within the Boston fault zone at approximately the same time as the main stage quartz-carbonate veins and are syn-deformational (Robert and Poulsen, in press).

Flat Veins (Late Extensional Veins): A second set of extensional veins occurring within the Boston deposit is represented by horizontally oriented flat veins. Flat veins, like ladder veins, form perpendicular to the minimum compressive stress associated with the Boston fault zone, generating areas of dilatancy. However, unlike ladder veins, flat veins are not confined to competent rock types and have been observed cutting across all other lithologies and previously mentioned vein types in the Boston deposit (Plates 3.12c,d,e and 3.16a). Flat veins are also much thicker and more laterally extensive than the ladder veins. Flat veins range from a few centimetres to tens of centimetres thick and can be up to several metres long. Internal layering parallel to the vein walls and elongation of quartz and carbonate grains perpendicular to the vein walls has been observed within many flat veins, indicating that these veins formed as a result of several consecutive opening and vein filling events (Plate 3.16a,b). Quartz and carbonate grains within the flat veins have been deformed and quartz typically displays strong undulose extinction. Locally, slabs of wallrock oriented at low to moderate angles to the vein walls also occur within the flat veins (Plate 3.16c). These wallrock slabs became incorporated into the flat veins during vein propagation and dilation (Robert and Poulsen, in press). Within the

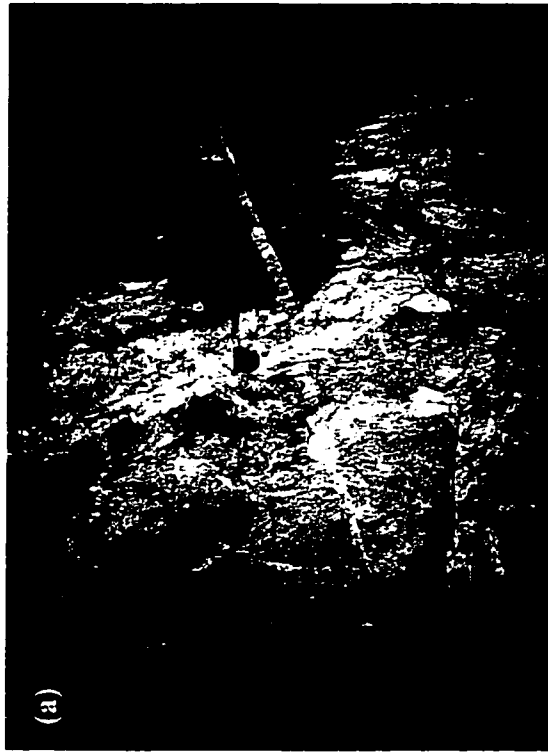


**Plate 3.16.** (a) Flat vein in the B2 zone crosscutting a subvertical quartz-carbonate vein; weathering has highlighted quartz (white) and carbonate (brown) crystals growing into the vein perpendicular to the vein walls (perpendicular to the maximum compressive stress in the Boston fault zone; lens cap is approximately 6cm in diameter); (b) a photomicrograph exposed under crossed nicols of elongate quartz and carbonate grains similar to in (a) growing into the flat vein at roughly right angles to the vein walls (vein wall is at the bottom of the photomicrograph); (c) a bridge of strongly altered wallrock that became incorporated into the flat vein as it opened (B2 zone).



Boston fault zone flat veins do not contain economically significant concentrations of gold and are not associated with the hydrothermal alteration or sulphidation of the wallrocks they cut. The flat veins cut across foliation at roughly right angles and appear to have formed as a direct consequence of compressional deformation associated with the development of the Boston fault zone. In the most strongly deformed portions of the Boston deposit the flat veins have been folded into sigmoidal shapes due to D3 deformation following their emplacement (Plate 3.12d,e). However, most flat veins within the Boston deposit are tabular and do not show any sign of folding or buckling (Plate 3.16a). The evidence presented above is consistent with the development of the flat veins during D3 deformation but relatively late in the life of the Boston fault zone. Furthermore, it is likely that the flat veins formed in response to the same deformational environment as the ladder veins, only under slightly more brittle conditions.

Phantom Veinlets (Brecciation): Numerous phantom veinlets, outlined by trails of fluid inclusions, occur within the main stage quartz-carbonate veins in the B2, B3, and B4 zones. The phantom veinlets are difficult to see in hand sample and thin section because they are mineralogically similar to, and have been deformed and recrystallized along with, the main stage quartz-carbonate veins that host them (Plate 3.17). The phantom veinlets create a stockworked array of irregular and cross cutting veinlets with no preferred orientation and appear to have formed in response to fracturing subsequent to main stage quartz-carbonate vein formation.

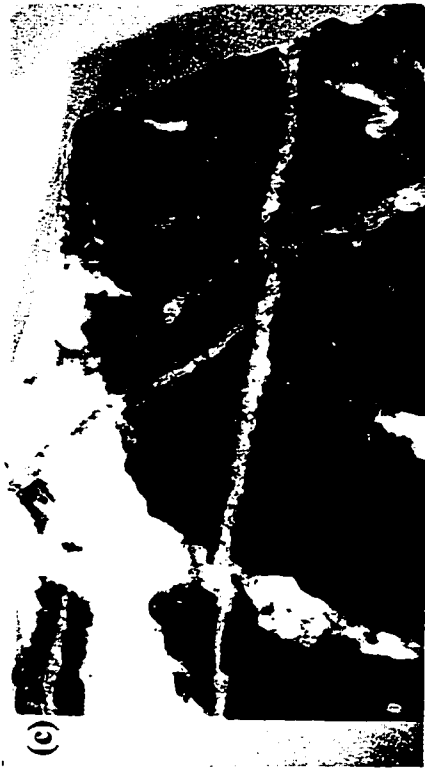


**Plate 3.17.** Photomicrographs (a) exposed in transmitted plane polarized light and (b) under crossed nicols of phantom veinlets hosted by a main stage quartz-carbonate vein in the B2 zone. The phantom veinlets and the quartz that hosts them have been extensively recrystallized and deformed. All that indicates the existence of these veinlets is a difference in fluid inclusion density between quartz within and outside of the veinlets. (c) Crosscutting late brittle veinlets within the B2 zone (scale is in centimetres).

6 7 8 9 10 11 12 13 14 15

In the B2 and B4 zones free gold has been observed in association with some phantom veinlets. The gold within these veinlets was most likely deposited at the same time as the main stage quartz-carbonate veins and then remobilized into the phantom veinlets during subsequent deformation associated with the development of the Boston fault zone. However, the exact timing of phantom veinlet emplacement and their relationship to the other vein types and lode-gold mineralization in the Boston deposit are poorly understood.

Late Brittle Veins (Rebrecciation): Throughout the Boston deposit thin, irregular veinlets with no preferred orientation occur both within and outboard of the main stage quartz-carbonate veins, cutting across all of the other vein types (Plate 3.17c). These veinlets are most prevalent in the B2 and B4 zones, and have even been observed cross cutting individual pyrite grains in the sulphidation halo adjacent to the main stage quartz-carbonate veins in these zones. The late veinlets generally contain clear, relatively undeformed quartz and carbonate and are always barren. Petrographically, these veinlets appear to have formed very late in the life of the hydrothermal system under conditions dominated by brittle deformation.

### ***3.2. The South Patch Occurrence***

The South Patch occurrence is a poorly understood lode-gold prospect located approximately 47 kilometres to the north of the Boston deposit near the northern end of the Hope Bay volcanic belt (Figure 1.2). Mineralized veining associated with the South

Patch occurrence occurs beneath Patch Lake and has not been observed in outcrop. The following discussion relies heavily on observations made by BHP geologists while logging drill core and later summarized in the "Hope Bay Project - Exploration Overview, 1999". and will be kept brief.

The South Patch occurrence was discovered during BHPs 1997 drill campaign and represents a 2.2 kilometre-long hydrothermal vein system encapsulated within strongly carbonatized and sericitized mafic volcanic rocks similar to the Boston deposit. Quartz-carbonate veining at South Patch occurs within the north-south-trending Patch Lake shear and appears to be structurally controlled, as it is in the Boston deposit, with quartz-carbonate veins occurring at or close to the contact between a package of mafic volcanic rocks and a quartz-feldspar porphyry. Hydrothermal alteration adjacent to auriferous veins at South Patch consists of paragonite, dolomite, chlorite, quartz, and pyrite, again similar to the Boston deposit, with gold forming inclusions within sulphide minerals or as free gold within the quartz-carbonate veins. Furthermore, both the South Patch showing and the Boston deposit are believed to occur within the limbs of large-scale folds.

#### **4. Sample Selection and Analytical Methods**

During the 1997 and 1998 field seasons, vein and wallrock samples were collected from surface showings and drill core both proximal and distal to the Boston deposit. Active drifting on two of the three main mineralized zones present in the Boston deposit, B2 and B3, allowed for additional samples to be taken underground on the 4000,

3935, and 3920 metre levels. Numerous mineralized and barren vein sets were sampled in this way. In addition, samples of altered and unaltered wall rock were collected from surface outcrop and drill-core both locally and regionally. In a comparison study, several samples of mineralized and barren rock were obtained from the South Patch gold prospect.

In total two hundred and sixteen samples were collected from the Boston deposit and surrounding area, and twenty-eight samples were provided from the South Patch showing. Sample numbers, descriptions, and UTM coordinates are given in Appendix A.

#### ***4.1. Petrography, XRD, and XRF Whole Rock Analyses***

Representative thin and polished sections of all of the rock types associated with the Boston deposit and South Patch occurrence were prepared for petrographic analysis. In addition, X-ray diffraction (XRD) and electron microprobe analysis was used to aid in the identification of end-member minerals difficult to distinguish on the basis of petrographic analysis alone (for example, calcite/dolomite/ankerite/siderite). Hand sample descriptions and mineralogy based on XRD, electron microprobe analysis, and thin section petrography is given in Appendix A.

Five samples of basalt and five samples of gabbro from the Boston area were sent to XRAL Laboratories in Ontario for whole rock X-ray fluorescence spectrometry (XRF). Whole rock analyses were used to confirm the original lithology of these samples. The XRF whole rock data are presented in Appendix B.

#### ***4.2. Fluid Inclusion Analysis***

Forty doubly polished thin sections of auriferous and barren veins from in the B2, B3, and B4 zones and surrounding area were prepared for fluid inclusion microthermometry. However, deformation and recrystallization of the vein material resulted in the poor overall quality of the fluid inclusions in many of these thin sections. In this study considerable effort was made to examine only undeformed populations of fluid inclusions that could be directly related to a specific veining event and showed no obvious signs of leaking or necking down. Unconstrained or deformed clusters and trails of fluid inclusions were avoided.

Fluid inclusion analysis was performed on a Linkam THMSG600 fluid inclusion heating/freezing stage at the University of Alberta. This stage was calibrated using Syn Fline synthetic fluid inclusion standards to a precision of  $\pm 0.1^{\circ}\text{C}$  at temperatures below  $0^{\circ}\text{C}$ . The accuracy of measurements made on this stage varies with the temperature of the phase change in question. For low-temperatures (below  $\sim 31^{\circ}\text{C}$ ), the measurements are accurate to within  $0.1^{\circ}\text{C}$ . High-temperature measurements (above  $\sim 31^{\circ}\text{C}$ ) are accurate to within  $1.0^{\circ}\text{C}$ .

The equivalent weight percent NaCl for  $\text{CO}_2$ -rich fluid inclusions was calculated from the final melting temperature of clathrate using an equation from Darling (1991). The equivalent weight percent NaCl for fluid inclusions that contained no  $\text{CO}_2$  was calculated from final ice melting temperatures using an equation from Bodnar (1993). The densities, molar volumes, mole fractions of  $\text{H}_2\text{O}$ ,  $\text{CO}_2$ , and NaCl, the molality NaCl, and the minimum pressure at the time of entrapment were calculated using the

MacFlinCor computer program for fluid inclusion data reduction and manipulation (Brown, 1989). Equations from Brown and Lamb (1986, 1989) were used in these calculations.

### ***4.3 Stable Isotopic Analysis***

Carbonates: Carbonate minerals from vein and wall rock material from the Boston deposit and surrounding area were analysed for their oxygen and carbon isotopic composition. At Boston, calcite, ferroan dolomite, and ankerite were separated from forty-one vein and eighty-seven wallrock samples both adjacent and distal to the mineralized zones. In a related study of the South Patch gold prospect, calcite, ferroan dolomite, and ankerite were separated from eight vein and twenty-four wallrock samples including samples from three mineralized zones.

Samples of vein carbonate were hand picked under technical-grade ethanol using a binocular microscope. Mineral separates were then dried and powdered to between 80 and 120  $\mu\text{m}$ . All samples were analysed by X-ray diffraction (XRD) to identify the type of carbonate mineral present.

Care was taken to select representative samples of wall rock material that were not weathered and contained no visible veining. These samples were powdered to between 80 and 120  $\mu\text{m}$ . The powdered samples of wallrock were analysed by XRD to determine the identity of all carbonate minerals present.

Carbon and oxygen were extracted as carbon dioxide ( $\text{CO}_2$ ) gas from between 30 and 40 mg of sample. Each sample was placed into a glass reaction tube and 3 ml of

phosphoric acid ( $\text{H}_3\text{PO}_4$ ) was introduced but not allowed to mix with the sample. The tube was then placed on a vacuum line overnight to ensure that all air was removed from the reaction vessel. After about twelve hours on the vacuum line the sample and  $\text{H}_3\text{PO}_4$  were mixed, liberating  $\text{CO}_2$  gas.

Achievement of isotopic equilibrium in the reaction between  $\text{H}_3\text{PO}_4$  and carbonate is both time and temperature dependent. Samples containing calcite were placed in a  $25^\circ\text{C}$  water bath and allowed to react for at least twenty-four hours to liberate the  $\text{CO}_2$  gas. Samples containing ferroan dolomite or ankerite were placed in a  $50^\circ\text{C}$  water bath and allowed to react for at least four days. Samples containing mixtures of calcite and ferroan dolomite or calcite and ankerite were taken through a stepped reaction procedure. The sample was placed in a  $25^\circ\text{C}$  water bath and allowed to react for one hour to liberate  $\text{CO}_2$  gas from calcite while minimizing the input from ferroan dolomite or ankerite. The  $\text{CO}_2$  gas was then extracted and the reaction vessel returned to vacuum. The sample was then placed in a  $50^\circ\text{C}$  water bath and allowed to react for at least four days, liberating  $\text{CO}_2$  gas from the remaining ferroan dolomite or ankerite.

Five samples of basalt from the South Patch showing contain both ankerite and siderite, based on XRD analysis. There are differences in  $\delta^{18}\text{O}$  and  $\delta^{13}\text{C}$  fractionation between ankerite and siderite. These differences may result in inaccurate results if  $\text{CO}_2$  gas liberated from both ankerite and siderite is analysed together. However, pure siderite prepared under controlled conditions in the laboratory takes more than seven days to react with  $\text{H}_3\text{PO}_4$  at  $50^\circ\text{C}$  (Carothers et al., 1988). The siderite that is present in the South Patch samples is most likely intergrown with other minerals. As a result, the  $\text{H}_3\text{PO}_4$  – siderite reaction may take months at  $50^\circ\text{C}$ . All ankerite extractions were performed after



reacting the samples with  $\text{H}_3\text{PO}_4$  for only four days, effectively minimizing any input of  $\text{CO}_2$  gas from the siderite.

After the sample and the acid had finished reacting, the sample was introduced into a glass line under vacuum. Any  $\text{H}_2\text{O}$  that may have been produced through the reaction of the  $\text{H}_3\text{PO}_4$  and the sample was removed by passing the sample through a  $\text{H}_2\text{O}$  trap, consisting of a cold finger submerged in a dry ice and ethanol slush. All water in the sample was frozen out of the sample by the cold trap, while  $\text{CO}_2$  passes through as a gas. The purified  $\text{CO}_2$  gas was finally frozen by a second cold finger submerged in liquid nitrogen. At this point the line was again opened to vacuum and all uncondensable gases (for example Ar) were removed. The trapped  $\text{CO}_2$  was then isolated and heated to room temperature so that the volume of the  $\text{CO}_2$  gas could be measured. The  $\text{CO}_2$  gas was then transferred to a glass tube that was taken to the mass spectrometer for analysis.

Carbon and oxygen isotopes were analysed on a Finnigan MAT 252 dual-inlet, multiple-collector, magnetic-sector, gas mass spectrometer. The sample was introduced into the mass spectrometer as  $\text{CO}_2$  gas. The fractionation factors used to account for the exchange of oxygen between the sample and the  $\text{H}_3\text{PO}_4$  acid were 1.01025 for calcite at  $25^\circ\text{C}$  (K. Muehlenbachs, pers. comm., 1999) and 1.01060 for dolomite and ankerite at  $50^\circ\text{C}$  (Kontak and Kerrich, 1997). Both oxygen and carbon isotope ratios are given in delta ( $\delta$ ) notation. Oxygen isotope ratios are reported relative to VSMOW, and carbon isotope ratios are reported relative to PDB. The carbonate stable isotope values have a  $2\sigma$  error of  $\pm 0.1\text{‰}$  (K. Muehlenbachs, pers. comm., 1999). Repeat analyses, conducted on several samples, confirmed the reproducibility of the results.

Quartz: Twelve quartz separates from mineralized veins and twenty-eight quartz separates from unmineralized veins associated with the Boston deposit, and four quartz separates from mineralized veins at South Patch were prepared for oxygen isotopic analysis. Vein quartz was hand picked under technical-grade ethanol. The separate was then dried and crushed to less than 0.2 mm and cleaned in a 3:1 mix of concentrated hydrochloric acid and nitric acid on a hotplate at approximately 100°C for at least one hour. Then the cleaned sample was rinsed with deionized water ten times, rinsed twice with technical grade acetone to ensure all water was removed from the sample, and finally dried on a hotplate. The samples were then analyzed in the stable isotopic laboratory at the University of Alberta.

Oxygen gas was liberated from between 10 and 20 mg of vein quartz using the bromine pentafluoride ( $\text{BrF}_5$ ) method. Nickel tubes were heated to 300°C for one hour to drive off all water. Helium gas was also introduced into the tubes to prevent moisture from getting into the line. The nickel tubes were then taken to a dry box where the samples were loaded. The tubes containing the sample were then attached to a line made of nickel pipes into which  $\text{BrF}_5$  had previously been introduced. Approximately five times as much  $\text{BrF}_5$  is required to react with a given amount of sample. The nickel tubes were heated with electric furnaces to 570°C for twelve hours for the reaction to take place. The tubes were then cooled to room temperature. The products of the reaction between  $\text{BrF}_5$  and quartz as well as any remaining  $\text{BrF}_5$  were then released into an evacuated monel line. The gas was passed through a trap cooled by liquid nitrogen, which removes all of the volatiles with the exception of  $\text{O}_2$  gas. The  $\text{O}_2$  gas was then converted to  $\text{CO}_2$  gas by reacting it with graphite at 500°C. The  $\text{CO}_2$  gas was then

transferred to another liquid nitrogen trap, isolated from the rest of the line, and then heated to room temperature so that its volume could be measured. The CO<sub>2</sub> gas was then transferred to a glass tube that was taken to the mass spectrometer for analysis as above.

Oxygen isotope reference standard NBS-28 (+9.6‰) was run to normalize the δ<sup>18</sup>O data to VSMOW. The silicate stable isotope results have a 2σ error of ±0.2‰ (K. Muehlenbachs, pers. comm., 1999). Repeat analyses conducted on several samples confirmed the reproducibility of the results.

Pyrite: Twenty-one pyrite separates from the wallrocks hosting the Boston deposit were prepared for stable isotopic analysis. Samples of pyrite were hand picked under technical-grade ethanol using a binocular microscope. Mineral separates were then dried and ground to approximately 2 mm before being sent to the stable isotope laboratory at the University of Calgary for analysis. The resulting δ<sup>34</sup>S data are accurate to within 0.3‰ and are reported relative to the CDT standard (S. Taylor, pers. comm., 2000)

Graphite: Six graphite separates from the wallrocks hosting the Boston deposit were also prepared for stable isotopic analysis. Graphite concentrates were hand picked under technical-grade ethanol. The separate was then dried and crushed to less than 0.2 mm and cleaned in a 3:1 mix of concentrated hydrochloric acid and nitric acid on a hotplate at approximately 100°C for at least one hour. The cleaned samples were then rinsed with deionized water ten times, rinsed twice with acetone, and finally dried on a hotplate. Graphite samples were also sent to the stable isotope laboratory at the University of

Calgary for analysis. The  $\delta^{13}\text{C}$  data have been normalized to the PDB standard and are accurate to within 0.2‰ (S. Taylor, pers. comm., 2000).

## **5. Results**

### ***5.1. XRF Whole Rock Analyses***

The results of the XRF whole rock analyses of ten samples of basalt and gabbro associated with the Boston deposit are presented in Appendix B.

Discontinuous gabbroic units occur throughout the basaltic package that hosts the Boston deposit. Where they have been hydrothermally and/or metamorphically altered the gabbros and basalts are very difficult to distinguish in both hand sample and thin section. The gabbros are, however, easily distinguished by their whole rock (XRF) geochemistry and by the stable isotopic composition of the carbonate minerals they contain. The gabbros tend to contain higher concentrations of potassium, rubidium, and barium than the basalts (Appendix B), and they are also commonly richer in iron and titanium (Locock, 1998a).

### ***5.2 Fluid Inclusions***

#### ***5.2.1. Fluid Inclusion Types***

In general, it is extremely uncommon to find primary fluid inclusions within the barren and auriferous quartz-carbonate veins that make up the Boston deposit. Locating

primary fluid inclusions that can be directly linked to gold mineralization within the mineralized zones is even more of a challenge. Minerals within the main stage quartz-carbonate veins and cross cutting ladder, flat, phantom, and late brittle veins have been extensively deformed and recrystallized. The fluid inclusions within these veins typically occur along healed micro-fractures, as irregular three-dimensional clusters or along recrystallized grain boundaries. These fluid inclusions tend to be small irregular secondary inclusions that are very difficult to work with. Furthermore, it can not be assumed that the fluid inclusions hosted by the deformed quartz and carbonate within these veins have retained a constant volume or have remained chemically closed systems since their entrapment.

That being said, primary fluid inclusions that have not been deformed have been preserved within the main stage quartz-carbonate veins in a few cases and under very unique circumstances. Primary fluid inclusions occur within quartz grains that have been included within large pyrite or carbonate grains in the main stage quartz-carbonate veins (Plate 5.1). The relative strength or plasticity of the pyrite or carbonate, respectively, appears to have taken up most of the strain associated with deformation, effectively protecting the quartz and its inclusions (Guha et al., 1991). Gold also typically occurs as inclusions within pyrite grains. It is likely, therefore, that the same fluid responsible for the deposition of the quartz and its inclusions, and by association the pyrite, was also responsible for the deposition of sulphide hosted gold in the Boston deposit.

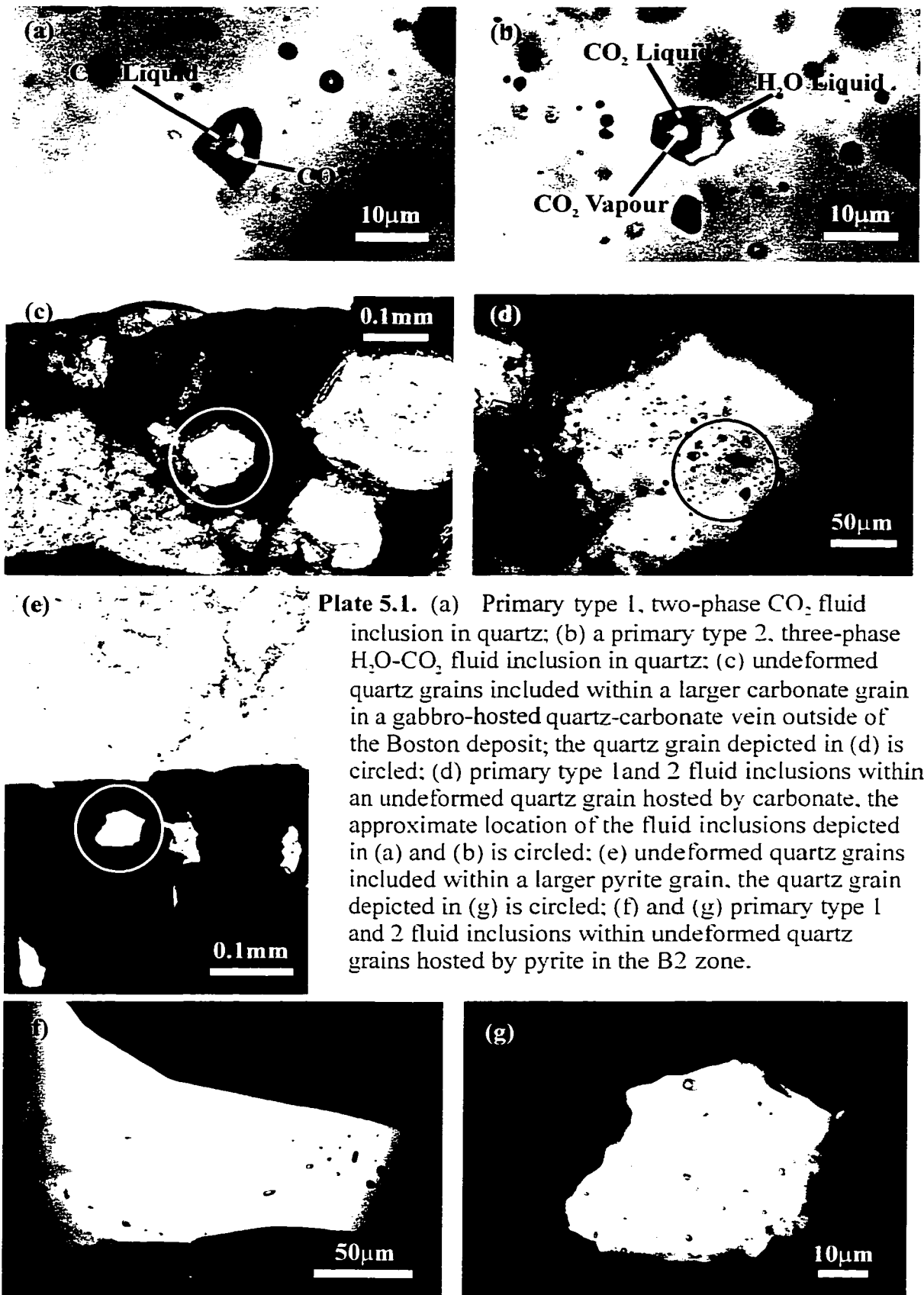


**Plate 5.1.** (a) Primary type 1, two-phase CO<sub>2</sub> fluid inclusion in quartz; (b) a primary type 2, three-phase H<sub>2</sub>O-CO<sub>2</sub> fluid inclusion in quartz; (c) undeformed quartz grains included within a larger carbonate grain in a gabbro-hosted quartz-carbonate vein outside of the Boston deposit; the quartz grain depicted in (d) is circled; (d) primary type 1 and 2 fluid inclusions within an undeformed quartz grain hosted by carbonate, the approximate location of the fluid inclusions depicted in (a) and (b) is circled; (e) undeformed quartz grains included within a larger pyrite grain, the quartz grain depicted in (g) is circled; (f) and (g) primary type 1 and 2 fluid inclusions within undeformed quartz grains hosted by pyrite in the B2 zone.

Type 1 Fluid Inclusions: Type 1 carbon dioxide-rich fluid inclusions occur as large 5 to 15  $\mu\text{m}$ . two-phase inclusions within both mineralized and barren quartz carbonate veins associated within the Boston fault zone (Plate 5.1a). These inclusions are preserved as primaries with negative crystal shapes within small, undeformed quartz grains that have been included within and protected from deformation by larger carbonate or pyrite grains (Plate 5.1 and 5.2d,e). Within sheltered, less deformed parts of the main stage quartz-carbonate veins in the Boston deposit, secondary type 1 fluid inclusions have also been observed, typically forming trails and three-dimensional clusters within deformed quartz and carbonate grains (Plate 5.2c). Type 1 inclusions always occur with type 2 inclusions; however, the reverse is not always true.

Type 2 Fluid Inclusions: Type 2 three-phase (liquid  $\text{H}_2\text{O}$ , liquid  $\text{CO}_2$ , and  $\text{CO}_2$  vapour) fluid inclusions are also present as primaries and secondaries in the main stage quartz-carbonate veins and extensional (ladder) veins in the Boston deposit and surrounding area (Plates 5.1 and 5.2). Type 2 fluid inclusions tend to be from less than 5 to 15  $\mu\text{m}$  in size (Plate 5.1b). In the main stage quartz-carbonate veins, primary type 2 fluid inclusions generally have negative crystal shapes and occur with or without type 1 inclusions in protected and undeformed quartz grains. Secondary type 2 fluid inclusions are the most prevalent fluid inclusion type within the main stage quartz-carbonate veins and ladder veins in all three mineralized zones, where they occur as trails and three-dimensional clusters within deformed quartz and carbonate grains (Plate 5.2a,b).

Secondary type 2 inclusions also appear to be the dominant fluid inclusion type within the phantom veinlets that occur within the main stage quartz-carbonate veins.

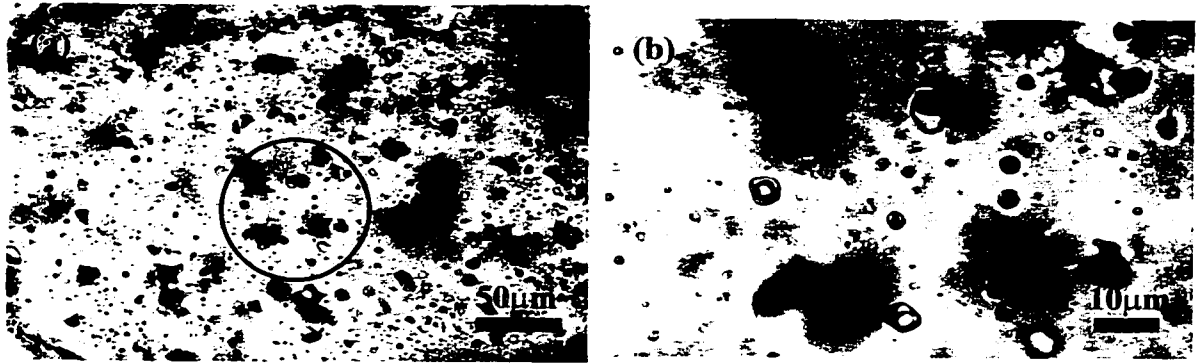
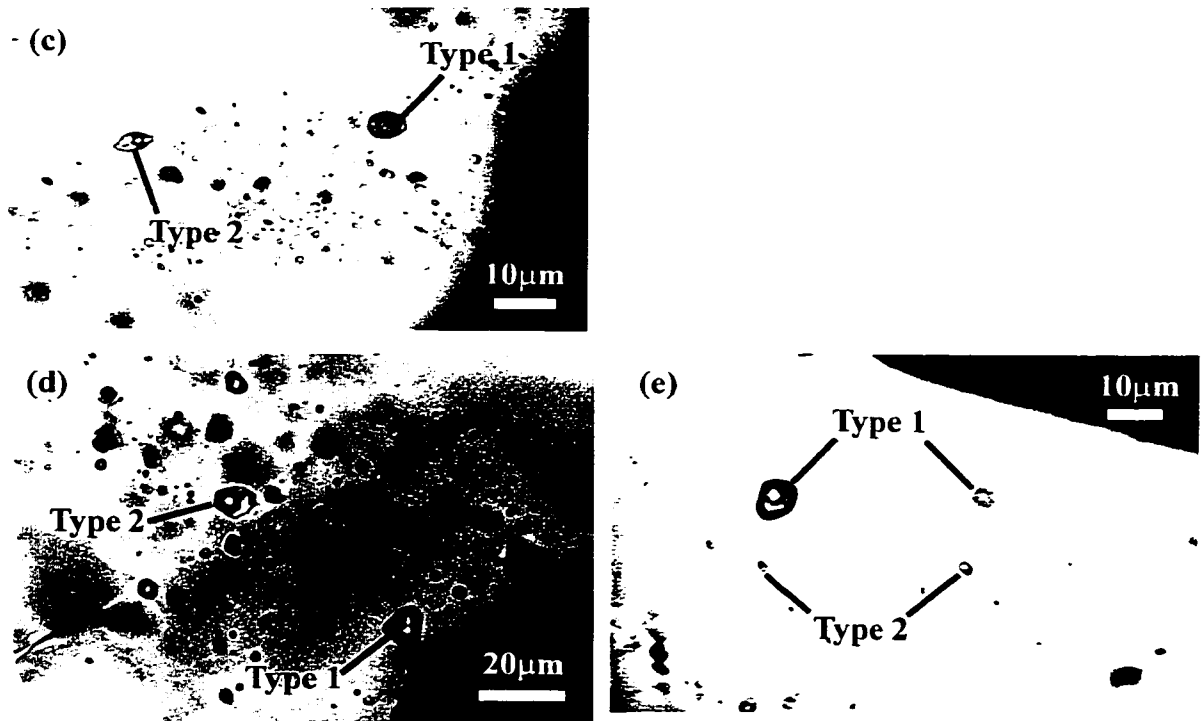


**Plate 5.2.** (a) Secondary type 2 fluid inclusions within a main stage quartz-carbonate vein in the B2 zone, the approximate location of the fluid inclusions depicted in (b) is circled; (b) close up of the secondary type 2 fluid inclusions depicted in (a), these fluid inclusions have negative crystal shapes and uniform fill volumes. (c), (d) and (e) show evidence for phase separation within main stage quartz-carbonate veins in the Boston area: (c) coexisting type 1 and type 2 fluid inclusions within a sheltered part of a main stage quartz-carbonate vein hosted by hydrothermally altered sediments within the Boston fault zone; (d) coexisting primary type 1 and 2 fluid inclusions within an undeformed quartz grain that was protected from deformation by a larger carbonate grain in a gabbro hosted quartz-carbonate vein (close up of Plate 5.1d); (e) coexisting primary type 1 and 2 fluid inclusions within an undeformed quartz grain that was protected from deformation by a larger pyrite grain in the B2 zone (close up of Plate 5.1f).





Deformation and recrystallization of the phantom veinlets has resulted in small irregularly shaped fluid inclusions with inconsistent fill volumes, such that they are unsuitable for microthermometric analysis. As a result, no measurements were done on fluid inclusions contained within the phantom veinlets.

Type 3 Fluid Inclusions: Secondary type 3 low salinity aqueous fluid inclusions occur within crosscutting brittle veinlets in the B2 zone (Plate 5.3c). These inclusions are liquid-rich and typically from less than 5 to 15  $\mu\text{m}$  in size (Plate 5.2a). Secondary type 3 inclusions tend to have irregular shapes, occurring as trails and three-dimensional clusters within late brittle veinlets.

Type 4 Fluid Inclusions: Secondary type 4, high salinity aqueous fluid inclusions have been observed within both the main stage quartz carbonate veins and crosscutting ladder veins in all three ore zones, typically occurring as trails of secondaries within healed microfractures (Plate 5.3d). Type 4 inclusions are large, 5 to 20  $\mu\text{m}$ , and have highly irregular shapes and tend to be more liquid-rich than type 3 inclusions (Plate 5.3b).

### **5.2.2. Microthermometry**

The results of the microthermometric examination of primary and secondary fluid inclusions from quartz-carbonate veins in the Boston deposit are summarized in Table 5.1 and illustrated in Figures 5.1 to 5.4. A complete list microthermometric measurements and associated compositional data for individual fluid inclusions is given in Appendix C.

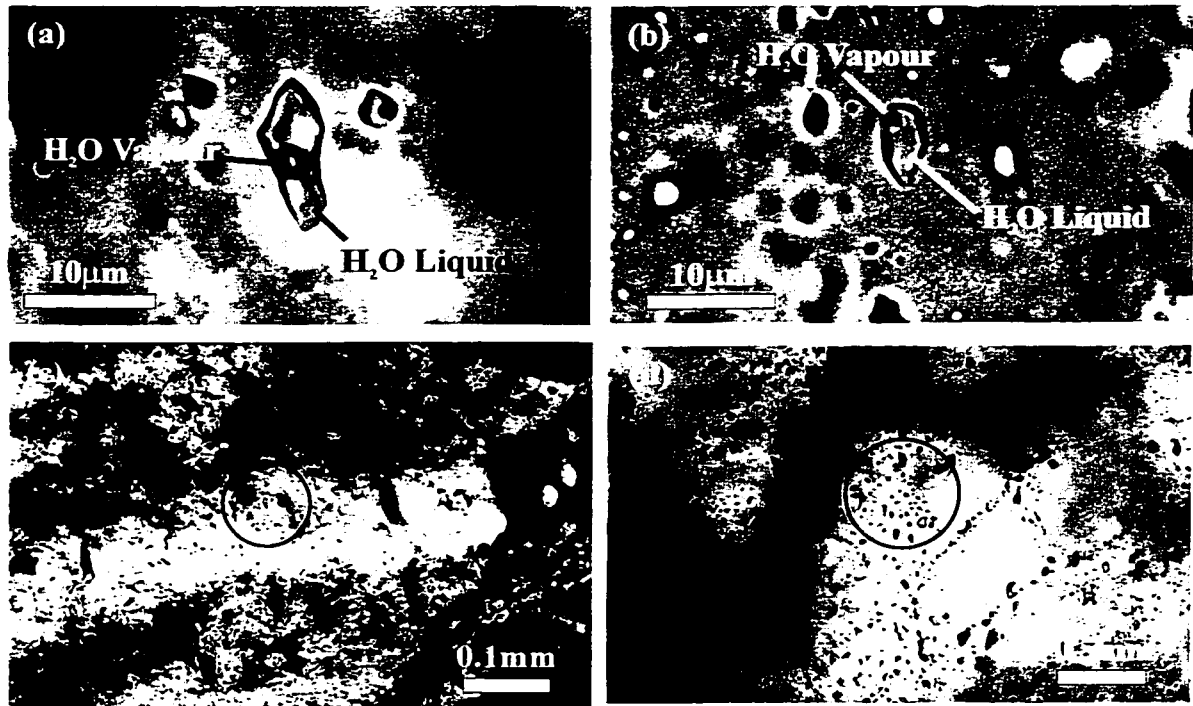


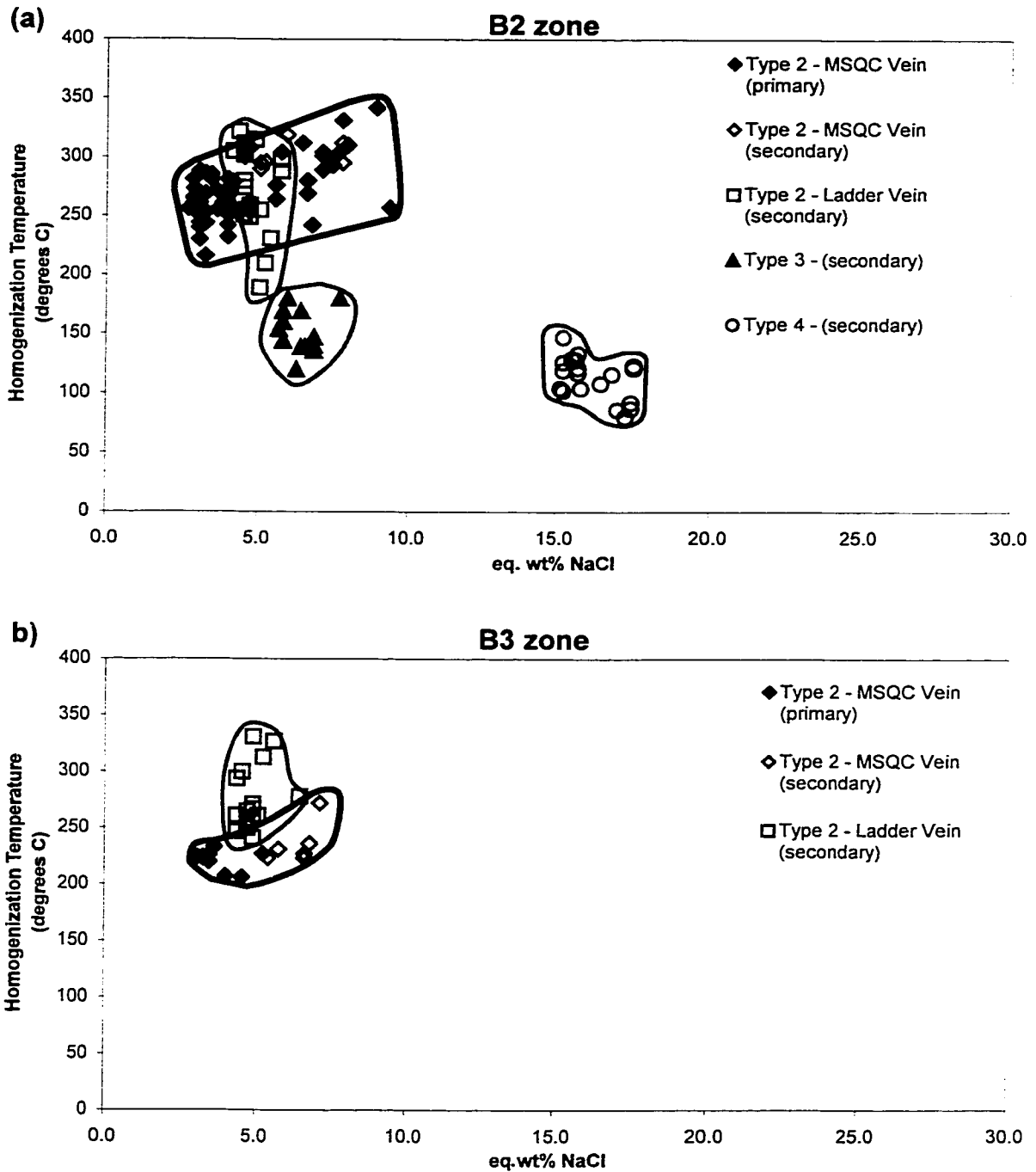
**Plate 5.3.** (a) Secondary type 3, two-phase  $H_2O$  fluid inclusion in quartz: (b) a secondary type 4, two-phase  $H_2O$  fluid inclusion in quartz: (c) type 3 fluid inclusions within a crosscutting quartz filled brittle veinlet in the B2 zone, the approximate location of the fluid inclusion depicted in (a) is circled: (d) type 4 fluid inclusions occurring as trails of secondaries along healed microfractures in the B2 zone, the approximate location of the fluid inclusion depicted in (b) is circled.

**Table 5.1.** Summary of the results of the microthermometric analysis of quartz-carbonate veins in the Boston deposit ( $T_{mCO_2}$  = the temperature at which the carbonic phase melts;  $T_e$  = the temperature of the eutectic;  $T_{mCE}$  = the temperature at which ice melts;  $T_{mCLATH}$  = the temperature at which clathrate melts; eq. wt% NaCl = the equivalent weight percent NaCl in solution;  $T_{hCO_2}$  = the temperature of homogenization of the carbonic phase;  $T_{h(L-V)}$  = the temperature of total homogenization; Min P = minimum pressure at Th; MSQC Vein = main stage quartz-carbonate vein; NA = not applicable).

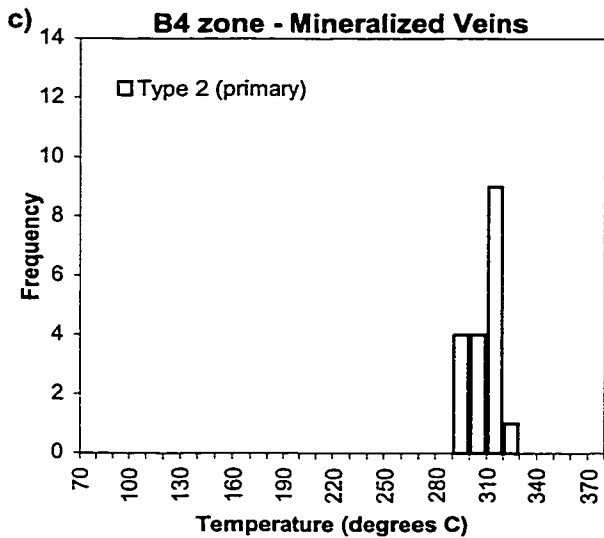
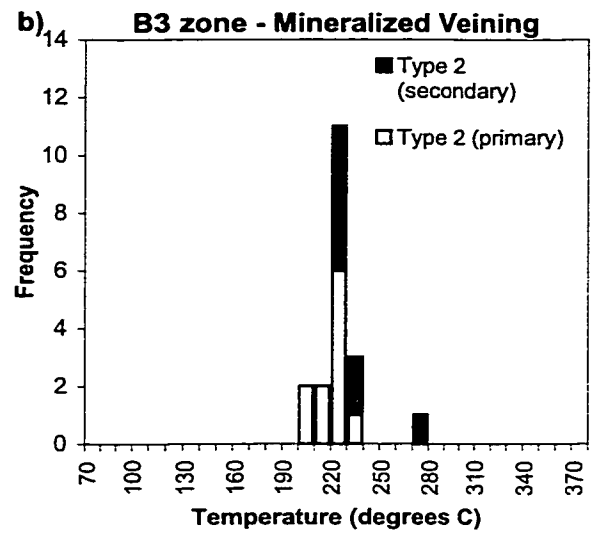
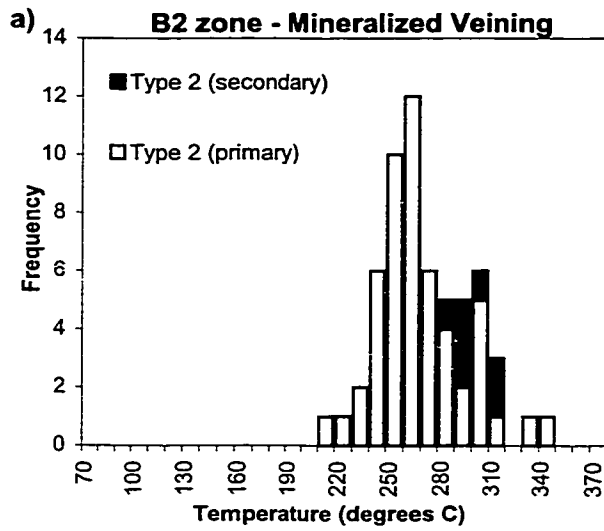
Parameter	Type 1 MSQC Vein (primary)	Type 2 MSQC Vein (primary)	Type 2 MSQC Vein (secondary)	All Type 2 Inclusions	Type 3 Late Brittle Vein (secondary)	Type 4 Late Brittle Vein (secondary)
Fluid Type	2-phase CO <sub>2</sub> inclusions	3-phase H <sub>2</sub> O-CO <sub>2</sub> inclusions	3-phase H <sub>2</sub> O-CO <sub>2</sub> inclusions	3-phase H <sub>2</sub> O-CO <sub>2</sub> inclusions	2-phase H <sub>2</sub> O inclusions	2-phase H <sub>2</sub> O inclusions
$T_{mCO_2}$ , °C	-56.6 (n = 17)	-56.8 ± 0.2 (n = 75)	-56.6 ± 0.04 (n = 46)	-56.7 ± 0.1 (n = 136)	NA	NA
$T_e$ , °C	NA	~ -20 (n = 4)	~ -22 to -17 (n = 15)	~ -28 to -17 (n = 23)	~ -33 to -24 (n = 10)	~ -35 (n = 22)
$T_{mCE}$ , °C	NA	NA	NA	NA	-6.1 to -3.5 (n = 16)	-13.8 to -10.9 (n = 22)
$T_{mCLATH}$ , °C	NA	5.1 to 9.0 (n = 91)	6.6 to 8.0 (n = 44)	5.1 to 8.0 (n = 153)	NA	NA
eq. wt.% NaCl	NA	2.6 to 9.3 (n = 91)	4.0 to 5.9 (n = 44)	2.6 to 9.3 (n = 153)	5.7 to 9.3 (n = 16)	14.9 to 17.6 (n = 22)
$T_{hCO_2}$ , °C	18.3 to 30.2 (n = 17)	27.0 to 31.1 (n = 59)	22.3 to 30.9 (n = 43)	22.3 to 31.1 (n = 110)	NA	NA

**Table 5.1 (continued)**

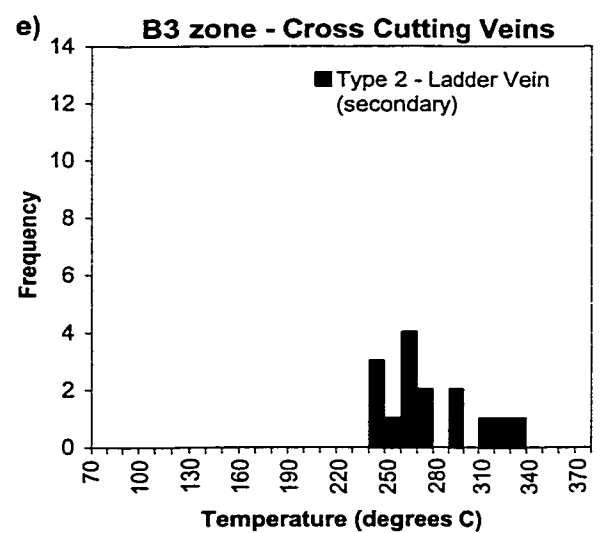
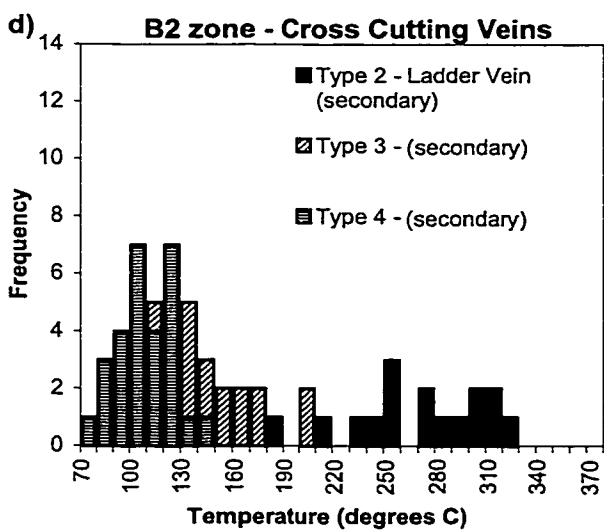
Parameter	Type 1 MSQC Vein (primary)	Type 2 MSQC Vein (primary)	Type 2 MSQC Vein (secondary)	Type 2 Ladder Vein (secondary)	All Type 2 Inclusions	Type 3 Late Brittle Vein (secondary)	Type 4 Late Brittle Vein (secondary)
Th <sub>(L-V)</sub> , °C	NA	206 to 342 (n = 81)	223 to 319 (n = 15)	189 to 331 (n = 33)	189 to 342 (n = 131)	102 to 207 (n = 15)	80 to 147 (n = 28)
CO <sub>2</sub> density, g/cm <sup>3</sup>	0.58 to 0.79 (n = 17)	0.27 to 0.66 (n = 51)	0.61 to 0.68 (n = 7)	0.35 to 0.75 (n = 27)	0.27 to 0.79 (n = 85)	NA	NA
Mole % CO <sub>2</sub>	55.64 to 75.63 (n = 17)	3 to 14 (n = 51)	10 to 16 (n = 7)	6 to 18 (n = 27)	3 to 18 (n = 85)	NA	NA
Mole% H <sub>2</sub> O	NA	86 to 96 (n = 51)	82 to 89 (n = 7)	81 to 93 (n = 27)	81 to 96 (n = 85)	97 to 98 (n = 15)	94 to 95 (n = 19)
Mole% NaCl	NA	1 to 3 (n = 51)	1 to 2 (n = 7)	1 to 2 (n = 27)	1 to 3 (n = 85)	2 to 3 (n = 15)	5 to 6 (n = 19)
Min P, kilobars	NA	1.9 to 3.6 (n = 51)	2.6 to 3.2 (n = 7)	2.0 to 2.8 (n = 26)	1.9 to 3.6 (n = 85)	NA	NA

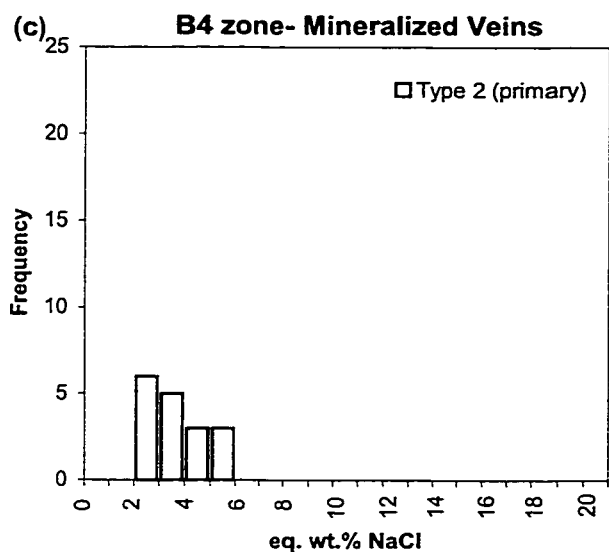
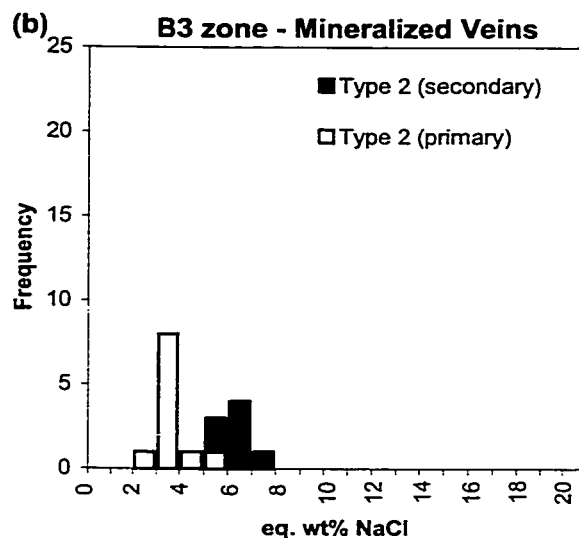
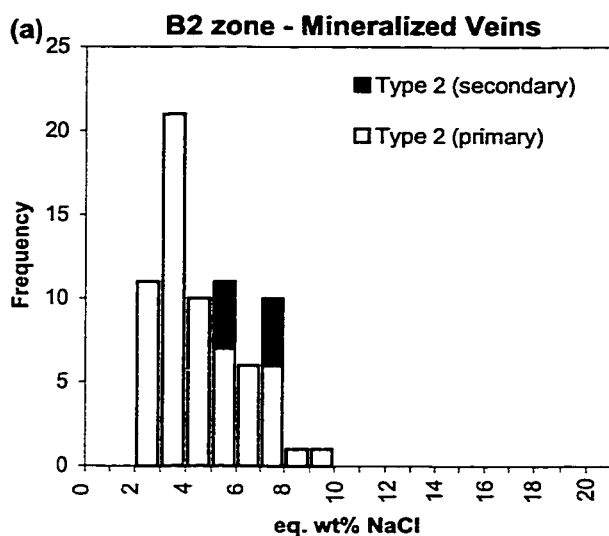


**Figure 5.1.** Salinity (eq. wt.% NaCl) vs homogenization temperature plots for mineralized and barren cross cutting veins in (a) the B2 zone, and (b) the B3 zone (MSQC vein = main stage quartz-carbonate vein).

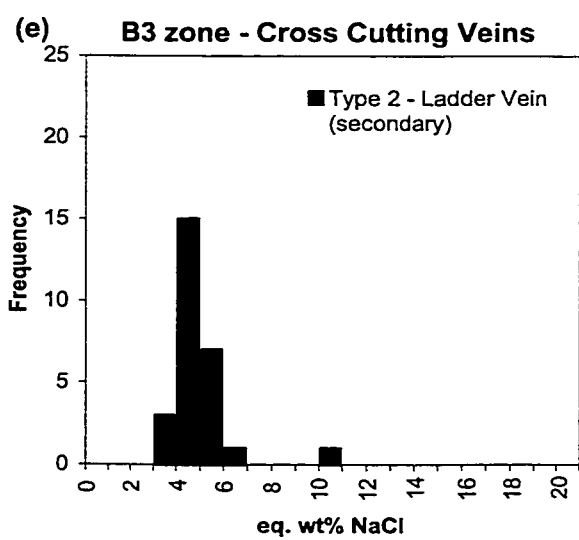
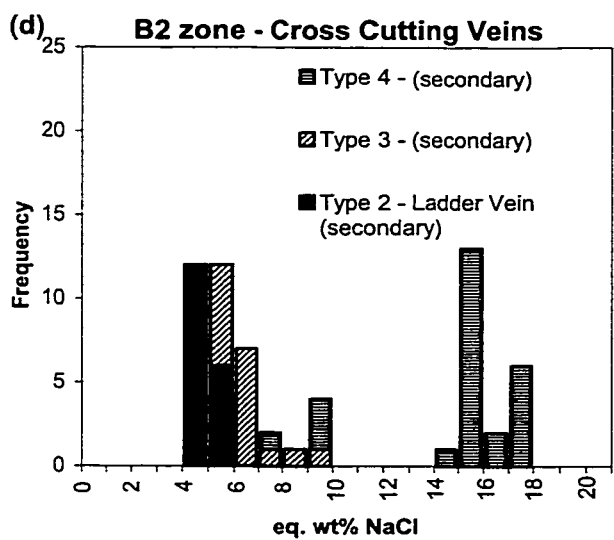


**Figure 5.2.** The homogenization temperature of primary and secondary type 2 fluid inclusions from (a) the B2 zone, (b) the B3 zone, and (c) the B4 zone, and secondary type 2, 3, and 4 inclusions within crosscutting veins in (d) the B2 zone, and (e) the B3 zone, (MSQC vein = main stage quartz-carbonate vein).





**Figure 5.3.** The salinity of primary and secondary type 2 fluid inclusions from (a) the B2 zone, (b) the B3 zone, and (c) the B4 zone, and secondary type 2, 3, and 4 fluid inclusions within cross cutting veins in (d) the B2 zone, and (e) the B3 zone.



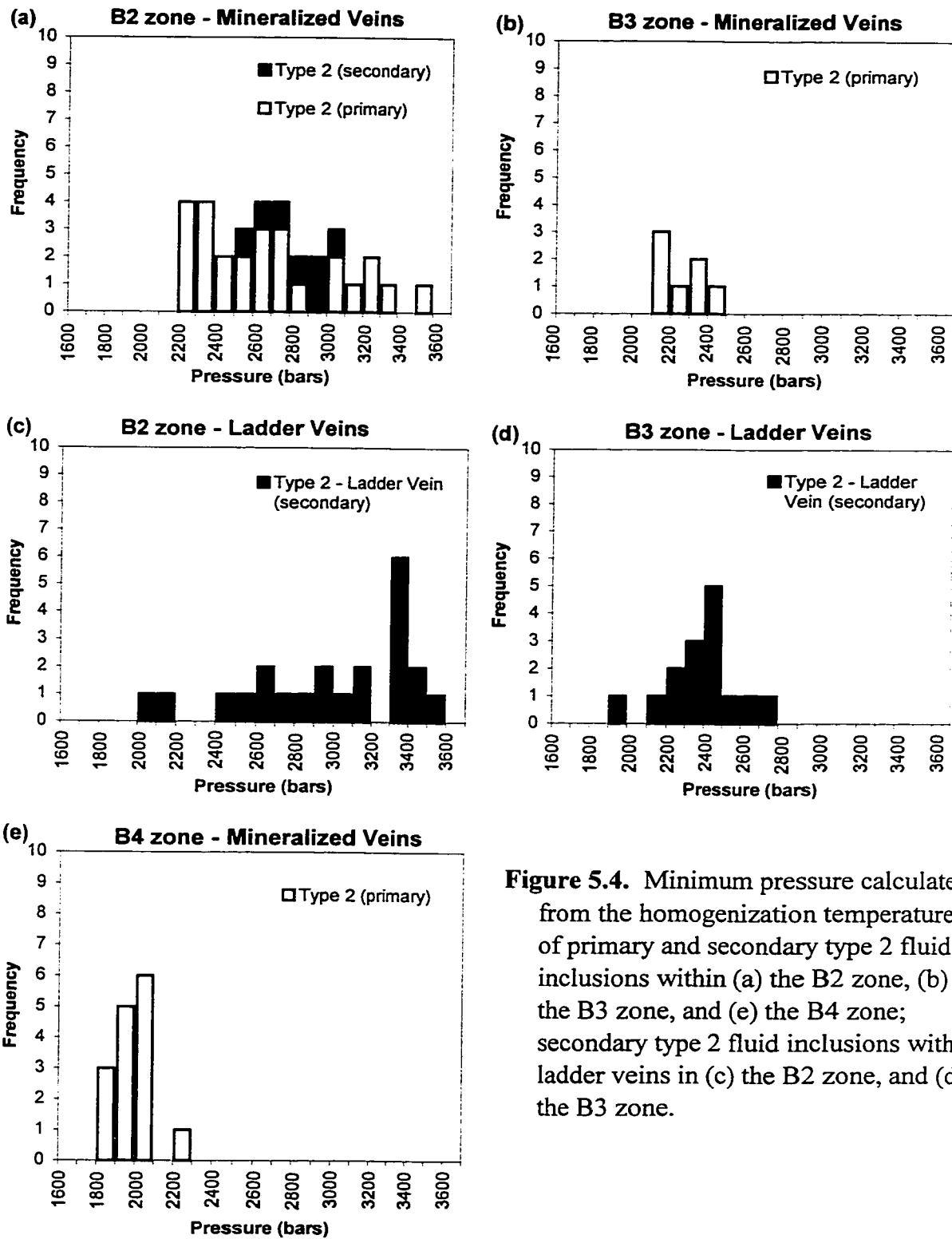


**Figure 5.4.** Minimum pressure calculated from the homogenization temperature of primary and secondary type 2 fluid inclusions within (a) the B2 zone, (b) the B3 zone, and (e) the B4 zone; secondary type 2 fluid inclusions with ladder veins in (c) the B2 zone, and (d) the B3 zone.



Type 1 Fluid Inclusions: Primary type 1 fluid inclusions homogenize by disappearance of the CO<sub>2</sub> vapour bubble between 18.3° and 30.2°C, with an average value of 26.0 ±4.0°C (n = 17), close to the critical temperature of pure carbon dioxide at 31.1°C. Carbon dioxide in Type 1 fluid inclusions melts at -56.6°C (n = 17). Pure CO<sub>2</sub> also has a melting temperature of -56.6°C. Thus, type 1 fluid inclusions appear to contain pure CO<sub>2</sub> with negligible concentrations of other dissolved gases. Type 1 inclusions are always associated with type 2 inclusions and may represent the phase separation of an aqueous-carbonic liquid into a CO<sub>2</sub>-rich gas phase and an H<sub>2</sub>O-rich liquid phase, the implications of which are discussed below (Plate 5.2c.d.e).

Type 2 Fluid Inclusions: Type 2 fluid inclusions from both the main stage quartz-carbonate veins and ladder veins homogenize to liquid at temperatures between 189° and 342°C, with an average value of 269 ±36°C (n = 131). Several type 2 inclusions that homogenize to a critical fluid were observed in the main stage quartz-carbonate veins in the B4 zone (Th between 315° and 319°C, n = 7). In addition, a small number of type 2 fluid inclusions that homogenize to the vapour phase were recorded in both the B2 and B3 zones (n = 9). Type 2 fluid inclusions that homogenize to the vapour phase were not included in average estimates in Table 5.1 or in Figures 5.1 and 5.2 due to their anomalously high homogenization temperatures which suggest they were trapped heterogeneously (Th between 325° and >400°C).

Type 2 fluid inclusions within the main stage quartz-carbonate veins and ladder veins typically have eutectic temperatures between -28° and -17°C (n = 23) suggesting that the solutes were dominated by NaCl (the pure NaCl-H<sub>2</sub>O system has a eutectic

temperature of  $-21.2^{\circ}\text{C}$ ). Thus, the salinities of type 2 fluid inclusions are reported in weight percent NaCl equivalent (eq. wt.% NaCl). However, the apparent range in eutectic temperatures suggests that these inclusions may contain minor amounts of other dissolved salts. Primary and secondary type 2 fluid inclusions from within the main stage quartz-carbonate veins and ladder veins have salinities of 2.6 to 9.3 eq. wt.% NaCl, with an average value of  $4.7 \pm 1.4$  eq. wt.% NaCl ( $n = 153$ ).

The homogenization temperatures of primary type 2 fluid inclusions from within the three mineralized zones range between  $206^{\circ}$  and  $342^{\circ}\text{C}$ , with an average value of  $272 \pm 34^{\circ}\text{C}$  ( $n = 81$ ). In several cases, within the main stage quartz-carbonate veins, primary type 1 ( $\text{CO}_2$  gas-rich) and primary type 2 ( $\text{H}_2\text{O}-\text{CO}_2$  liquid rich) fluid inclusions are trapped together within undeformed quartz grains sheltered from deformation by larger pyrite or carbonate grains (Plate 3.2c, d, e). The coexistence of primary type 1 and 2 fluid inclusions indicates that the hydrothermal fluid was undergoing phase separation at the time of entrapment and was therefore on the liquid-vapour curve for the  $\text{H}_2\text{O}-\text{CO}_2$ -NaCl system. Fluid inclusions trapped during phase separation will homogenize at the temperature of trapping (Brown, 1998). Therefore, the homogenization temperature calculated for these inclusions reflects the actual temperature of the hydrothermal fluid at the time of entrapment. A pressure of 1.9 to 3.6 kilobars, with an average value of  $2.5 \pm 0.5$  kilobars ( $n = 51$ ), was calculated for the hydrothermal fluid using the trapping temperature of primary type 2 fluid inclusions within the three mineralized zones (method outlined in Brown and Lamb, 1986, 1989).

Slight temperature differences become apparent when primary type 2 fluid inclusions within the main stage quartz-carbonate veins in the B2, B3, and B4 zones are

compared (Figure 5.2a,b,c). Primary type 2 fluid inclusions in main stage quartz-carbonate veins from the B3 zone homogenize at slightly lower temperatures ( $222 \pm 9^\circ\text{C}$ ,  $n = 11$ ) than primary type 2 fluid inclusions in the B2 zone ( $270 \pm 26^\circ\text{C}$ ,  $n = 52$ ), whereas primary type 2 fluid inclusions from the B4 zone homogenize at slightly higher temperatures ( $310 \pm 10^\circ\text{C}$ ,  $n = 18$ ).

It is possible that the variation observed in the average homogenization temperatures of primary type 2 fluid inclusions in the three mineralized zones resulted from differences in the thickness of the main stage quartz-carbonate veins in the three zones. Veins in the B3 zone tend to form a stockworked array of relatively thin veins which are more susceptible to heat loss than the thick (up to thirty metres thick in some cases) fissure veins characteristic of the B2 and B4 zones. This may have resulted in the slightly lower temperature of fluid inclusions from the B3 zone.

Alternatively, the scarcity of workable populations of primary fluid inclusions in the B3 and B4 zones may have introduced a bias into the selection of samples for microthermometric analysis. In general, the main stage quartz carbonate veins that make up the three mineralized zones in the Boston deposit have been strongly deformed and recrystallized. As a result, out of seventeen doubly polished thin sections prepared, only one workable population of primary type 2 fluid inclusions was discovered in each of the B3 and B4 zones.

It is likely that minerals deposited later in the life of the hydrothermal system will have experienced less deformation than minerals that were deposited by an earlier and possibly higher temperature phase of the hydrothermal fluid. The lower homogenization temperatures recorded for the type 2 fluid inclusions from the B3 zone may therefore,

simply reflect the influence of a late, lower temperature stage of the auriferous fluid.

Similarly, primary type 2 fluid inclusions with higher homogenization temperatures in the B4 zone may have come from quartz that was deposited by a higher temperature phase of the auriferous fluid.

However, the ranges in homogenization temperatures recorded for primary type 2 fluid inclusions in the three mineralized zones at Boston overlap (Figure 5.2a, b, c) and it is likely that they represent the same auriferous hydrothermal fluid. Mesothermal lode-gold deposits are generally believed to form as the result of long-lived hydrothermal systems. The range in the temperatures displayed by primary type 2 fluid inclusions within the main stage quartz-carbonate veins should therefore be considered an estimate of the total range in the temperature of the hydrothermal fluid responsible for lode-gold mineralization in the Boston deposit.

Secondary, type 2 fluid inclusions within extensional (ladder) veins in the B2 and B3 zones have homogenization temperatures and salinities that are almost identical to that of primary type 2 fluid inclusions in the mineralized zones (Figures 5.1, 5.2, and 5.3). Type 2 fluid inclusions within ladder veins in the B2 zone have average homogenization temperatures of  $271 \pm 39^{\circ}\text{C}$  ( $189^{\circ}$  to  $322^{\circ}\text{C}$ ,  $n = 16$ ), and salinities of  $4.8 \pm 0.5$  eq. wt.% NaCl (4.1 to 5.8 eq. wt.% NaCl,  $n = 18$ ). In the B3 zone type 2 fluid inclusions within ladder veins have homogenization temperatures of  $278 \pm 29^{\circ}\text{C}$  ( $241^{\circ}$  to  $331^{\circ}\text{C}$ ,  $n = 17$ ) and salinities of  $4.9 \pm 0.5$  eq. wt.% NaCl (4.0 to 5.9 eq. wt.% NaCl,  $n = 27$ ). Minimum pressures between 2.0 and 2.8 kilobars, with an average value of  $2.8 \pm 0.5$  kilobars ( $n = 26$ ), were calculated for secondary type 2 fluid inclusions hosted by ladder veins in the B2 and B3 zones using the homogenization temperature of these inclusions

(method outlined in Brown and Lamb, 1986, 1989). This is also well within the range of pressures calculated for the hydrothermal fluid represented by primary type 2 fluid inclusions within the main stage quartz-carbonate veins (1.9 to 3.6 kilobars; Figure 5.4).

Primary and secondary type 2 fluid inclusions in the main stage quartz-carbonate veins and ladder veins contain between 3 and 18 mole percent CO<sub>2</sub> (n = 85) with a density of 0.3 to 0.8 g/cm<sup>3</sup> (n = 85). Carbon dioxide in the majority of type 2 fluid inclusions melts around -56.7 ±0.1°C (n = 136). Pure CO<sub>2</sub> melts at -56.6°C. Therefore, the presence of other dissolved gases in type 2 fluid inclusions appears to be negligible. However, rare CO<sub>2</sub> melting temperatures as low as -57.1°C have been recorded which may indicate the local presence of a minor amount of some other dissolved gas species, such as CH<sub>4</sub>, N<sub>2</sub>, or H<sub>2</sub>S. The CO<sub>2</sub> phase of type 2 fluid inclusions typically homogenizes to liquid between 22.3 and 31.1°C, with an average value of 29.2 ±2.0°C (n = 70), although several inclusions (n = 40) in which the carbonic phase homogenizes critically or to the vapour phase have also been recorded (Appendix C).

Type 3 Fluid Inclusions: Type 3 fluid inclusions homogenize by disappearance of the vapour bubble between 120° and 207°C, with an average value of 159 ±25°C (n = 15). These inclusions contain no CO<sub>2</sub> and are generally gas poor. At 25°C these inclusions have vapour volume fractions of 0.05 ±0.02 (n = 16). The eutectic temperature of type 3 inclusions is between -33° and -24°C, with an average value of -26 ±4°C (n = 10). The salinity of type 3 fluid inclusions, calculated in weight percent NaCl equivalent, is between 5.7 and 9.3 eq. wt.% NaCl, with an average value of 6.7 ±1.1 eq. wt.% NaCl (n = 16). The minimum pressure that was calculated for type 3 fluid inclusions from

isochores at the temperature of homogenization is between 5 and 15 bars and is likely a gross underestimation of the true trapping pressure of these fluid inclusions and will not be considered further.

Type 4 Fluid Inclusions: Type 4 fluid inclusions homogenize to the liquid phase between 80° and 147°C, with an average value of  $113 \pm 18^\circ\text{C}$  (n = 28). These inclusions contain even less vapour than type 3 inclusions (estimated vapour volume fractions at 25°C of around 0.02, n = 41). The eutectic temperature of type 4 fluid inclusions is approximately  $-35^\circ\text{C}$  (n = 22). These inclusions have salinities that fall between 14.9 and 17.6 eq. wt.% NaCl, with an average value of  $16.1 \pm 0.9$  eq. wt.% NaCl (n = 22). One group of highly saline fluid inclusions with eutectic temperatures around  $-55^\circ\text{C}$  (n = 11) was also observed in the B2 zone. Minimum pressures between 4 and 6 bars ( $5 \pm 1$  bars, n = 19) were calculated for type 4 fluid inclusions using the temperature of homogenization and like the pressures calculated for type 3 fluid inclusions are a gross underestimate of the true trapping pressure and are not considered further.

Accurate microthermometric measurements were not possible on fluid inclusions within the flat veins. Fluid inclusions within these veins are very small, typically  $\ll 5$   $\mu\text{m}$ , and have a dark appearance making them difficult to work with (Plate 5.2e). Quartz within the flat veins has been strongly deformed and recrystallized. The fluid inclusions within these veins tend to be irregular two- and three-phase fluid inclusions with varied liquid-to-vapour ratios. Consequently any microthermometric information that could have been obtained from these inclusions would be meaningless.

### **5.3. Stable Isotopes**

#### **5.3.1. Carbonate and Quartz (Mineralized Veins)**

The results of the stable isotopic analyses of ferroan dolomite and ankerite from gold-bearing veins in the Boston deposit are presented in Appendix D and summarised in Table 5.2 and Figure 5.5a,b. The results of the stable isotopic analyses of vein quartz are presented in Appendix E and Figure 5.5c, and are summarised in Table 5.3.

The stable isotopic compositions of ferroan dolomite and ankerite separated from auriferous veins in the Boston deposit are very tightly grouped (Figure 5.5a,b), varying by only 1.6‰ in both  $\delta^{13}\text{C}$  (-4.7 to -3.1‰, n = 15) and  $\delta^{18}\text{O}$  (11.2 to 12.8‰, n = 15). The total range in the  $\delta^{18}\text{O}$  composition of quartz separated from the auriferous veins is also small, varying by only 2.1‰ (12.8 to 14.9‰, n = 12; Figure 5.5c).

Even if the three mineralized zones in the Boston deposit are looked at separately the  $\delta^{13}\text{C}$  values of carbonate minerals appears to be quite similar (Figure 5.5a).

Carbonate minerals separated from B2 zone have  $\delta^{13}\text{C}$  values of -4.6 to -3.1‰, with an average value of  $-3.1 \pm 0.6\text{‰}$  (n = 5), whereas carbonates separated from the B3 zone have  $\delta^{13}\text{C}$  values of -4.7 to -3.2‰, with an average value of  $-4.0 \pm 0.5\text{‰}$ , n = 9. The only sample analysed from the B4 zone has a  $\delta^{13}\text{C}$  value of -3.1‰.

In contrast, the  $\delta^{18}\text{O}$  values of carbonate and quartz separated from the three mineralized zones shows some isotopic separation (Figure 5.5b,c). The  $\delta^{18}\text{O}$  values of

**Table 5.2.** Summary of the results of the stable isotopic analysis of calcite, ankerite, and ferroan dolomite separated from mineralized and barren veins, and wallrocks associated with the Boston deposit (Avg = average value, SD = standard deviation; \* = outlying values were not included in calculated range and average).

Host Rock	$\delta^{13}\text{C PDB, ‰}$		$\delta^{18}\text{O VSMOW, ‰}$		No. of Analyses	No. of Analyses	Typical Whole Rock Value		Reference
	Range	Avg $\pm$ SD	Range	Avg $\pm$ SD			$\delta^{13}\text{C PDB, ‰}$	$\delta^{18}\text{O VSMOW, ‰}$	
B2 Zone	-4.6 to -3.1	-3.1 $\pm$ 0.6	12.0 to 12.8	12.4 $\pm$ 0.3	5	5			
B3 Zone	-4.7 to -3.2	-4.0 $\pm$ 0.5	11.2 to 12.2	11.7 $\pm$ 0.3	9	9			
B4 Zone	-3.1	—	12.8	—	1	1			
<b>All Zones</b>	<b>-4.7 to -3.1</b>	<b>-3.9 <math>\pm</math>0.6</b>	<b>11.2 to 12.8</b>	<b>12.0 <math>\pm</math>0.5</b>	<b>15</b>	<b>15</b>	<b>-10.0 to +2.2</b>	<b>9 to 14</b>	Groves and Foster, 1991; de Ronde et al., 1997; Kerrich, 1987
Basalt	-2.8 to +0.7	-1.8 $\pm$ 0.8	10.7 to 13.8*	12.4 $\pm$ 0.9*	33*	33*	0 $\pm$ 2	8.5 to 14.7	Muehlenbachs, 1986; Wood et al., 1986; Muehlenbachs and Clayton, 1972
Basalt Vein	-2.9 to 0.5	-1.7 $\pm$ 1.0	12.2 to 13.9*	12.9 $\pm$ 0.7*	7*	7*			
Gabbro	-3.8 to -2.3	-3.2 $\pm$ 0.5	10.3 to 14.8	12.0 $\pm$ 1.9	13	13	-5 $\pm$ 2	5.5 to 11.0	Muehlenbachs, 1986; Ohmoto and Rye, 1979; Taylor and Sheppard, 1986
Gabbro Vein	-2.9/-3.5/-3.6	—	9.4/11.0/11.0	—	3	3			



**Table 5.2 (continued)**

Host Rock	$\delta^{13}\text{C PDB, ‰}$		$\delta^{18}\text{O VSMOW, ‰}$		No. of Analyses	Typical Whole Rock Value	Reference	
	Range	Avg $\pm$ SD	Range	Avg $\pm$ SD				$\delta^{13}\text{C PDB, ‰}$
Turbiditic Sediment	-6.7 to -3.9	-5.0 $\pm$ 1.0	10.9 to 14.1	12.3 $\pm$ 0.8	11	> -15	8 to 25	Faure, 1986a; Lohgstaffe, 1987
Turbiditic Sediment Vein	-3.1 to -4.8*	-4.1 $\pm$ 0.6*	11.8 to 12.6*	12.1 $\pm$ 0.3*	7*			
Graphitic Argillite	-6.9 to -2.5	-3.9 $\pm$ 1.8	12.5 to 18.9	15.6 $\pm$ 2.2	6	> -15	10 to 30	Faure, 1986a; Lohgstaffe, 1987
Graphitic Argillite Vein	-1.6	—	15.9	—	1			
Andesite Dyke	-3.3 to -2.0	-2.6 $\pm$ 0.5	11.8 to 14.0	12.7 $\pm$ 0.7	7	-5 $\pm$ 2	5.5 to 11.0	Muehlenbachs, 1986; Ohmoto and Rye, 1979; Taylor and Sheppard, 1986
Strongly Deformed Rock	-3.2 to -1.6	-2.2 $\pm$ 0.5	12.0 to 13.2	12.7 $\pm$ 0.4	8			
Strongly Deformed Rock Vein	-3.0 to -1.7	-2.1 $\pm$ 0.6	14.2 to 16.1	15.3 $\pm$ 0.8	4			

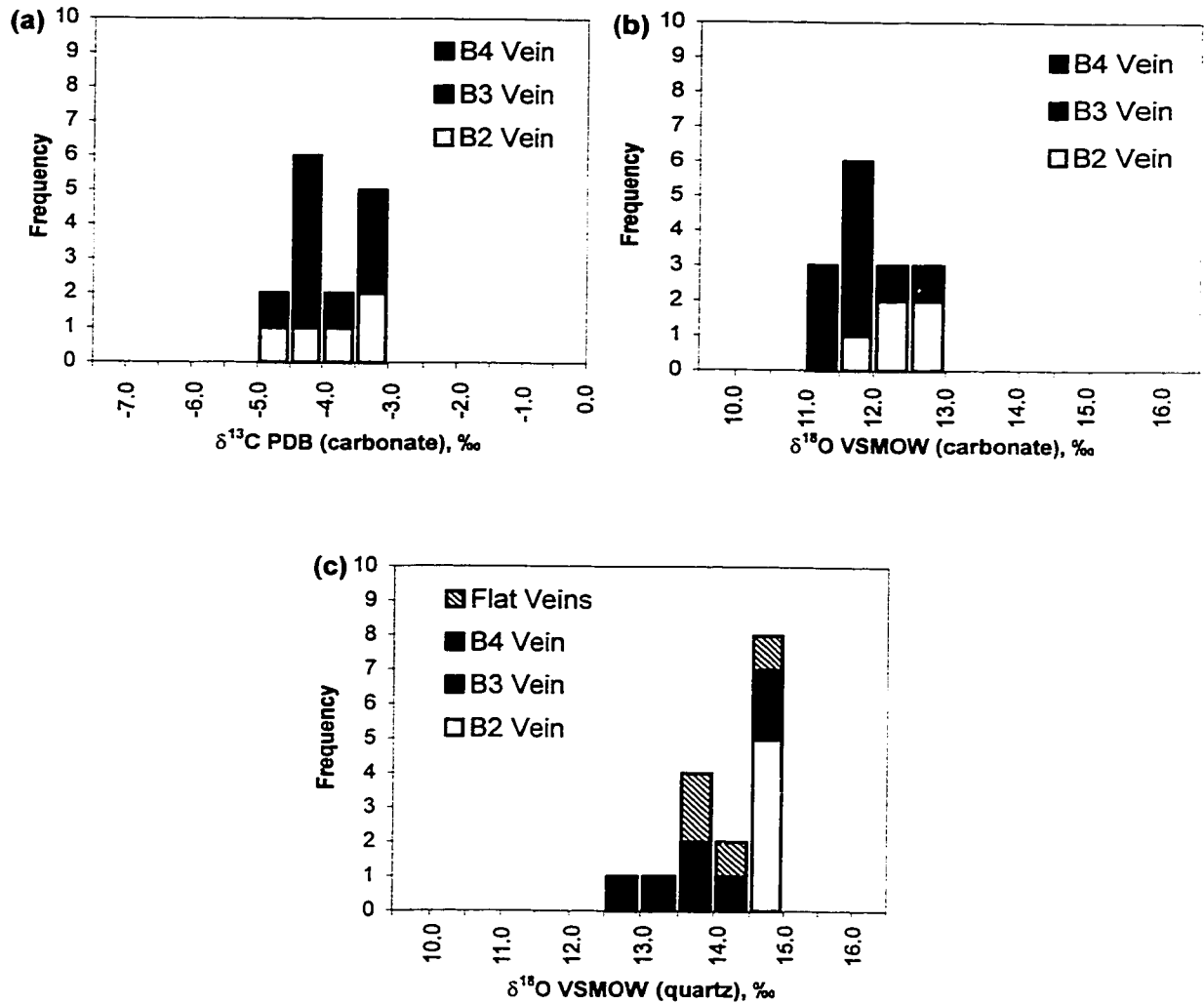


**Figure 5.5.** The (a) carbon and (b) oxygen stable isotopic composition of carbonate separated from gold-bearing veins within the B2, B3, and B4 zones; and (c) the oxygen stable isotopic composition of quartz separated from gold-bearing and flat veins in the B2, B3, and B4 zones.

**Table 5.3.** Summary of the results of the stable isotopic analysis of quartz separated from mineralized and barren veins in the Boston deposit (Avg = average value; SD = standard deviation)

Host Rock	$\delta^{18}\text{O}$ VSMOW, ‰		No. of Analyses
	Range	Avg $\pm$ SD	
B2 Zone	14.6 to 14.9	14.7 $\pm$ 0.1	5
B3 Zone	12.8 to 14.3	13.6 $\pm$ 0.6	5
B4 Zone	14.7/14.8	—	2
<b>All Zones</b>	<b>12.8 to 14.9</b>	<b>14.3 <math>\pm</math>0.7</b>	<b>12</b>
Flat Vein	13.8 to 14.6	14.2 $\pm$ 0.3	4
Basalt	14.2 to 16.6	15.6 $\pm$ 0.7	8
Gabbro	10.2 to 13.4	11.8 $\pm$ 1.2	6
Turbiditic Sediment	13.2 to 14.6	14.1 $\pm$ 0.6	4
Graphitic Argillite	14.1 to 16.4	15.5 $\pm$ 0.9	4
Strongly Deformed Rock	12.9/14.8	—	2

carbonate separated from the B2 zone fall between 12.0 and 12.8‰ with an average value of  $12.4 \pm 0.3\text{‰}$  ( $n = 5$ ); one carbonate sample from the B4 zone has a  $\delta^{18}\text{O}$  value of 12.8‰; and carbonate minerals in the B3 zone have  $\delta^{18}\text{O}$  values of 11.2 to 12.2‰ with an average value of  $11.7 \pm 0.3\text{‰}$  ( $n = 9$ ). Quartz separated from the B2 zone has  $\delta^{18}\text{O}$  compositions between 14.6 to 14.9‰, with an average value of  $14.7 \pm 0.1\text{‰}$  ( $n = 5$ ); two samples of quartz separated from the B4 zone have  $\delta^{18}\text{O}$  compositions of 14.7 and 14.8‰; whereas quartz from the B3 zone has slightly lower  $\delta^{18}\text{O}$  compositions of 12.8 to 14.3‰, with an average value of  $13.6 \pm 0.6\text{‰}$  ( $n = 5$ ).

It is not reasonable to assume that the variation observed in the stable isotopic composition of minerals separated from the B2, B3, and B4 zones is simply a factor of differences in the composition of the particular carbonate species analysed. A one per mil shift in  $\delta^{18}\text{O}$  values was observed in both quartz and carbonate separated from the auriferous veins and, therefore, must be a quality that was originally present in the fluid itself. It is also unlikely that the  $\delta^{18}\text{O}$  shift was the result of error introduced during preparation of the samples. Several samples of carbonate and quartz from all three mineralized zones were duplicated and re-run to ensure that the results were consistent.

The slight  $\delta^{18}\text{O}$  shift observed in carbonates in the main stage quartz-carbonate veins in the three mineralized zones may be related to the numerous cross cutting extensional and late brittle veinlets that occur within these veins. Although great care was taken to avoid these veinlets during sample selection and preparation, their abundance within some auriferous veins in the B2 and B4 zones made this impossible. Provided that all other variables remain constant, quartz and carbonate deposited within the late veins from a lower temperature fluid will be enriched in the heavy isotope of

oxygen relative to the main stage veins according to the quartz-water or carbonate-water fractionation factor (Matsuhisa et al., 1979). As a result, a slight  $\delta^{18}\text{O}$  enrichment may have been created in samples from the B2 and B4 zones, where small amounts of quartz and carbonate deposited within the late veins were unavoidably analysed together with quartz and carbonate deposited within the main stage quartz-carbonate veins.

In general, the  $\delta^{13}\text{C}$  values of carbonate minerals are not as sensitive to small fluctuations in temperature as  $\delta^{18}\text{O}$  values (Ohmoto and Rye, 1979). As a result, the  $\delta^{13}\text{C}$  values of carbonate minerals deposited within main stage quartz-carbonate veins in the Boston deposit tend to be fairly uniform (Figure 5.5a).

That being said there is a great deal of overlap in the stable isotopic composition of quartz and carbonate separated from the three mineralized zones in the Boston deposit (Figures 5.5). Isotopically quartz and carbonate in the B2, B3, and B4 zones appear to have been deposited at roughly the same time from the same auriferous fluid and for all intents and purposes can be considered one uniform population.

The  $\delta^{18}\text{O}$  values of quartz separated from flat veins within the Boston deposit range from 13.8 and 14.6‰, with an average value of  $14.2 \pm 0.3\text{‰}$  ( $n = 4$ , Figure 5.5c). These values also fall within the range of  $\delta^{18}\text{O}$  values calculated for quartz separated from the three mineralized zones that make up the Boston deposit.

### **5.3.2. Carbonate (Country Rocks)**

The distribution of  $\delta^{13}\text{C}$  versus  $\delta^{18}\text{O}$  values for ferroan dolomite, ankerite and calcite separated from mineralized veins within the Boston deposit and disseminated throughout the hydrothermally and metamorphically altered igneous and sedimentary

rocks that host and surround the Boston deposit are plotted in Figure 5.6a. The results of the stable isotopic analyses of these minerals are presented in Appendix D and are summarised in Table 5.2.

It is clear from Figure 5.6a that the stable isotopic composition of carbonate minerals disseminated throughout the different rock types in the Boston area form distinct isotopic populations that show more variation than carbonate minerals within the gold-bearing veins. Only immediately adjacent to the main stage quartz-carbonate veins, where the effects of hydrothermal alteration were most intense, do carbonate minerals in the wallrocks have stable isotopic compositions that are similar to carbonate minerals from within the gold-bearing veins themselves (Figure 5.6b). Carbonate minerals within the wallrocks directly adjacent to auriferous quartz-carbonate veins in the Boston deposit have  $\delta^{13}\text{C}$  values of -4.0 to -2.9‰, with an average value of  $-3.3 \pm 0.4\text{‰}$  ( $n = 5$ ) and  $\delta^{18}\text{O}$  values of 11.8 to 13.0‰, with an average value of  $12.4 \pm 0.4\text{‰}$  ( $n = 5$ ). Ankerite and ferroan dolomite deposited within the auriferous quartz-carbonate veins have  $\delta^{13}\text{C}$  values of -4.7 to -3.1‰, with an average value of  $-3.9 \pm 0.6\text{‰}$  ( $n = 15$ ) and  $\delta^{18}\text{O}$  values 11.3 to 12.8‰, with an average value of  $12.0 \pm 0.5\text{‰}$  ( $n = 15$ ).

In contrast, secondary carbonate minerals deposited within the country rocks distal to the mineralized veins have distinct stable isotopic compositions that appear to be similar to the stable isotopic composition of the rock types that host them (Figure 5.6a and Table 5.2).

Mafic Volcanic Rocks: Highly altered pillowed basalts that have interacted with, and been altered by cold seawater on the sea floor generally have whole rock  $\delta^{18}\text{O}$

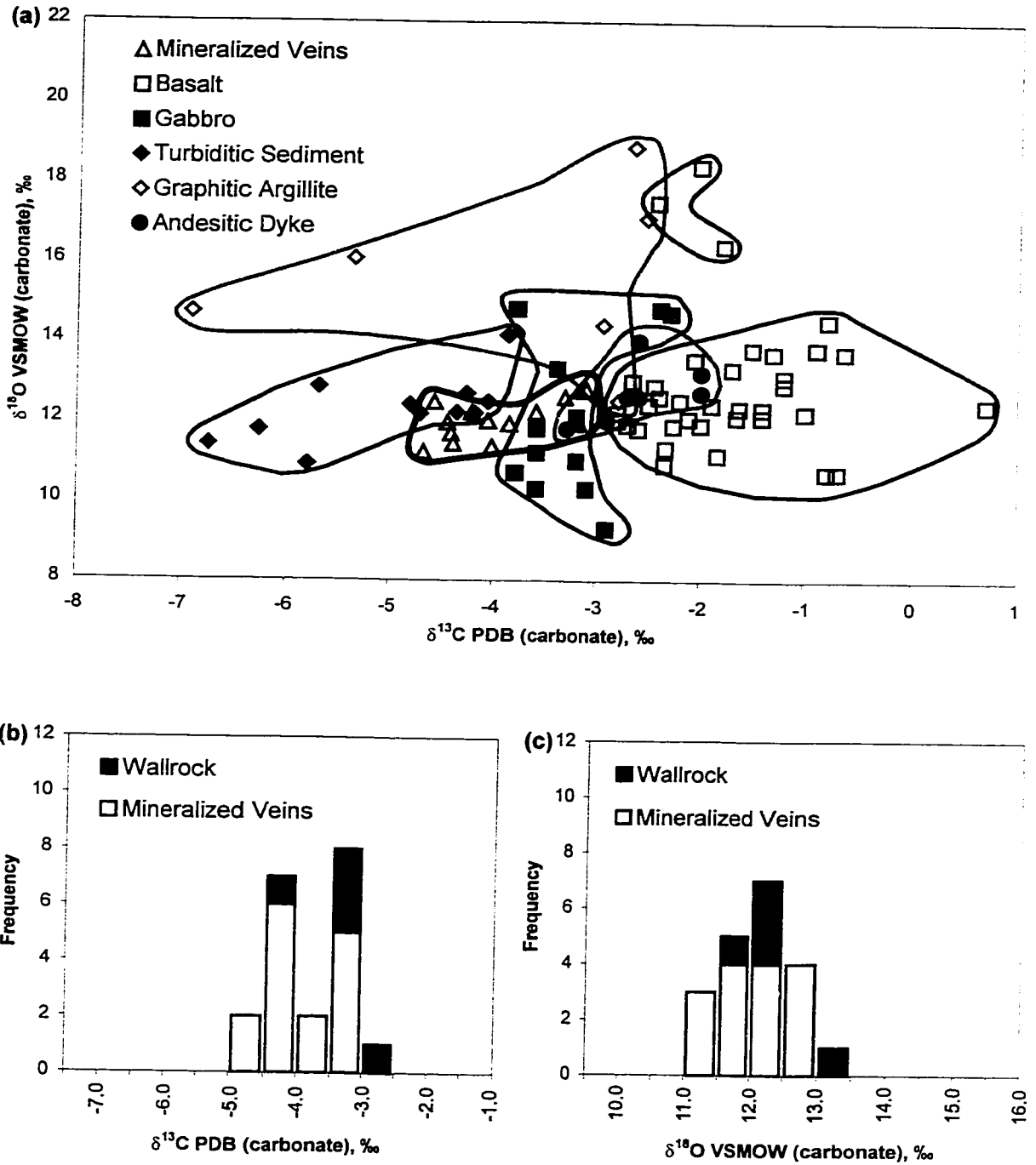


**Figure 5.6.** The stable isotopic composition of carbonate minerals separated from gold-bearing veins and (a) disseminated throughout the country rocks distal to the Boston deposit; and (b) and (c) wallrocks directly adjacent to the mineralized veins within the Boston deposit.

compositions between 8.5 and 14.7‰ (Muehlenbachs and Clayton, 1972). These rocks also typically contain disseminated carbonate minerals with  $\delta^{13}\text{C}$  compositions of  $0 \pm 2\text{‰}$  (Muehlenbachs, 1987, Wood et al., 1986). Secondary carbonates disseminated throughout the greenschist facies basaltic rocks in the Boston area were found to have similar stable isotopic compositions to typical seafloor altered pillowed basalts. Secondary carbonate minerals within altered basaltic rocks in the Boston area were found to have  $\delta^{13}\text{C}$  values of -2.8 to 0.7‰, with an average value of  $-1.8 \pm 0.8\text{‰}$  ( $n = 36$ ), and excluding samples JSB-016, JSB-026, and JSB-175, have  $\delta^{18}\text{O}$  values of 10.7 to 13.8‰, with an average value of  $12.4 \pm 0.9\text{‰}$  ( $n = 33$ ).

Secondary carbonate within samples JSB-016, JSB-026, and JSB-175 were found to have anomalously high  $\delta^{18}\text{O}$  compositions of 16.4, 17.5, and 18.4‰ respectively, and plot as an isolated group in Figure 5.6a. These three samples originated from an anomalous wedge of relatively unaltered basaltic rock that occurs within the Boston fault zone approximately halfway between and slightly to the north of the B2 and B3 zones. Carbonate minerals with  $\delta^{18}\text{O}$  values such as these may have been deposited by a fluid that was isotopically unique or at a much lower temperature than the fluid responsible for hydrothermal alteration and gold mineralization in the rest of the Boston deposit. However, at this time the true nature of this unit and the carbonate minerals it contains is not well understood.

Gabbros: Greenschist facies gabbroic rocks surrounding the Boston deposit contain secondary carbonate minerals with  $\delta^{13}\text{C}$  values of -3.8 to -2.3‰, with an average value of  $-3.2 \pm 0.5\text{‰}$  ( $n = 13$ ), and  $\delta^{18}\text{O}$  values of 10.3 to 14.8‰, with an average value of 12.0



$\pm 1.9\text{‰}$  ( $n = 13$ , Figure 5.6a). Fresh igneous rocks, including gabbros, generally have whole rock  $\delta^{13}\text{C}$  values of around  $-5 \pm 2\text{‰}$  (Muehlenbachs, 1986; Ohmoto and Rye, 1979) and whole rock  $\delta^{18}\text{O}$  compositions between 5.5 and 11.0‰ (Taylor and Sheppard, 1986).

In the marine environment the low temperature hydrothermal alteration of a fresh package of gabbroic rock by circulating seawater shortly after their emplacement will typically result in a slight  $\delta^{13}\text{C}$  and  $\delta^{18}\text{O}$  whole rock enrichment (Muehlenbachs, 1986). However, the whole rock stable isotopic composition of the intrusive gabbroic rocks will generally never become as enriched in  $\delta^{13}\text{C}$  and  $\delta^{18}\text{O}$  as is commonly observed in hydrothermally altered pillowed basalts that were extruded directly onto the seafloor (Muehlenbachs, 1986).

Secondary carbonate minerals disseminated throughout the metamorphically altered gabbroic rocks in the Boston area were found to be slightly enriched in  $\delta^{13}\text{C}$  and  $\delta^{18}\text{O}$  with respect to the whole rock  $\delta^{13}\text{C}$  and  $\delta^{18}\text{O}$  values typical of fresh igneous rocks. However, the  $\delta^{13}\text{C}$  composition of secondary carbonate within the gabbroic rocks is not as enriched as secondary carbonate from within altered basaltic rocks in the same area, and forms a distinct population in Figure 5.6a.

Andesitic Dyke: Secondary carbonate disseminated throughout a metre wide, hydrothermally altered andesitic dyke that runs subparallel to the Boston fault zone between the B2 and B3 zones also has a stable isotopic composition that resembles the whole rock stable isotopic composition of slightly altered igneous rock. Carbonate minerals within the andesitic dyke have  $\delta^{13}\text{C}$  values of  $-3.3$  to  $-2.0\text{‰}$ , with an average

value of  $-2.6 \pm 0.5\text{‰}$  ( $n = 7$ ), and  $\delta^{18}\text{O}$  values of 11.8 to 14.0‰, with an average value of  $12.7 \pm 0.4\text{‰}$  ( $n = 7$ ).

Turbiditic Sediments: Clastic sedimentary rocks generally have whole rock  $\delta^{18}\text{O}$  compositions that fall somewhere between those of unaltered igneous rocks and clay minerals, depending on the relative proportion of each component in the rock, with most samples having  $\delta^{18}\text{O}$  values between 8 and 25‰ (Longstaffe, 1987). The whole rock  $\delta^{13}\text{C}$  composition of marine clastic sedimentary rocks is generally very low, typically less than  $-15\text{‰}$  (Faure, 1986a).

Secondary carbonate minerals within metamorphically altered turbiditic sediments in the Boston area were found to have stable isotopic compositions that are depleted in  $\delta^{13}\text{C}$  with respect to secondary carbonate minerals within metamorphically altered basalts and gabbros in the Boston area (Figure 5.6a). The  $\delta^{13}\text{C}$  values of secondary carbonate minerals in the turbiditic sediments fall between  $-6.7$  and  $-3.9\text{‰}$ , with an average value of  $-5.0 \pm 1.0\text{‰}$  ( $n = 11$ ). On the other hand the  $\delta^{18}\text{O}$  values of secondary carbonate minerals separated from the turbiditic sediments fall between 10.9 and 14.1‰, with an average value of  $12.3 \pm 0.8\text{‰}$  ( $n = 11$ ) and are similar to the  $\delta^{18}\text{O}$  values calculated for secondary carbonate minerals disseminated throughout metamorphically altered basalts and gabbros in the Boston area.

Graphitic Argillites: Secondary carbonate minerals disseminated throughout the greenschist facies graphitic argillites in the Boston area have  $\delta^{13}\text{C}$  values of  $-6.9$  to  $-2.5\text{‰}$ , with an average value of  $-3.9 \pm 1.8\text{‰}$  ( $n = 6$ ), and  $\delta^{18}\text{O}$  values of 12.5 to 18.9‰,

with an average value of  $15.6 \pm 2.2\text{‰}$  ( $n = 6$ ). For the most part the  $\delta^{13}\text{C}$  composition of secondary carbonate minerals within graphitic argillites and turbiditic sediments from the Boston area are similar. However, the  $\delta^{18}\text{O}$  composition of secondary carbonate minerals from within the graphitic argillites tends to be enriched with respect to secondary carbonate minerals within turbiditic sediments from the same area (Figure 5.6a).

In general clastic sedimentary rocks become enriched in  $\delta^{18}\text{O}$  according to the amount of clay minerals they contain. Argillites are the product of the weak metamorphism of a mudstone or shale and are composed primarily of clay minerals. As a result, argillites generally have  $\delta^{18}\text{O}$  whole rock compositions that fall between 10 and 30‰ (Longstaffe, 1987). The whole rock  $\delta^{13}\text{C}$  composition of all marine sedimentary rocks is typically less than -15‰ (Faure, 1986a).

Carbonate Sediment: A sample of a syngenetic carbonate unit from the Discovery area, approximately 58km north of the Boston deposit (Figure 1.2), was found to have a  $\delta^{13}\text{C}$  value of 0.2‰ and a  $\delta^{18}\text{O}$  value of 20.0‰ (Appendix D). Precambrian carbonate sediments precipitating out of cold seawater generally have  $\delta^{13}\text{C}$  values of approximately  $0.4 \pm 2.7\text{‰}$  (Ohmoto and Rye, 1979; Schidlowski et al., 1975). Assuming that the stable isotopic composition of marine carbonates has not changed significantly through geologic time, a  $\delta^{18}\text{O}$  value of approximately 20.0‰ would also be characteristic of this rock type (Faure, 1986b).

Strongly Deformed Samples: Within the Boston fault zone all rock types have been subjected to intense deformation and pervasive hydrothermal alteration. In these highly

altered and deformed samples the true nature of the rocks becomes impossible to determine in hand sample and thin section. Secondary carbonate minerals within several samples of intensely foliated and hydrothermally altered rock were found to have  $\delta^{13}\text{C}$  compositions of -3.2 to -1.6‰, with an average value of  $-2.2 \pm 0.5\text{‰}$  ( $n = 8$ ), and  $\delta^{18}\text{O}$  compositions of 12.0 to 13.2‰, with an average value of  $12.7 \pm 0.4\text{‰}$  ( $n = 8$ ). These samples are more similar, at least isotopically, to the stable isotopic composition of secondary carbonate minerals within the metamorphically altered basaltic and gabbroic rocks than they are to secondary carbonate minerals within the sedimentary rocks in the Boston area (Figures 5.6a and 5.7a,b). It is therefore likely that the strongly altered rocks that were analysed in this study were originally igneous rather than sedimentary in composition. Graphitic argillites occur in close proximity to the B2 and B4 zones and are structurally important in the formation of these two mineralized zones; however, the sedimentary rocks do not appear to directly host auriferous veins in the Boston deposit.

In Figures 5.8 to 5.15 the isotopic composition of secondary carbonate from within the metamorphically altered igneous and sedimentary rocks in the Boston area have been plotted with respect to distance from the mineralized veins. In these figures there does not appear to be a consistent relationship between the sample location and the isotopic composition of the secondary carbonate minerals in the country rocks. Rather, as noted above, secondary carbonate minerals within the different lithologies have a range of stable isotopic compositions that appears to reflect the stable isotopic composition of the rocks that host them.

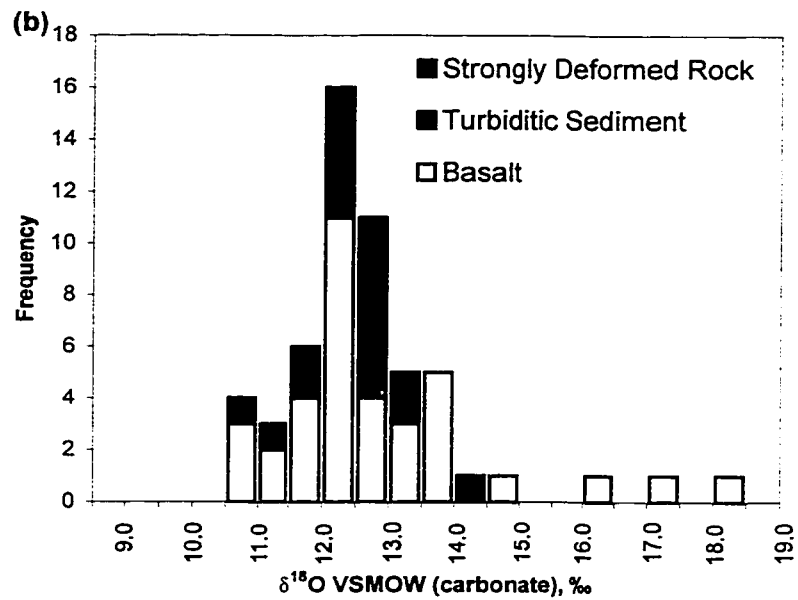
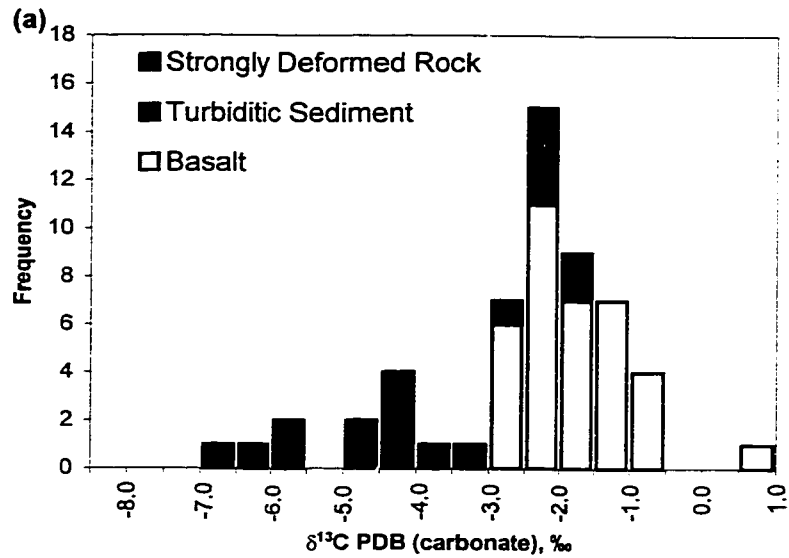


**Figure 5.7.** The (a) carbon, and (b) oxygen stable isotopic composition of secondary carbonate minerals disseminated throughout metamorphically altered basaltic rocks, turbiditic sediments, and strongly deformed rocks associated with the Boston deposit

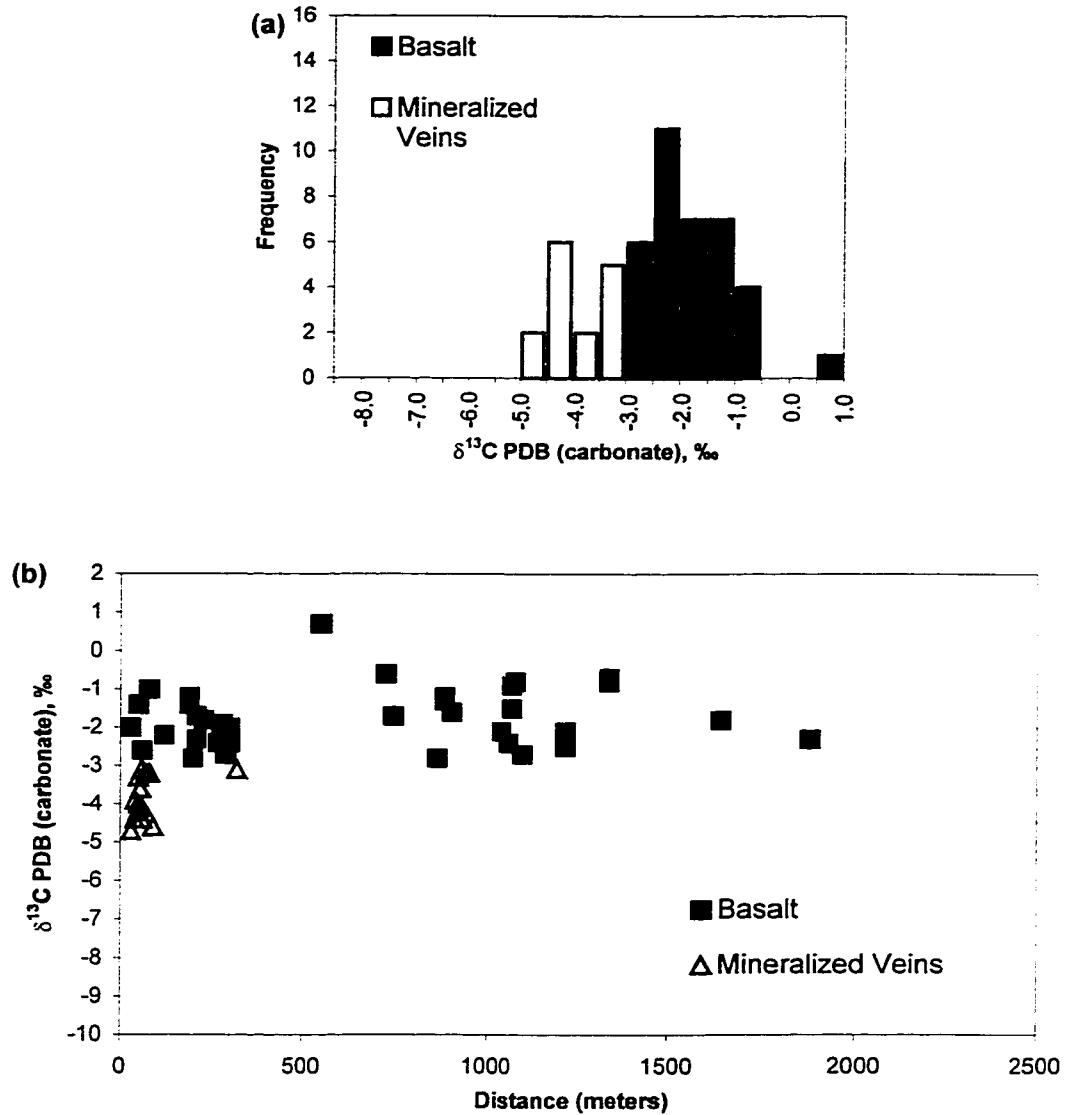


**Figure 5.8.** The carbon stable isotopic composition of secondary carbonate minerals within (a) gold-bearing veins and altered basaltic rocks in the Boston area and (b) the carbon stable isotopic composition of secondary carbonate minerals from within basaltic rocks with respect to distance from mineralized veins in the Boston area (all distances measured from 7505000N and 441150E, approximately halfway between the B2 and B3 zones).

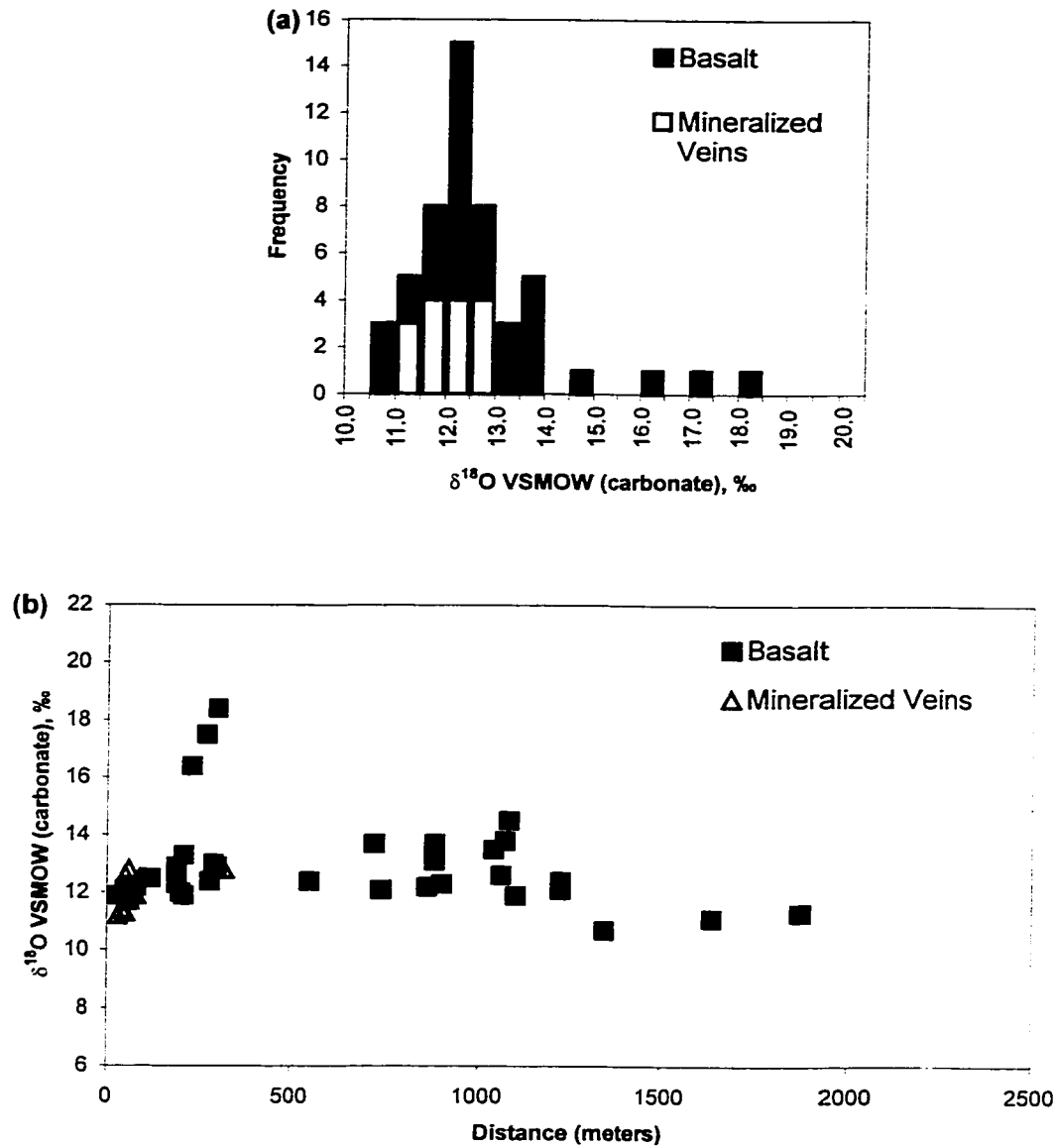


**Figure 5.9.** The oxygen stable isotopic composition of secondary carbonate minerals within (a) gold-bearing veins and altered basaltic rocks in the Boston area and (b) the oxygen stable isotopic composition of secondary carbonate minerals from within basaltic rocks with respect to distance from mineralized veins in the Boston area (all distances measured from 7505000N and 441150E, approximately halfway between the B2 and B3 zones).

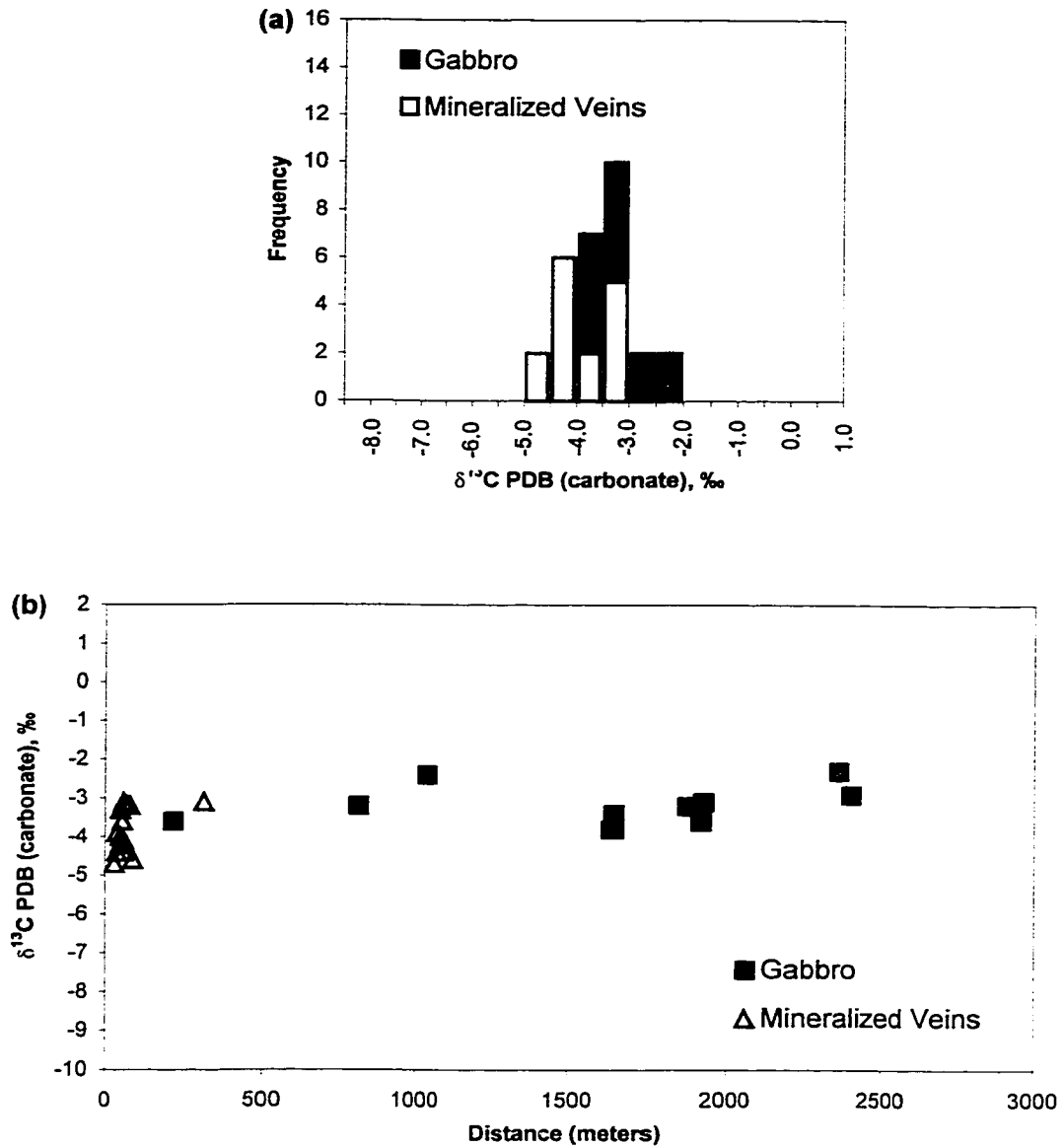


**Figure 5.10.** The carbon stable isotopic composition of secondary carbonate minerals within (a) gold-bearing veins and altered gabbroic rocks in the Boston area and (b) the carbon stable isotopic composition of secondary carbonate minerals from within gabbroic rocks with respect to distance from mineralized veins in the Boston area (all distances measured from 7505000N and 441150E, approximately halfway between the B2 and B3 zones).



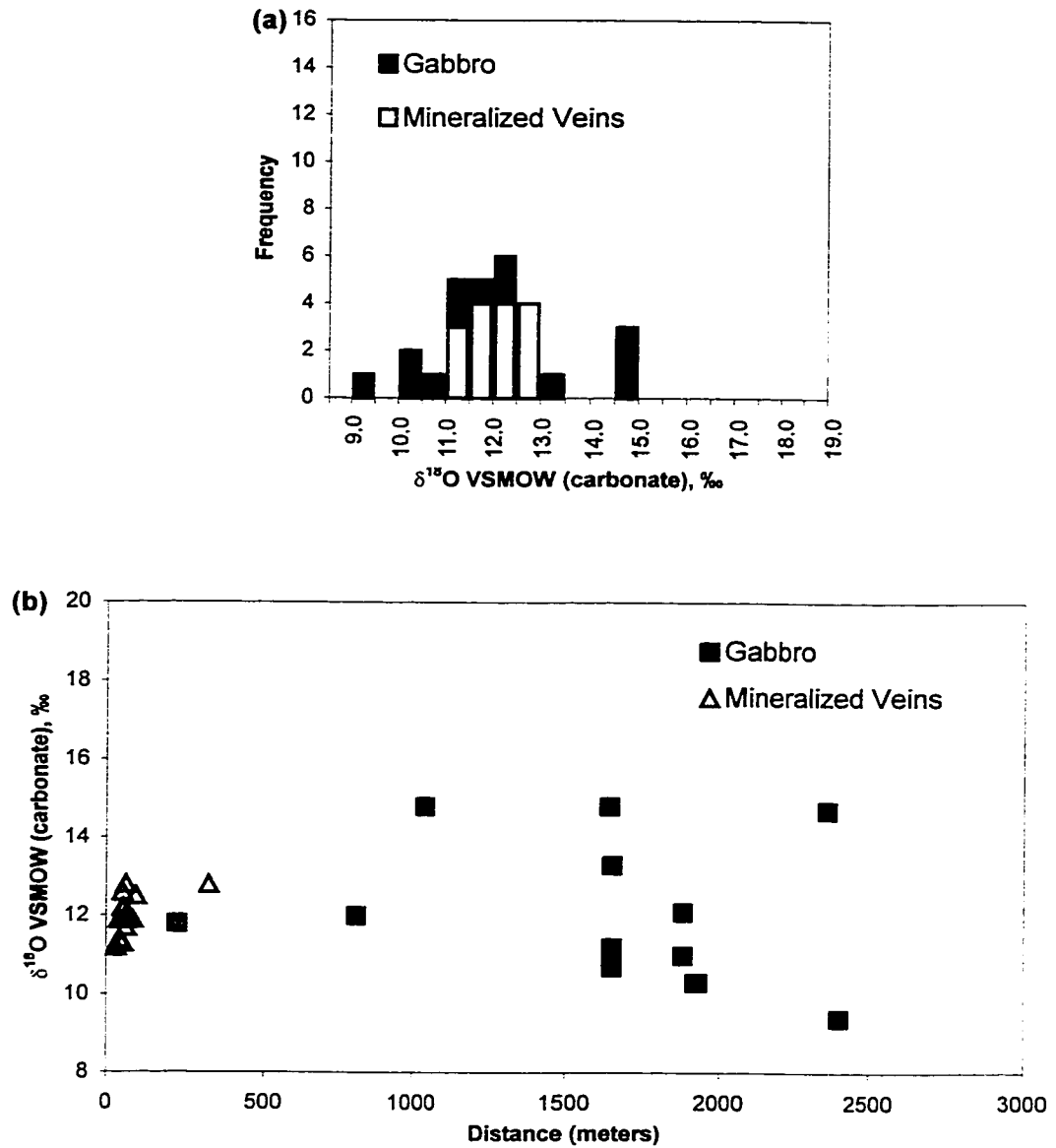


**Figure 5.11.** The oxygen stable isotopic composition of secondary carbonate minerals within (a) gold-bearing veins and altered gabbroic rocks in the Boston area and (b) the oxygen stable isotopic composition of secondary carbonate minerals from within gabbroic rocks with respect to distance from mineralized veins in the Boston area (all distances measured from 750500N and 441150E, approximately halfway between the B2 and B3 zones).

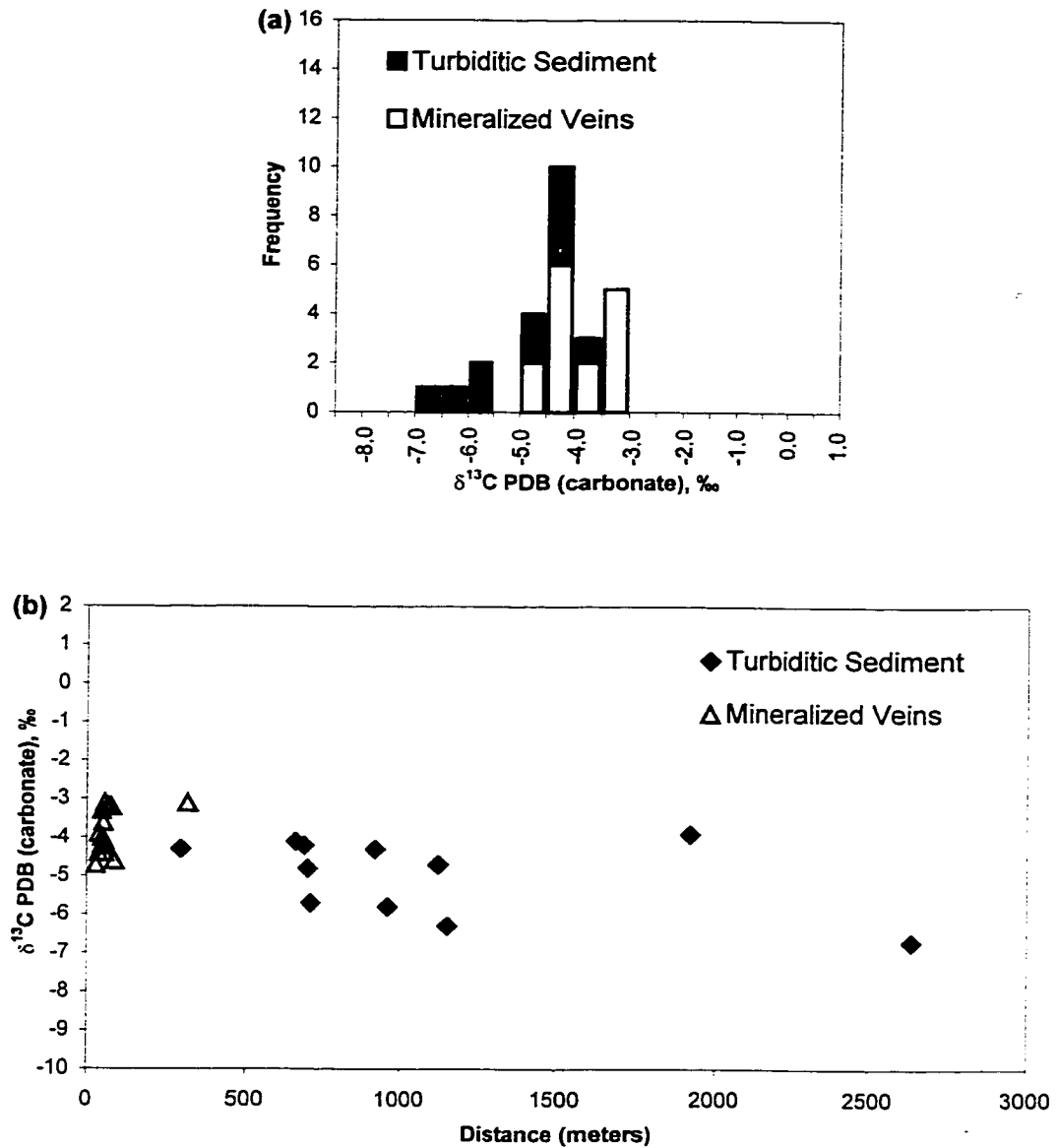


**Figure 5.12.** The carbon stable isotopic composition of secondary carbonate minerals within (a) gold-bearing veins and altered turbiditic sediments in the Boston area and (b) the carbon stable isotopic composition of secondary carbonate minerals from within turbiditic sediments with respect to distance from mineralized veins in the Boston area (all distances measured from 7505000N and 441150E, approximately halfway between the B2 and B3 zones).

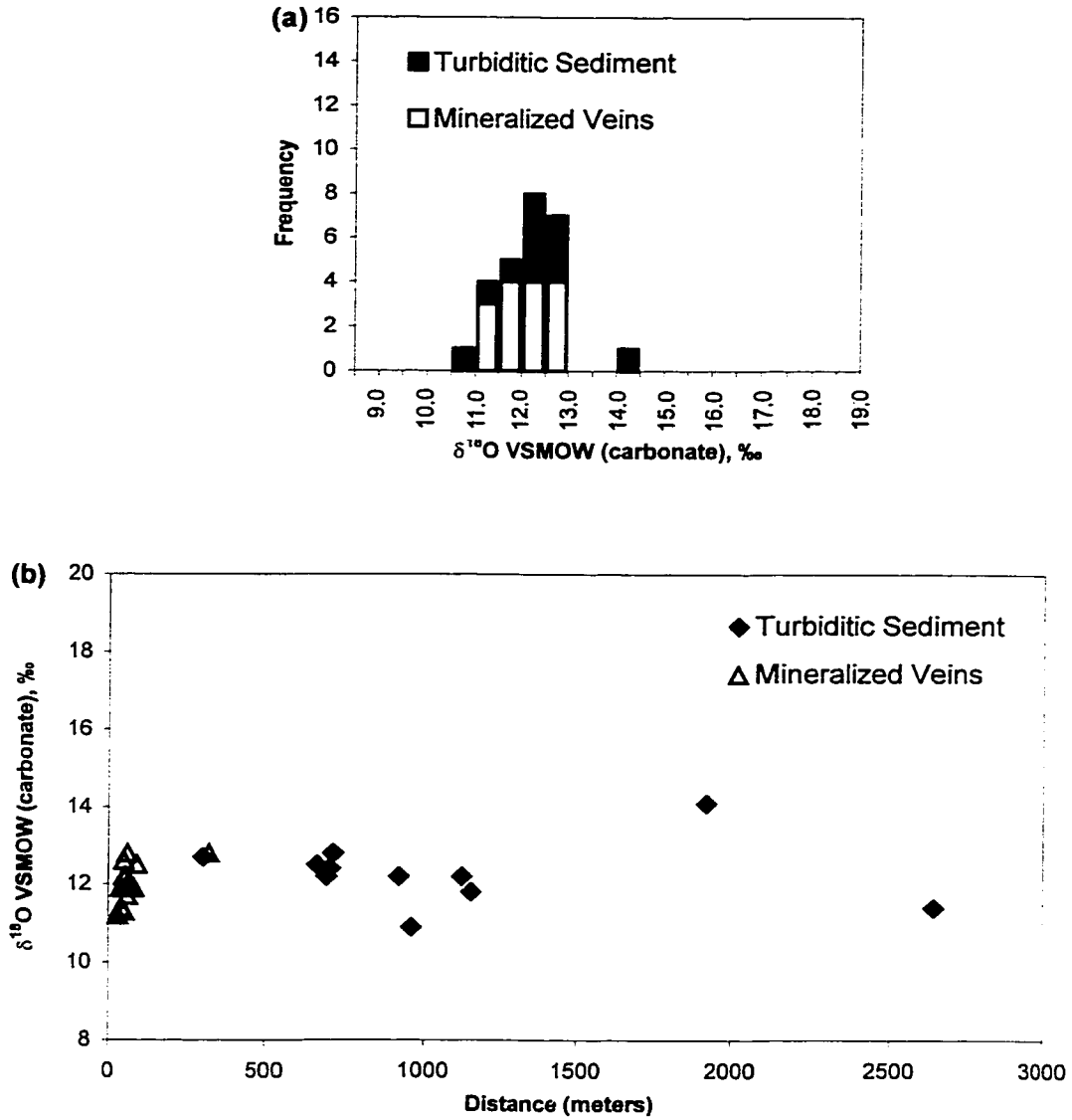


**Figure 5.13.** The oxygen stable isotopic composition of secondary carbonate minerals within (a) gold-bearing veins and altered turbiditic sediments in the Boston area and (b) the oxygen stable isotopic composition of secondary carbonate minerals from within turbiditic sediments with respect to distance from mineralized veins in the Boston area (all distances measured from 7505000N and 441150E, approximately halfway between the B2 and B3 zones).

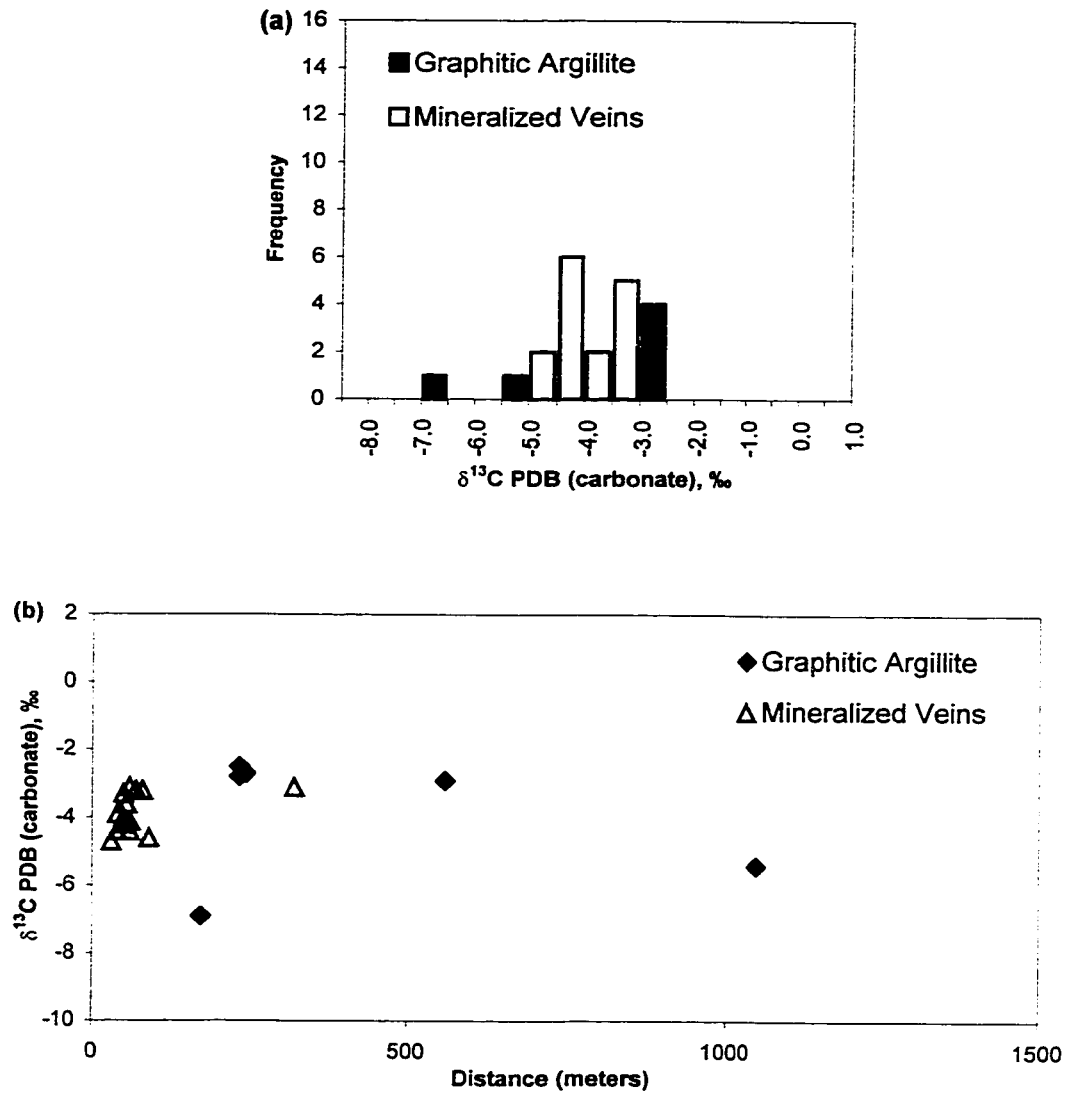


**Figure 5.14.** The carbon stable isotopic composition of secondary carbonate minerals within (a) gold-bearing veins and altered graphitic argillites in the Boston area and (b) the carbon stable isotopic composition of secondary carbonate minerals from within graphitic argillites with respect to distance from mineralized veins in the Boston area (all distances measured from 7505000N and 441150E, approximately halfway between the B2 and B3 zones).

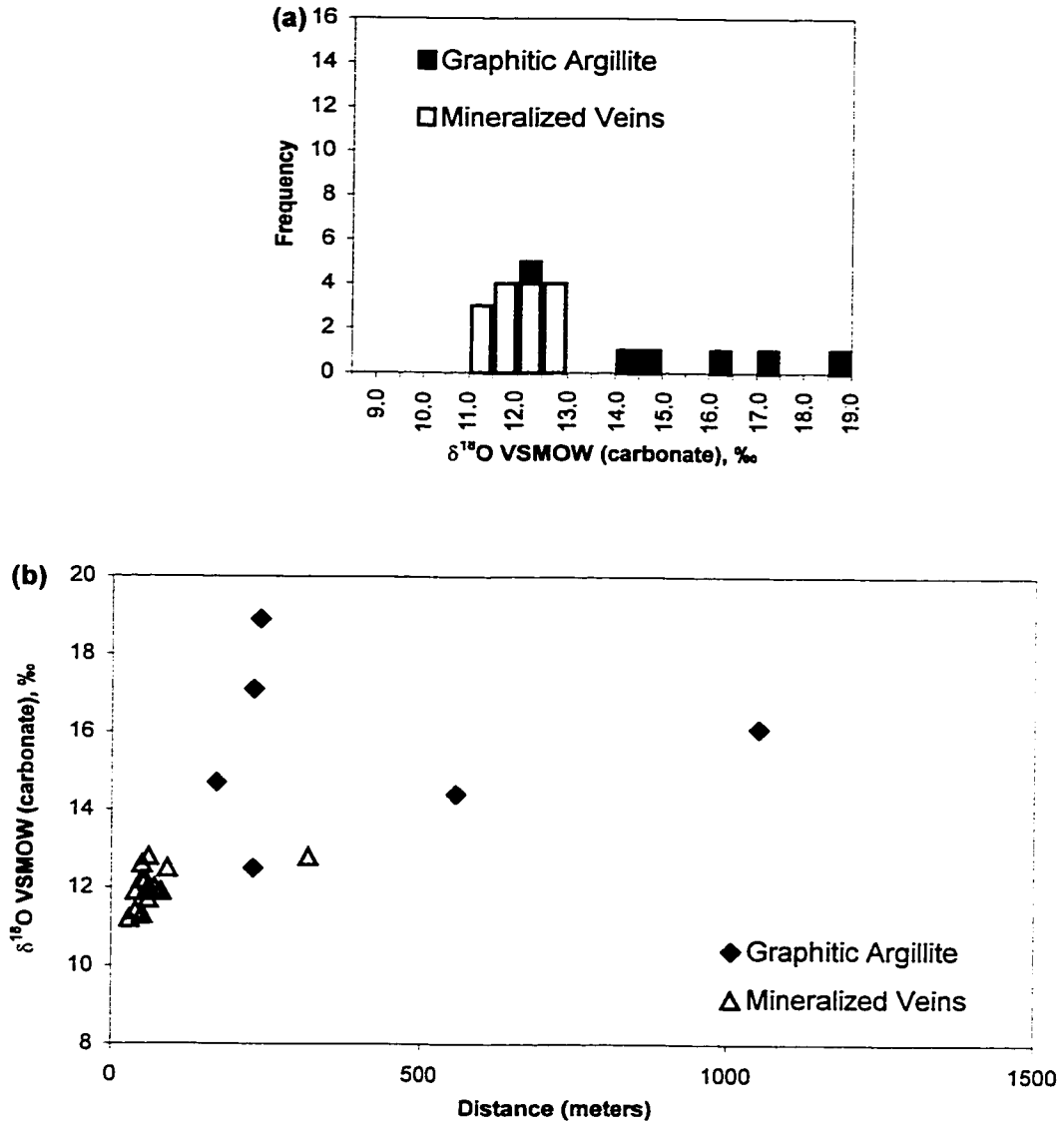


**Figure 5.15.** The oxygen stable isotopic composition of secondary carbonate minerals within (a) gold-bearing veins and altered graphitic argillites in the Boston area and (b) the oxygen stable isotopic composition of secondary carbonate minerals from within graphitic argillites with respect to distance from mineralized veins in the Boston area (all distances measured from 7505000N and 441150E, approximately halfway between the B2 and B3 zones).

### 5.3.3. Carbonate and Quartz (Regional Veining)

The results of the stable isotopic analyses of ferroan dolomite, ankerite and calcite separated from foliation parallel and cross-cutting regional quartz-carbonate veining in the Boston area are presented in Appendix D and Figure 5.16a, and are summarised in Table 5.2. The results of the stable isotopic analyses of vein quartz are presented in Appendix E and Figure 5.16b, and are summarised in Table 5.3. For the most part, quartz and carbonate separated from regional veins in the Boston area reflect the whole rock stable isotopic composition of the country rocks that host them, just as was observed in the stable isotopic composition of carbonate minerals disseminated throughout the country rocks themselves.

Basalt-Hosted Regional Veins: Carbonate minerals in basalt hosted regional veins have  $\delta^{13}\text{C}$  compositions of -2.9 to 0.5‰, with an average value of  $-1.7 \pm 1.0\text{‰}$  ( $n = 10$ ), and with the exception of samples JSB-026 and JSB-175,  $\delta^{18}\text{O}$  compositions of 12.2 to 13.9‰, with an average value of  $12.9 \pm 0.7\text{‰}$  ( $n = 7$ ). This is identical to the range of  $\delta^{13}\text{C}$  and  $\delta^{18}\text{O}$  values calculated for secondary carbonate minerals from within the basalts themselves ( $\delta^{13}\text{C} = -2.8$  to  $0.7\text{‰}$ ;  $\delta^{18}\text{O} = 10.7$  to  $13.8\text{‰}$ ).

Ferroan dolomite separated from a vein in sample JSB-026 has a  $\delta^{18}\text{O}$  value of 20.0‰, and ankerite and calcite separated from a vein in sample JSB-175 have  $\delta^{18}\text{O}$  values of 16.9 and 18.1‰ respectively, and plot as an isolated group in Figure 5.16a. As discussed in the previous section samples JSB-026 and JSB-175 originated from an unaltered wedge of basalt that occurs within the Boston fault zone approximately halfway between and slightly to the north of the B2 and B3 zones. Like the secondary carbonate

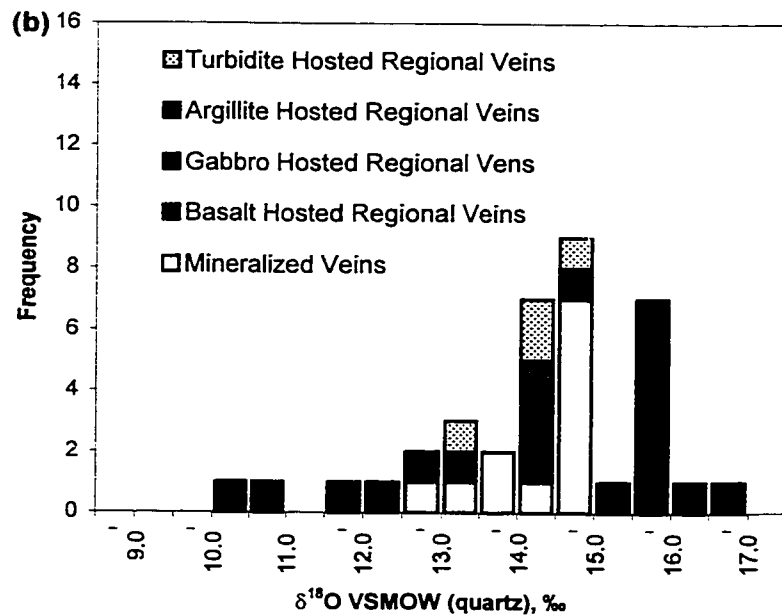
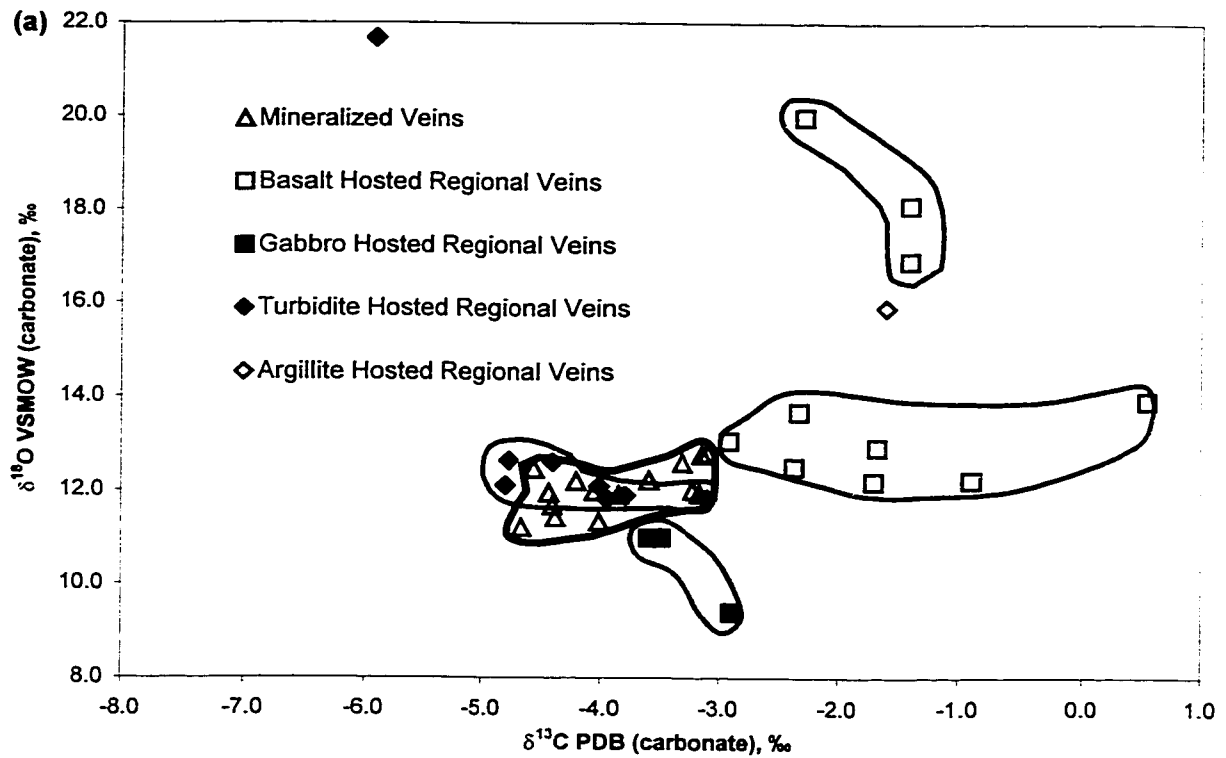


**Figure 5.16.** (a) The stable isotopic composition of carbonate minerals separated from gold-bearing and regional veins associated with the Boston deposit; and (b) the oxygen stable isotopic composition of quartz separated from gold-bearing and regional veins in the Boston area.

disseminated throughout the basaltic wedge itself, carbonate separated from veins in these samples has abnormally high  $\delta^{18}\text{O}$  values.

Quartz separated from barren veins hosted by basaltic rocks in the Boston area has  $\delta^{18}\text{O}$  values of 14.2 to 16.6‰, with an average value of  $15.6 \pm 0.7\text{‰}$  ( $n = 7$ ). These values are slightly higher than, but for the most part overlap with the whole rock  $\delta^{18}\text{O}$  values typical of seafloor altered pillowed basalts ( $\delta^{18}\text{O} = 8.5$  to  $14.7\text{‰}$ ; Muehlenbachs and Clayton, 1972).

Gabbro-Hosted Regional Veins: Three samples of carbonate separated from veins hosted by gabbroic rocks in the Boston area were found to have  $\delta^{13}\text{C}$  values of -2.9, -3.5, and -3.6‰, and corresponding  $\delta^{18}\text{O}$  values of 9.4, 11.0, and 11.0‰. These values fall well within the range of  $\delta^{13}\text{C}$  and  $\delta^{18}\text{O}$  values calculated for secondary carbonate minerals within the greenschist facies gabbroic rocks in the Boston area ( $\delta^{13}\text{C} = -3.8$  to  $-2.3\text{‰}$ ;  $\delta^{18}\text{O} = 10.3$  to  $14.8\text{‰}$ ).

Quartz separated from veins within the gabbroic rocks has  $\delta^{18}\text{O}$  values of 10.2 to 13.4‰, with an average value of  $11.8 \pm 1.2\text{‰}$  ( $n = 6$ ). The isotopic composition of the vein quartz is also within the whole rock stable isotopic composition typical of igneous rocks in general ( $\delta^{18}\text{O} = 5.5$  and  $11.0\text{‰}$ ; Taylor and Sheppard, 1986).

Turbiditic Sediment-Hosted Regional Veins: With the exception of sample JSB-106, quartz-carbonate veins hosted by turbiditic sediments distal to the Boston deposit have  $\delta^{13}\text{C}$  values of -4.8 to -3.1‰, with an average value of  $-4.1 \pm 0.6\text{‰}$  ( $n = 7$ ), and  $\delta^{18}\text{O}$  values of 11.8 to 12.6‰, with an average value of  $12.1 \pm 0.3\text{‰}$  ( $n = 7$ ). The isotopic



composition of the carbonate minerals in these veins is quite uniform and overlaps with the isotopic composition of secondary carbonate minerals within the immediately surrounding country rocks ( $\delta^{13}\text{C} = -6.7$  to  $-3.9\text{‰}$ ;  $\delta^{18}\text{O} = 10.9$  to  $14.1\text{‰}$ ), and the auriferous veins in the Boston deposit ( $\delta^{13}\text{C} = -4.7$  to  $-3.1\text{‰}$ ;  $\delta^{18}\text{O} = 11.2$  to  $12.8\text{‰}$ ; Figure 5.16a).

Ankerite separated from a vein in sample JSB-106 has a  $\delta^{13}\text{C}$  value of  $-5.9\text{‰}$ , which is depleted with respect to carbonate from other veins but within the isotopic range of carbonate minerals in the surrounding sediments. However, ankerite in this sample has a  $\delta^{18}\text{O}$  value of  $21.7\text{‰}$ , and is greatly enriched in the heavy isotope of oxygen with respect to all other samples analysed (Figure 5.16a). Veining in this sample, therefore, appears to be unrelated to other barren veins associated with the Boston deposit.

However, the oxygen isotopic composition of carbonate in sample JSB-106 is still within the  $\delta^{18}\text{O}$  whole rock range typical of clastic sedimentary rocks in general ( $\delta^{18}\text{O} = 8$  and  $25\text{‰}$ ; Longstaffe, 1987).

Quartz in the turbidite hosted veins has  $\delta^{18}\text{O}$  values of  $13.2$  to  $14.6\text{‰}$ , with an average value of  $14.1 \pm 0.6\text{‰}$  ( $n = 4$ ). The isotopic composition of the vein quartz also falls within the  $\delta^{18}\text{O}$  whole rock range typical of clastic sedimentary rocks.

Graphitic Argillite-Hosted Regional Veins: The graphitic argillites at Boston are commonly interfingered with the basaltic rocks. One sample of ankerite and four samples of quartz were separated from barren veins within the graphitic argillites.

Ankerite separated from a vein in sample JSB-167 has a  $\delta^{13}\text{C}$  value of  $-1.6\text{‰}$ , which is enriched with respect to secondary carbonate within the graphitic sediments in other parts

of the Boston deposit ( $\delta^{13}\text{C} = -6.9$  to  $-2.5\text{‰}$ ), and extremely enriched with respect to the  $\delta^{13}\text{C}$  whole rock value marine sediments in general ( $\delta^{13}\text{C} < -15\text{‰}$ ; Faure, 1986a). It is possible that the fluid responsible for the deposition of ankerite within this vein was in equilibrium with secondary carbonate in the surrounding basaltic rocks, not the argillites themselves.

On the other hand, ankerite in sample JSB-167 has a  $\delta^{18}\text{O}$  value of  $15.9\text{‰}$ , and quartz from four samples in this area have  $\delta^{18}\text{O}$  values of  $14.1$  to  $16.4\text{‰}$ , with an average value of  $15.5 \pm 0.9\text{‰}$  ( $n = 4$ ). These values overlap with the  $\delta^{18}\text{O}$  values of secondary carbonate disseminated throughout the graphitic argillites that host these veins ( $\delta^{18}\text{O} = 12.5$  to  $18.9\text{‰}$ ), and are also within the whole rock stable isotopic range characteristic of clay rich sedimentary rocks ( $\delta^{18}\text{O} = 10$  to  $30\text{‰}$ ; Longstaffe, 1987).

Veins Hosted by Strongly Deformed Samples: Carbonate minerals separated from barren quartz-carbonate veins within rocks that have experienced intense hydrothermal alteration and deformation within the Boston fault zone have  $\delta^{13}\text{C}$  compositions of  $-3.0$  to  $-1.7\text{‰}$  ( $-2.1 \pm 0.6\text{‰}$ ,  $n = 4$ ) and  $\delta^{18}\text{O}$  compositions of  $14.2$  to  $16.1\text{‰}$  ( $15.3 \pm 0.8\text{‰}$ ,  $n = 4$ ). Two samples of quartz separated from barren quartz-carbonate veins within the strongly altered and deformed samples have  $\delta^{18}\text{O}$  compositions of  $12.9$  and  $14.8\text{‰}$ . The  $\delta^{13}\text{C}$  values of carbonate separated from veins in these samples are similar to the  $\delta^{13}\text{C}$  values of secondary carbonate minerals within the surrounding wallrocks ( $\delta^{13}\text{C} = -3.2$  to  $-1.6\text{‰}$ ,  $n = 8$ ).

The  $\delta^{18}\text{O}$  value of carbonate separated from the barren veins is slightly higher than the  $\delta^{18}\text{O}$  value of carbonate within the surrounding country rocks ( $\delta^{18}\text{O} = 12.0$  to

13.2‰). Graphitic argillites containing carbonate minerals with enriched  $\delta^{18}\text{O}$  values ( $\delta^{18}\text{O} = 12.5$  to  $18.9\%$ ,  $n = 6$ ) occur in close proximity to the B2 and B4 zones and may have influenced the stable isotopic composition of the fluid in these veins.

In Figures 5.17 to 5.22 the isotopic compositions of quartz and carbonate separated from several foliation parallel and cross cutting regional veins are plotted with respect to distance from the mineralized zones. With the possible exception of veins hosted by the basaltic rocks (Figure 5.17), these plots show no relationship between isotopic composition and distance from the mineralized zones.

#### **5.3.4. Pyrite**

The results of the stable isotopic analyses of twenty samples of pyrite separated from barren and auriferous wallrock from in and around the Boston deposit are presented in Appendix F and are summarised in Table 5.4. The sulphur stable isotopic results plotted in Figure 5.23.

Mineralized Veins: Pyrite separated from the sulphidation halo around gold-bearing veins in the B2, B3, and B4 zones has a very tight isotopic range, varying by only 1.3‰. The  $\delta^{34}\text{S}$  values of pyrite separated from the sulphidation halo around gold-bearing veins fall between 2.1 and 3.5‰, with an average value of  $2.7 \pm 0.4\%$  ( $n = 8$ ). Even when looked at individually the  $\delta^{34}\text{S}$  values of pyrite separated from sulphidation halos around mineralized veins in the three zones are almost identical (Figure 5.23): pyrite separated from the B2 zone has  $\delta^{34}\text{S}$  values of 2.1 to 3.0‰, with an average value of  $2.6 \pm 0.4\%$  ( $n = 4$ ); three samples of pyrite separated from the B3 zone have  $\delta^{34}\text{S}$  values of 2.4, 3.1, and

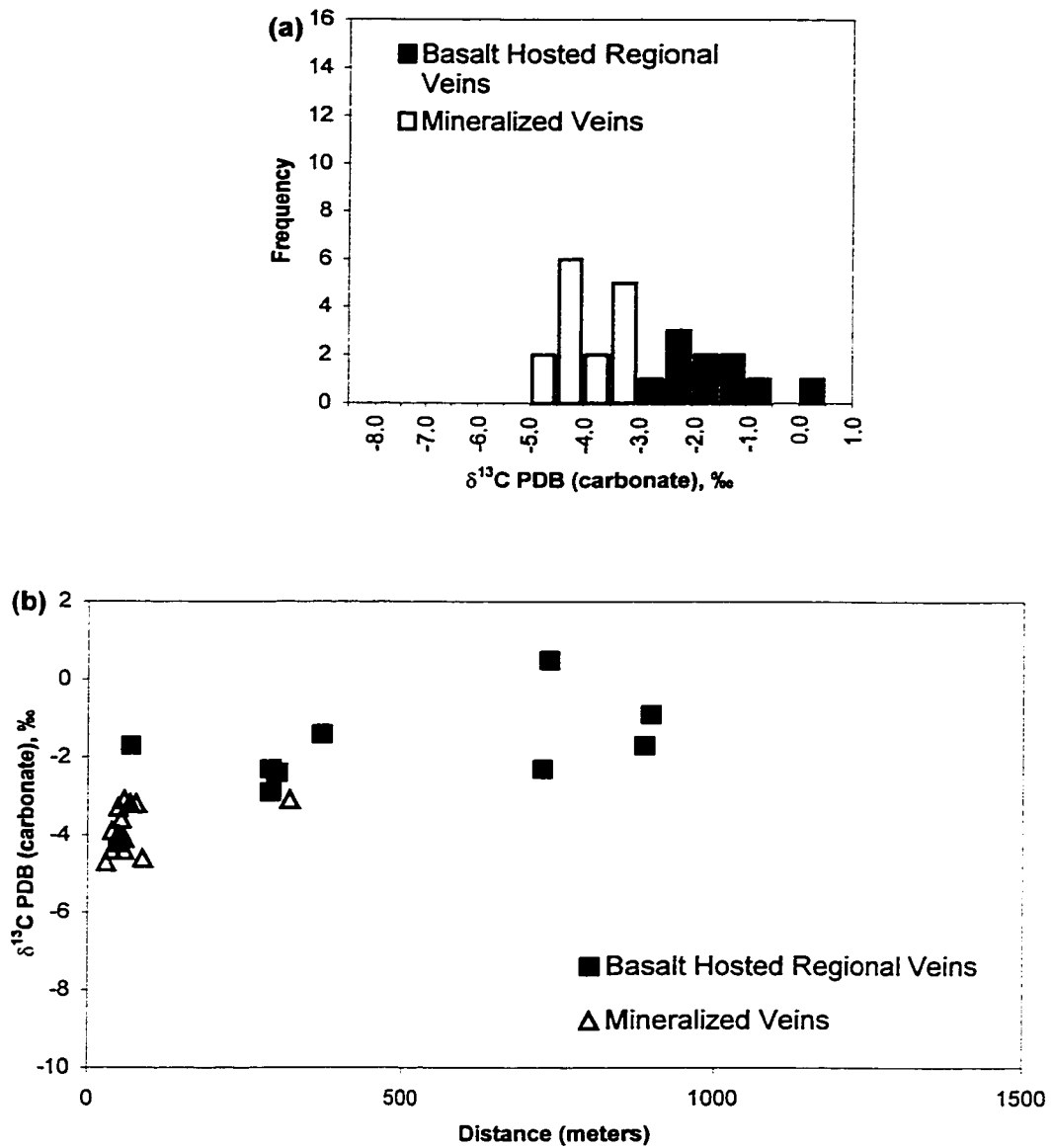


**Figure 5.17.** The carbon stable isotopic composition of carbonate minerals separated from (a) gold-bearing veins and regional veins hosted by basalts in the Boston area and (b) the carbon stable isotopic composition of carbonate minerals separated from regional veins hosted by basalts with respect to distance from mineralized veins in the Boston area (all distances measured from 7505000N and 441150E, approximately halfway between the B2 and B3 zones).

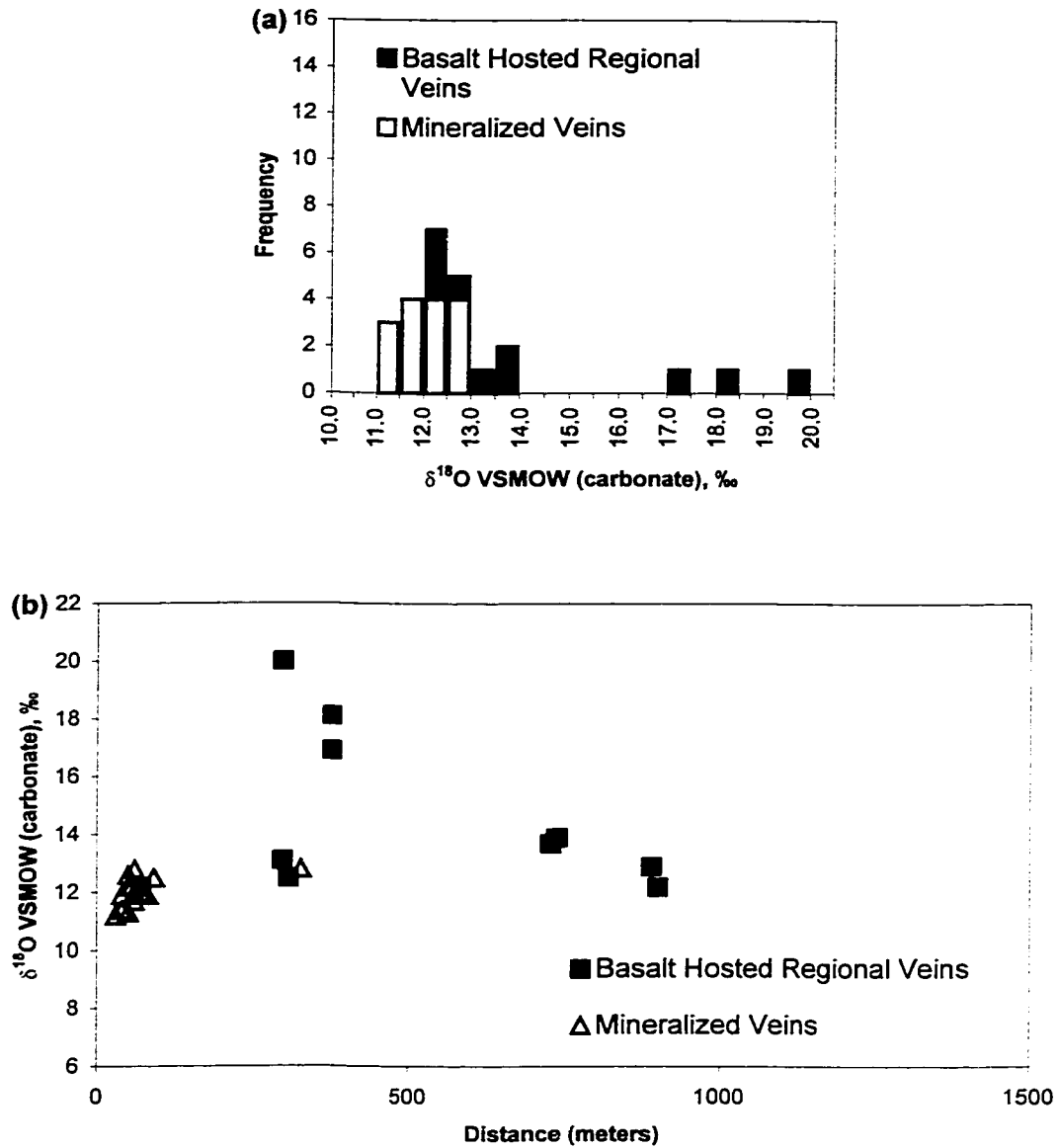


**Figure 5.18.** The oxygen stable isotopic composition of carbonate minerals separated from (a) gold-bearing veins and regional veins hosted by basalts in the Boston area and (b) the oxygen stable isotopic composition of carbonate minerals separated from regional veins hosted by basalts with respect to distance from mineralized veins in the Boston area (all distances measured from 7505000N and 441150E, approximately halfway between the B2 and B3 zones).

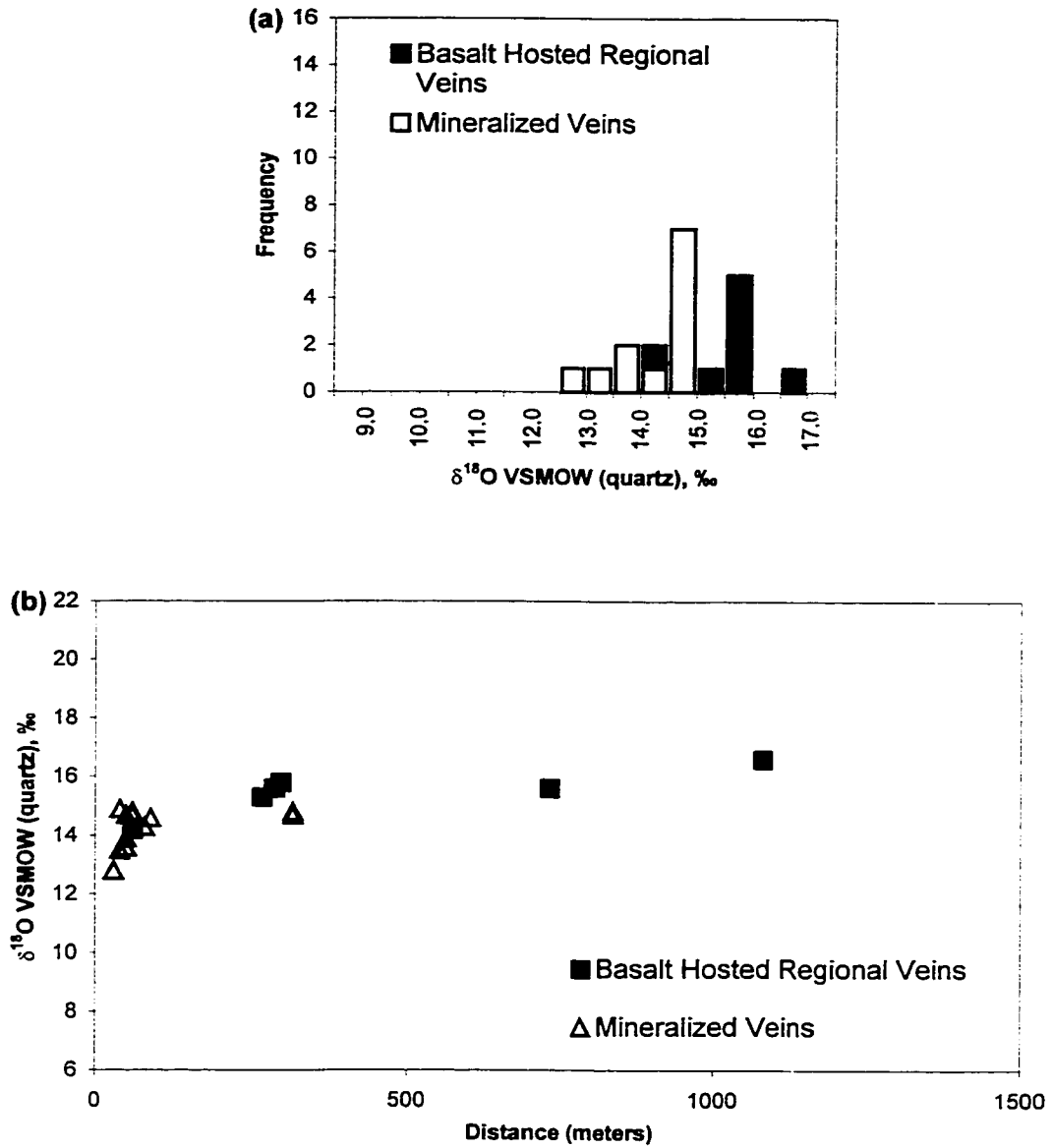


**Figure 5.19.** The oxygen stable isotopic composition of quartz separated from (a) gold-bearing veins and regional veins hosted by basalts in the Boston area and (b) the oxygen stable isotopic composition of quartz separated from regional veins hosted by basalts with respect to distance from mineralized veins in the Boston area (all distances measured from 7505000N and 441150E, approximately halfway between the B2 and B3 zones).

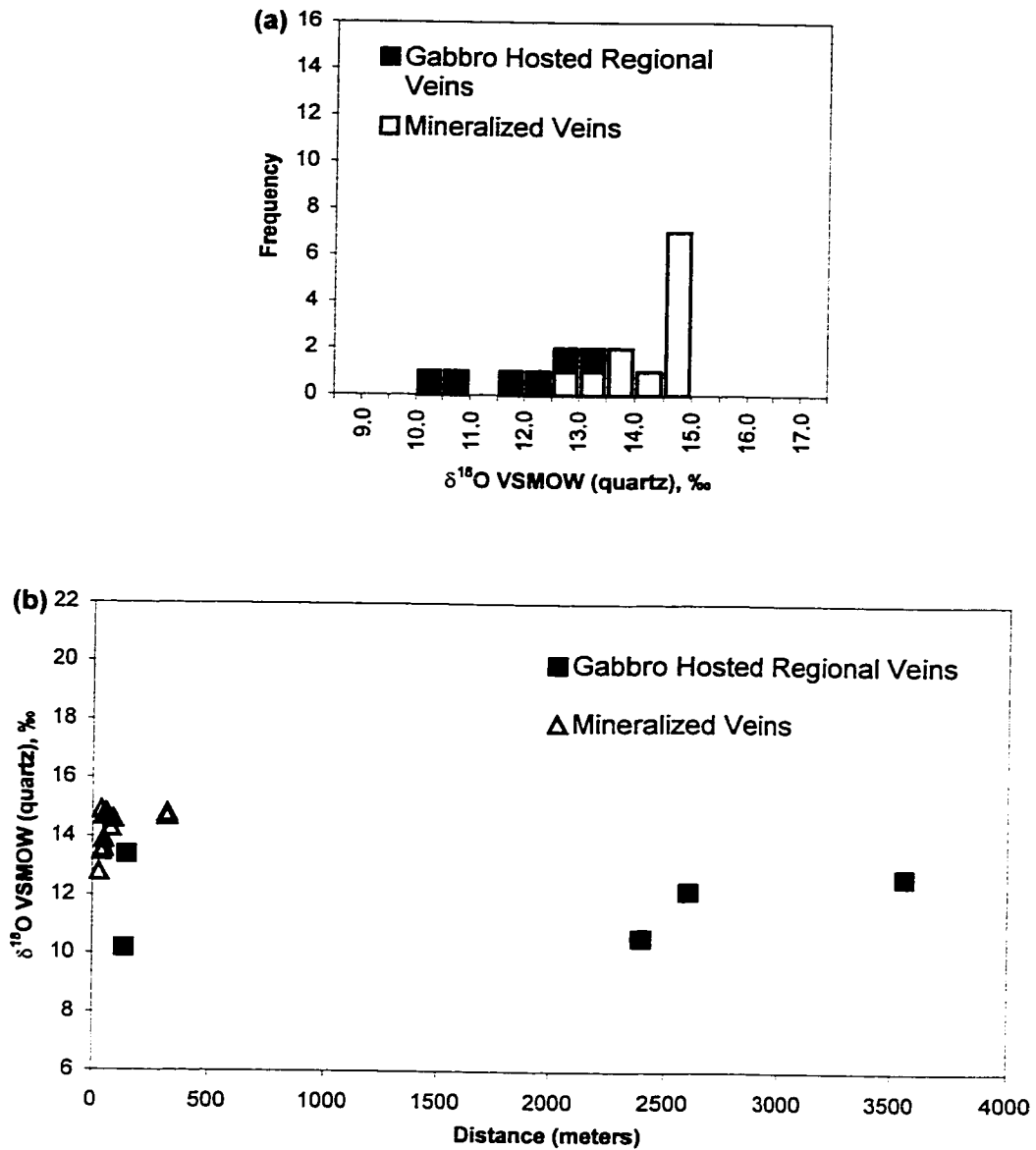


**Figure 5.20.** The oxygen stable isotopic composition of quartz separated from (a) gold-bearing veins and regional veins hosted by gabbros in the Boston area and (b) the oxygen stable isotopic composition of quartz separated from regional veins hosted by gabbros with respect to distance from mineralized veins in the Boston area (all distances measured from 7505000N and 441150E, approximately halfway between the B2 and B3 zones).

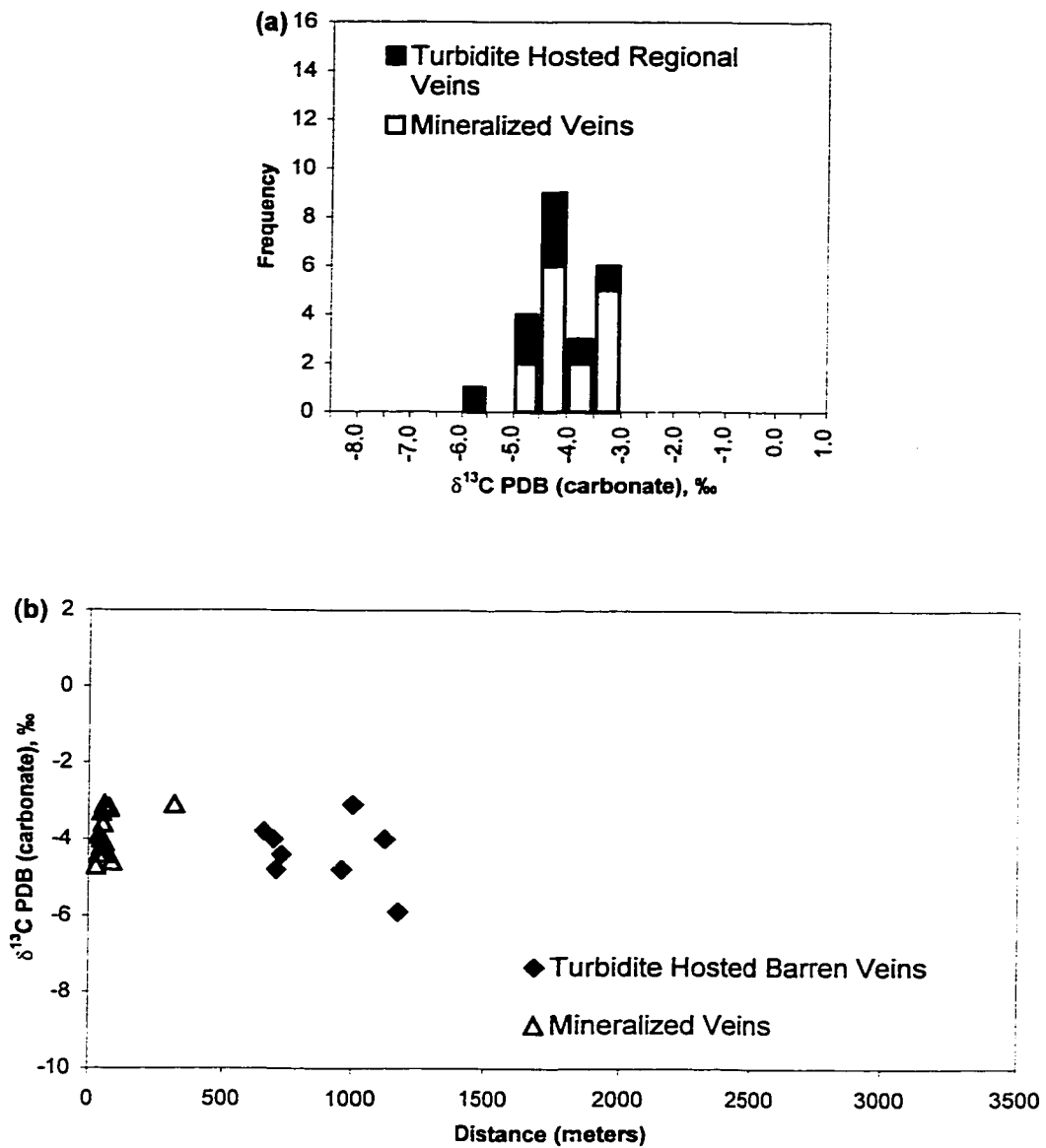


**Figure 5.21.** The carbon stable isotopic composition of carbonate minerals separated from (a) gold-bearing veins and regional veins hosted by turbiditic sediments in the Boston area and (b) the carbon stable isotopic composition of carbonate minerals separated from regional veins hosted by turbiditic sediments with respect to distance from mineralized veins in the Boston area (all distances measured from 7505000N and 441150E, approximately halfway between the B2 and B3 zones).



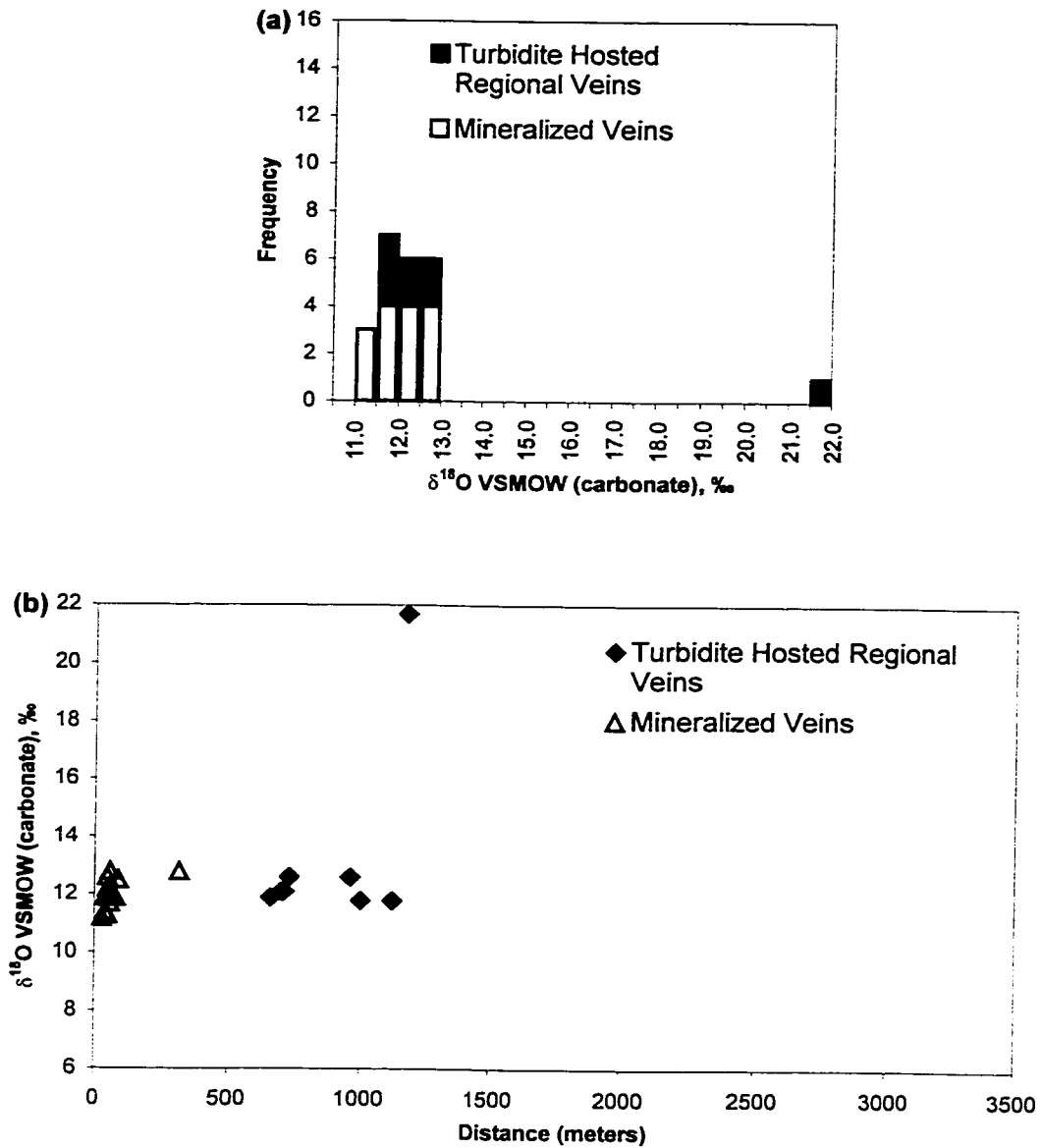


**Figure 5.22.** The oxygen stable isotopic composition of carbonate minerals separated from (a) gold-bearing veins and regional veins hosted by turbiditic sediments in the Boston area and (b) the oxygen stable isotopic composition of carbonate minerals separated from regional veins hosted by turbiditic sediments with respect to distance from mineralized veins in the Boston area (all distances measured from 7505000N and 441150E, approximately halfway between the B2 and B3 zones).

**Table 5.4.** Summary of the results of the stable isotopic analysis of pyrite separated from adjacent to mineralized and barren veins and from vugs and bands within turbiditic and graphitic sediments associated with the Boston deposit (Avg = average value; SD = standard deviation).

Host Rock	Occurrence	$\delta^{34}\text{S}$ CDT ‰		No. of Analysis
		Range	Avg $\pm$ SD	
B2 Zone	Sulphidation Halo	2.1 to 3.0	2.6 $\pm$ 0.4	4
B3 Zone	Sulphidation Halo	2.4/3.1/3.5	—	3
B4 Zone	Sulphidation Halo	2.5	—	1
<b>All Zones</b>	<b>Sulphidation Halo</b>	<b>2.1 to 3.5</b>	<b>2.7 <math>\pm</math>0.4</b>	<b>8</b>
Basalt	Sulphidation Halo	3.4	—	1
Gabbro	Sulphidation Halo	2.2	—	1
Turbiditic Sediment	Sulphidation Halo	2.2	—	1
Graphitic Argillite	Sulphidation Halo	2.5	—	1
Strongly Deformed Rock	Sulphidation Halo	1.6	—	1
Turbiditic Sediment	Pyrite Vugs	0.3/0.9	—	2
Graphitic Argillite	Pyrite Bands and Clots	3.4 to 4.7	4.2 $\pm$ 0.6	4

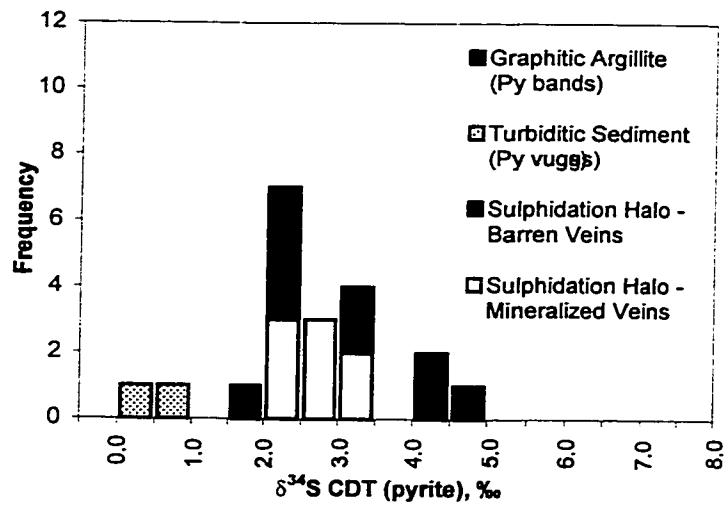


**Figure 5.23.** The sulphur stable isotopic composition of pyrite separated from the sulphidation halo around mineralized and barren veins, and from clots within graphitic argillite and vugs within turbidites in the Boston area.

3.5‰; and the only sample of pyrite separated from the B4 zone has a  $\delta^{34}\text{S}$  value of 2.5‰.

Unmineralized Veins: Pyrite was also separated from the sulphidation halos around unmineralized quartz-carbonate veins within the basalts, gabbros, turbiditic and argillic sediments, and strongly altered rocks that occur in the area surrounding the Boston deposit. Pyrite separated from sulphidation halos around unmineralized veins in the Boston area has  $\delta^{34}\text{S}$  values of 1.6 to 3.4‰, with an average value of  $2.4 \pm 0.6\text{‰}$  ( $n = 6$ ). In all cases, and regardless of host rock lithology, pyrite separated from the sulphidation halos around unmineralized quartz-carbonate veins have similar stable isotopic compositions to those of pyrite separated from gold bearing sulphidation halos around the veins ( $\delta^{34}\text{S} = 2.1$  and  $3.5\text{‰}$ ; Figure 5.23).

Pyrite Not Associated With Veining: Pyrite that does not appear to be associated with veining also commonly occurs throughout the turbiditic and argillic sediments. Pyrite of this type typically forms foliation parallel bands and clots in the argillic sediments. The sulphur isotopic composition of pyrite separated from these bands and clots is between 3.4 and 4.7‰, with an average value of  $4.2 \pm 0.6\text{‰}$  ( $n = 4$ ), and are slightly enriched in  $\delta^{34}\text{S}$  with respect to pyrite separated from the mineralized veins ( $\delta^{34}\text{S} = 2.1$  to  $3.5$ ; Figure 5.23). Two samples of pyrite separated from vugs within the turbiditic sediments were also analysed and found to have  $\delta^{34}\text{S}$  values of 0.3 and 0.9‰. Pyrite in these two samples is depleted in the heavy isotope of sulphur with respect to pyrite separated from the sulphidation halo around quartz-carbonate veins (Figure 5.23).

### ***5.3.5. Graphite***

The results of the stable isotopic analyses of six samples of graphite separated from graphitic argillites associated with the Boston deposit are presented in Appendix G.

The stable isotopic composition of graphite separated from argillic sediments in the Boston area have  $\delta^{13}\text{C}$  values that fall between -29.0 and -25.0‰, with an average value of  $-27.1 \pm 1.7\text{‰}$  ( $n = 6$ ). Typical reduced organic carbon in marine sediments has  $\delta^{13}\text{C}$  values between -30 and -10‰ with an average value of approximately -25‰ (Ohmoto and Rye, 1979 and Ohmoto, 1986). The graphite in the argillic sediments at Boston is therefore isotopically consistent with a marine sedimentary origin.

### ***5.4. Stable Isotopes from the South Patch Occurrence***

In a reconnaissance study of the South Patch gold prospect thirty-two samples of carbonate and four samples of quartz from auriferous vein and country rock material were prepared for stable isotopic analysis. The results of the stable isotopic analyses of ferroan dolomite, ankerite, and calcite from the South Patch occurrence are presented in Appendix D and are summarized in Table 5.5 and Figure 5.24. The results of the stable isotopic analyses of vein quartz are presented in Appendix E.

#### ***5.4.1. Carbonate and Quartz (Mineralized Veins)***

Carbonate minerals separated from the mineralized veins in the South Patch occurrence have  $\delta^{13}\text{C}$  values that vary by only 1.7‰ (-3.8 to -2.1‰), with an average value of  $-2.7 \pm 0.6\text{‰}$  ( $n = 8$ ), and with the exception of samples SPJS-011 and SPJS-032,

**Table 5.5.** Summary of the results of the stable isotopic analysis of calcite, ankerite, and ferroan dolomite separated from mineralized and barren veins, and wallrocks associated with the South Patch occurrence (Avg = average value, SD = standard deviation; \* = outlying values were not included in calculated range and average).

Host Rock	$\delta^{13}\text{C PDB, ‰}$		$\delta^{18}\text{O VSMOW, ‰}$		No. of Analyses	No. of Analyses	Typical Wallrock Value		Reference
	Range	Avg $\pm$ SD	Range	Avg $\pm$ SD			$\delta^{13}\text{C PDB, ‰}$	$\delta^{18}\text{O VSMOW, ‰}$	
Mineralized Veining	-3.8 to -2.1	-2.6 $\pm$ 0.6	8	11.6 to 13.2*	12.0 $\pm$ 0.5*	6*	-10.0 to +2.2	9 to 14	Groves and Foster, 1991; de Ronde et al., 1997; Kerrich, 1987
Basalt	-2.7 to -0.2	-1.8 $\pm$ 0.6	18	11.4 to 13.9	12.5 $\pm$ 0.8	18	0 $\pm$ 2	8.5 to 14.7	Muehlenbachs, 1986; Wood et al., 1986; Muehlenbachs and Clayton, 1972
Gabbro	-3.4 to 4.1	-3.7 $\pm$ 0.3	5	10.9 to 12.5	11.8 $\pm$ 0.7	5	-5 $\pm$ 2	5.5 to 11.0	Muehlenbachs, 1986; Ohmoto and Rye, 1979; Taylor and Sheppard, 1986

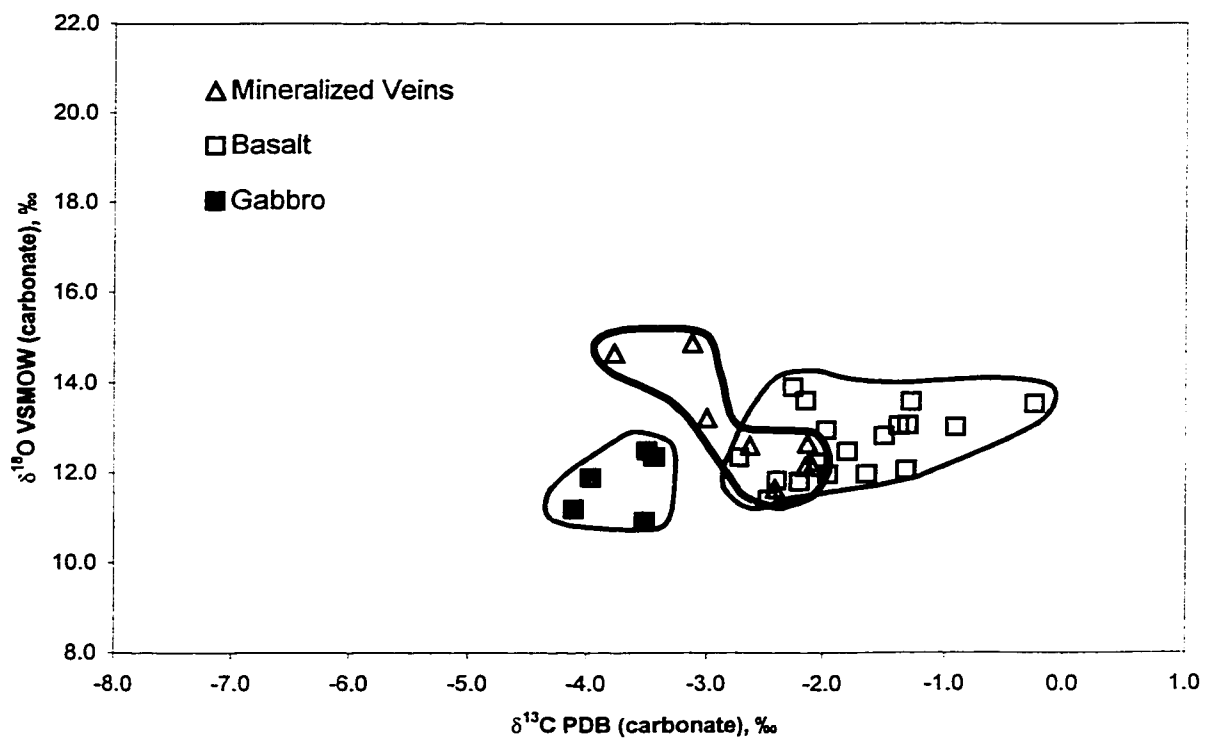


**Figure 5.24.** The stable isotopic composition of secondary carbonate minerals within gold-bearing veins and metamorphically altered country rocks associated with the South Patch occurrence.

$\delta^{18}\text{O}$  values that vary by only 1.6‰ (11.6 to 13.2‰), with an average value of 12.0 ±0.5‰ (n = 6). Excluding sample SPJS-018 ( $\delta^{18}\text{O}$  = 10.2‰), quartz within these veins has  $\delta^{18}\text{O}$  values that vary by only 0.3‰ (14.3, 14.5, and 14.6‰). The isotopic composition of carbonate and quartz separated from auriferous quartz-carbonate veins in the South Patch occurrence is very tightly grouped and overlaps with the stable isotopic composition of carbonate and quartz separated from gold-bearing veins in the Boston deposit ( $\delta^{13}\text{C}$  carbonate = -4.7 to -3.1‰, n = 15;  $\delta^{18}\text{O}$  carbonate = 11.2 to 12.8‰, n = 15;  $\delta^{18}\text{O}$  quartz = 12.8 to 14.9‰, n = 3) suggesting mineralized quartz-carbonate veining in both the South Patch occurrence and the Boston deposit originated from an isotopically similar hydrothermal fluid.

Ferroan dolomite separated from sample SPJS-011, and calcite separated from sample SPJS-032, have enriched  $\delta^{18}\text{O}$  values of 14.7 and 14.9‰ respectively, compared to carbonate separated from other mineralized veins in the South Patch area. In hand sample and thin section these two samples contain evidence of pervasive late carbonate filled fracturing of indeterminate origin and as a result must be considered with scepticism.

#### ***6.4.2 Carbonate (Country Rocks)***

Greenschist facies basaltic rocks associated with the South Patch occurrence contain secondary carbonate with  $\delta^{13}\text{C}$  values of -2.7 to -0.2‰, with an average value of -1.8 ±0.6‰ (n = 18), and  $\delta^{18}\text{O}$  values of 11.4 to 13.9‰, with an average value of 12.5 ±0.8‰ (n = 18). Greenschist facies gabbroic rocks in the South Patch area contain secondary carbonate minerals with  $\delta^{13}\text{C}$  values of -4.1 to -3.4‰, with an average value of



$-3.7 \pm 0.3\text{‰}$  ( $n = 5$ ), and  $\delta^{18}\text{O}$  values of 10.9 to 12.5‰, with an average value of  $11.8 \pm 0.7\text{‰}$  ( $n = 5$ ).

The stable isotopic composition of secondary carbonate minerals within the altered basaltic and gabbroic rocks associated with the South Patch occurrence resemble the whole rock isotopic composition typical of hydrothermally altered pillow basalts ( $\delta^{13}\text{C} = 0 \pm 2\text{‰}$ ; Muehlenbachs, 1986; Wood et al., 1986;  $\delta^{18}\text{O} = 8.5$  to  $14.7\text{‰}$ ; Muehlenbachs and Clayton, 1972) and fresh gabbroic rocks ( $\delta^{13}\text{C} = -5 \pm 2\text{‰}$ ; Muehlenbachs, 1986; Ohmoto and Rye, 1979;  $\delta^{18}\text{O} = 5.5$  to  $11.0\text{‰}$ ; Taylor and Sheppard, 1986) respectively (Table 5.5). This is also similar to what was observed in the carbonate minerals within the country rocks surrounding the Boston deposit.

## **6. Discussion**

### ***6.1. Fluid Types and Paragenesis***

The petrographic, fluid inclusion, and stable isotopic data presented above indicate that at least three chemically distinct fluids have invaded the Boston fault zone and surrounding wallrocks during the life of the hydrothermal system responsible for the Boston lode-gold deposit. Of these only one fluid seems to be directly linked to gold deposition.

### ***6.1.1. Auriferous Fluid***

As mentioned in the previous sections, a significant portion of the gold associated with the Boston deposit occurs as inclusions within pyrite grains that have been deposited within and surrounding main stage quartz-carbonate veins (Plate 3.13). In a few cases, undeformed quartz grains that contain primary type 1 (CO<sub>2</sub> gas-rich) and primary type 2 (H<sub>2</sub>O-CO<sub>2</sub> liquid-rich) fluid inclusions have also been preserved within pyrite grains (Plates 5.1 e, f, g and 5.2e). Petrographically, the quartz, pyrite, and gold appear to have been deposited during the same mineralizing event. Therefore, the fluid contained within the primary type 1 and type 2 fluid inclusions appears to be directly related to sulphidation and gold deposition within the Boston deposit. Furthermore, the coexistence of primary type 1 and 2 fluid inclusions within the undeformed quartz grains hosted by pyrite in the main stage quartz-carbonate veins indicates that when these inclusions were trapped the fluid was undergoing phase separation. Therefore, the homogenization temperature and pressure calculated from the primary type 2 fluid inclusions corresponds to actual temperature of the hydrothermal fluid. The auriferous fluid responsible for lode-gold deposition, sulphidation, and hydrothermal alteration in the Boston deposit was a low salinity (2.6 to 9.3 eq. wt.% NaCl), H<sub>2</sub>O-CO<sub>2</sub> fluid that had an average temperature of 272 ±34°C and average pressure of 2.5 ±0.5 kilobars. Other dissolved gases such as N<sub>2</sub> and CH<sub>4</sub> do not appear to have been important as indicated by the CO<sub>2</sub> melting point of type 1 and type 2 fluid inclusions (-56.6°C for type 1 fluid inclusions and -56.8 ±0.2°C for type 2 fluid inclusions).

Secondary type 2 fluid inclusions are the most abundant fluid inclusion type that occurs within unmineralized quartz-carbonate ladder veins in the Boston deposit. Trails

and three-dimensional clusters of type 2 fluid inclusions occur throughout these veins. Secondary type 2 fluid inclusions within the quartz carbonate ladder veins have similar homogenization temperatures (189° to 331°C, n = 33), pressures (2.0 to 2.8 kilobars, n = 26), and salinities (4.0 to 5.9 eq. wt.% NaCl, n = 44) as the primary type 2 fluid inclusions associated with auriferous main stage quartz-carbonate veins in the Boston deposit (homogenization temperatures = 206° to 342°C, n = 81; homogenization pressures = 1.9 to 3.6 kilobars, n = 51; salinity = 2.6 to 9.3, n = 91; Figures 5.1 to 5.4). This suggests that the auriferous fluid responsible for the main stage quartz-carbonate veining and gold deposition within the three mineralized zones was also present during the formation of the quartz-carbonate ladder veins. As previously mentioned, ladder veins or flat veins in other Archean lode gold deposits are commonly mineralized (for example, the Hollinger-McIntyre deposit, Ontario, Burrows et al., 1993; and the Sigma mine, Quebec, Robert and Brown, 1986b; Robert and Kelly, 1987), however in the Boston deposit they appear to be sub-economic.

Trails and three-dimensional clusters of secondary, H<sub>2</sub>O-CO<sub>2</sub> liquid-rich, type 2 fluid inclusions also occur within healed micro-fractures and veinlets hosted by deformed quartz grains throughout the main stage quartz-carbonate veins in the Boston deposit (Plate 5.2a,b). The fluid inclusions occurring within these fractures were trapped sometime after the formation of the main stage quartz-carbonate veins and ladder veins during an episode of brittle fracturing and deformation of the vein minerals. In the B2 and B3 zones two relatively undeformed populations of secondary fluid inclusions were examined in detail. It was discovered that the secondary fluid inclusions within these fractures have similar microthermometric properties (homogenization temperature = 223

to 319°C, n = 15; homogenization pressure = 2.6 to 3.2 kilobars, n = 7; salinity = 5.1 to 7.8 eq. wt.% NaCl, n = 15) to primary type 2 fluid inclusions associated with hydrothermal alteration and gold deposition within the Boston deposit (homogenization pressure = 206 to 342, n = 81; homogenization pressure = 1.9 to 3.6 kilobars, n = 51; salinity = 2.6 to 9.3, n = 91).

The phantom veinlets within the three mineralized zones appear to be the result of a post vein filling stage of brittle fracturing. The occurrence of deformed H<sub>2</sub>O-CO<sub>2</sub> fluid inclusions within the phantom veinlets suggests that the auriferous fluid responsible for deposition of gold and pyrite within the main stage quartz-carbonate veins was still present during the formation of these veinlets. It is likely that this fluid was also present during the deposition and/or remobilization of coarse gold into the phantom veinlets in the B2 and B4 zones late in the life of this system. However, due to the poor quality of the quartz hosting fluid inclusions in the phantom veinlets detailed microthermometric measurements were not possible and no data were collected.

Coarse gold has not been observed within main stage quartz-carbonate veins and phantom veinlets in the B3 zone. It appears that once sealed the irregular stockworked veins that make up the B3 zone were much more difficult to remobilize than the thick, foliation parallel, vertically dipping fissure veins that make up the B2 and B4 zones. Consequently, less hydrothermal fluid was focused in any given area of the B3 zone. Gold and sulphide minerals tend to be more uniformly disseminated throughout the wallrock adjacent to the stockworked quartz-carbonate veins in the B3 zone and for the most part, the quartz-carbonate veins themselves appear to be barren.

### **6.1.2. Barren Fluids**

In addition to the auriferous fluid responsible for gold mineralization and hydrothermal alteration associated with the Boston deposit, at least two other types of hydrothermal fluid have invaded the Boston fault zone. The two barren fluids are represented by low salinity (5.7 and 9.3 eq. wt.% NaCl, n = 16), type 3, aqueous fluid inclusions and highly saline (14.9 and 17.6 eq. wt.% NaCl, n = 22), type 4, aqueous fluid inclusions (Plate 5.3a,b). In general type 3 and 4 fluid inclusions are gas poor and contain no CO<sub>2</sub>. The average homogenization temperature of type 3 fluid inclusions is between 102° and 207°C (n = 15). Type 4 fluid inclusions homogenize at temperatures between 80° and 147°C (n = 28). However, these temperatures do not represent trapping conditions and are probably an underestimate of the true trapping temperature of these inclusions.

Type 3 fluid inclusions occur as trails of secondaries within late barren quartz-carbonate veinlets that have been observed cross cutting all other vein types and host lithologies within the Boston deposit (Plate 5.3c). Petrographically these veinlets contain relatively undeformed quartz and carbonate and appear to have been emplaced relatively late in the life of the Boston deposit under conditions dominated by brittle deformation.

Late quartz-carbonate veinlets tend to occur most commonly within the B2 and B4 zones. This association can be explained if the style of main stage quartz-carbonate veining and the competency of the rocks hosting the three mineralized zones are considered. During late movements of the Boston fault zone the thick, quartz-carbonate fissure veins present in the B2 and B4 zones will be more easily refractured than the

thinner, stockworked quartz-carbonate veins characteristic of the B3 zone. Furthermore, the hydrothermally altered graphitic sediments and basalts associated with veining in the B2 and B4 zones will also be much more easily remobilized by shifts in the Boston fault zone than the more competent basalts and gabbros that host veining in the B3 zone. Consequently, late hydrothermal fluids would have more easily invaded the B2 and B4 zones relative to the B3 zone.

Type 3 fluid inclusions from within the barren quartz-carbonate veinlets have similar salinities (5.7 and 9.3 eq. wt.% NaCl, n = 16) to primary type 2 fluid inclusions from within auriferous quartz-carbonate veins in the Boston deposit (2.6 to 9.3 eq. wt.% NaCl; n = 91; Figure 5.3). It is possible that type 3 fluid inclusions represent a residual fluid that may have been present in the Boston fault zone late in the life of this system.

Type 4 fluid inclusions occur as irregular trails of secondaries within healed microfractures in both the main stage quartz-carbonate veins and crosscutting ladder veins in the Boston deposit (Plate 5.3d). Late, highly saline fluids, similar to the fluid in the aqueous type 4 fluid inclusions in the Boston deposit have been reported within gold-bearing quartz-carbonate veins in Archean lode-gold deposits throughout the world. In Canada, aqueous fluid inclusions with highly variable salinities have been observed in the Sigma mine, Quebec (Boullier et al., 1998; Robert and Kelly, 1987) and the Hollinger-McIntyre deposit, Ontario (Smith et al., 1984). These fluids have been interpreted to be the result of the invasion of late basement brines and are believed to be unrelated to lode-gold deposition in these deposits (Boullier et al., 1998).

## **6.2. Stable Isotopes**

### **6.2.1. The $\delta^{18}\text{O}_{\text{H}_2\text{O}}$ Composition of the Auriferous Fluid**

The oxygen stable isotopic composition of the hydrothermal fluid responsible for the deposition of quartz, carbonate, and gold within quartz-carbonate veins in the Boston deposit was calculated using the quartz-water and dolomite-water fractionation equations of Clayton et al. (1972) and Matthews and Katz (1977) respectively, at the average temperature of the auriferous fluid ( $272 \pm 34^\circ\text{C}$ ,  $n = 81$ ). Very little variation was recorded in the  $\delta^{18}\text{O}$  composition of ferroan dolomite, ankerite, and quartz separated from auriferous quartz-carbonate veins in the Boston lode-gold deposit (Figure 5.5b,c). The  $\delta^{18}\text{O}$  composition of carbonate minerals separated from the B2, B3, and B4 zones vary by only 1.6‰ (11.2 to 12.8‰,  $n = 15$ ), and quartz separated from gold-bearing veins in the three zones has  $\delta^{18}\text{O}$  values that vary by only 2.1‰ (12.8 to 14.9‰,  $n = 12$ ). Assuming that dolomite-water fractionation is also applicable to ankerite, the fluid in equilibrium with carbonate from the three mineralized zones was determined to have  $\delta^{18}\text{O}_{\text{H}_2\text{O}}$  values of 4.1 to 5.7‰, with an average value of  $5.0 \pm 0.5\%$  ( $n = 15$ ), whereas the fluid in equilibrium with quartz was determined to have  $\delta^{18}\text{O}_{\text{H}_2\text{O}}$  values of 4.9 to 7.0‰, with an average value of  $6.4 \pm 0.7\%$  ( $n = 12$ ). The oxygen isotopic composition of the fluid calculated using carbonate and quartz values overlaps extensively indicating that the quartz and carbonate within the main stage quartz-carbonate veins were deposited from an isotopically uniform hydrothermal fluid. The restricted range in  $\delta^{18}\text{O}_{\text{H}_2\text{O}}$  values also implies that these minerals were in isotopic equilibrium with each other as well as the hydrothermal fluid when they were deposited.

The metamorphic devolatilization of igneous and volcanogenic sedimentary rocks associated with greenstone belts typically produces fluids with  $\delta^{18}\text{O}_{\text{H}_2\text{O}}$  compositions of 5 to 13‰, whereas magmatic waters generally have  $\delta^{18}\text{O}_{\text{H}_2\text{O}}$  compositions of 5.5 to 10‰ (Taylor, 1979). The  $\delta^{18}\text{O}_{\text{H}_2\text{O}}$  fluid values calculated above for the Boston deposit are broadly compatible with both of these sources, and based on the oxygen isotope data alone it is not possible to distinguish between a metamorphic and a magmatic source for the hydrothermal fluid. Either of these sources for the fluid is reasonable considering that the granodioritic intrusions west of the Hope Bay volcanic belt appear to be broadly contemporaneous with the peak of metamorphism and deformation in this area.

Several samples of quartz were also separated from unmineralized flat veins within the Boston deposit and found to have uniform  $\delta^{18}\text{O}$  compositions of 13.8 to 14.6‰ (n = 4) that are similar to the gold-bearing quartz-carbonate veins in the Boston deposit (12.8 to 14.9‰, n = 12; Figure 5.5c). However, due to the poor quality of the fluid inclusions contained within the flat veins microthermometric measurements were not possible. As a result, no temperature data are available from the flat veins in the Boston deposit and the  $\delta^{18}\text{O}_{\text{H}_2\text{O}}$  value could not be calculated. Nevertheless, it appears that a hydrothermal fluid with a similar isotopic composition was responsible for the deposition of quartz within both the flat veins and the gold-bearing main stage quartz-carbonate veins in the Boston deposit.

### ***6.2.2. The $\delta^{13}\text{C}_{\text{CO}_2}$ Composition of the Auriferous Fluid***

The  $\delta^{13}\text{C}$  composition of ferroan dolomite and ankerite separated from auriferous main stage quartz-carbonate veins in the Boston deposit has a restricted range ( $\delta^{13}\text{C} =$



-4.7 to -3.1‰, n = 15; Figure 5.5a), similar to the range in  $\delta^{18}\text{O}$  values presented above. The  $\delta^{13}\text{C}_{\text{CO}_2}$  value of the hydrothermal fluid in equilibrium with ferroan dolomite and ankerite within these veins was calculated using the dolomite- $\text{CO}_2$  fractionation equation of Ohmoto and Rye (1979), at the average temperature of the auriferous fluid ( $272 \pm 34^\circ\text{C}$ , n = 81). Generally speaking, carbon isotopic fractionation between carbonate minerals is poorly constrained at temperatures above  $200^\circ\text{C}$ , but is believed to be less than 1.0‰ (Ohmoto and Rye, 1979). Therefore, it is reasonable to assume that the dolomite- $\text{CO}_2$  fractionation equation can be used to calculate the  $\delta^{13}\text{C}_{\text{CO}_2}$  value of the hydrothermal fluid in equilibrium with both ferroan dolomite and ankerite without significantly affecting the results. The  $\delta^{13}\text{C}_{\text{CO}_2}$  value of carbon dioxide in equilibrium with carbonate in the main stage quartz-carbonate veins was calculated to be between -3.8 and -2.2‰, with an average value of  $-3.0 \pm 0.6\text{‰}$  (n = 15).

Several possible sources of  $\text{CO}_2$  exist in the Hope Bay volcanic belt that may have contributed carbon to the hydrothermal fluid responsible for quartz-carbonate veining in the Boston deposit. Carbon may have originated from the oxidation or hydrolysis of disseminated graphite in sedimentary rocks or from the metamorphic decarbonation or leaching of carbonates from sedimentary and igneous rocks. Carbon may also have been derived from an as yet undiscovered magmatic source.

Graphitic argillites are commonly interfingering with the basaltic rocks in the Hope Bay volcanic belt. The  $\delta^{13}\text{C}$  values of graphite separated from argillites associated with the B2 and B4 zones fall between -29.0 to -25.0‰ (n = 6; Appendix G) and resemble typical reduced organic carbon in marine sedimentary rocks ( $\delta^{13}\text{C} = -30$  and -10‰, with an average value of approximately -25‰; Ohmoto and Rye, 1979; Ohmoto,

1986). Using the graphite-CO<sub>2</sub> fractionation equation of Ohmoto and Rye (1979), the  $\delta^{13}\text{C}_{\text{CO}_2}$  value of CO<sub>2</sub> produced by the interaction between a hydrothermal fluid and graphite in the argillites was calculated to be between -15.5 to -11.5‰, with an average value of  $-13.6 \pm 1.7\text{‰}$  (n = 6) at 272°C, if equilibrium is assumed. The  $\delta^{13}\text{C}_{\text{CO}_2}$  value of the auriferous hydrothermal fluid responsible for the main stage quartz-carbonate veining in the Boston deposit falls between -3.8 and -2.2‰ (n = 15). Therefore, the auriferous hydrothermal fluid does not appear to have been in equilibrium with graphite in the argillic sediments. Furthermore, CH<sub>4</sub> is also produced during the reaction between H<sub>2</sub>O and graphite. The auriferous fluid in the Boston deposit does not contain CH<sub>4</sub> and it is unlikely that interaction between the fluid and graphite provided much CO<sub>2</sub> to the hydrothermal system.

Alternatively, CO<sub>2</sub> may have been derived by the metamorphic decarbonation or leaching of carbonates from within carbonate rich sedimentary and volcanic rocks prior to entering the Boston fault zone. Carbonate rich sedimentary have been described several times by BHP geologists working within the Hope Bay volcanic belt. One sample of ferroan dolomite separated from a syngenetic carbonate unit collected in the Discovery area approximately 58 kilometres north of the Boston deposit (Figure 1.2) was analysed and found to have a  $\delta^{13}\text{C}$  value of 0.2‰. Pillowed basalts that have not been affected by hydrothermal alteration associated with lode-gold mineralization also occur throughout the Hope Bay volcanic belt. These rocks commonly contain disseminated calcite with  $\delta^{13}\text{C}$  values of around 0‰ that was most likely deposited in the presence of ocean water during or shortly after the basalt was extruded on the seafloor. In general, the  $\delta^{13}\text{C}_{\text{CO}_2}$  value of carbon dioxide produced by the dissolution of marine carbonates is

approximately  $0.4 \pm 2.7\text{‰}$  (Schidlowski et. al., 1975; Ohmoto and Rye, 1979) and is slightly enriched in the heavy isotope of carbon with respect to  $\text{CO}_2$  in the auriferous hydrothermal fluid ( $\delta^{13}\text{C}_{\text{CO}_2} = -3.8$  to  $-2.2\text{‰}$ ,  $n = 15$ ).

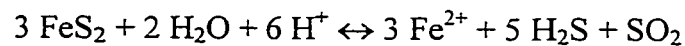
Carbon dioxide derived from a juvenile magmatic source generally has a  $\delta^{13}\text{C}_{\text{CO}_2}$  value of  $-5 \pm 2\text{‰}$  (Ohmoto and Rye, 1979), which is slightly depleted in the heavy isotope of carbon with respect to  $\text{CO}_2$  in the auriferous hydrothermal fluid ( $\delta^{13}\text{C}_{\text{CO}_2} = -3.8$  to  $-2.2\text{‰}$ ,  $n = 15$ ). In fact, the  $\delta^{13}\text{C}_{\text{CO}_2}$  value of the hydrothermal fluid is intermediate between juvenile magmatic carbon and  $\text{CO}_2$  produced by decarbonation or leaching of marine carbonate from sedimentary and igneous rocks ( $0.4 \pm 2.7\text{‰}$ ; Schidlowski et. al., 1975; Ohmoto and Rye, 1979). Other authors working on Archean lode-gold deposits have reported similar  $\delta^{13}\text{C}_{\text{CO}_2}$  values and have concluded that the  $\text{CO}_2$  was derived from a combination of magmatic carbon and the metamorphism of carbonate-bearing rocks (Golding and Wilson, 1983; Rye et al., 1976). Igneous rocks occur to the west of the Hope Bay volcanic belt that are of an appropriate age (Figure 2.1) and may have supplied carbon to the hydrothermal fluid; however, a suitable magmatic source has not yet been discovered in direct association with the Boston deposit and at this point a magmatic contribution to the auriferous fluid is only speculation.

### ***6.2.3. The $\delta^{34}\text{S}_{\text{H}_2\text{S}}$ Composition of the Auriferous Fluid***

Various amounts of sulphur, copper, arsenic, and gold have also been added to the wallrocks that host the Boston deposit by the hydrothermal fluid. Pyrite separated from the sulphidation halo adjacent to barren and auriferous quartz-carbonate veins has relatively uniform  $\delta^{34}\text{S}$  values of 1.6 to 3.5‰ ( $n = 14$ ; Figure 5.23). In lode-gold deposits

sulphur is typically transported in solution in the form of HS<sup>-</sup>. According to Ohmoto and Rye (1979) under equilibrium conditions isotopic fractionation between H<sub>2</sub>S and HS<sup>-</sup> dissolved in the hydrothermal fluid is negligible. Therefore, δ<sup>34</sup>S<sub>H<sub>2</sub>S</sub> values of 0.3 to 2.2‰, with an average of 1.2 ±0.5‰ (n = 14) were calculated for sulphur in the hydrothermal fluid using the pyrite-H<sub>2</sub>S fractionation equation of Ohmoto and Rye (1979) and the average homogenisation temperature of primary type 2 fluid inclusions (272 ±34°C, n = 81).

Pyrite and chalcopyrite are the most common sulphide minerals in igneous and sedimentary rocks throughout the Hope Bay volcanic belt, and may have been the source of sulphur in the auriferous fluid according to the following equation (Ohmoto and Rye, 1979).



Although lots of variation exists, the decomposition of sulphides in igneous and sedimentary rocks by a circulating hydrothermal fluid will generally liberate H<sub>2</sub>S with δ<sup>34</sup>S<sub>H<sub>2</sub>S</sub> values of 1 to 3‰ (Ohmoto and Rye, 1979) that are quite similar to those calculated for the auriferous hydrothermal fluid (δ<sup>34</sup>S<sub>H<sub>2</sub>S</sub> = 0.3 to 2.2‰). However, magmatic fluids contain sulphur with δ<sup>34</sup>S values of approximately 0.0 ±3‰ (Ohmoto and Goldhaber, 1997). As a result, the sulphur isotopic data, like the oxygen and carbon data discussed above, cannot be interpreted unambiguously. Sulphur, and by association copper, arsenic, and gold, present in the Boston deposit may have been leached from basaltic and/or sedimentary rocks by a metamorphically derived fluid. Alternatively,

these components may have been contributed to the hydrothermal system by a yet undiscovered magmatic source or combination of these two sources.

#### ***6.2.4. The $\delta^{13}\text{C}$ and $\delta^{18}\text{O}$ Composition of Secondary Carbonate in the Country Rocks***

It is apparent from Figure 5.6a that secondary calcite, ankerite, and ferroan dolomite within the metamorphically altered igneous and sedimentary rocks in the area surrounding the Boston deposit have a range of stable isotopic compositions that are different from the mineralized zones. The contrast observed in  $\delta^{13}\text{C}$  and  $\delta^{18}\text{O}$  values with distance from the mineralized veins can be explained if the system responsible for quartz-carbonate veining, hydrothermal alteration, and lode-gold mineralization in the Boston deposit was fluid dominated. Within the hydrothermal center where fluid flow is at a maximum, the fluid to rock ratio will be very large. Minerals deposited within auriferous quartz-carbonate veins and the wallrocks immediately adjacent to them will be in equilibrium with the fluid and the  $\text{CO}_2$  it contains. As a result, the stable isotopic composition of minerals deposited in the hydrothermal center will reflect the stable isotopic composition of the hydrothermal fluid. Away from the hydrothermal center the fluid to rock ratio will be low. Any hydrothermal fluid interacting with the surrounding country rocks will equilibrate with them and as a result, the stable isotopic composition of the carbonate minerals deposited within the country rocks distal to the hydrothermal center will tend to reflect the rocks that host them.

At Boston there is evidence for extensive fluid-rock interaction along vein conduits during hydrothermal fluid discharge. Carbonate minerals deposited in the wallrocks immediately adjacent to gold-bearing veins in the Boston fault zone have  $\delta^{13}\text{C}$

values of -4.0 to -2.9‰ (n = 5) and  $\delta^{18}\text{O}$  values of 11.8 to 13.0‰ (n = 5), and resemble carbonate minerals deposited within the gold-bearing veins themselves ( $\delta^{13}\text{C} = -4.7$  to -3.1‰, n = 15;  $\delta^{18}\text{O} = 11.3$  to 12.8‰, n = 15; Figure 5.6b). Furthermore, due to the high ratio of fluid to rock along the vein conduits the isotopic composition of carbonate minerals deposited within the veins is believed to reflect the isotopic composition of the auriferous fluid with little contamination from the country rocks.

Inspection of the data in Figure 5.6a leads to the inference of a low water to rock ratio in the country rocks surrounding the Boston deposit. Carbonate minerals deposited within hydrothermally and metamorphically altered country rocks not associated with mineralized veining tend to have distinct isotopic compositions. Assuming that temperature has remained constant during alteration, the water to rock ratio was low, and that carbonate deposited within the country rocks was in equilibrium with the fluid and the  $\text{CO}_2$  it contains, differences in the stable isotopic composition of carbonate hosted by different rock types in the Boston area can be directly related to differences in the whole rock isotopic composition of these rock types.

The water to rock ratio appears to have decreased very rapidly with distance from the mineralized veins in the Boston fault zone. Calcite separated from igneous and sedimentary rocks outside of the Boston fault zone is likely the product of seafloor diagenesis or metamorphism and therefore its stable isotopic composition appears to be unrelated to the isotopic composition of the hydrothermal fluid and entirely dependent on the original isotopic composition of the host rocks. As a result an isotopic trend with distance from the mineralized veins was not observed in Figures 5.8 to 5.15.

### ***6.2.5. The $\delta^{13}\text{C}$ and $\delta^{18}\text{O}$ Composition of Quartz and Carbonate in Regional Veins***

The stable isotopic composition of several samples of quartz and carbonate separated from barren veins hosted by metamorphically altered igneous and sedimentary rocks in the Boston area have been calculated and are plotted in Figure 5.16. Aside from a few isolated samples discussed earlier, quartz and carbonate separated from the barren veins have stable isotopic compositions that resemble secondary carbonate minerals disseminated throughout the surrounding country rocks. Assuming that the temperature remained constant, the fluid that deposited quartz and carbonate within these veins must have been in isotopic equilibrium with the surrounding country rocks and the water to rock ratio within these veins must have been low.

Consistent with the above statement, carbonate minerals separated from veins hosted by basaltic rocks in the Boston area have  $\delta^{13}\text{C}$  values of -2.9 to 0.5‰ (n = 10) and  $\delta^{18}\text{O}$  values of 12.2 to 13.9‰ (n = 7), which overlap almost perfectly with the isotopic composition of carbonate minerals separated from the basalts that host them ( $\delta^{13}\text{C} = -2.8$  to 0.7‰, n = 36;  $\delta^{18}\text{O} = 10.7$  to 13.8‰, n = 33). However, when looked at with respect to distance from the Boston deposit, carbonate minerals in the metamorphically altered basalt hosted quartz-carbonate veins have stable isotopic compositions that appear to shift gradually toward enriched  $\delta^{13}\text{C}$  values relative to the mineralized zones (Figure 5.17b). Where microthermometric analyses were possible, the primary and secondary type 2 fluid inclusions within the barren veins were found to be similar (homogenization temperature = 181° to 292°C, n = 15; homogenization pressure = 2.8 to 2.9 kilobars, n = 3; salinity = 2.8 to 10.7 eq. wt.% NaCl, n = 15) to primary type 2 fluid inclusions within mineralized

veins in the Boston fault zone (homogenization temperature = 206° to 342°C, n = 81; homogenization pressure = 1.9 to 3.6 kilobars, n = 51; salinity = 2.6 to 9.3 eq. wt.% NaCl, n = 91). Due to the increased permeability within the veins, higher water to rock ratios may have been preserved to much greater distances from the hydrothermal center than was possible within the surrounding wallrocks. As a result, the shift from fluid-dominated to wallrock-dominated  $\delta^{13}\text{C}$  values will be more gradual in carbonates deposited within the barren veins than it is in carbonates deposited within the basaltic rocks themselves. As previously mentioned, cold seawater alteration of pillow basalts on the sea floor will produce rocks with  $\delta^{13}\text{C}$  values around 0‰ (Muehlenbachs, 1986). This is consistent with the  $\delta^{13}\text{C}$  enrichment observed in carbonate minerals separated from basalt-hosted veins farther away from the Boston deposit (Figure 5.17b).

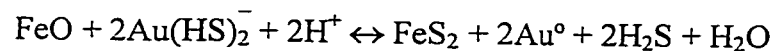
However, the isotopic shift observed in Figure 5.17b is very slight and only based on carbonate separated from ten vein samples. Furthermore, a corresponding distance-related shift was not observed in the  $\delta^{18}\text{O}$  values of carbonate and quartz separated from these veins (Figures 5.18b and 5.19b). At this time the true nature of the  $\delta^{13}\text{C}$  shift recorded in carbonate minerals separated from basalt hosted barren veins in the Boston area is not completely understood.

### **6.3. *Deposition of Gold***

As mentioned previously a significant portion of the gold in the B2 and B4 zones and the majority of the gold in the B3 zone occurs with sulphides, in particular pyrite, arsenopyrite, and chalcopyrite (Plate 3.13). Gold typically occurs as inclusions within



sulphide minerals or as fracture fill and thin coatings on the surface of sulphide grains. Sulphide alteration commonly forms a halo that extends more than 15 centimetres into the wallrock on either side of auriferous veins (Plate 3.11). Sulphidation is directly related to an increase in pH and the release of reduced iron into the hydrothermal fluid that accompanies the replacement of chlorite in the wallrock by carbonate, paragonite, and muscovite. Pyrite is precipitated in the wallrock when part of the iron from the hydrothermal alteration of chlorite reacts with  $\text{HS}^-$  in the fluid under slightly acidic conditions (Kishida and Kerrich, 1987). If the fluid also contains dissolved arsenic and copper, arsenopyrite and chalcopyrite may be deposited as a result of a similar process. The following reaction illustrates how sulphidation and gold deposition may occur in the wallrocks adjacent to the main stage quartz-carbonate veins in the B2, B3, and B4 zones.



Gold is typically transported in solution as a bisulphide complex. The stability of the gold-bisulphide complex is directly related to availability of  $\text{HS}^-$  in the fluid (Reed, 1997; Gibert et al., 1998). By removing  $\text{HS}^-$  from the fluid, wallrock sulphidation may act as a catalyst, triggering the precipitation of gold in lode-gold deposits (Kishida and Kerrich, 1987). Gold will become included within growing sulphide grains as hydrothermal alteration and sulphidation of the wallrocks continues.

Within the B2 and B4 zones gold also occurs as coarse crystals within deformed and recrystallized quartz-filled phantom veinlets within the main stage quartz-carbonate veins. It is possible that the gold was remobilized and redeposited in the phantom

veinlets during D3 deformation. Conversely, rapid drops in fluid pressure would have accompanied hydraulic fracturing during the formation of the main stage quartz-carbonate veins. Rapid pressure fluctuations may have triggered phase separation in a hydrothermal fluid. Carbon dioxide, H<sub>2</sub>S, and other dissolved gasses will be lost to the vapour phase as a result. Gold may have been deposited within the phantom veinlets as a result of the increase in pH and the decrease in availability of HS<sup>-</sup> in the fluid that would have accompanied phase separation and the loss of CO<sub>2</sub> and H<sub>2</sub>S to the vapour phase (Gibert et al., 1998).

As mentioned previously, quartz within the phantom veinlets typically contains small (approximately 5 μm), irregularly shaped, H<sub>2</sub>O-CO<sub>2</sub> fluid inclusions with variable fill volumes. A preliminary petrographic and microthermometric examination of these fluid inclusions revealed that they are similar to the type 2 fluid inclusions commonly associated with gold and pyrite in other parts of the main stage quartz-carbonate veins. However, due to the poor quality of the quartz hosting these fluid inclusions detailed microthermometric measurements were not possible and no data were collected.

#### ***6.4. The South Patch Occurrence***

Isotopically, carbonate minerals separated from auriferous quartz-carbonate veins and secondary carbonate minerals disseminated throughout the metamorphically altered basaltic and gabbroic rocks associated with the South Patch occurrence and the Boston deposit, are almost identical ( Tables 5.2 and 5.5, and Figures 5.6a and 5.24). This

suggests that the fluids responsible hydrothermal alteration and lode-gold mineralization in the South Patch occurrence and Boston deposit were, at least isotopically, very similar. Furthermore, the fluid to rock ratio in both deposits appears to have shifted from fluid dominated, within the hydrothermal center, to rock dominated within a small distance from the mineralized veins. This suggests that the auriferous hydrothermal fluid in both the Boston deposit and the South Patch occurrence was largely confined to the gold-bearing quartz-carbonate veins and directly adjacent wallrocks during the life of the mineralizing system.

#### ***6.5. Similarity to other Archean lode-gold deposits***

Archean quartz-carbonate vein lode-gold deposits are a characteristic feature of Archean greenstone belts within granite-greenstone terrains throughout the world. Deposits of this type typically occur in environments characterized by low- to medium-grade metamorphic rocks, brittle to ductile rock behaviour, and compressive deformation. Mineralized veining commonly occurs in close proximity to belt scale shear zones, resulting in broadly linear arrays of major gold deposits or districts (Groves and Foster, 1991; Robert, 1995; de Ronde et al., 1997). Mineralized quartz-carbonate veins may occur in any of the rock types present in a given greenstone belt, although deposits hosted by mafic volcanic and associated ultramafic igneous rocks are by far the most common. Furthermore, within a given shear zone mineralized veining tends to be structurally controlled, becoming most intense at the contacts between rocks of differing competency (Groves and Foster, 1991; Robert, 1995; de Ronde et al., 1997).

The structural setting and metamorphic grade generally associated with Archean lode-gold deposits appears to be typical of the Boston deposit as well. As discussed above, the Boston deposit occurs within the Boston fault zone and is hosted by deformed lower-greenschist facies mafic-volcanic and gabbroic rocks. The Boston fault zone is part of a larger north-south-trending structure, the Hope Bay fault, which traverses the entire length of the Hope Bay volcanic belt. The quartz-carbonate veins that make up the Boston deposit have been affected by both brittle and ductile deformation related to compression in the vicinity of the Boston fault zone. Finally, in a manner similar to other Archean lode-gold deposits, the intensity of quartz-carbonate veining within the Boston fault zone increases significantly as the contacts between competent volcanic rocks and ductile sedimentary rocks are approached.

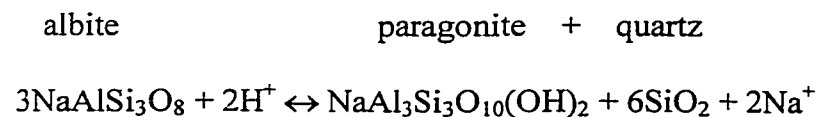
#### ***6.5.1. Mineralization and wallrock alteration***

In most Archean lode-gold deposits, including the Boston deposit, gold occurs with sulphide minerals, in particular pyrite and arsenopyrite, both within the quartz carbonate veins and as an integral part of the wallrock alteration immediately adjacent to these veins (Groves and Foster, 1991; Robert, 1995). Gold forms coatings, fracture-fillings, and inclusions within sulphide grains in a halo that extends several centimetres into the wallrocks on either side of the quartz-carbonate veins. Gold also occurs as isolated grains of free gold within particularly rich veins.

Hydrothermal alteration similar to what has been observed in the Boston deposit has been described numerous times in various lode-gold deposits throughout the world, for example: the Sigma mine, Quebec (Robert and Brown, 1986a), the Kerr-Addison

mine (Kishida and Kerrich, 1987) and the Timmins (Porcupine) area (Smith and Kesler, 1985) Ontario, the Kambalda area (Phillips and Groves, 1983) and the Kalgoorlie area (Phillips, 1986) western Australia, and the Fazenda Brasileiro mine, Bahia (Teixeira et al., 1990), and is summarized in Table 6.1. In the wallrocks surrounding most Archean lode-gold deposits a distinctly zoned hydrothermal alteration mineral assemblage has overprinted the metamorphic mineral assemblage. Slight variations in silicate and carbonate mineralogy are common. However, an overall trend to intense carbonation related to the introduction of significant amounts of CO<sub>2</sub> into the wallrocks from the hydrothermal fluid, and shift from chlorite-dominated to sericite-dominated alteration is the same in every deposit.

One difference apparent in Table 6.1 is that in most Archean lode-gold deposits albite is the dominant sodium-bearing phase both proximal and distal to the hydrothermal center. Hydrothermal alteration in the Boston deposit is characterized by a complete lack of albite and instead contains abundant paragonite as the dominant sodium-bearing phase. The relationship between albite and paragonite is illustrated by the following equation (Reed, 1997):



According to the equation above, the hydrothermal fluid responsible for wallrock alteration and lode-gold mineralization in the Boston area did not contain enough sodium

**Table 6.1.** Wallrock alteration associated with the Boston deposit and typical basalt hosted Archean lode-gold deposits: Archean lode-gold deposit information adapted from Groves and Foster (1991).

Distance from hydrothermal center	Boston	Typical Archean lode-gold deposit
Main ore zone	Quartz-carbonate veining; silicification; ankerite/dolomite + dravite + paragonite ± muscovite ± siderite; rare phlogopite; abundant pyrite, arsenopyrite, and chalcopyrite	Quartz-carbonate veining; silicification; ankerite + biotite or sericite, some albite; rare green mica; abundant Fe-sulphides ± arsenopyrite; stibnite locally abundant
Proximal alteration	Ankerite-dolomite + sericite (paragonite and muscovite) ± high-Mg chlorite (clinochlore); trace pyrite and chalcopyrite	Ankerite-dolomite + biotite or sericite ± high-Mg chlorite; some Fe-sulphides
Distal alteration	Calcite + chlorite + sericite (paragonite ± muscovite); trace pyrite and chalcopyrite	Calcite + chlorite + amphibole + albite; minor Fe-sulphides

or was slightly too acidic for albite to precipitate. Instead paragonite was deposited as the stable sodium bearing silicate.

### **6.5.2. Nature of the mineralizing fluids**

Table 6.2 lists selected microthermometric and stable isotopic data for the Boston deposit and South Patch occurrence along with similar data compiled by Groves and Foster (1991) and de Ronde et al. (1997) for other Archean lode-gold deposits throughout the world. It is apparent from Table 6.2 that the gold-bearing fluids responsible for lode-gold mineralization in Archean greenstone belts world wide, including the Boston deposit, are very similar.

Archean lode-gold deposits are characterized by low-salinity (3 to 6 eq. wt.% NaCl), slightly reducing, H<sub>2</sub>O-CO<sub>2</sub> fluids, with nearly neutral pH. Minimum temperatures of 200 to 400°C and pressures of 0.5 to 4.5 kilobars are typical. The auriferous fluid is generally water dominated (75 to 90 mole percent). The CO<sub>2</sub> fraction is of moderate density (0.3 to 0.9 g/cm<sup>3</sup>) and constitutes 10 to 25 mole percent of the fluid. Minor CH<sub>4</sub> and N<sub>2</sub> are also present in many deposits but rarely make up more than 1 mole percent of the fluid. Variable degrees of phase separation have also commonly been recognized (Groves and Foster, 1991; Robert, 1995; de Ronde et al., 1997).

The auriferous hydrothermal fluid in the Boston deposit is also a low salinity (2.6 to 9.3 eq. wt.% NaCl, n = 91), H<sub>2</sub>O-CO<sub>2</sub> fluid with a similar temperature (206 to 342°C, n = 81), and pressure (1.9 to 3.6 kilobars, n = 51) to typical of Archean lode-gold deposits throughout the world. Carbon dioxide with a density of 0.3 to 0.7 g/cm<sup>3</sup> (n = 51) makes up between 3 and 14 mole percent (n = 51) of the auriferous fluid in the Boston deposit,

**Table 6.2.** Fluid characteristics and selected stable isotope values for the Boston deposit, the South Patch occurrence, and Archean lode-gold deposits in general: Archean lode-gold deposit data modified after Groves and Foster (1991) and de Ronde et al. (1997); NA = Not Available.

Parameter	Boston Fluid	South Patch Fluid	General Fluid in Archean Lode-Gold Deposits	Data Source
Mineralizing fluid	3-phase H <sub>2</sub> O-CO <sub>2</sub> inclusions	NA	3-phase H <sub>2</sub> O-CO <sub>2</sub> inclusions	Fluid inclusions
T, °C	206 to 342	NA	200 to 450	Fluid inclusions
P <sub>fluid</sub> , kb	1.9 to 3.6	NA	1 to 4.5	Fluid inclusions
Wt.% NaCl Equiv.	2.6 to 9.3	NA	< 6	Fluid inclusions
CO <sub>2</sub> Density (g/cm <sup>3</sup> )	0.3 to 0.7	NA	0.3 to 0.9	Fluid inclusions
Mole % CO <sub>2</sub>	3 to 14	NA	10 to 25	Fluid inclusions
Mole % H <sub>2</sub> O	86 to 96	NA	75 to 90	Fluid inclusions
Evidence for phase separation	Yes	NA	Yes	Fluid inclusions
Gold deposition mechanism	Sulphidation (poss. phase separation)	Sulphidation (poss. phase separation)	Sulphidation and/or Phase separation	Fluid inclusions, petrography, chemistry
δ <sup>18</sup> O <sub>carbonate</sub> , ‰	+11.2 to +12.8	+11.6 to +13.2	+9 to +14	Stable isotopes
δ <sup>18</sup> O <sub>quartz</sub> , ‰	+12.8 to +14.9	+10.2 to +14.6	+8 to +16	Stable isotopes
δ <sup>18</sup> O <sub>H<sub>2</sub>O</sub> , ‰	+4.1 to +7.0	NA	+2.5 to +10	Stable isotopes
δ <sup>13</sup> C <sub>carbonate</sub> , ‰	-4.7 to -3.1	-3.8 to -2.1	-10 to +2.2	Stable isotopes
δ <sup>13</sup> C <sub>CO<sub>2</sub></sub> , ‰	-3.8 to -2.2	NA	-7 to +1	Stable isotopes
δ <sup>34</sup> S <sub>pyrite</sub> , ‰	+1.6 to +3.5	NA	+0.8 to +8.1	Stable isotopes
δ <sup>34</sup> S <sub>fluid</sub> , ‰	δ <sub>34</sub> S <sub>H<sub>2</sub>S</sub> = + 0.3 to +2.2	NA	δ <sup>34</sup> S <sub>fluid</sub> = +1 to +3	Stable isotopes



with water making up the other 86 to 96 mole percent ( $n = 51$ ). Other dissolved gasses such as  $\text{CH}_4$  and  $\text{N}_2$  do not appear to have been important in the Boston deposit as they are in other Archean lode-gold deposits (Groves and Foster, 1991).

The gold-bearing fluid in Archean lode-gold deposits generally has  $\delta^{18}\text{O}_{\text{fluid}}$  values of 2.5 to 10‰,  $\delta^{13}\text{C}_{\text{fluid}}$  values of -7 to 1‰, and  $\delta^{34}\text{S}_{\text{fluid}}$  values of 1 to 3‰ (Groves and Foster, 1991). The mineralized fluid in the Boston deposit contains  $\text{H}_2\text{O}$  ( $\delta^{18}\text{O}_{\text{H}_2\text{O}} = 4.1$  to  $7.0\text{‰}$ ,  $n = 27$ ),  $\text{CO}_2$  ( $\delta^{13}\text{C}_{\text{CO}_2} = -3.8$  to  $-2.2\text{‰}$ ,  $n = 15$ ), and  $\text{H}_2\text{S}$  ( $\delta^{34}\text{S}_{\text{H}_2\text{S}} = 0.3$  to  $2.2\text{‰}$ ,  $n = 14$ ) with isotopic compositions that are comparable to Archean lode-gold deposits worldwide. In fact, the stable isotopic data for quartz, carbonate, and sulphide separated from mineralized veins in the Boston deposit, South Patch occurrence, and other Archean lode-gold deposits are almost identical, suggesting isotopically similar sources for the mineralized fluids.

## 7. Conclusions

The system responsible for lode-gold mineralization and hydrothermal alteration in the Boston deposit appears to have been fluid dominated, but largely confined to quartz-carbonate veins and adjacent wallrocks within the Boston fault zone. The auriferous fluid was a low salinity ( $4.4 \pm 1.6$  eq. wt.% NaCl,  $n = 91$ ),  $\text{H}_2\text{O}$ - $\text{CO}_2$  fluid that was at an average temperature of  $272 \pm 34^\circ\text{C}$  ( $n = 81$ ) and average pressure of  $2.5 \pm 0.5$  kilobars ( $n = 51$ ). The fluid has a  $\delta^{18}\text{O}_{\text{H}_2\text{O}}$  value of 4.1 to  $7.0\text{‰}$  ( $n = 27$ ), a  $\delta^{13}\text{C}_{\text{CO}_2}$  value of -3.8 to  $-2.2\text{‰}$  ( $n = 15$ ), and a  $\delta^{34}\text{S}_{\text{H}_2\text{S}}$  value of 0.3 to  $2.2\text{‰}$  ( $n = 14$ ). Based on the microthermometric and isotopic data alone it is difficult to evaluate the relative

importance of magmatic versus metamorphic input to the hydrothermal fluid.

Granodioritic intrusions synchronous with the peak of metamorphism and deformation in the Hope Bay volcanic belt are common to the west of the Boston deposit. It is entirely possible that at deeper levels in the crust a metamorphically derived hydrothermal fluid may have incorporated carbon, sulphur, and possibly some gold from an as yet undiscovered magmatic source before entering the Boston area. Nesbitt and Muehlenbachs (1989) suggested that deeply circulating, highly evolved meteoric water may have played an important role in the development of mesothermal lode-gold deposits. However, at the present time the true origin of the fluids responsible for lode-gold mineralization in the Boston deposit remains poorly understood.

The tight grouping of microthermometric and stable isotopic data from the Boston deposit suggests that gold was deposited in this area from an auriferous fluid with uniform physical and geochemical characteristics. Furthermore, the structural style and nature of the hydrothermal alteration, mineralization, and fluid chemistry characteristic of the Boston deposit was also observed in the South Patch occurrence and has been described in numerous other lode-gold deposits in Archean greenstone belts throughout the world (Groves and Foster, 1991; Robert, 1995; de Ronde et al., 1997), indicating that these deposits formed in similar tectonic environments from similar gold-bearing fluids.

There is a great potential for the discovery of additional major lode-gold deposits within the Hope Bay volcanic belt. Highly mineralized greenstone belts in Archean cratons throughout the world, generally contain clusters of hundreds to thousands of individual gold deposits that outline giant gold mining districts or camps (for example; the Abitibi belt, Quebec; the Timmins (Porcupine) district, Ontario; and the Kalgoorlie

area, western Australia; Groves and Foster, 1991; Robert, 1995). Several small to medium size gold showings and prospects, including the South Patch occurrence, have been discovered in the northern end of the Hope Bay volcanic in which the style of mineralization and hydrothermal alteration resembles what has been described for the Boston deposit in this study. However, to this date the Boston deposit remains relatively isolated in the southern portion of the belt. There is no reason to believe that future exploration along the strike of the Hope Bay fault will not reveal the presence of additional lode-gold resources in this area.

## 8. References

- Bevier, M.L., and Gebert, J.S., 1991, U-Pb geochronology of the Hope Bay-Elu Inlet area, Bathurst block, northeastern Slave structural province, Northwest Territories: *Canadian Journal of Earth Sciences*, v. 28, p. 1925-1930.
- BHP internal report (various authors), 1999, Hope Bay Project – Exploration Overview: unpublished BHP internal report, 335 p.
- Bleeker, W., and Villeneuve, M., 1995, Structural studies along the Slave portion of the Snorcle transect: Geological Survey of Canada, Continental Geoscience Division, Snorcle Workshop, p. 8-13.
- Bodnar, R.J., 1993, Revised equation and table for determining the freezing point depression of H<sub>2</sub>O-NaCl solutions: *Geochimica et Cosmochimica Acta*, v. 57, p. 683-684.
- Boullier, A., Firdaous, K., and Robert, F., 1998, On the significance of aqueous fluid inclusions in gold-bearing quartz vein deposits from the southeastern Abitibi subprovince (Quebec, Canada): *Economic Geology*, v. 93, p. 216-223.

- Bowring, S.A., King, J.E., Housh, T.B., Isachsen, C.E., and Podosek, F.A., 1989b, Neodymium and lead isotopic evidence for enriched early Archaean crust in North America: *Nature*, v. 340, 222-225.
- Bowring, S.A., Williams, I.S., and Compson, W., 1989a, 3.96 Ga gneisses from the Slave province, Northwest Territories, Canada: *Geology*, v. 17, p. 971-975.
- Brown, P.E., 1998, Fluid inclusion modeling for hydrothermal systems: *in* J.P. Richards and P.B. Larson ed., *Techniques in hydrothermal ore deposit geology*, *Reviews in Economic Geology*, v. 10, p. 151-171.
- Brown, P.E., 1989, FLINCOR: a microcomputer program for the reduction and investigation of fluid inclusion data: *American Mineralogist*, v. 74, p. 1390-1393.
- Brown, P.E., and Lamb, W.M., 1986, Mixing of H<sub>2</sub>O-CO<sub>2</sub> in fluid inclusions; geobarometry and Archean gold deposits: *Geochimica et Cosmochimica Acta*, v. 50, p. 847-852.
- Brown, P.E., and Lamb, W.M., 1989, P-V-T properties of fluids in the system H<sub>2</sub>O ± CO<sub>2</sub> ± NaCl: new graphical presentations and implications for fluid inclusion studies: *Geochimica et Cosmochimica Acta*, v. 53, p. 1209-1221.

- Burrows, D.R., Spooner, E.T.C., Wood, P.C., and Jemielita, R.A., 1993, Structural controls on formation of the Hollinger-McIntyre Au quartz vein system in the Hollinger shear zone, Timmins, southern Abitibi greenstone belt, Ontario: *Economic Geology*, v. 88, p. 1643-1663.
- Carothers, W.W., Adami, L.H., and Rosenbauer, R.J., 1988, Experimental oxygen isotopic fractionation between siderite-water and phosphoric acid liberated CO<sub>2</sub>-siderite: *Geochimica et Cosmochimica Acta*, v. 52, p. 2445-2450.
- Clark, D.B., 1996, The geology of the Boston deposit, Hope Bay volcanic belt, Northwest Territories, Canada: Unpublished M.Sc. thesis, Queen's University, Kingston, Ontario, 94p.
- Clayton, R.N., O'Neil, J.R., and Mayeda, T.K., 1972, Oxygen isotope exchange between quartz and water: *Journal of Geophysical Research*, v. 77, P. 3057-3067.
- Darling, R.S., 1991, An extended equation to calculate NaCl contents from clathrate melting temperatures in H<sub>2</sub>O-CO<sub>2</sub>-NaCl fluid inclusions: implications fro P-T isochore location: *Geochimica et Cosmochimica Acta*, v. 55, p. 3869-3871.
- Davis, W.J., and Bleeker, W., 1997, Timing of plutonism and regional deformation in the Yellowknife – Sleepy Dragon area, southern Slave Province: in *NWT geoscience*

forum 25<sup>th</sup> anniversary Yellowknife; program and abstracts of talks and posters, Indian and Northern Affairs Canada, Yellowknife, NWT, Canada, p. 34-36.

Davis, W.J., and Hegner, E., 1992, Neodymium isotopic evidence for the tectonic assembly of late Archean crust in the Slave Province, Northwest Canada: *Contributions to Mineralogy and Petrology*, v. 111, p. 493-504.

Davis, W.J., Fryer, B.J., and King, J.E., 1994, Geochemistry and evolution of late Archean plutonism and its significance to the tectonic development of the Slave craton: *Precambrian Research*, v. 67, p. 207-241.

Davis, W.J., Gariépy, C., and van Breemen, O., 1996, Pb isotopic composition of late Archean granites and the extent of recycling early Archean crust in the Slave province, northwest Canada: *Chemical Geology*, v. 130, p. 255-269.

Faure, G., 1986a, Carbon: *in* John Wiley and Sons, ed., *Principles of isotope geology*, second edition, p. 491-520.

Faure, G., 1986b, Oxygen and hydrogen in the lithosphere: *in* John Wiley and Sons, ed., *Principles of isotope geology*, second edition, p. 460-484.

Fraser, J.A., 1964, Geological notes on the northeastern District of Mackenzie, Northwest Territories: Geological Survey of Canada, Paper 63-40, 21p.

- Fyson, W.K., Dube, A., and Padgham, W.A., 1993, A new tectonically oriented compilation map of the Slave Province: *in* Program with Abstracts, Joint annual meeting of the Geological Association of Canada and the Mineralogical Association of Canada 18, p 33.
- Gao, Z.L., and Kwak, T.A.P., 1997, The geochemistry of wall rock alteration in turbidite-hosted gold vein deposits, central Victoria, Australia: *Journal of Geochemical Exploration*, v. 59, p. 259-274.
- Gebert, J., 1989a, Preliminary mapping in the Hope Bay metavolcanic belt, Bathurst block, Slave province, NWT: Canada-NWT Mineral Development Agreement, 8p.
- Gebert, J., 1989b, The geology of the Hope Bay and Elu Inlet metavolcanic belts northeastern Slave province, NWT: *in* Northwest Territories Geology Division-Department of Indian Affairs and Northern Development, Exploration Overview 1989: Mining, Exploration and Geological Investigations, p. 33-34.
- Gebert, J., 1990a, Geology of the Hope Bay and Elu Inlet metavolcanic belts, Bathurst block, northeastern Slave province, N.W.T.: *in* Northwest Territories Geology Division-Department of Indian Affairs and Northern Development, Exploration Overview 1990: Mining, Exploration and Geological Investigations, p. 26-27.



- Gebert, J.S., 1990b, Hope Bay project: *in* GNWT-DIAND Geoscience Projects 1989, Annual Report, March 1990, Canada-Northwest Territories Mineral Development Agreement, p. 21-27.
- Gebert, J.S., 1992, Geology of the Hope Bay and Elu Inlet metavolcanic belts, northeastern Slave province, NWT: *in* Richardson, D.G., and Irving, M., ed., Project Summaries, Canada-Northwest Territories Mineral Development Subsidiary Agreement 1987-1991, Geological Survey of Canada Open File 2484, p. 15-17.
- Gebert, J.S., 1993, Geology and Mineral potential of the Archean Hope Bay and Elu Inlet volcanic belts, northeastern Slave structural province, district of Mackenzie, N.W.T.: NWT Geology Division-Department of Indian and Northern Affairs Canada: Canada/NWT Mineral Development Agreement, 103p.
- Gibert, F., Pascal, M.L., and Pichavant, M., 1998, Gold solubility and speciation in hydrothermal solutions: experimental study of the stability of hydrosulphide complex of gold ( $\text{AuHS}^{\ominus}$ ) at 350 to 450°C and 500 bars: *Geochimica et Cosmochimica Acta*, v. 62, p. 2931-2947.
- Golding, S.D., and Willson, A.F., 1983, Geochemical and stable isotopic studies of the No. 4 lode, Kalgoorlie, Western Australia: *Economic Geology*, v. 78, p. 438-450.

- Groves, D.I., and Foster, R.P., 1991, Archean lode gold deposits: *in* Gold Metallogeny and Exploration, Chapter 3, p. 63-103.
- Guha, J., Lu, H.Z., Dube, B., Robert, F., and Gagnon, M., 1991, Fluid characteristics of vein and altered wall rock in Archean mesothermal gold deposits: Economic Geology, v. 86, p. 667-684.
- Hebel, M., 1999, U-Pb geochronology and lithochemistry of the Hope Bay greenstone belt, Slave structural province, Northwest Territories, Canada: Unpublished M.Sc. thesis, University of British Columbia, Vancouver, British Columbia, microfiche.
- Henderson, J.B., 1970, Stratigraphy of the Archean Yellowknife Supergroup, Yellowknife – Prosperous Bay area, District of Mackenzie: Geological Survey of Canada, Paper 70, 26 p.
- Hodgson, C.J., 1989, The structure of shear-related, vein-type gold deposits: a review: Ore Geology Reviews, v. 4, p. 231-273.
- Hoffman, P.F., 1989, Precambrian geology and tectonic history of North America: *in* Bally, A.W., and Palmer, A.R., eds, Vol. A., The geology of North America – an overview, The Geological Society of America, p. 447-512.

- Hurst, M.E., 1935, Vein formation at Porcupine: *Economic Geology*, v. 30, p. 103-127.
- Isachsen, C.E., Bowring, S.A., and Padgham, W.A., 1991, U-Pb zircon geochronology of the Yellowknife volcanic belt, NWT, Canada: new constraints on the timing and duration of greenstone belt magmatism: *Journal of Geology*, v. 99, p. 55-67.
- Isachsen, C., and Bowring, S.A., 1994, Evolution of the Slave craton: *Geology*, v. 22, p. 917-920
- Kishida, A., and Kerrich, R., 1987, Hydrothermal alteration zoning and gold concentration at the Kerr-Addison Archean lode gold deposit, Kirkland lake, Ontario: *Economic Geology*, v. 82, p. 649-690.
- Kontak, D. J., and Kerrich, R., 1997, An isotopic (C, O, Sr) study of vein gold deposits in the Meguma Terrain, Nova Scotia: Implication for source reservoirs: *Economic Geology*, v. 92, p. 161-180.
- Kusky, T.M., 1989, Accretion of the Archean Slave province: *Geology*, v. 17, p. 63-67.
- Kusky, T.M., and Vearncombe, J.R., 1997, Structural Aspects: *in* M.J. DeWit and L.D. Ashwal, ed., *Greenstone belts*, Oxford University Press, p. 92-124.

- Leclair, S., 1990a, Interactions of granitoids and the gold mineralization Ida Point, N.W.T.: *in* GNWT-DIAND Geoscience Projects 1989, Annual Report, March 1990, Canada-Northwest Territories Mineral Development Agreement, p. 21-27.
- Leclair, S., 1990b, The Ida Point gold showing, Hope Bay greenstone belt, NWT: *in* Northwest Territories Geology Division-Department of Indian Affairs and Northern Development, Exploration Overview 1990: Mining, Exploration and Geological Investigations, p. 35-36.
- Leclair, S., 1991, Mineralization at the margin of a tonalitic intrusion: the Ida Point gold Hope Bay greenstone belt, NWT: Universite du Quebec a Montreal, Canada-NWT Mineral Development Agreement, 60p.
- Leclair, S.G., 1992, The Ida Point gold showing, Hope Bay greenstone belt, Northwest Territories: *in* Richardson, D.G., and Irving, M., ed., Project Summaries, Canada-Northwest Territories Mineral Development Subsidiary Agreement 1987-1991, Geological Survey of Canada Open File 2484, p. 61-63.
- Locock, A., 1998a, Petrology of the major lithological units of the Boston gold deposit: BHP Minerals Canada Ltd. Internal Report, 31p.
- Locock, A., 1998b, Preliminary results of U-Pb zircon age dating of the Boston main dyke: BHP Minerals Canada Ltd. Internal Report, 4p.

- London, D., and Manning, D.A.C., 1995, Chemical variation and significance of tourmaline from southwest England: *Economic Geology*, v. 90, p. 495-519.
- Longstaffe, F.J., 1987, Stable isotope studies of diagenetic processes: *in* T.K. Kyser ed., Short course in stable isotope geochemistry of low temperature fluids, Mineralogical Association of Canada, v. 13, p.187-257.
- Love, D.A., and Roberts, R.G., 1991, The geology and geochemistry of gold mineralization and associated alteration at the Rundle gold deposit, Abitibi subprovince, Ontario: *Economic Geology*, v. 86, p. 644-666.
- Mathews, A., and Katz, A., 1977, Oxygen isotope fractionation during dolomitization of calcium carbonate: *Geochimica et Cosmochimica Acta*, v. 41, p. 1431-1438.
- Matsuhisa, Y., Goldsmith, J.R., and Clayton, R.N., 1979, Oxygen isotopic fractionation in the system quartz-albite-anorthite-water: *Geochimica et Cosmochimica Acta*, v. 43, p. 1131-1140.
- McBirney, A.R., 1994, Basalts and magma series: *in* Jones and Bartlett Publishers, Boston, London, *Igneous Petrology* 2<sup>nd</sup> edition, p 220-270.

- Muehlenbachs, K., 1986, Alteration of the oceanic crust and the  $^{18}\text{O}$  history of seawater: *in* J.W. Valley, H.P. Taylor, Jr., and J.R. O'Neil, ed., Reviews in Mineralogy Volume 16, Stable isotopes in high temperature geological processes, Mineralogical Society of America, p. 425-444.
- Muehlenbachs, K., and Clayton, R.N., 1972, Oxygen isotope studies of fresh and weathered submarine basalts: Canadian Journal of Earth Science, v. 9, p. 172-184.
- Nesbitt, B.E., and Muehlenbachs, K., 1989, Geology, geochemistry, and genesis of mesothermal lode gold deposits of the Canadian Cordillera: evidence for ore formation from evolved meteoric water: *in* R.R. Keays, W.R.H. Ransay, and D.I. Groves eds., The Geology of Gold Deposits: the Perspective in 1988, Economic Geology, Monograph 6, p. 553-563.
- Ohmoto, H., 1986, Stable isotope geochemistry of ore deposits: *in* J.W. Valley, H.P. Taylor, Jr., and J.R. O'Neil, ed., Reviews in Mineralogy Volume 16, Stable isotopes in high temperature geological processes, Mineralogical Society of America, p. 491-560.
- Ohmoto, H., and Goldhaber, M.B., 1997, Sulfur and carbon isotopes: *in* H.L. Barnes ed., Geochemistry of hydrothermal ore deposits, 3<sup>rd</sup> edition, New York, Wiley, p. 517-612.

- Ohmoto, H., and Rye, R.O., 1979, Isotopes of sulfur and carbon: *in* H.L. Barnes ed.,  
Geochemistry of hydrothermal ore deposits, 2<sup>nd</sup> edition, New York, Wiley, p.  
509-567.
- Padgham, W.A., 1985, Observations and speculations on supracrustal successions in the  
Slave Structural province: *in* L.D. Ayres, P.C. Thurston, K.D. Card, and  
W.Weber, eds., Geological Association of Canada Special Paper 28, p156-167.
- Padgham, W.A., 1990, The Slave Province, an overview: Geological Survey of Canada,  
Open-File Report, 2168, p. 1-41.
- Padgham, W.A., and Fyson, W.K., 1992, The Slave province: a distinct Archean craton:  
Canadian Journal of Earth Science, v. 29, p. 2072-2086.
- Phillips, G.N., 1986, Geology and alteration in the Golden Mile, Kalgoorlie: Economic  
Geology, v. 81, p. 779-808.
- Phillips, G.N., and Groves, D.I., 1983, The nature of Archean gold-bearing fluids as  
deduced from gold deposits of western Australia: Journal of the Geological  
Society of Australia, v. 30, p. 25-39.

- Reed, M.H., 1997, Hydrothermal alteration and its relationship to ore fluid composition: *in* H.L. Barnes ed., *Geochemistry of hydrothermal ore deposits*, 3<sup>rd</sup> edition, New York, Wiley, p. 303-366.
- Relf, C., 1992, Two distinct shortening events during late Archean orogeny I the west-central Slave Province, Northwest Territories, Canada: *Canadian Journal of Earth Sciences*, v. 29, p. 2104-2117.
- Robert and Poulsen, in press, Structural controls on veins in gold deposits in greenstone belts: *in* *The application of structural geology to the interpretation of ore forming processes: from satellites to outcrops*, *Reviews in Economic Geology*, v. 14.
- Robert, F., 1996, Quartz-carbonate vein gold: *in* *Geology of Canadian Mineral Deposit Types*, Geological Survey of Canada, p. 350-366.
- Robert, F., and Brown, A.C., 1986a, Archean gold-bearing quartz veins at the Sigma mine, Abitibi greenstone belt, Quebec: Part II. Vein paragenesis and hydrothermal alteration: *Economic Geology*, v. 81, p. 593-616.
- Robert, F., and Brown, A.C., 1986b, Archean gold-bearing quartz veins at the Sigma mine, Abitibi greenstone belt, Quebec: Part I. Geologic relations and formation of the vein system: *Economic Geology*, v. 81, p. 578-592.



- Robert, F., and Kelly, W.C., 1987, Ore-forming fluids in Archean gold-bearing quartz veins at the Sigma mine, Abitibi greenstone belt, Quebec, Canada: *Economic Geology*, v. 82, p. 1464-1482.
- De Ronde, C.E.J., Channer, D.M.DeR., and Spooner, E.T.C., 1997, Archean fluids: *in* M.J. DeWit and L.D. Ashwal, ed., *Greenstone belts*, Oxford University Press, p. 309-335.
- Rye, R.O, Schuiling, R.D., Rye, D.M., Jansen, J.B.H., 1976, Carbon, hydrogen, and oxygen isotope studies of the regional metamorphic complex at Naxos, Greece: *Geochimica et Cosmochimica Acta*, v. 40, p. 1031-1049.
- Schidlowski, M., Eichmann, R., and Junge, C.E., 1975, Precambrian sedimentary carbonates: carbon and oxygen isotope geochemistry and implications for the terrestrial oxygen budget: *Precambrian Research*, v. 2, p. 1-69.
- Smith, J.P., O'Neal, J.R., and Erlank, A.J., 1984, Oxygen isotope compositions of minerals and rocks and chemical alteration patterns in pillow lavas from the Barberton greenstone belt, South Africa: *in* A. Kroner, G.N. Hanson, and A.M. Goodwin eds., *Archean geochemistry, the origin and evolution of the Archean continental crust*, Springer-Verlag, Berlin, p 115-137.

- Smith, T.J., and Kesler, S.E., 1985, Relation of fluid inclusion geochemistry to wallrock alteration and lithogeochemical zonation at the Hollinger-McIntyre gold deposit, Timmins, Ontario: Canadian Institute of Mining and Metallurgy Bulletin, v. 78, p. 35-46.
- Smith, T.J., and Kesler, S.E., 1985, Relation of fluid inclusion geochemistry to wallrock alteration and lithogeochemical zonation at the Hollinger-McIntyre gold deposit, Timmins, Ontario, Canada: CIM Bulletin, v. 78, p. 35-46.
- Sylvester, P.J., Harper, G.D., Byerly, G.R., and Thurston, P.C., 1997, Volcanic Aspects: *in* M.J. DeWit and L.D. Ashwal, ed., Greenstone belts, Oxford University Press, p. 56-90.
- Taylor, H.P., 1979, Oxygen and hydrogen isotope relationships in hydrothermal ore deposits: *in* H.L. Barnes ed., Geochemistry of hydrothermal ore deposits, 2<sup>nd</sup> edition, New York, Wiley, p. 236-277.
- Taylor, H.P., and Sheppard, S.M.F., 1986, Igneous rocks: I. Processes of isotopic fractionation and isotope systematics: *in* J.W. Valley, H.P. Taylor, Jr., and J.R. O'Neil, ed., Reviews in Mineralogy Volume 16, Stable isotopes in high temperature geological processes, Mineralogical Society of America, p. 227-272.

- Teixeira, J.B.G., Kishida, A., Marimon, M.P.C., Xavier, R.P., and McReath, I., 1990, The Fazenda Brasileiro gold deposit, Bahia: geology, hydrothermal alteration, and fluid inclusion studies: *Economic Geology*, v. 85, p. 990-1009.
- Tompson, P.H., 1996, Regional geology of Archean granitoid rocks adjacent to the Hope Bay volcanic belt, northeastern Slave province, Canadian Shield: BHP Minerals Canada Ltd. Internal Report, 39p.
- Tompson, P.H., 1997, Regional geology of Archean granitoid rocks adjacent to the Hope Bay and Elu Inlet volcanic belts, northeastern Slave structural province, Canadian Shield: BHP Minerals Canada Ltd. Internal Report, 56p.
- Twiss, R.J., and Moores, E.M., 1973, Chapter 10 Mechanics of natural fractures and faults: in W.H. Freeman and Company, New York eds., *Structural Geology*, p. 186-214.
- van Breemen, O., Davis, W.J., and King, J.E., 1992, Temporal distribution of granitoid plutonic rocks in the Archean Slave Province, northwest Canadian Shield: *Canadian Journal of Earth Sciences*, v. 29: 2186-2199.
- Wood, P.C., Burrows, D.R., Thomas, A.V., and Spooner, E.T.C., 1986, The Hollinger-McIntyre Au-quartz vein system, Timmins, Ontario, Canada: geologic characteristics, fluid properties and light stable isotope geochemistry: *in* A.J.

Macdonald ed., Proceedings Volume, Gold'86, an International Symposium on the Geology of Gold, Konsult International Inc., Ontario, p. 56-80.

**Appendix A.** Location information, hand sample descriptions, and mineralogy based on x-ray defraction analysis (XRD), thin-section, and hand sample petrography (ank - ankerite; aspy - arsenopyrite; cal - calcite; carb - carbonate; chl - chlorite; cpy - chalcopyrite; dol - dolomite; fol - foliation; graph - graphite; musc - muscovite; parag - paragonite; plag - plagioclase; py - pyrite, Qtz - quartz; gal - galena; ser - sericite; tr - trace;  $\alpha$ -cut - crosscut; BAS - basalt; GAB - gabbro; SED - sediment; GWY - graywacke; ARG - argillite; WK - weak hydrothermal alteration; MD - moderate hydrothermal alteration; ST - strong hydrothermal alteration; V - vein).

### Boston Deposit

Sample No.	Rock Type	Location (UTM 83N, 83E)	DDH No. and Depth to Sample (m)	Mineralogy - based on thin-section petrography and/or XRD	Hand Sample Description
JSB-001	BAS WK	7505012N 441162E	Decline - Face 225	Ankerite (50%), Quartz (30%), Clinocllore/Paragonite (15%), Rutile (5%), Pyrite (tr)	Light green/beige, weakly altered, weakly fol basalt, pervasive sericite alt throughout. Sample contains x-cutting veins of light green parag/carb.
JSB-003	Strongly Deformed Rock	7504789N 441353E	97NOD-175 101.4-101.5	Ankerite (37%), Quartz (33%), Paragonite (14%), Rutile (10%), Py (3%), Cpy (2%), Clinocllore (1%) Aspy/Po (tr)	Very strongly altered unit consisting of dark brown bands of sericite alt and thicker (5mm) wavy bands and lenses of black/dark gray carbonate alteration.
JSB-004	BAS ST	7504789N 441353E	97NOD-175 101.5-101.7	Quartz, Dolomite, Paragonite	—
JSB-006	Strongly Deformed Rock	7504789N 441353E	97NOD-175 118.5-118.9	Quartz, Ankerite, Clinocllore, Paragonite, Magnetite, Rutile, Pyrite	Strongly altered unit consisting of deformed brown sericite rich bands and dark gray/black folded carb rich bands.
JSB-007	ARG MD	7504789N 441353E	97NOD-175 128.3-128.5	Pyrite (40%), Ankerite (33%), Quartz (20%), Graph (5%), Sphalerite (1%), Parag (<1%), Cpy (tr)	Dark gray/black coloured moderately deformed sed with mottled appearance. Network of wispy parag/graph bands surround irregular carb rich lenses.
JSB-008	ARG MD	7504789N 441353E	97NOD-175 127.1-127.3	Parag (30%), Graph (25%), Quartz (19%), Ankerite (15%), Pyrite (10%), Sphalerite (1%), Cpy (tr)	Dark gray/black, strongly deformed sed with wispy bands of parag/graph throughout defining fol, thicker carb rich bands occur between parag/graph bands.

JSB-009	BAS WK	7504789N 441353E	97NOD-175 224.2-224.6	Dolomite (40%), Quartz (30%), Paragonite (22%), Clinocllore (5%), Rutile (3%)	—
JSB-010	BAS MD	7504789N 441353E	97NOD-175 235.7-236.1	Paragonite (35%), Ankerite (30%), Quartz (25%), Rutile (9%), Clinocllore (1%), Pyrite (tr)	Pervasively altered unit with thin wispy green/beige/brown stringers of sericite alternating with gray lenses of carb/qtz alternation throughout, gives sample a mottled appearance.
JSB-012	B3 VEIN	7504945N 441158E	B3 Cross-cut (3935m level) Face XC3(2)-09	Quartz, Ankerite, Dravite, Paragonite, Muscovite, Clinocllore, Pyrite, Aspy/Cpy	Milky bull qtz vein with white to gray clots of coarse carb crystals, py occurs within vein close to vein walls. Numerous irregular x-cutting qtz/carb filled fractures occur within vein and surrounding wallrock. Wallrock is dark brown/green/gray, strongly deformed, carbonatized and pyritized. Light green parag also occurs within wallrock close to vein.
JSB-013	B3 VEIN	7504945N 441158E	B3 Cross-cut (3935m level) South Wall XC3(2)-09	Quartz, Dolomite, Dravite, Paragonite, Muscovite, Clinocllore, Pyrite, Cpy	Milky bull qtz vein containing irregular clots of coarse white to gray carb crystals. Numerous fractures filled with clear qtz occur within vein. Wallrock is dark brown/green/gray and strongly altered, only moderate py occurs within wallrock, no py occurs within vein.
JSB-014	B3 VEIN	7504945N 441158E	B3 Cross-cut (3935m level) Face XC3(2)-09	Quartz, Dolomite, Sericite, Gold, Rutile, Pyrite, Cpy, Aspy	Sample is qtz flooded and intensely pyritized, numerous sub-mm to cm-scale qtz/carb veinlets and large irregular clots of deformed py crystals occur throughout sample. Overall the sample is dark brown/gray and has a mottled appearance.
JSB-015	Ladder Vein in BAS MD	7504948N 441146E	B3 Cross-cut (3935m level) Face XC3(2)-03	Ankerite/Siderite (54%), Quartz (40%), Pyrite (5%), Cpy (1%), Clinocllore (tr)	Intensely carbonatized wallrock containing cm-scale x-cutting milky qtz ladder veins, carb rich wallrock appears to be boudinaged and is hosted by mod hydrothermally altered basalt.
JSB-016	BAS	7505356N 441327E	Decline - Near Portal	Clinocllore, Quartz, Dolomite, Muscovite, Plagioclase, Rutile	—
JSB-018	GAL in VEIN in BAS WK	7505109N 441314E	97NOD-163 136.0-136.2	Quartz, Carbonate, Clinocllore, Paragonite, Magnesite, Galena, Sphalerite, Pyrite	Milky qtz and carbonate vein containing galena and sphalerite. Galena occurs between qtz grains in a dendritic pattern and forms up to 80% of the vein locally. Irregular clasts of beige/green wallrock also occur within vein.
JSB-020	BAS WK	7504789N 441353E	97NOD-175 481.8-482.6	Ankerite (40%), Clinocllore (30%), Quartz (25%), Paragonite (5%), Rutile (tr), Py/Cpy (tr)	—

JSB-021	Flat Vein in Strongly Deformed Rock	7504940N 441175E	B3 Cross-cut (3935m level) South Wall XC3(2)-11	Quartz, Carbonate, Pyrite	Flat vein consisting of fractured milky qtz and coarse grained white carb crystals. Carb occurs along vein margins and grows into the vein, vein is hosted by gray/green strongly carbonatized wallrock. Minor py occurs within wallrock but does not appear to be related to veining.
JSB-022	B3 VEIN	7504940N 441175E	B3 Cross-cut (3935m level) Face XC3(2)-11	Dolomite (55%), Dravite (20%), Quartz (10%), Pyrite (6%), Rutile (5%), Aspy (3%), Clinocllore (1%), Gold (tr), Cpy (tr)	Milky bull qtz vein containing coarse carb crystals along vein margins, vein has an irregular stockworked appearance. Wallrock is gray/dark green/brown and strongly altered, fine grained rutile and coarse cubes of py and aspy (9%) and carb occur in wallrock.
JSB-023	B3 VEIN	7504940N 441175E	B3 Cross-cut (3935m level) Face XC3(2)-11	Dolomite (37%), Pyrite (15%), Dravite (15%), Quartz (10%), Aspy (10%), Rutile (5%), Parag (5%), Phlogopite (2%), Chlino (1%), Gold (tr), Cpy (tr)	Stockwork of x-cutting milky qtz and carb filled veins (mm to cm-scale), carb appears to grow in to the vein perpendicular to the vein walls. Wallrock consists of green/gray strongly carbonate and sericite altered gabbro, substantial py/aspy also occurs throughout wallrock.
JSB-025	BAS WK	7505212N 441310E	97NOD-174 240.5-240.7	Quartz (40%), Ankerite (30%), Muscovite (20%), Clinocllore (7%), Plagioclase (2%), Py (1%)	Bright green/beige, well foliated, parag rich basalt, wispy bands of sericite define foliation throughout. Foliation parallel qtz/carb veinlets also occur throughout sample.
JSB-026	BAS	7505212N 441310E	97NOD-174 239.6-239.9	Dolomite (45%), Clinocllore/Paragonite (30%), Quartz (22%), Rutile (3%), Py/Cpy (tr)	Dark forest green basalt, several x-cutting qtz/carb filled veins occur throughout, qtz/carb clots give unit a grainy appearance, rutile (eucoxene) alteration occurs throughout.
JSB-027	BAS	7505212N 441310E	97NOD-174 215.2-215.4	Ankerite (40%), Clinocllore (30%), Quartz (20%), Dravite (5%), Rutile (3%), Plagioclase (2%), Py Cpy (tr)	—
JSB-028	GAB	7504837N 441366E	97NOD-168 328.4-328.6	Dolomite/Magnesite(?) (40%), Quartz (25%), Parag/Musc (15%), Clinocllore (12%), Rutile (5%), Pyrite (tr)	—
JSB-029	GAB+V	7504837N 441366E	97NOD-168 320.3-321.0	Dolomite/Magnesite(?), Quartz, Parag/Musc, Clinocllore, Rutile, Pyrite, Cpy/Aspy	B3 gabbro consisting of bright green wispy bands of paragonite and light brown rutile alternating with gray bands of carb and qtz, py cubes with pressure shadows occur throughout. Sample contains numerous x-cutting qtz/dol veins, dol tends to occur along vein margins with qtz filling centre of vein.
JSB-030	DYKE	7504633N 441358E	97NOD-170 179.5	Qtz, Clinocllore, Calcite/Ankerite, Musc/Parag, Plagioclase, Py/Cpy	Beige, fine grained, very weakly foliated sample, fine py grains occur throughout as individual grains, mm-scale irregular patches of pink alt also occur throughout sample. Overall sample has an igneous texture.

JSB-031	DYKE	7505034N 441172E	Decline - Drill Bay #19	Quartz, Dolomite, Paragonite, Muscovite, Pyrite	Beige, fine grained, weakly fol sample containing fine (mm-scale) py grains, py occurs as individual crystals and irregular clots of grains, mm-scale irregular patches of pink alt also occur throughout sample.
JSB-032	B3 VEIN	7504977N 441150E	97B33935-133 47.6-47.7	Quartz (70%), Dolomite (15%), Dravite (13%), Pyrite (2%), Rutile (tr)	Milky qtz vein containing irregular clots of coarse grained carb and clasts of strongly altered, dark gray/green/brown wallrock. Fine grained py occurs with wallrock clasts locally. A cross-cutting qtz/carb ladder vein occurs within this sample, qtz and carb within this vein grow into vein perpendicular to vein walls.
JSB-033	GAL(B3)	7504977N 441150E	97B33935-132 71.0-71.3	Quartz, Dolomite/Magnesite(?), Paragonite, Clinocllore, Rutile	---
JSB-034	BAS	---	97PGD-04 103.9-104.3	Quartz, Clinocllore, Calcite, Plagioclase, Rutile, Py/Cpy	Dark forest green basalt, very fine grained and unfoliated, fine grained rutile and irregular calcite filled fractures occur throughout. Cal appears to be limited to these fractures. Overall sample has an igneous texture.
JSB-035	FLAT VEIN in BASMD	7505034N 441096E	97B23920-138 18.4-18.5	Ankerite, Quartz, Paragonite, Clinocllore, Rutile, Py/Cpy	Qtz/carb filled flat vein, qtz/carb grow into the vein perpendicular to the vein walls. Vein is hosted by well foliated, gray/green/brown gabbro, rutile (leucocene occurs throughout wallrock). Vein cuts wallrock at 65 degrees to foliation.
JSB-037	DYKE	7504929N 441410E	94NOD-108 673.1-673.3	Dolomite (80%), Quartz (12%), Pyrite (5%), Paragonite (2%), Rutile (1%), Muscovite (tr)	Beige, weakly foliated, fine grained unit containing coarse grained py as individual grains and groups of grains, qtz pressure shadows commonly occur adjacent to py grains.
JSB-039	BAS	7505007N 441504E	94NOD-123 670.1-670.3	Clinocllore (60%), Carbonate (20%), Quartz (16%), Plagioclase (2%), Rutile (2%), Paragonite (tr), Pyrite (tr)	---
JSB-041	GAB+V	7503494N 443026E	94NOD-135 195.6-195.9	Clinocllore (33%), Calcite (27%), Quartz (16%), Dravite (12%), Rutile (6%), Musc (6%)	Very dark forest green, fine grained, weakly foliated, pervasively calcite altered sample. Sample contains qtz/cal vein.
JSB-043	BAS WK	7504944N 441162E	B3 Cross-cut (3935m level) 25m South wall	Quartz, Dolomite	---
JSB-045	FLAT VEIN	7504946N 441154E	B3 Cross-cut (3935m level) 19m North wall	Quartz, Carbonate	Milky white bull qtz vein containing coarse grained white carb locally.



JSB-046	B2 VEIN	7505078N 441171E	B2 Cross-cut (4000m level) South wall	Ankerite, Quartz, Dravite, Pyrite, Chalcocopyrite	Milky bull qtz vein, very little carb occurs within vein. Wallrock is dark gray and pervasively carbonate enriched and contains 10% py cubes, py has a pitted appearance due to numerous inclusions of qtz and carb. Numerous late brittle qtz/carb filled fractures x-cut vein and wallrock, locally pyrite grains are also cut by these fractures, later fractures can be seen offsetting earlier fractures in this sample.
JSB-047	B2 VEIN	7505078N 441171E	B2 Cross-cut (4000m level) South wall	Quartz (75%), Dravite (15%), Pyrite (7%), Ankerite (2%), Parag (1%), Gold (tr), Cpy (tr)	Visible gold occurs along the outer margin of a sericite/dravite/pyrite stringer hosted by a strongly deformed and recrystallized qtz/carb vein. The stringer and the gold appear to occupy a late fracture within the qtz/carb vein. Pyrite occurs in close association with gold in this fracture. Numerous other x-cutting fractures filled with clear qtz occur within this sample.
JSB-048	GWY	7504962N 441481E	97NOD-176 211.5-211.8	Quartz (37%), Sericite (28%), Plagioclase (18%), Carbonate (15%), Rutile (2%), Py/Cpy (tr)	---
JSB-051	GAB+V	—	97PGD-05 102.9 to 103.0m	Ankerite/Calcite (45%), Quartz (35%), Clinoclhore (10%), Phlogopite (8%), Rutile (1%), Py/Cpy (1%)	Very weakly altered gabbro containing qtz/calc/ank vein.
JSB-055	B2 VEIN	7505050N 441152E	B2 Cross-cut (3920m level) 30m South wall	Quartz, Ankerite, Sericite, Dravite, Pyrite, Aspy	Vein of massive milky bull qtz containing irregular clots or coarse, white to gray carb. Stringers of intensely carbonatized wallrock occur within vein approximately parallel to vein margins and appear to be pieces of wallrock incorporated into vein during vein growth. Wallrock is gray/green/brown and has been intensely carbonate enriched, py/aspy occur next to vein in wallrock.
JSB-056	B2 VEIN	7505052N 441148E	B2 Cross-cut (3920m level) 36m South wall	Quartz (79%), Ankerite (12%), Pyrite (3%), Dravite (3%), Parag/Musc (2%), Rutile (1%)	Vein of milky bull qtz containing irregular clots of coarse (cm-scale) carb and clasts and stringers of strongly altered wallrock, py occurs within vein with wallrock stringers locally. Numerous x-cutting qtz/carb ladder veins occur within vein, perpendicular to vein walls. Wallrock is dark gray/black and strongly pyritized (mm to cm cubes make up 40% of wallrock locally).
JSB-057	B2 VEIN	7505052N 441148E	B2 Cross-cut (3920m level) 36m South wall	Quartz (60%), Ankerite (20%), Parag/Musc (10%), Clinoclhore (5%), Pyrite (3%), Rutile (2%), Cpy (tr)	Vein containing coarse grained gray to white carb and irregular patches of milky qtz. Vein is oriented parallel to well developed foliation in wallrock. Wallrock is dark gray/black and contains 10% py locally as clots of grains. A x-cutting qtz/carb ladder vein occurs within this vein perpendicular to vein walls, qtz/carb grow into the ladder vein perpendicular to vein walls. The ladder vein terminates at margins of main stage vein and does not continue into wallrocks on either side.

JSB-058	B2 VEIN	7505054N 441140E	B2 Cross-cut (3920m level) 44m North wall	Ankerite (70%), Quartz (28%), Dravite (2%)	Vein consisting of coarse grained gray to white carb, irregular patches of milky bull quartz, and minor dravite locally (2%).
JSB-059	B2 VEIN	7505054N 441140E	B2 Cross-cut (3920m level) 44m North wall	Pyrite (70%), Ankerite (15%), Quartz (10%) Parag/Musc (3%), Dravite (1%), Rutile (1%), Gold (tr), Cpy/Aspy (tr)	Milky bull qtz vein containing irregular clots of coarse grained carb and stringers of strongly altered wallrock, py occurs with wallrock stringers in vein locally. Wallrock is gray and intensely carbonatized and pyritized. Qtz/carb ladder veins x-cut the main vein at right angles, terminating abruptly at vein margins, qtz/carb within the ladder vein grows out from the vein walls into the centre of the vein.
JSB-060	B2 VEIN	7505054N 441140E	B2 Cross-cut (3920m level) 44m North wall	Quartz, Carbonate, Pyrite, Dravite, Sericite, Paragonite, Pyrite, Aspy, Rutile	Deformed (boudinaged) 7cm thick milky bull qtz vein containing clots of coarse grained carb and stringers of strongly altered wallrock. Wallrock stringers occur parallel to vein margins, are occasionally associated with py clots and were probably incorporated into the vein during growth. Wallrock is dark gray/brown, strongly altered, well foliated and contains clots of py and light green parag locally. Qtz/carb ladder veins occur throughout vein, terminating abruptly at vein margins, qtz and carb within the ladder veins grows into the veins from the vein walls.
JSB-066	DYKE	7505025N 441090E	97B23920-144 46.4-46.8	Ankerite (45%), Quartz (35%), Clinocllore (10%), Parag/Musc (8%), Py/Cpy (2%), Rutile (tr)	Beige, weakly foliated almost massive, fine grained sample containing fine pyrite cubes throughout, py cubes commonly have qtz filled pressure shadows.
JSB-067	DYKE	7505136N 441187E	Decline - Face 263	Chinolochlore, Quartz, Dolomite/Calcite, Plagioclase, Rutile	Dark green, fine grained sample that does not appear to have been hydrothermally altered.
JSB-068	B2 VEIN	7505015N 441089E	97B23920-147 30.0-30.1	Ankerite/Calcite (55%), Quartz (15%), Dravite (12%), Rutile (5%), Pyrite (10%), Aspy (3%), Cpy (tr)	Milky bull qtz vein containing clots of coarse (cm-scale) grained white carb. Wallrock is dark gray and strongly carbonatized, pyrite occurs throughout wallrock as coarse cubes (mm to cm-scale). A late x-cutting qtz/carb veinlet with a thin (mm-scale) py/aspy halo also occurs within this sample.
JSB-069	ARG	7504799N 441314E	97NOD-181 35.0-35.2	Ankerite (30%), Parag (25%), Graph (20%), Py (14%), Qtz (10%), Sphalerite (<1%), Rutile (tr), Cpy (tr)	Gray to dark gray/black banded, strongly fol and folded unit, mm-scale bands of graph/parag and carb rich sediment altered throughout.
JSB-070	B3 VEIN	7504958N 441183E	B3 Ore Drift (3935m level) West wall 97B3N-5	Dolomite (35%), Quartz (30%), Pyrite (20%), Dravite (10%), Rutile (4%), Aspy (1%), Gold (tr), Cpy (tr)	Milky bull qtz vein containing clots of coarse (cm-scale) grained white carb. Numerous irregular fractures filled with clear qtz occur throughout sample. Wallrock is dark gray, strongly altered and intensely pyritized containing up to 90% py locally.

JSB-071	GAB+V	7502440N 441960E	Regional Surface Sample	—	—
JSB-072	GAB+V	7501480N 442000E	Regional Surface Sample	—	—
JSB-073	GAB+V	7502720N 441849E	Regional Surface Sample	Ankerite (50%), Plagioclase (20%), Quartz (10%), Clino/Musc (10%), Rutile (6%), Pyrite (4%)	Beige/gray, well layered sample with darker black/gray bands throughout, associated with a dark gray quartz vein. Sample contains qtz/ank vein.
JSB-074	SED+V	7502840N 441680E	Regional Surface Sample	Ankerite/Siderite (35%), Plagioclase (30%), Quartz (25%), Pyrite (7%), Clino/Musc (2%), Rutile (1%)	—
JSB-075	B3 VEIN	7505030N 441213E	B3 Cross-cut (4000m level) West wall	Quartz (70%), Dolomite (29%), Sericite (1%), Dravite (tr)	Milky bull qtz vein that contains irregular clots of coarse (cm-scaled) grained light gray to white carb throughout.
JSB-076	B2 VEIN	7505037N 441148E	B2 Cross-cut (4000m level) West wall	Quartz (75%), Dravite (20%), Ankerite/Calcite (4%), Pyrite (1%), Gold (tr), Rutile (tr)	Milky bull qtz vein, irregular clots of coarse (cm-scaled) grained light gray to white carb occur locally, typically along vein margins. Numerous irregular qtz filled fractures occur throughout vein and wallrock. Wallrock is dark gray, strongly altered, and locally contains up to 90% py as irregular clots of mm-scale grains. Coarse (cm- scale) py cube occur within vein close to vein margins locally.
JSB-077	FLAT VEIN	7505005N 441317E	97NOD-w165 271.8-272.0	Quartz, Ankerite	Milky bull qtz and carb vein, carb crystals grow into vein from vein margins at approximately right angles.
JSB-078	B2 VEIN	7505005N 441317E	97NOD-w165 364.2-364.3	Quartz (55%), Carbonate (20%), Dravite (10%), Rutile (3%), Pyrite (8%), Cpy (4%), Gold (tr)	Milky bull qtz vein containing irregular clasts and stringers of strongly altered wallrock, pyrite occurs with wallrock as clots of grains. Numerous x-cutting carb filled veinlets occur throughout sample, these veinlets x-cut both qtz and wall rock stringers and therefore must be late.
JSB-079	B2 VEIN	7505047N 441153E	B2 Cross-cut (3920m level) South wall XC2(2)-B	Quartz (50%), Ankerite (20%), Dravite(15%), Pyrite (10%), Sericite (2%), Cpy (2%), Rutile (1%), Gold (tr), Aspy (tr)	Qtz floored unit with a mottled appearance. Sample contains irregular clots of coarse grained gray to white carb, brecciated clasts of dark gray strongly altered wallrock and clots of mm to cm-scale py grains. Irregular patches and cm-scale x-cutting veins of milky qtz occur throughout sample.

JSB-080	LADDER VEIN	7504940N 441160E	B2 Cross-cut (3920m level) South wall	Quartz (50%), Ankerite (43%), Parag/Musc (5%), Rutile (2%), Dravite (tr), Pyrite (tr)	Dark gray strongly carbonatized unit containing several x-cutting milky qtz filled ladder veins. Light green parag occurs adjacent to ladder veins in this sample.
JSB-081	B3 VEIN	7504939N 441163E	B2 Cross-cut (3920m level) South wall	Quartz (55%), Ankerite (44%), Clinocllore/Paragonite (1%)	Deformed milky bull qtz vein containing irregular clots of coarse (mm-scale) carbonate.
JSB-082	FLAT VEIN	7504939N 441163E	B2 Cross-cut (3920m level) South wall	Quartz, Ankerite	Milky bull qtz and coarse grained white carb. Carb crystals several cm in diameter have been observed in this sample.
JSB-083	B4 VEIN	7504706N 441393E	97NOD-182 180.8-180.9	Quartz, Ankerite, Sericite, Dravite, Pyrite, Gold	Milky qtz vein containing irregular stringers of sericite/dravite/pyrite, these stringers appear to occur within fractures in the qtz vein. Sub-mm grains of visible gold also occur along one of these fractures.
JSB-085	B4 VEIN	7504706N 441393E	97NOD-182 158.7-158.8	Quartz, Ankerite, Calcite, Paragonite, Muscovite, Kaolinite(?), Pyrite	Milky qtz vein containing irregular stringers and clasts of strongly altered wallrock and clots of coarse grained carb. Carb tends to occur adjacent to vein walls. Wallrock is dark gray/black, well foliated and contains substantial py as clots of cubes. Clots of light green paragonite also occur adjacent to vein locally.
JSB-097	BAS WK+V	7504119N 441537E	98NOD225 173.8-174.2	Calcite (40%), Clinocllore (35%), Quartz (15%), Rutile (10%), Paragonite (5%)	Well foliated, beige/gray coloured unit, pervasive calcite alteration with concentrations of calcite in irregular stringers and lenses throughout. Sample contains qtz/cat vein.
JSB-100	BAS WK	7504097N 441427E	98NOD227 202.7-202.8	Quartz, Ankerite, Paragonite, Clinocllore, Calcite	Dark forest green, very weakly altered basalt with minor thin wispy bands of light brown sericite alteration locally, pervasive calcite alteration throughout with large lenses of calcite occurring parallel to foliation.
JSB-102	GWY	7507649N 441018E	98NOD223 221.4-221.5	Quartz, Ankerite, Clinocllore, Muscovite, Plagioclase	Very dark gray, massive, weakly foliated, moderately fine grained sample.
JSB-103	GAB	7503408N 441459E	98NOD224 61.2-61.3	Quartz, Ankerite, Calcite, Clinocllore, Plagioclase	—
JSB-104	GAB+V	7503408N 441459E	98NOD224 63.1-63.2	Quartz, Dolomite, Clinocllore, Paragonite, Plagioclase, Rutile, Pyrite	Moderately altered beige/green banded unit, mm-scale beige bands of carb alt. with dark forest green bands of clino/parag/rutile throughout sample. Coarse py cubes are also common. Sample contains qtz/dol vein.
JSB-105	GAB WK	7503408N 441459E	98NOD224 63.8-63.9	Ankerite (40%), Plagioclase (25%), Quartz (15%), Muscovite (10%), Rutile (5%), Clinocllore (5%)	Beige/green coloured grainy unit with rutile (leucocene) needles throughout, unit does not appear to be foliated.

JSB-106	GWY+V	7503870N 441502E	98NOD228 96.6-96.8	Quartz (37%), Clino/Musc (28%), Plagioclase (19%), Ankerite (16%), Rutile (1%), Py/Cpy (tr)	Gray, fine grained, very weakly foliated, almost massive sample. Sample contains qtz/ank vein.
JSB-112	BAS	7503408N 441459E	98NOD224 231.3-231.5	Quartz, Calcite, Clinocllore, Plagioclase, Epidote	Light beige, weakly foliated and pervasively calcite altered unit. Bands of very fine grained and coarser grained basalt alternate throughout, possibly pillow selvages.
JSB-113	GWY+V	7505882N 440942E	98NOD218 43.9-43.7	Quartz, Ankerite, Muscovite, Clinocllore, Rutile	Gray, massive, unfoliated, moderately fine grained sample. Sample contains qtz/ank vein.
JSB-115	GWY + V	7505882N 440942E	98NOD218 245.3-245.6	Quartz, Ankerite, Clinocllore, Plagioclase, Muscovite	Dark gray, mod fine grained, massive sample with numerous x-cutting qtz/dol filled fractures throughout.
JSB-116	GWY MD+V	7505882N 440942E	98NOD218 71.1-71.2	Quartz, Ankerite, Clinocllore, Muscovite, Paragonite	Gray to dark gray fine grained to moderately fine grained sample, well foliated with remnant graded bedding preserved. Sample contains qtz/ank vein.
JSB-118	BAS	7504233N 441496E	98NOD214 250.4-250.6	Quartz, Calcite, Clinocllore, Paragonite, Muscovite	Dark green, weakly foliated, pervasively calcite altered unit, rutile (teucoxene) clots occur throughout. Wispy clinocllore/parag bands and cal filled veinlets occur locally.
JSB-121	BAS ST	7504233N 441496E	98NOD214 117.1-117.2	Paragonite (50%), Carbonate (20%), Quartz (15%), Clinocllore (13%), Rutile (2%), Pyrite (tr)	---
JSB-122	GAB WK+V	7504233N 441496E	98NOD214 60.0-60.5	Quartz, Ankerite, Paragonite, Clinocllore	Beige, fine grained, well foliated sample. Sample contains qtz/ank vein.
JSB-125	BAS	7503750N 441366E	98NOD215 177.5-177.7	Quartz, Ankerite, Calcite, Clinocllore, Paragonite, Rutile	Dark green/beige, well foliated basalt. Unit is pervasively cal enriched with bands of brown sericite alteration (<1 mm) occurring locally, substantial rutile also occurs throughout.
JSB-126	Strongly Deformed Rock	7503750N 441366E	98NOD215 108.6-109.0	Clinocllore (40%), Paragonite (20%), Ankerite/Calcite (29%), Quartz (10%), Rutile (1%), Py/Cpy (tr)	Dark gray/black, well foliated, strongly deformed sample, wispy sericite/graph bands define foliation. Sample contains qtz/ank/calclite vein.
JSB-127	Strongly Deformed Rock	7503750N 441366E	98NOD215 42.2-42.4	Paragonite (40%), Clinocllore (20%), Ankerite (24%), Quartz (15%), Rutile (1%), Py/Cpy (tr)	Well foliated, dark gray/black sample, bands of sericite/graph define foliation, bands of fine grained pyrite occur parallel to foliation throughout.
JSB-128	BAS	7503750N 441366E	98NOD215 67.4-67.6	Dolomite (50%), Clinocllore (30%), Quartz (15%), Paragonite (3%), Rutile (2%)	Beige/green coloured basalt with patches of dark forest green clinocllore and very fine grained rutile occurring throughout. Unit has a patchy appearance due to the patchy dol alteration.
JSB-131	BAS WK+V	7504278N 441037E	98NOD233 23.3-23.5	Calcite (35%), Paragonite (25%), Clinocllore (18%), Paragonite (15%), Quartz (5%), Rutile (2%)	Beige/green/grey coloured well foliated unit, pervasively calcite alteration with irregular lenses and bands of calcite throughout. Sample contains qtz/cal vein.

JSB-132	BAS WK	7503124N 441645E	98NOD219 117.2-117.4	Clinocllore (55%), Calcite (30%), Pyrite (7%), Rutile (5%), Quartz (3%)	Beige/green/grey coloured well foliated unit, pervasively calcite altered with irregular lenses and bands of calcite throughout.
JSB-133	GAB	7503124N 441645E	98NOD219 166.2-166.4	Clinocllore (50%), Plagioclase (30%), Calcite (10%), Paragonite (5%), Quartz (3%), Rutile (2%), Pyrite (tr)	Dark forest green coloured. Pervasively calcite altered gabbro with a grainy appearance and well developed foliation.
JSB-134	SED	7503124N 441645E	98NOD219 143.3-143.5	Calcite (30%), Quartz (24%), Graph (20%), Muse (12%), Clinocllore (8%), Py (5%), Cpy (1%), Spht/Aspy/Po (tr)	Gray and dark gray/black, very fine grained, well banded sample, graph rich bands alternate with lighter gray bands, stringers of pyrite/calcite occur locally.
JSB-135	GWY	7503124N 441645E	98NOD219 143.7-143.8	Quartz (35%), Ankerite (25%), Clinocllore (20%), Paragonite (18%), Rutile (2%), Pyrite (tr)	Dark gray, moderately fine grained, weakly foliated sample.
JSB-136	GAB+V	7503124N 441645E	98NOD219 152.1-152.4	Clinocllore (45%), Plagioclase (30%), Calcite (15%), Quartz (5%), Rutile (3%), Paragonite (2%)	Dark forest green coloured. Pervasively calcite altered gabbro with mm-scale cal/clino/plag grains giving it a coarse grained appearance. Sample displays well developed foliation. Sample contains qtz/cal vein.
JSB-137	ARG WK+V	7503921N 441308E	98NOD216 109.2-109.5	Ankerite (35%), Quartz (30%), Graph (25%), Pyrite (6%), Cpy (4%), Sphalerite (tr)	Dark gray/black graph rich, strongly deformed sample with mottled appearance. Sample contains qtz/ank vein.
JSB-138	BAS MD+V	7503921N 441308E	98NOD216 32.3-32.8	Quartz, Ankerite, Calcite, Paragonite, Clinocllore, Magnetite	Deformed beige/gray/brown coloured unit, irregular sericite bands and stringers occur throughout giving the sample a mottled appearance. Sample contains qtz/cal/ank vein.
JSB-139	BAS	7503921N 441308E	98NOD216 257.1-257.3	Quartz, Ankerite, Clinocllore, Muscovite, Paragonite, Rutile	Very weakly altered, beige/dark green, fine grained basalt, fine grained rutile occurs throughout.
JSB-140	ARG	7503921N 441308E	98NOD216 198.9-199.1	Graph (50%), Calcite (18%), Quartz (15%), Parag (15%), Pyrite (2%), Spht/Cpy (tr)	Very dark gray to black, fine grained, graphite rich sample, irregular qtz/cal filled veinlets occur locally throughout sample.
JSB-143	BAS MD	7503921N 441308E	98NOD216 55.3-55.5	Quartz, Ankerite, Paragonite, Clinocllore	Sample consists of wispy (mm-scale) bands of brown/beige sericite alteration and thicker (mm to cm-scale) bands and lenses of gray carb alteration. Overall the sample has a mottled appearance.
JSB-145	SED	7504750N 441384E	94NOD148 67.3-67.5	---	---
JSB-147	BAS+V	7504278N 441037E	98NOD233 86.3-86.5	Clinocllore (50%), Calcite (30%), Quartz (15%), Magnetite (6%), Epidote (4%), Plagioclase (4%), Rutile (1%)	Very dark green, weakly foliated, pervasively cal altered basalt, fine grained rutile (leucocene) occurs throughout. Sample contains qtz/cal vein.

JSB-149	7505707N 440821E	GWY+V	98NOD213 411.8-411.9	Quartz, Dolomite, Muscovite, Paragonite, Plagioclase, Rutile	Dark gray, weakly foliated sample, moderately fine grained sample, fine leucoxene and wispy mm-scale bands of sericite throughout. Sample contains qtz/dol vein.
JSB-150	7503895N 441405E	GWY+V	98NOD202 31.7-32.1	Quartz (35%), Musc (25%), Parag (15%), Ankerite (15%), Clino (7%), Py (3%), Graph (tr), Sphalerite (tr)	Gray and dark gray banded, several cm-scale finer grained bands contain evidence of graded bedding. Sample contains qtz/ank vein.
JSB-151	7503895N 441405E	GAB MD	98NOD202 119.3-119.9	Quartz, Dolomite, Paragonite, Clinocllore, Rutile	Light green/gray, well foliated sample with cream coloured leucoxene alteration throughout, boudinaged x-cutting carb filled veins occur locally.
JSB-152	7503895N 441405E	BAS WK+V	98NOD202 85.4-85.6	Quartz, Ankerite, Paragonite, Clinocllore, Pyrite	Beige/gray, well foliated unit with beige/brown mm-scale stringers of sericite alteration parallel to foliation, qtz eyes and py grains with pressure shadows also occur throughout sample. Sample contains qtz/dol vein.
JSB-154	7503895N 441405E	BAS ST	98NOD202 200.0-200.2	Quartz, Ankerite, Paragonite, Muscovite, Clinocllore, Magnetite, Pyrite	Dark gray, fine grained, carb rich sample, thin bands of brown/beige sericite alteration occur throughout, py occurs as irregular clots of grains.
JSB-155	7503895N 441405E	BAS ST	98NOD202 87.9-88.3	Quartz, Ankerite, Paragonite, Muscovite, Clinocllore, Magnetite	Dark gray, fine grained, carb rich sample, thin bands of brown/beige sericite alt occur throughout, patches of quartz occur locally.
JSB-156	7503895N 441405E	Strongly Deformed Rock	98NOD202 385.4-385.6	Ankerite (40%), Quartz (35%), Clinocllore (10%), Parag/Musc (10%), Rutile (4%), Py (tr), Cpy/Po (tr)	Dark gray/black/brown, strongly deformed and altered sample, wispy bands of sericite alteration define foliation, irregular lenses of light gray carb alteration occur between sericite stringers giving sample a mottled appearance. Sample contains qtz/ank vein.
JSB-159	7504137N 441469E	BAS WK+V	98NOD199 169.5-169.8	Quartz, Ankerite, Clinocllore, Paragonite	Beige/brown, fine grained, pervasively sericite altered sample. Sample contains qtz/ank vein.
JSB-162	7504137N 441469E	ARG WK+V	98NOD199 75.0-75.2	Quartz (55%), Carbonate (20%), Graph (15%), Py (6%), Musc/Parag (4%), Sph/Cpy/Po (tr)	Weakly foliated, very dark gray/black graphitic rich argillite. Sample contains qtz/carb vein.
JSB-164	7505689N 440889E	GWY WK+V	98NOD198 152.4-152.7	Quartz, Muscovite, Clinocllore, Plagioclase, Dolomite	Gray/brown, fine grained, poorly foliated sample. Sample contains qtz/dol vein.
JSB-165	7505689N 440889E	GWY WK+V	98NOD198 36.2-36.4	Quartz, Ankerite, Muscovite, Paragonite, Clinocllore, Plagioclase, Rutile	Dark gray to gray, mod fine grained, weakly foliated sample. Sample contains qtz/ank vein.
JSB-166	7505626N 441524E	GWY+V	98NOD207 214.3-214.6	Quartz, Ankerite, Muscovite, Paragonite, Clinocllore, Plagioclase, Rutile	Gray/dark gray, fine grained, very weakly foliated sample, appears to range from true graywacke to argillite. Sample contains qtz/ank vein.

JSB-167	ARG MD+V	7505626N 441524E	98NOD207 114.5-115.0	Clinoclhore (40%), Parag/Musc (25%), Ankerite (18%), Quartz (15%), Rutile (2%), Py/Cpy (tr)	Dark gray/black, poorly foliated, deformed sample, irregular clots and stringers of pyrite occur roughly parallel to foliation throughout. Sample contains qtz/ank vein.
JSB-168	GWY	7505626N 441524E	98NOD207 38.9-39.2	Quartz (35%), Dolomite (25%), Plagioclase (20%), Clinoclhore (15%), Muscovite (4%), Rutile (1%), Py/Cpy (tr)	Fine grained, green/gray, massive and unfoliated sample.
JSB-171	Strongly Deformed Rock	7505485N 440876E	98NOD211 133.1-133.4	Quartz, Ankerite, Muscovite, Paragonite, Clinoclhore, Rutile	Dark gray to gray, fine grained, well banded, strongly altered sample, clots and lenses of carbonate occur throughout. Sample contains qtz/ank vein.
JSB-172	Strongly Deformed Rock	7505485N 440876E	98NOD211 48.8-49.2	Quartz (35%), Parag/Musc (30%), Ankerite (20%), Clinoclhore (10%), Plagioclase (5%), Rutile (tr), Py/Cpy (tr)	Beige/gray, well foliated, strongly altered, fine grained sample with mm-scale rounded quartz grains throughout. Sample contains qtz/ank vein.
JSB-174	ARG+V	7507649N 441018E	98NOD223 55.4-55.7	Quartz, Dolomite, Muscovite, Paragonite, Clinoclhore	Dark gray, weakly foliated, moderately fine grained, deformed sample. Sample contains qtz/dol vein.
JSB-175	BAS+V	7505278N 441270E	94NOD147 29.8-30.2	Clinoclhore (40%), Clacite (25%), Quartz (15%), Plag (10%), Musc (5%), Rutile (4%), Py (1%) (Ank(80%)/Qtz(20%) vein)	Dark forest green, weakly foliated basalt with numerous x-cutting calcite filled fractures throughout, calcite appears to be confined to fractures. Sample contains ank/qtz vein.
JSB-177	BAS MD+V	7505278N 441270E	94NOD147 60.5-61.0	Paragonite (40%), Ankerite/Siderite (22%), Quartz (18%), Clino/Musc (13%), Rutile (7%), Py/Cpy/Aspy (tr)	Beige/green/brown, pervasively sericitic altered unit with thin bands of carbonate alteration occurring throughout. Sample contains qtz/carb vein.
JSB-179	BAS ST+V	7505278N 441270E	94NOD147 208.1-208.6	Ankerite (55%), Quartz (30%), Parag/Musc (7%), Pyrite (6%), Rutile (2%)	Dark gray mottled unit with irregular light green or brown stringers of parag/misc throughout, py also commonly occurs with these stringers. Sample contains qtz/ank vein.
JSB-180	Strongly Deformed Rock	7505278N 441270E	94NOD147 220.1-220.3	Ankerite (85%), Quartz (10%), Parag/Clinoclhore (4%), Rutile (1%), Py/Cpy (tr)	Very dark gray, strongly altered sample, numerous x-cutting veins occur throughout, coarse ankerite crystals and pyrite/sericitic stringers occur throughout sample. Sample contains qtz/ank vein.
JSB-184	BAS WK+V	7505049N 440978E	93NOD044 262.0-262.2	Ankerite, Quartz, Paragonite, Clinoclhore	Weakly altered basalt containing a qtz/ank vein.
JSB-185	ARG	7504512N 440865E	93NOD033 33.3 to 33.4	Quartz, Dolomite, Phlogopite, Paragonite, Pyrophyllite, Clinoclhore	Dark gray/black sample with mm-scale bands and stringers of graph/sericitic occurring throughout defining a well developed foliation, carb lenses and clots also occur throughout sample.
JSB-188	BAS	7504512N 440865E	93NOD033 169.2-169.4	Clinoclhore (60%), Calcite (28%), Quartz (10%), Rutile (2%)	Very fine grained, dark forest green basalt, numerous oval shaped light green calcite rich patches throughout, calcite also occurs as bands and veinlets throughout sample



JSB-189	ARG	7505003N 440954E	93NOD035 35.7-36.1	Quartz, Dolomite, Clinocllore, Muscovite, Paragonite, Dolomite	Well handed, dark gray/black sample, very thin sercite/graph bands define foliation, lenses of carb and clots of fine grained py occur throughout sample. Sample contains qtz/dol vein.
JSB-191	BAS ST	7505003N 440954E	93NOD035 250.2-250.3	Quartz, Ankerite, Clinocllore, Paragonite, Muscovite	Brown/gray/green strongly altered and foliated unit consisting of alternating sercite rich bands and carb/qtz rich bands and lenses. Weathers rusty brown due to iron content.
JSB-193	BAS	7504717N 441239E	93NOD063 33.2-33.4	Clinocllore (35%), Calcite (22%), Quartz (18%), Plag (15%), Magnetite (5%), Rutile (4%), Py (1%), Sercite (tr)	Dark forest green massive, weakly foliated, pervasively calcite altered sample with light green cream coloured spots throughout, rutile (leucoxene) also occurs throughout.
JSB-194	Strongly Deformed Rock	7504717N 441239E	93NOD063 413.1-413.4	Quartz, Ankerite, Clinocllore, Paragonite, Rutile, Magnetite	—
JSB-195	GWY	7505126N 441448E	94NOD104 52.0-52.2	Dolomite (60%), Quartz (20%), Parag/Musc (17%), Rutile (2%), Py/Cpy (1%)	Gray, weakly foliated sample, graded bedding is observed cutting foliation at a 30 degree angle.
JSB-199	BAS	7505126N 441448E	94NOD104 347.2-347.3	Calcite (50%), Clinocllore (30%), Quartz (18%), Rutile (2%), Pyrite (tr)	Light gray/green, fine grained, well foliated, pervasively calcite altered sample, fine grained rutile (leucoxene) and irregular zones of dark green clinocllore occurs throughout giving unit a mottled appearance.
JSB-200	BAS	7505126N 441448E	94NOD104 407.5-407.7	Quartz, Ankerite, Calcite, Clinocllore, Paragonite, Muscovite	—
JSB-202	BAS	7505007N 441504E	94NOD123 559.3-559.4	Calcite (40%), Clinocllore (35%), Quartz (15%), Plagioclase (8%), Rutile (2%), Sercite (tr)	Very fine grained, dark forest green unit with numerous patches of light green, weakly foliated unit that has been pervasively calcite altered, calcite rich patches throughout give unit a mottled appearance.
JSB-207	GAB	7504929N 441410E	94NOD108 84.6-84.7	Ankerite (50%), Quartz (20%), Paragonite (15%), Clinocllore (10%), Pyrite (3%), Rutile (2%)	Gray/beige/green, weakly foliated, fine grained sample, locally has a very mottled appearance.
JSB-208	Strongly Deformed Rock	7504929N 441410E	94NOD108 110.4-110.5	Quartz, Ankerite, Clinocllore, Paragonite, Magnetite	—
JSB-210	BAS MD	7504929N 441410E	94NOD108 345.3-345.4	Quartz, Ankerite, Clinocllore, Paragonite	—
JSB-211	BAS	7504750N 441410E	Surface Sample	Quartz, Ankerite, Calcite, Clinocllore, Plagioclase, Illite, Actinolite	—

JSB-212	GAB	7505150N 439450E	Surface Sample	Quartz, Dolomite, Calcite, Clinocllore, Plagioclase, Muscovite	---
JSB-216	SED ST	7504724N 441207E	97NOD169 128.5	Carbonate, Quartz, Sericite, Pyrite	Dark gray/black, well foliated (banded) sample, clots of fine grained py occur locally with long axis parallel to foliation.

### South Patch Occurrence

Sample No.	Rock Type	Location (UTM 83N, 83E)	DDH No. and Depth to Sample (m)	Mineralogy - based on thin-section petrography and/or XRD	Hand Sample Description
SPJS-001	BAS	7549600N 434300E	Surface Sample	Quartz, Calcite, Clinocllore, Plagioclase	Greenschist facies basalt, calcite filled fractures and wispy veinlets throughout, trace py, carbonate minerals restricted to fractures.
SPJS-003	Carbonate Unit	7556000N 428300E	Surface Sample	Dolomite, Quartz, Clinocllore, Illite	Pervasively dolomitized unit showing karst weathering to a rusty dull brown colour, fresh surface gray, massive to weakly foliated, minor qtz/carb veining throughout.
SPJS-005	BAS	7547831N 435234E	97PSD06 176	Quartz, Ankerite, Calcite, Clinocllore, Plagioclase	Greenschist facies unaltered basalt, massive unfoliated unit.
SPJS-006	GAB ST	7547831N 435179E	97PSD07 46	Quartz, Ankerite, Clinocllore, Paragonite, Plagioclase	Deformed/folded mm- to cm-scale bands of ank and ser alteration, strongly altered unit.
SPJS-008	Mineralized Vein	7547831N 435179E	97PSD07 211	Quartz, Dolomite, Pyrite	Qtz/carb vein, massive milky qtz with carb occurring between qtz crystals throughout, minor py also in vein.
SPJS-009	BAS MD	7547831N 435179E	97PSD07 317	Ankerite/Siderite (47%), Quartz (20%), Paragonite (16%), Rutile (10%), Clinocllore (7%), Muscovite (tr), Py/Cpy (tr)	Moderately altered sample, intense carb alteration with cm-scale gray carb bands separated by very thin, wispy ser bands that define a well developed foliation.
SPJS-010	BAS MD	7547831N 435349E	97PSD08 161	Quartz, Ankerite/Siderite, Paragonite, Magnetite, Rutile	Moderately altered sample, strongly foliated with alternating mm-scale ser and carb bands defining foliation throughout, carb bands tend to be boudinaged.
SPJS-011	Mineralized Vein	7547831N 435250E	97PSD09 126	Quartz, Dolomite, Clinocllore	Milky qtz vein with minor intergranular carb and stringers of dark green chl, vein fractured by several mm-scale x-cutting qtz/carb filled veinlets.
SPJS-012	Mineralized Vein	7546723N 435374E	98PSD26 55	Quartz, Dolomite, Sericite, Clinocllore, Pyrite, Gold	Qtz/carb vein, massive milky qtz with carb occurring between qtz crystals throughout, visible gold occurs with carb in qtz vein, stringers of chl/py also in vein.
SPJS-013	Mineralized Vein	7546723N 435374E	98PSD26 62	Quartz (70%), Ankerite (29%), Muscovite (1%), Gold (tr)	Qtz/carb vein, similar to SPJS-012, with minor mm-scale x-cutting qtz veinlets throughout, visible gold occurs with carb in vein.

SPJS-014	BAS WK	7546723N 435374E	98PSD26 75	Dolomite (45%), Quartz (20%), Parag/Musc (20%), Clinocllore (8%), Rutile (4%), Cpy (tr)	Weakly altered sample, beige/green massive unfoliated unit.
SPJS-016	BAS WK	7546723N 435443E	97PSD14 36	Ankerite/Siderite (45%), Quartz (25%), Paragonite (20%), Rutile (9%), Py/Cpy (tr), Clinocllore (tr)	Weakly to moderately altered sample, moderately well developed foliation throughout, pervasive carb alteration gives the sample an orange/brown appearance.
SPJS-017	BAS MD	7546723N 435443E	97PSD14 158	Quartz, Ankerite/Siderite, Paragonite	Moderately to strongly altered sample, strongly foliated with a soapy feel, mm-scale bands of ser/carb alteration define foliation throughout.
SPJS-018	Mineralized Vein	7546723N 435443E	97PSD14 170	Quartz, Dolomite, Pyrite, Gold	Qtz/carb vein, mainly milky qtz with intergranular carb, visible gold occurs within carb in the vein, py also occurs within qtz vein.
SPJS-019	BAS WK	7546723N 435443E	97PSD14 197	Dolomite/Calcite (35%), Clinocllore/Musc (30%), Quartz (27%), Rutile (8%), Anorthite (tr), Plagioclase (tr), Cpy (tr)	Very weak to unaltered sample, well foliated, minor bleaching along some foliation planes, pervasive calcite alteration throughout.
SPJS-020	BAS	7546743N 435514E	98PSD30 97	Quartz, Ankerite, Clinocllore, Paragonite, Pyrite	Very weak to unaltered sample, moderately well foliated unit.
SPJS-021	BAS	7546743N 435514E	98PSD30 140	Clinocllore (35%), Dolomite (30%), Quartz (10%), Rutile (8%), Paragonite (7%), Cpy (tr)	Grainy beige/green unit, leucoxene alteration throughout.
SPJS-022	BAS MD	7546723N 435420E	97PSD13 96	Quartz, Ankerite/Siderite, Clinocllore, Paragonite	Moderately altered sample, beige coloured moderately well foliated unit, rusty orange/brown appearance due to pervasive carb alteration.
SPJS-023	BAS+V	7546723N 435420E	97PSD13 153	Ankerite, Quartz, Paragonite, Clinocllore	Quartz floxed unit, pervasive carb (coarse grained) with qtz near centre of sample, ser/chl stringers throughout occurring parallel to dominant fol, late x-cutting qtz/carb filled fractures also occur locally
SPJS-027	GAB MD	7549800N 434748E	98PSD25 182	Quartz, Dolomite, Clinocllore, Muscovite, Plagioclase, Rutile	Moderately altered sample, well developed foliation defined by cm to mm-scale bands of ser and carb alteration, py occurs along foliation locally.
SPJS-028	BAS WK	7549800N 434748E	98PSD25 338	Clinocllore (35%), Plagioclase (25%), Calcite (20%), Rutile (10%), Quartz (7%), Parag/Musc (3%), Pyrite (tr)	Grainy light gray/green coloured rock consisting of ser, chl, qtz, poorly foliated unit.
SPJS-029	BAS WK	7549800N 434550E	98PSD43 110	Quartz, Ankerite, Calcite, Clinocllore, Plagioclase, Paragonite	Weakly altered sample, weakly foliated green to green/beige unit, pervasively calcite enriched with bands of ser/chl/carb throughout.

SPJS-030	BAS	7549800N 434550E	98PSD43 146	Clinocllore (40%), Rutile (17%), Calcite (15%), Quartz (10%), Muscovite (15%), Epidote (2%), Py/Aspy/Cpy (1%), Plag (tr)	Possible flow top breccia, intensely chl enriched with minor calcite throughout, trace py and cpy also occur throughout.
SPJS-031	GAB MD	7549800N 434550E	98PSD43 263	Quartz, Ankerite, Calcite, Clinocllore, Muscovite, Rutile, Pyrite	Moderately altered sample, mottled foliation with bands of chl/ser and carb throughout, minor py occurs along foliation planes locally, irregular cal filled veinlets occur throughout sample.
SPJS-032	Mineralized Vein	7549800N 434550E	98PSD43 250	Ankerite/Calcite (45%), Quartz (30%), Clinocllore (7%), Muscovite (3%), Rutile (tr), Py (tr)	Intensely fractured unit, fractures and mm-scale veinlets filled with carb throughout, qtz/carb matrix with numerous chl/py stringers throughout.
SPJS-033	GAB WK	7549675N 434425E	98PSD34 63	Quartz, Dolomite, Clinocllore, Plagioclase	Weakly altered sample, weakly foliated with minor bleaching along fol plains locally, dark green fol parallel chl stringers also occur locally.
SPJS-036	Mineralized Vein	7549675N 434425E	98PSD34 261	Quartz, Ankerite, Clinocllore, Rutile, Muscovite	Intense carb alteration with qtz flooding and irregular stringers of ser/py throughout giving sample a mottled appearance, foliation irregular and weakly developed.
SPJS-037	BAS MD	7549675N 434425E	98PSD34 285	Quartz, Ankerite, Clinocllore, Plagioclase, Paragonite	Moderately altered sample, beige coloured with moderately developed fol.

### Major Elements

Sample	Unit	% SiO <sub>2</sub>	% Al <sub>2</sub> O <sub>3</sub>	% CaO	% MgO	% Na <sub>2</sub> O	% K <sub>2</sub> O	% Fe <sub>2</sub> O <sub>3</sub>	% MnO	% TiO <sub>2</sub>	% P <sub>2</sub> O <sub>5</sub>	% Cr <sub>2</sub> O <sub>3</sub>	% LOI	% Sum
JSB-034	Basalt	40.4	12.9	11.70	5.83	2.45	0.07	13.50	0.23	1.010	0.08	0.03	12.20	100.3
JSB-147	Basalt	37.7	16.2	4.94	10.10	2.29	0.19	18.60	0.24	1.610	0.14	0.02	8.25	100.3
JSB-188	Basalt	39.9	9.8	17.70	4.97	2.27	0.04	9.06	0.31	0.598	0.05	0.13	15.60	100.4
JSB-193*	Basalt	48.4	11.9	6.58	5.45	2.51	0.16	15.70	0.19	1.744	0.15	-0.01	7.30	100.2
JSB-199*	Basalt	46.6	13.1	9.88	5.92	2.74	0.03	10.10	0.15	0.800	0.07	0.04	10.80	100.3
JSB-029	Gabbro	22.0	8.6	7.37	16.30	0.79	1.42	14.80	0.24	0.513	0.01	0.36	27.60	100.0
JSB-041*	Gabbro	47.6	15.4	8.79	5.10	2.72	0.65	11.30	0.17	0.996	0.11	0.04	7.35	100.2
JSB-073*	Gabbro	38.1	13.3	8.98	5.06	3.82	0.61	14.60	0.25	1.766	0.13	-0.01	13.60	100.3
JSB-105	Gabbro	45.0	11.3	7.48	4.59	4.33	0.71	11.50	0.19	1.134	0.09	-0.01	13.90	100.2
JSB-207*	Gabbro	36.3	15.5	10.40	5.21	2.02	0.36	12.80	0.26	0.838	0.05	0.05	16.70	100.4
Duplicate of JSB-029	Gabbro	22.1	8.6	7.39	16.30	0.78	1.44	14.80	0.24	0.511	0.02	0.36	27.70	100.3

### Trace Elements

Sample	Unit	ppm Rb	ppm Sr	ppm Y	ppm Zr	ppm Nd	ppm Ba
JSB-034	Basalt	3	67	21	54	2	24
JSB-147	Basalt	3	177	29	114	9	328
JSB-188	Basalt	3	52	12	34	-2	31
JSB-193*	Basalt	3	199	29	108	8	20
JSB-199*	Basalt	3	63	15	51	3	-20
JSB-029	Gabbro	64	86	11	31	-2	165
JSB-041*	Gabbro	20	168	18	70	-2	251
JSB-073*	Gabbro	15	166	38	130	7	151
JSB-105	Gabbro	18	75	25	74	5	100
JSB-207*	Gabbro	11	84	19	47	2	88
Duplicate of JSB-029	Gabbro	64	86	12	30	-2	163

**Appendix B. X-ray fluorescence spectrometry (XRF)**  
 data for five samples of basalt and five samples of gabbro that were difficult to identify in hand sample.  
 \* - indicates that sample identification changed from field identification after taking into account the XRF whole rock data, petrography, and geochemistry (the lower recording limit of this technique is 0.01% and 2 ppm; 20 ppm for Ba).

## Appendix C. Microthermometric measurements for veins in the Boston deposit.

- P = Primary Fluid Inclusion  
 PS = Pseudosecondary Fluid Inclusion  
 S = Secondary Fluid Inclusion  
 VolFrac Vap = Approximate volume fraction of vapor at 25°C  
 VolFrac CO<sub>2</sub> = Approximate volume fraction of the carbonic phase at Th<sub>CO2</sub>  
 Tm<sub>CO2</sub> = The temperature at which the carbonic phase melts (degrees C)  
 Te = The temperature of the eutectic (degrees C)  
 Tm<sub>ICE</sub> = The temperature at which ice melts (degrees C)  
 Tm<sub>CLATH</sub> = The temperature at which clathrate melts (degrees C)  
 eq wt% NaCl = The equivalent weight percent NaCl content of the Fluid Inclusion  
 Th<sub>CO2</sub> = The temperature of homogenization of the carbonic phase (degrees C)  
 Th<sub>(L-V)</sub> = The temperature of total homogenization (degrees C)  
 \* = Fluid inclusion shows evidence of necking down and was not included in average.
- L = Homogenize to Liquid  
 V = Homogenize to Vapor  
 C = Homogenize to a Critical fluid  
 D = Fluid Inclusion Decrepitated  
 XH<sub>2</sub>O = Mole fraction H<sub>2</sub>O  
 XNaCl = Mole fraction NaCl  
 XCO<sub>2</sub> = Mole Fraction CO<sub>2</sub>  
 d<sub>AQ</sub> = Density of the aqueous phase (g/cm<sup>3</sup>)  
 d<sub>CO2</sub> = Density of the carbonic phase (g/cm<sup>3</sup>)  
 d<sub>BULK</sub> = Density of the bulk inclusion (g/cm<sup>3</sup>)  
 Mol Vol CO<sub>2</sub> = Molar volume of CO<sub>2</sub>  
 Mol Vol Bulk = Molar volume of the bulk inclusion  
 M NaCl = Molality NaCl  
 Min P = Minimum pressure at Th (bars)

### Main Stage Quartz-Carbonate Veins

Sample	Inc	Type	Vol Frac Vap	Vol Frac CO <sub>2</sub>	Tm <sub>CO2</sub>	Te	Tm <sub>ICE</sub>	Tm <sub>CLATH</sub>	eq-wt % NaCl	Th <sub>CO2</sub>	Th <sub>(L-V)</sub>	XH <sub>2</sub> O	XCO <sub>2</sub>	XNaCl	d <sub>AQ</sub>	d <sub>CO2</sub>	d <sub>BULK</sub>	Mol Vol CO <sub>2</sub>	Mol Vol Bulk	M NaCl	Min P	
JSB-046	1	1	P	0.10	1.0	-56.6	—	—	—	30.1	L	—	—	—	—	0.59	—	—	74.97	—	—	—
(H-D)	2	1	P	0.10	1.0	-56.6	—	—	—	29.8	L	—	—	—	—	0.60	—	—	73.28	—	—	—
Chip #1	3	1	P	0.10	1.0	-56.6	—	—	—	23.2	L	—	—	—	—	0.74	—	—	59.82	—	—	—
B2 zone	4	2	P	—	0.30	-56.6	—	7.7	4.5	27.8	L	300	L	0.88	1.02	0.66	0.92	66.57	23.21	0.83	3170	
	5	2	P	—	0.30	-56.6	—	7.6	4.7	29.2	L	308	L	0.89	1.03	0.63	0.91	70.43	23.36	0.83	3192	
	6	1	P	0.10	1.0	-56.6	—	—	—	18.3	L	—	—	—	—	0.79	—	—	55.64	—	—	—
	7*	2*	P*	—	0.30*	-56.6*	—	8.2*	3.6*	28.5*	L*	242*	L*	—	—	—	—	—	—	—	—	—
	8	1	P	0.15	1.0	-56.6	—	—	—	29.3	L	—	—	—	—	0.62	—	—	71.10	—	—	—
	9	2	P	—	0.30	-56.6	—	6.9	5.9	30.7	L	350	V	0.89	1.03	0.63	0.89	70.43	23.36	0.83	3562	
	10	2	P	—	0.30	-56.6	—	6.6	6.5	30.7	L	355	V	0.89	1.40	0.55	0.89	79.44	23.62	1.16	3629	
	11	2	P	—	0.30	-56.6	—	6.6	6.5	30.4	L	355	V	0.89	1.40	0.55	0.89	79.44	23.62	1.16	2906	

12	1	P	0.10	1.0	-56.6	--	--	--	23.7	L	--	--	--	--	0.73	--	60.37	--	--		
13	1	P	0.10	1.0	-56.6	--	--	--	23.6	L	--	--	--	--	0.73	--	60.25	--	--		
14	1	P	0.10	1.0	-56.6	--	--	--	26.0	L	--	--	--	--	0.69	--	63.40	--	--		
15	1	P	0.10	1.0	-56.6	--	--	--	26.3	L	--	--	--	--	0.69	--	63.88	--	--		
16	1	P	0.10	1.0	-56.6	--	--	--	28.9	L	--	--	--	--	0.63	--	69.70	--	--		
17	1	P	0.10	1.0	-56.6	--	--	--	27.9	L	--	--	--	--	0.66	--	66.99	--	--		
18	1	P	0.10	1.0	-56.6	--	--	--	27.8	L	--	--	--	--	0.66	--	66.76	--	--		
19	1	P	0.10	1.0	-56.6	--	--	--	26.7	L	--	--	--	--	0.68	--	64.56	--	--		
20	1	P	0.10	1.0	-56.6	--	--	--	30.2	L	--	--	--	--	0.58	--	75.63	--	--		
21	1	P	0.10	1.0	-56.6	--	--	--	29.4	L	--	--	--	--	0.62	--	71.49	--	--		
Avg.	1/2	P	0.10	0.83	-56.6	--	--	7.1	5.6	27.5	334	0.89	0.09	0.02	1.17	0.65	0.90	68.21	23.43	0.96	3292

Sample	Inc	Type	Vol Frac	Vol Frac	Vol Frac	Tmco2	Te	Tmice	Tmclatu	eq.wt %	Tmco2	Th(q-v)	XH2O	XCO2	XNaCl	dAQ	dco2	dBULK	Mol Vol CO2	Mol Vol Bulk	M NaCl	M Min P		
JSB-015	1	1	P	0.5	1.0	-56.6	--	--	9.0	2.0	21.6	L	--	--	--	--	--	--	58.25	--	--	--		
(FI-A)	2	1	P	0.5	1.0	-56.6	--	--	9.0	2.0	21.0	L	--	--	--	--	--	--	57.72	--	--	--		
Chip #1	3	2	P	0.20	0.20	-56.7	--	--	8.4	3.2	29.5	L	D	L	--	--	--	--	--	--	--	--		
B3 zone	4	2	P	0.20	0.20	--	--	--	7.7	4.5	--	206	L	--	--	--	--	--	--	--	--	--		
	5	2	P	0.10	0.10	--	--	--	8.0	4.0	--	207	L	--	--	--	--	--	--	--	--	--		
	6	2	P	0.20	0.20	--	--	--	--	--	--	214	L	--	--	--	--	--	--	--	--	--		
	7	2	P	0.20	0.20	--	--	--	8.4	3.2	29.5	V	224	L	0.96	0.03	0.01	1.01	0.33	0.88	135.06	21.97	0.56	2436
	8	2	P	0.20	0.20	--	--	--	8.4	3.2	29.7	V	223	L	0.96	0.03	0.01	1.01	0.33	0.88	132.39	21.96	0.56	2426
	9	2	P	0.25	0.25	--	--	--	8.5	3.0	30.6	V	224	L	0.94	0.05	0.01	1.01	0.38	0.85	117.40	23.05	0.52	2208
	10	2	P	0.25	0.25	-56.6	--	--	8.3	3.4	30.8	V	226	L	0.94	0.05	0.01	1.02	0.39	0.86	112.41	22.99	0.59	2253
	11	2	P	0.25	0.25	-56.6	--	--	8.3	3.4	31.0	V	226	L	0.94	0.05	0.01	1.02	0.42	0.87	105.72	22.92	0.59	2265
	12	2	P	0.20	0.20	--	--	--	8.2	3.6	--	--	233	L	--	--	--	--	--	--	--	--	--	--
	13	2	P	0.20	0.20	-56.6	--	--	8.3	3.4	29.7	V	220	L	0.96	0.03	0.01	1.02	0.33	0.88	132.39	21.96	0.59	2375
	14	2	P	0.20	0.20	-56.6	--	--	7.3	5.2	31.1	C	227	L	0.94	0.04	0.02	1.03	0.42	0.91	105.72	21.77	0.93	2534
	15	1	P	0.75	1.0	--	--	--	--	--	--	--	--	--	--	--	--	--	--	--	--	--	--	--
16*	1*	P*	0.75*	1.0	-56.6*	--	--	--	8.9*	2.2*	20.7*	L*	--	--	--	--	--	--	--	--	--	--	--	--
17*	1*	P*	0.75*	1.0	-56.6*	--	--	--	8.9*	2.2*	--	--	--	--	--	--	--	--	--	--	--	--	--	--
Avg.	1/2	P	0.58	0.44	-56.6	--	--	--	8.3	3.4	29.2	221	0.95	0.04	0.01	1.02	0.46	0.87	106.34	22.37	0.62	2357		

Sample	Inc	Type	Vol Frac Vap	Vol Frac CO <sub>2</sub>	T <sub>inc</sub>	T <sub>inc</sub>	Te	T <sub>inc</sub>	T <sub>inc</sub>	T <sub>inc</sub>	eq.wt % NaCl	Th <sub>CO<sub>2</sub></sub>	Th <sub>(L-V)</sub>	XH <sub>2</sub> O	XCO <sub>2</sub>	XNaCl	d <sub>ΛQ</sub>	d <sub>CO<sub>2</sub></sub>	d <sub>BULK</sub>	Mol Vol CO <sub>2</sub>	Mol Vol Bulk	M NaCl	Min P
JSB-047	1	2	P	0.30	-57.0	---	---	6.2	---	289	L	---	---	---	---	---	---	---	---	---	---	---	---
(FI-C)	2	2	P	0.20	-57.0	---	---	6.0	---	293	L	---	---	---	---	---	---	---	---	---	---	---	---
Chip #2	3	2	P	0.30	-57.0	---	---	6.2	7.1	27.0	V?	304	L	0.93	0.05	0.02	1.05	0.27	0.81	162.51	24.71	1.30	2873
B2 zone	4	2	P	0.30	-57.0	---	---	5.7	7.9	29.4	V?	310	L	0.92	0.05	0.02	1.05	0.32	0.83	136.35	24.52	1.46	2941
	5	2	P	0.30	-57.0	---	---	6.6	6.5	---	---	312	L	---	---	---	---	---	---	---	---	---	---
	6	2	P	0.30	-56.9	---	---	6.5	6.6	---	---	269	L	---	---	---	---	---	---	---	---	---	---
	7	2	P	0.30	-57.0	---	---	5.8	7.8	---	---	331	L	---	---	---	---	---	---	---	---	---	---
	8	2	P	0.30	-57.0	---	---	5.9	7.6	---	---	303	L	---	---	---	---	---	---	---	---	---	---
	9	2	P	0.30	-56.9	---	---	5.1	8.9	29.5	V?	342	L	0.92	0.05	0.03	1.06	0.33	0.84	135.06	24.50	1.66	3317
	10	2	P	0.30	-57.1	---	---	6.9	5.9	---	---	> 400	V	---	---	---	---	---	---	---	---	---	---
	11	2	P	0.30	-57.0	---	---	---	---	---	---	> 400	V	---	---	---	---	---	---	---	---	---	---
	12	2	P	0.30	-57.0	---	---	7.1	5.6	---	---	264	L	---	---	---	---	---	---	---	---	---	---
	13	2	P	0.30	-57.1	---	---	6.5	6.6	---	---	280	L	---	---	---	---	---	---	---	---	---	---
	14	2	P	0.30	-57.0	---	---	---	---	---	---	> 400	V	---	---	---	---	---	---	---	---	---	---
	15	2	P	0.30	-57.0	---	---	7.0	5.8	29.3	V	304	L	0.93	0.05	0.02	1.03	0.32	0.82	137.62	24.54	1.03	2836
	16*	2*	P*	0.30*	---	---	---	---	---	28.3*	V*	218*	L*	---	---	---	---	---	---	---	---	---	---
	17*	2*	P*	0.30*	---	---	---	---	---	30.2*	?	260*	L*	---	---	---	---	---	---	---	---	---	---
	18*	2*	P*	0.20*	---	---	---	7.4*	5.1*	28.5*	V*	195*	L*	---	---	---	---	---	---	---	---	---	---
Avg.	2	P	---	0.29	-57.0	---	---	6.3	7.0	28.8	---	300	---	0.93	0.05	0.02	1.05	0.31	0.83	142.89	24.57	1.36	2992

Sample	Inc	Type	Vol Frac Vap	Vol Frac CO <sub>2</sub>	T <sub>inc</sub>	T <sub>inc</sub>	Te	T <sub>inc</sub>	T <sub>inc</sub>	T <sub>inc</sub>	eq.wt % NaCl	Th <sub>CO<sub>2</sub></sub>	Th <sub>(L-V)</sub>	XH <sub>2</sub> O	XCO <sub>2</sub>	XNaCl	d <sub>ΛQ</sub>	d <sub>CO<sub>2</sub></sub>	d <sub>BULK</sub>	Mol Vol CO <sub>2</sub>	Mol Vol Bulk	M NaCl	Min P
JSB-059	1	2	P	0.20	-56.6	--20	---	8.4	3.2	31.0	L	253	L	0.94	0.05	0.01	1.01	0.52	0.91	84.90	21.57	0.56	2870
(FI-C)	2	2	P	0.25	-56.7	---	---	7.4	5.1	30.6	L	---	---	---	---	---	---	---	---	---	---	---	---
Chip #4	3	2	P	0.20	-56.6	--20	---	8.5	3.0	31.0	L	230	L	0.94	0.05	0.01	1.01	0.52	0.91	84.65	21.57	0.52	2582
B2 zone	4	2	P	0.20	---	---	---	8.4	3.2	30.8	L	244	L	0.94	0.05	0.01	1.01	0.54	0.92	80.84	21.51	0.56	2773
	5	2	P	0.25	---	---	---	8.5	3.0	30.8	L	244	L	0.92	0.07	0.01	1.01	0.54	0.90	80.84	22.55	0.52	2551
	6	2	P	0.25	-56.6	--20	---	8.4	3.2	---	---	216	L	---	---	---	---	---	---	---	---	---	---
	7*	2*	P*	0.20*	-56.6*	--20*	---	8.4*	3.2*	31.0*	L*	271*	L*	---	---	---	---	---	---	---	---	---	---



8	2	P	—	0.25	-56.6	—	—	8.5	3.0	30.9	L	240	L	0.92	0.07	0.01	1.01	0.53	0.89	82.72	22.58	0.52	2493
9	2	P	—	0.25	-56.6	—	—	—	—	—	—	247	L	—	—	—	—	—	—	—	—	—	—
10	2	P	—	0.35	-56.6	—	—	7.5	4.9	28.6	L	325	V	—	—	—	—	—	—	—	—	—	—
11	2	P	—	0.35	-56.6	—	—	7.4	5.1	28.2	L	330	V	—	—	—	—	—	—	—	—	—	—
12	2	P	—	0.35	-56.6	—	—	7.5	4.9	28.6	L	325	V	—	—	—	—	—	—	—	—	—	—
13	2	P	—	0.25	-56.6	—	—	7.6	4.7	—	—	253	L	—	—	—	—	—	—	—	—	—	—
Avg.	2	P	—	0.26	-56.6	-20	—	8.0	3.9	30.1	264	0.93	0.06	0.01	1.01	0.53	0.91	82.79	21.95	0.54	2654		

Sample	Inc	Type	Vol Frac Vap	Vol Frac CO <sub>2</sub>	T <sub>m,CO<sub>2</sub></sub>	T <sub>e</sub>	T <sub>m,ICE</sub>	T <sub>m,CLATH</sub>	eq.wt % NaCl	T <sub>h,CO<sub>2</sub></sub>	T <sub>h,(v)</sub>	XH <sub>2</sub> O	XCO <sub>2</sub>	XNaCl	d <sub>AQ</sub>	d <sub>CO<sub>2</sub></sub>	d <sub>BULK</sub>	Mol Vol CO <sub>2</sub>	Mol Vol Bulk	M NaCl	Min P		
																						Mol Vol CO <sub>2</sub>	Mol Vol Bulk
JSB-046	1	2	P	—	0.15	-56.7	—	7.8	4.3	29.4	L	> 350	—	—	—	—	—	—	—	—	—	—	
(FI-A)	2	2	P	—	0.15	-56.7	—	8.0	4.0	29.6	L	281	L	0.95	0.04	0.01	1.02	0.61	0.96	71.97	20.46	0.69	3646
Chip #2	3	2	P	—	0.15	—	—	7.6	4.7	—	—	262	L	—	—	—	—	—	—	—	—	—	—
B2 zone	4	2	P	—	0.15	-56.7	—	8.5	3.0	30.0	L	261	L	0.95	0.04	0.01	1.01	0.60	0.95	73.89	20.49	0.52	3317
	5	2	P	—	0.15	-56.7	—	8.2	3.6	30.0	L	271	L	0.95	0.04	0.01	1.02	0.60	0.95	73.89	20.49	0.62	3464
	6	2	P	—	0.15	-56.7	—	8.0	4.0	—	—	273	L	—	—	—	—	—	—	—	—	—	—
	7	2	P	—	0.15	—	—	8.0	4.0	—	—	232	L	—	—	—	—	—	—	—	—	—	—
	8	2	P	—	0.15	—	—	8.0	4.0	—	—	242	L	—	—	—	—	—	—	—	—	—	—
	9	2	P	—	0.15	-56.7	—	7.9	4.1	—	—	279	L	—	—	—	—	—	—	—	—	—	—
	10	2	P	—	0.15	—	—	7.9	4.1	30.0	L	254	L	0.95	0.04	0.01	1.02	0.60	0.96	73.89	20.48	0.73	3268
	11	2	P	—	0.15	-56.7	—	8.5	3.0	—	—	250	L	—	—	—	—	—	—	—	—	—	—
	12*	2*	P*	—	0.15*	—	—	8.1*	3.8*	—	—	311*	L*	—	—	—	—	—	—	—	—	—	—
	13*	2*	P*	—	0.15*	-56.7*	—	8.1*	3.8*	—	—	324*	V*	—	—	—	—	—	—	—	—	—	—
	14	2	P	—	0.15	—	—	8.0	4.0	—	—	251	L	—	—	—	—	—	—	—	—	—	—
Avg.	2	P	—	0.15	-56.7	—	—	8.0	3.9	29.8	260	0.95	0.04	0.01	1.02	0.60	0.95	73.41	20.48	0.64	3424		

Sample	Inc	Type	Vol Frac Vap	Vol Frac CO <sub>2</sub>	T <sub>m,CO<sub>2</sub></sub>	T <sub>e</sub>	T <sub>m,ICE</sub>	T <sub>m,CLATH</sub>	eq.wt % NaCl	T <sub>h,CO<sub>2</sub></sub>	T <sub>h,(v)</sub>	XH <sub>2</sub> O	XCO <sub>2</sub>	XNaCl	d <sub>AQ</sub>	d <sub>CO<sub>2</sub></sub>	d <sub>BULK</sub>	Mol Vol CO <sub>2</sub>	Mol Vol Bulk	M NaCl	Min P		
																						Mol Vol CO <sub>2</sub>	Mol Vol Bulk
JSB-055	1	2	P	—	0.30	-56.6	—	8.0	4.0	29.5	V	267	L	0.93	0.05	0.01	1.02	0.33	0.81	135.06	24.53	0.69	2435
(FI-A)	2	2	P	—	0.30	—	—	8.0	4.0	—	—	—	—	—	—	—	—	—	—	—	—	—	—
Chip #2	3	2	P	—	0.30	—	—	8.0	4.0	—	—	259	L	—	—	—	—	—	—	—	—	—	—

B2 zone	4	2	P	—	0.30	-56.6	—	—	8.1	3.8	30.0	V	261	L	0.93	0.06	0.01	1.02	0.34	0.82	128.08	24.47	0.66	2395
	5	2	P	—	0.30	-56.6	—	—	8.2	3.6	30.0	V	255	L	0.93	0.06	0.01	1.02	0.34	0.82	128.08	24.47	0.62	2310
	6	2	P	—	0.30	-56.6	—	—	4.8	9.3	—	—	257	L	—	—	—	—	—	—	—	—	—	—
	7	2	P	—	0.30	—	—	—	7.8	4.3	—	—	255	L	—	—	—	—	—	—	—	—	—	—
	8	2	P	—	0.30	—	—	—	8.1	3.8	—	—	—	—	—	—	—	—	—	—	—	—	—	—
	9	2	P	—	0.30	-56.6	—	—	8.0	4.0	—	—	267	L	—	—	—	—	—	—	—	—	—	—
	10	2	P	—	0.30	-56.6	—	—	6.4	6.8	—	—	242	L	—	—	—	—	—	—	—	—	—	—
	11	2	P	—	0.30	—	—	—	8.2	3.6	—	—	—	—	—	—	—	—	—	—	—	—	—	—
	12	2	P	—	0.30	—	—	—	8.1	3.8	—	—	255	L	—	—	—	—	—	—	—	—	—	—
Avg.		2	P	—	0.30	-56.6	—	—	7.6	4.6	29.8		258		0.93	0.06	0.01	1.02	0.34	0.81	130.41	24.49	0.66	2380

Sample	Inc	Type	Vol Frac Vap	Vol Frac CO <sub>2</sub>	Te	T <sub>m,CO2</sub>	T <sub>m,ICE</sub>	T <sub>m,CLATH</sub>	eq.wt % NaCl	T <sub>h,CO2</sub>	T <sub>h,(L-V)</sub>	XH <sub>2</sub> O	XCO <sub>2</sub>	XNaCl	d <sub>AQ</sub>	d <sub>CO2</sub>	d <sub>BULK</sub>	Mol Vol CO <sub>2</sub>	Mol Vol Bulk	M NaCl	Min P			
																						Mol Vol CO <sub>2</sub>	Mol Vol Bulk	M NaCl
JSB-055	1	2	P	—	0.30	-56.8	—	—	8.4	3.2	30.8	L	269	L	0.90	0.09	0.01	1.01	0.54	0.87	80.84	23.68	0.56	2609
(FI-A)	2	2	P	—	0.30	-56.9	—	—	8.4	3.2	30.8	L	286	L	0.90	0.09	0.01	1.01	0.54	0.87	80.94	23.68	0.56	2794
Chip #3	3	2	P	—	0.30	-56.9	—	—	8.6	2.8	31.0	C	273	L	0.91	0.08	0.01	1.01	0.52	0.86	84.65	23.78	0.49	2616
B2 zone	4	2	P	—	0.30	—	—	—	8.6	2.8	—	—	266	L	—	—	—	—	—	—	—	—	—	—
	5	2	P	—	0.30	-56.9	—	—	7.1	5.6	—	—	276	L	—	—	—	—	—	—	—	—	—	—
	6	2	P	—	0.30	-56.9	—	—	8.5	3.0	30.6	V	269	L	0.93	0.06	0.01	1.01	0.38	0.82	117.40	24.35	0.52	2472
	7	2	P	—	0.30	-56.9	—	—	8.3	3.4	30.9	L	285	L	0.90	0.09	0.01	1.02	0.53	0.87	82.72	23.73	0.59	2789
	8	2	P	—	0.30	-56.9	—	—	8.6	2.8	30.0	V	261	L	0.93	0.06	0.01	1.01	0.34	0.81	128.08	24.48	0.49	2391
	9	2	P	—	0.30	-56.9	—	—	8.7	2.6	30.0	V	256	L	0.94	0.06	0.01	1.01	0.34	0.81	128.08	24.48	0.45	2316
	10	2	P	—	0.30	-56.9	—	—	8.6	2.8	30.0	V	264	L	0.93	0.06	0.01	1.01	0.34	0.81	128.08	24.48	0.49	2422
Avg.		2	P	—	0.30	-56.9	—	—	8.4	3.2	30.5		271		0.92	0.07	0.01	1.01	0.44	0.84	103.85	24.08	0.52	2551

JSB-085	1	2	P	—	0.45	-56.7	—	—	7.0	5.8	30.0	V	314	L	0.88	0.11	0.02	1.03	0.34	0.72	128.08	29.78	1.03	2210
(FI-A)	2	2	P	—	0.50	-56.7	—	—	—	—	30.5	L	315	C	—	—	—	—	—	—	—	—	—	—
Chip #1	3	2	P	—	0.50	-56.7	—	—	8.5	3.0	30.7	V	317	C	0.86	0.14	0.01	1.01	0.38	0.70	115.08	31.40	0.52	2031
B4 zone	4	2	P	—	0.50	-56.7	—	—	8.6	2.8	30.7	V	315	C	0.86	0.14	0.01	1.01	0.38	0.70	115.08	31.40	0.49	2006

5	2	P	—	0.50	-56.7	—	—	8.5	3.0	30.4	V	318	L	0.86	0.13	0.01	1.01	0.36	0.69	121.42	31.62	0.52	2018
6	2	P	—	0.50	-56.7	—	—	7.2	5.4	30.0	V	317	L	0.86	0.12	0.02	1.03	0.34	0.69	128.08	31.80	0.96	2014
7*	2*	P*	—	0.50*	-56.7*	—	—	7.4*	5.1*	30*	V*	269*	L*	—	—	—	—	—	—	—	—	—	—
8	2	P	—	0.50	-56.7	—	—	7.4	5.1	30.0	V	292	L	0.86	0.12	0.01	1.03	0.34	0.69	128.08	31.80	0.90	1852
9	2	P	—	0.50	-56.7	—	—	7.5	4.9	30.4	V	297	L	0.86	0.13	0.01	1.03	0.36	0.69	121.42	31.60	0.86	1889
10	2	P	—	0.50	-56.7	—	—	8.4	3.2	30.1	V	305	L	—	—	—	—	—	—	—	—	—	—
11*	2*	P*	—	0.35*	-56.8*	—	—	8.8*	2.4*	30.1*	V*	253*	L*	—	—	—	—	—	—	—	—	—	—
12	2	P	—	0.50	-56.8	—	—	8.4	3.2	30.4	V	317	C	0.86	0.13	0.01	1.01	0.36	0.69	121.42	31.62	0.56	2007
13*	2*	P*	—	0.5*	-56.8*	—	—	7.1*	5.6*	—	—	276*	L*	—	—	—	—	—	—	—	—	—	—
14	2	P	—	0.50	-56.8	—	—	7.9	4.1	—	—	294	L	—	—	—	—	—	—	—	—	—	—
15	2	P	—	0.40	-56.8	—	—	7.7	4.5	30.0	V	299	L	0.90	0.09	0.01	1.02	0.34	0.75	128.08	27.65	0.80	1878
16	2	P	—	0.50	-56.7	—	—	8.3	3.4	30.1	V	303	L	0.87	0.13	0.01	1.02	0.35	0.68	126.53	31.78	0.59	1910
17	2	P	—	0.50	-56.8	—	—	8.1	3.8	29.9	V	312	L	0.87	0.12	0.01	1.02	0.34	0.68	129.56	31.86	0.66	1972
18	2	P	—	0.50	-56.8	—	—	8.4	3.2	30.4	V	327	C	0.86	0.13	0.01	1.01	0.36	0.69	121.42	31.62	0.56	1973
19	2	P	—	0.50	-56.8	—	—	8.7	2.6	30.2	V	306	C	0.87	0.13	0.01	1.01	0.35	0.68	124.92	31.74	0.45	1925
20	2	P	—	0.50	-56.8	—	—	8.5	3.0	30.5	V	304	L	0.86	0.13	0.01	1.01	0.37	0.69	119.50	31.55	0.52	1928
21	2	P	—	0.50	-56.8	—	—	8.6	2.8	30.5	V	319	C	0.86	0.13	0.01	1.01	0.37	0.69	119.50	31.56	0.49	2020
Avg.	2	P	—	0.5	-56.7	—	—	8.1	3.8	30.3	310	—	—	0.86	0.12	0.01	1.02	0.36	0.69	123.21	31.25	0.66	1976

Sample	Inc	Type	Vol Frac Nap	Vol Frac CO <sub>2</sub>	T <sub>incO2</sub>	T <sub>e</sub>	T <sub>injCE</sub>	T <sub>injLATH</sub>	eq.Wt % NaCl	T <sub>HCO2</sub>	T <sub>H2O</sub>	X <sub>H2O</sub>	X <sub>CO2</sub>	X <sub>NaCl</sub>	d <sub>AQ</sub>	d <sub>CO2</sub>	d <sub>BULK</sub>	Mol Vol CO <sub>2</sub>	Mol Vol Bulk	M NaCl	Min P	
JSB-023	1	2	S	—	0.10	-56.6	—	—	6.2	7.1	—	—	—	—	—	—	—	—	—	—	—	—
(FI-A)	2	2	S	—	0.10	—	—	—	6.5	6.6	—	—	—	—	—	—	—	—	—	—	—	—
Chip #2	3	2	S	—	0.10	—	-25	—	6.5	6.6	—	—	—	—	—	—	—	—	—	—	—	—
B3 zone	4	2	S	—	0.10	—	—	—	6.5	6.6	—	—	—	—	—	—	—	—	—	—	—	—
	5	2	S	—	0.10	—	-25	—	7.2	5.4	—	—	—	—	—	—	—	—	—	—	—	—
	6	2	S	—	0.10	—	—	—	7.0	5.8	—	—	—	—	—	—	—	—	—	—	—	—
	7	2	S	—	0.10	—	—	—	—	—	—	—	—	—	—	—	—	—	—	—	—	—
	8	2	S	—	0.10	-56.6	—	—	6.4	6.8	—	—	—	—	—	—	—	—	—	—	—	—
Avg.	2	S	—	0.10	-56.6	-25	—	—	6.6	6.4	—	—	—	—	—	—	—	—	—	—	—	—

Sample	Inc	Type	Vol		Te	T <sub>m</sub> CR	T <sub>m</sub> CLATH	eq.wt % NaCl	Th <sub>CO2</sub>	Th <sub>(L-V)</sub>	XH <sub>2</sub> O	XCO <sub>2</sub>	XNaCl	d <sub>AQ</sub>	d <sub>CO2</sub>	d <sub>BULK</sub>	Mol Vol CO <sub>2</sub>	Mol Vol Bulk	M NaCl	Min P	
			Frac Vap	Frac CO <sub>2</sub>																	
JSB-047	1	2	S	0.40	-56.6	--	7.3	5.2	29.1	L	296	0.84	0.15	0.01	1.03	0.63	0.87	70.09	25.80	0.93	2620
(FI-A)	2	2	S	0.40	-56.6	--	6.9	5.9	28.9	L	319	0.84	0.15	0.02	1.04	0.63	0.87	69.44	25.76	1.06	2876
Chip #3	3	2	S	0.30	-56.6	--	6.2	7.1	28.5	L	301	0.88	0.10	0.02	1.04	0.64	0.92	68.29	23.26	1.30	3198
B2 zone	4	2	S	0.40	-56.6	--	5.8	7.8	26.9	L	312	0.82	0.16	0.02	1.05	0.68	0.90	64.77	25.46	1.43	2943
	5	2	S	0.30	-56.6	--	7.4	5.1	28.0	L	290	0.88	0.10	0.01	1.03	0.66	0.92	67.03	23.23	0.90	3054
	6	2	S	0.40	-56.6	--	5.8	7.8	28.0	L	--	--	--	--	--	--	--	--	--	--	--
	7	2	S	0.40	-56.6	--	5.8	7.8	28.0	L	295	0.83	0.15	0.02	1.05	0.66	0.89	67.03	25.60	1.43	2725
	8	2	S	0.30	-56.6	--	7.4	5.1	29.7	L	295	0.89	0.10	0.01	1.03	0.61	0.90	72.41	23.42	0.90	3036
Avg.	2	S	0.36	-56.6	-26	--	6.6	6.5	28.4	301	0.85	0.13	0.02	1.04	0.64	0.90	68.44	24.65	1.13	2922	

### Unmineralized Main Stage Quartz-Carbonate Veins

Sample	Inc	Type	Vol		Te	T <sub>m</sub> CR	T <sub>m</sub> CLATH	eq.wt % NaCl	Th <sub>CO2</sub>	Th <sub>(L-V)</sub>	XH <sub>2</sub> O	XCO <sub>2</sub>	XNaCl	d <sub>AQ</sub>	d <sub>CO2</sub>	d <sub>BULK</sub>	Mol Vol CO <sub>2</sub>	Mol Vol Bulk	M NaCl	Min P
			Frac Vap	Frac CO <sub>2</sub>																
JSB-041	1	1	P	0.05	-56.7	--	--	--	28.1	L	--	--	--	--	0.65	--	67.47	--	--	--
(FI-A)	2	1	P	0.05	-56.7	--	--	--	26.6	L	--	--	--	--	0.68	--	64.39	--	--	--
Chip #1	3	1	P	0.05	-56.7	--	--	--	25.3	L	--	--	--	0.71	--	--	62.37	--	--	--
Unmin	4	1	P	0.06	-56.7	--	--	--	28.1	L	--	--	--	0.65	--	--	67.47	--	--	--
Gab	5	1	P	0.05	-56.7	--	--	--	28.1	L	--	--	--	0.65	--	--	67.47	--	--	--
	6	1	P	0.05	-56.7	--	--	--	28.6	L	--	--	--	0.64	--	--	68.79	--	--	--
	7	1	P	0.05	-56.7	--	--	--	27.9	L	--	--	--	0.66	--	--	66.99	--	--	--
	8	1	P	0.05	-56.7	--	--	--	28.7	L	--	--	--	0.64	--	--	69.09	--	--	--
	9	1	P	0.05	-56.7	--	--	--	26.7	L	--	--	--	0.68	--	--	64.56	--	--	--
	10	1	P	0.05	-56.7	--	--	--	26.6	L	--	--	--	0.68	--	--	64.39	--	--	--
	11	1	P	0.05	-56.7	--	--	--	26.9	L	--	--	--	0.68	--	--	64.92	--	--	--
	12	1	P	0.05	-56.7	--	--	--	27.0	L	--	--	--	0.68	--	--	65.11	--	--	--
	13	1	P	0.05	-56.7	--	--	--	26.8	L	--	--	--	0.68	--	--	64.74	--	--	--
	14	1	P	0.05	-56.8	--	--	--	26.3	L	--	--	--	0.69	--	--	63.88	--	--	--
	15	2	P	0.50	-56.7	--	--	--	--	--	--	--	--	--	--	--	--	--	--	--

16	2	P	—	0.30	-56.7	--25	—	8.5	3.0	29.6	L	288	L	0.89	0.10	0.01	1.01	0.61	0.89	71.97	23.42	0.52	2906
17	1	P	0.05	1.0	-56.7	—	—	—	—	27.9	L	—	—	—	—	—	—	0.66	—	66.99	—	—	—
18	1	P	0.05	1.0	-56.7	—	—	—	—	29.0	L	—	—	—	—	—	—	0.63	—	70.03	—	—	—
19	2	P	—	0.30	-56.7	—	—	—	—	30.5	L	274	L	—	—	—	—	—	—	—	—	—	—
20	1	P	0.05	1.0	-56.7	—	—	—	—	27.4	L	—	—	—	—	—	—	0.67	—	65.90	—	—	—
21	2	P	—	0.30	-56.7	—	—	8.3	3.4	29.8	L	—	L	0.89	0.10	0.01	1.02	0.60	0.89	72.87	23.45	0.59	2832
22	2	P	—	0.30	-56.7	—	—	8.6	2.8	30.0	L	—	L	0.90	0.10	0.01	1.01	0.60	0.89	73.89	23.49	0.49	2829
Avg.	1/2	P	0.05	0.85	-56.7	-25	—	8.5	3.1	27.9	281	—	—	0.90	0.10	0.01	1.01	0.66	0.89	67.16	23.45	0.53	2856

Sample	Inc	Type	Vol		Frac	Vol	Frac	Te	T <sub>MI</sub>	T <sub>CL</sub>	T <sub>GL</sub>	T <sub>HT</sub>	T <sub>HT</sub>	T <sub>HT</sub>	X <sub>H<sub>2</sub>O</sub>	X <sub>CO<sub>2</sub></sub>	X <sub>NaCl</sub>	d <sub>AQ</sub>	d <sub>CO<sub>2</sub></sub>	d <sub>BULK</sub>	Mol Vol	Mol Vol	M	Min P
			Frac	Vol																				
JSB-137	1	2	S	—	0.10	—	—	—	—	—	—	—	—	—	—	—	—	—	—	—	—	—	—	—
(FL-A)	2	2	S	—	0.05	—	—	—	—	—	—	—	—	—	—	—	—	—	—	—	—	—	—	—
Chip #1	3	2	S	—	0.05	—	—	—	—	—	—	—	—	—	—	—	—	—	—	—	—	—	—	—
Uminin	4	2	S	—	0.05	—	--23	—	—	—	—	—	—	—	—	—	—	—	—	—	—	—	—	—
Sed	5	2	S	—	0.05	—	—	—	—	—	—	—	—	—	—	—	—	—	—	—	—	—	—	—
	6	2	S	—	0.05	—	—	—	—	—	—	—	—	—	—	—	—	—	—	—	—	—	—	—
	7	2	S	—	0.10	—	—	—	—	—	—	—	—	—	—	—	—	—	—	—	—	—	—	—
	8	2	S	—	0.05	—	—	—	—	—	—	—	—	—	—	—	—	—	—	—	—	—	—	—
	9	2	S	—	0.06	—	--24	—	—	—	—	—	—	—	—	—	—	—	—	—	—	—	—	—
	10	2	S	—	0.05	—	—	—	—	—	—	—	—	—	—	—	—	—	—	—	—	—	—	—
	11	2	S	—	0.05	—	—	—	—	—	—	—	—	—	—	—	—	—	—	—	—	—	—	—
	12	2	S	—	0.05	—	—	—	—	—	—	—	—	—	—	—	—	—	—	—	—	—	—	—
	13	2	S	—	0.05	—	—	—	—	—	—	—	—	—	—	—	—	—	—	—	—	—	—	—
	14	1	S	0.50	1.0	-56.8	—	—	—	—	—	—	—	—	—	—	—	—	—	—	—	—	—	—
	15	1	S	0.60	1.0	-56.9	—	—	—	—	—	—	—	—	—	—	—	—	—	—	—	—	—	—
Avg.	1/2	S	0.55	0.18	-56.9	-24	—	—	—	—	—	—	—	—	—	—	—	—	—	—	—	—	—	—

### Extensional (Ladder) Veins

Sample	Inc	Type	Vol		Te	T <sub>mix</sub>	T <sub>mix</sub>	T <sub>mix</sub>	eq.wt	T <sub>H<sub>2</sub>O</sub>	X <sub>H<sub>2</sub>O</sub>	X <sub>CO<sub>2</sub></sub>	X <sub>NaCl</sub>	d <sub>AQ</sub>	d <sub>CO<sub>2</sub></sub>	d <sub>BULK</sub>	Mol Vol		M	Min P			
			Frac Vap	Frac CO <sub>2</sub>													CO <sub>2</sub>	Bulk					
JSB-059	1	2	S	0.25	-56.6	--22	--	7.0	5.8	30.6	L	298	L	0.91	0.07	0.02	1.03	0.56	0.92	78.30	22.47	1.03	3270
(FI-C)	2	2	S	0.30	-56.6	--22	--	7.9	4.1	22.3	L	305	L	0.87	0.12	0.01	1.02	0.75	0.94	58.83	22.87	0.73	3472
Chip #3	3	2	S	0.30	-56.6	--20	--	7.7	4.5	25.0	L	312	L	0.88	0.11	0.01	1.03	0.71	0.93	61.85	23.01	0.80	3448
B2 zone	4	2	S	0.30	-56.6	--	--	7.5	4.9	24.4	L	D	L	--	--	--	--	--	--	--	--	--	--
	5	2	S	0.25	-56.6	--20	--	7.5	4.9	27.2	L	315	L	0.90	0.09	0.01	1.03	0.67	0.94	65.33	22.14	0.86	3655
	6	2	S	0.30	-56.6	--20	--	7.8	4.3	25.3	L	322	L	0.88	0.11	0.01	1.02	0.71	0.93	62.26	23.03	0.76	3526
	7	2	S	0.25	-56.6	--19	--	7.7	4.5	26.0	L	302	L	0.90	0.09	0.01	1.03	0.70	0.94	63.27	22.08	0.80	3556
	8	2	S	0.25	-56.6	--19	--	7.0	5.8	24.0	L	288	L	0.89	0.09	0.02	1.04	0.73	0.96	60.62	21.97	1.03	3474
	9	2	S	0.30	-56.6	--19	--	7.6	4.7	24.1	L	259	L	--	--	--	--	--	--	--	--	--	--
	10	2	S	0.30	-56.6	--19	--	7.7	4.5	24.5	L	251	L	--	--	--	--	--	--	--	--	--	--
	11	2	S	0.25	-56.6	--19	--	7.7	4.5	24.0	L	274	L	--	--	--	--	--	--	--	--	--	--
	12	2	S	0.25	-56.6	--17	--	7.6	4.7	24.6	L	249	L	--	--	--	--	--	--	--	--	--	--
	13	2	S	0.25	--	--	--	--	--	--	--	--	--	--	--	--	--	--	--	--	--	--	--
	14	2	S	0.25	-56.6	--	--	7.7	4.5	22.6	L	280	L	0.89	0.09	0.01	1.03	0.74	0.96	59.12	21.92	0.80	3412
Avg.	2	S	0.27	-56.6	-20	--	7.6	4.8	25.0	288	288	0.89	0.10	0.01	1.03	0.70	0.94	63.70	22.44	0.85	3477		

Sample	Inc	Type	Vol		Te	T <sub>mix</sub>	T <sub>mix</sub>	T <sub>mix</sub>	eq.wt	T <sub>H<sub>2</sub>O</sub>	X <sub>CO<sub>2</sub></sub>	X <sub>NaCl</sub>	d <sub>AQ</sub>	d <sub>CO<sub>2</sub></sub>	d <sub>BULK</sub>	Mol Vol		M	Min P				
			Frac Vap	Frac CO <sub>2</sub>												CO <sub>2</sub>	Bulk						
JSB-059	1	2	S	0.30	-56.8	--21	--	7.4	5.1	29.8	L	255	L	0.89	0.10	0.01	1.03	0.60	0.90	72.87	23.43	0.90	2579
(FI-C)																							
Chip #1																							
B2 zone																							

Sample	Inc	Type	Vol		Te	T <sub>mix</sub>	T <sub>mix</sub>	T <sub>mix</sub>	eq.wt	T <sub>H<sub>2</sub>O</sub>	X <sub>CO<sub>2</sub></sub>	X <sub>NaCl</sub>	d <sub>AQ</sub>	d <sub>CO<sub>2</sub></sub>	d <sub>BULK</sub>	Mol Vol		M	Min P				
			Frac Vap	Frac CO <sub>2</sub>												CO <sub>2</sub>	Bulk						
JSB-059	1	2	S	0.25	--	--20	--	7.3	5.2	29.3	L	210	L	0.91	0.08	0.02	1.03	0.62	0.93	70.79	22.30	0.93	2256
(FI-C)	2	2	S	0.25	-56.7	--20	--	7.4	5.1	27.9	L	189	L	0.90	0.08	0.02	1.03	0.66	0.94	66.80	22.18	0.90	2040
Chip #2	3	2	S	0.25	-56.7	--	--	7.2	5.4	23.9	L	231	L	0.89	0.09	0.02	1.03	0.73	0.96	60.50	21.97	0.96	2719













**Appendix D.** Carbon and oxygen isotope data for carbonate minerals.  $\delta^{13}\text{C}$  values reported relative to PDB,  $\delta^{18}\text{O}$  values reported relative to VSMOW. All values have a  $2\sigma$  error of  $\pm 0.1\%$ . Calcites were reacted at  $25^\circ\text{C}$  for a minimum of 24 hours. A fractionation factor of 10.01025 was used to account for the oxygen exchange between sample and acid during preparation (Muehlenbachs, pers. comm., 1999). Fe-dolomites and ankerites were reacted at  $50^\circ\text{C}$  for a minimum of 4 days. A fractionation factor of 10.01060 was used to correct for acid fractionation (Kontak and Kerrich, 1997).

### Boston Deposit

Sample	Mineralogy Based on XRD	Unit	$\delta^{13}\text{C PDB, } \%$		$\delta^{18}\text{O VSMOW, } \%$		$\delta^{13}\text{C PDB, } \%$		$\delta^{18}\text{O VSMOW, } \%$	
			Calcite	Calcite	Calcite	Calcite	Ankerite or Fe-Dolomite	Ankerite or Fe-Dolomite		
JSB-046	Ankerite	B2 Vein					-4.6			12.5
JSB-056	Ankerite	B2 Vein					-4.1			12.0
JSB-057	Ankerite	B2 Vein					-3.3			12.6
JSB-058	Ankerite	B2 Vein					-3.1			12.8
JSB-059	Ankerite	B2 Vein					-3.6			12.2
JSB-012	Ankerite	B3 Vein					-4.4			11.9
JSB-013	Fe-Dolomite	B3 Vein					-3.9			11.9
JSB-014	Fe-Dolomite	B3 Vein					-4.2			12.2
JSB-022	Fe-Dolomite	B3 Vein					-4.0			11.3
JSB-023	Fe-Dolomite	B3 Vein					-4.4			11.7
JSB-032	Fe-Dolomite	B3 Vein					-4.7			11.2
JSB-033	Fe-Dolomite	B3 Vein					-3.2			12.0
JSB-070	Fe-Dolomite	B3 Vein					-4.4			11.4
JSB-075	Fe-Dolomite	B3 Vein					-3.2			11.9
JSB-085	Ankerite	B4 Vein					-3.1			12.8
JSB-046	Ankerite	B2 Wallrock					-2.9			12.3
JSB-057	Ankerite	B2 Wallrock					-3.3			12.3
JSB-012	Ankerite	B3 Wallrock					-4.0			11.8

**Appendix D. (Continued)**

Sample	Mineralogy Based on XRD	Unit	$\delta^{13}\text{C PDB, ‰}$		$\delta^{18}\text{O VSMOW, ‰}$		$\delta^{18}\text{O VSMOW, ‰}$	
			Calcite	Ankerite or Fe-Dolomite	Calcite	Ankerite or Fe-Dolomite	Calcite	Ankerite or Fe-Dolomite
JSB-022	Fe-Dolomite	B3 Wallrock						13.0
JSB-032	Fe-Dolomite	B3 Wallrock					-3.1	12.3
JSB-026	Fe-Dolomite	Basalt Vein					-2.3	20.0
JSB-081	Ankerite	Basalt Vein					-1.7	12.2
JSB-097	Calcite	Basalt Vein	-0.9		12.2			
JSB-100	Calcite	Basalt Vein	-1.7		12.9			
JSB-131	Calcite	Basalt Vein	0.5		13.9			
JSB-147 <sup>†</sup>	Calcite	Basalt Vein	-2.3		13.7			
JSB-177	Ankerite	Basalt Vein					-2.4	12.5
JSB-175	Calcite and Ankerite	Basalt Vein	-1.4		18.1		-1.4	16.9
JSB-179	Ankerite	Basalt Vein					-2.9	13.1
JSB-001	Ankerite	Basalt					-2.0	11.9
JSB-009	Fe-Dolomite	Basalt					-2.3	11.9
JSB-010	Ankerite	Basalt					-2.8	12.0
JSB-016	Fe-Dolomite	Basalt					-1.8	16.4
JSB-025	Ankerite	Basalt					-2.7	13.0
JSB-026	Fe-Dolomite	Basalt					-2.4	17.5
JSB-034 <sup>†</sup>	Calcite	Basalt	-2.3		10.9			
JSB-097	Calcite	Basalt	-1.6		12.3			
JSB-100	Calcite and Ankerite	Basalt	-1.3		13.7		-1.2	13.1
JSB-112	Calcite	Basalt	-1.8		11.1			
JSB-118	Calcite	Basalt	-1.7		12.1			
JSB-125	Calcite and Ankerite	Basalt	-2.5		12.4		-2.1	12.1
JSB-132	Calcite	Basalt	-2.3		11.3			
JSB-138*	Ankerite	Basalt					-0.8	14.5
JSB-139	Ankerite	Basalt					-2.1	13.5
JSB-143*	Ankerite	Basalt					-1.5	13.8
JSB-147 <sup>†</sup>	Calcite	Basalt	-0.6		13.7			

**Appendix D. (Continued)**

Sample	Mineralogy Based on XRD	Unit	$\delta^{13}\text{C PDB, ‰}$		$\delta^{18}\text{O VSMOW, ‰}$		$\delta^{18}\text{O VSMOW, ‰}$	
			Calcite	Ankerite or Fe-Dolomite	Calcite	Ankerite or Fe-Dolomite	Calcite	Ankerite or Fe-Dolomite
JSB-152	Ankerite	Basalt						
JSB-154*	Ankerite	Basalt						11.9
JSB-155*	Ankerite	Basalt						13.8
JSB-159	Ankerite	Basalt						12.6
JSB-175	Calcite	Basalt	-2.0		18.4			12.2
JSB-179	Ankerite	Basalt						12.9
JSB-184	Ankerite	Basalt						12.1
JSB-188 <sup>†</sup>	Calcite	Basalt	0.7		12.4			
JSB-191	Ankerite	Basalt						11.8
JSB-193 <sup>†</sup>	Calcite	Basalt	-1.9		12.4			
JSB-199 <sup>†</sup>	Calcite	Basalt	-1.7		13.3			
JSB-200	Calcite and Ankerite	Basalt	-1.4		12.3			12.9
JSB-202	Calcite	Basalt	-1.0		12.2			
JSB-210	Ankerite	Basalt						12.5
JSB-211	Calcite and Ankerite	Basalt	-0.7		10.7			10.7
JSB-041 <sup>†</sup>	Calcite	Gabbro Vein	-2.9		9.4			
JSB-051*	Calcite and Ankerite	Gabbro Vein	-3.5		11.0			11.0
JSB-041 <sup>†</sup>	Calcite	Gabbro	-2.9		9.3			
JSB-073 <sup>†</sup>	Ankerite	Gabbro						14.7
JSB-103	Calcite and Ankerite	Gabbro	-3.8		14.8			11.2
JSB-104	Fe-Dolomite	Gabbro						13.3
JSB-105 <sup>†</sup>	Ankerite	Gabbro						10.7
JSB-122*	Ankerite	Gabbro						12.0
JSB-133	Calcite	Gabbro	-3.6		10.3			
JSB-136	Calcite	Gabbro	-3.1		10.3			
JSB-151	Fe-Dolomite	Gabbro						14.8
JSB-207 <sup>†</sup>	Ankerite	Gabbro						11.8
JSB-212	Calcite and Fe-Dolomite	Gabbro	-3.2		11.0			12.1

### Appendix D. (Continued)

Sample	Mineralogy Based on XRD	Unit	$\delta^{13}\text{C PDB, ‰}$		$\delta^{18}\text{O VSMOW, ‰}$		$\delta^{15}\text{O VSMOW, ‰}$	
			Calcite	Ankerite or Fe-Dolomite	Calcite	Ankerite or Fe-Dolomite	Calcite	Ankerite or Fe-Dolomite
JSB-106	Ankerite	Turbiditic Sed. Vein		-5.9		21.7		
JSB-113	Ankerite	Turbiditic Sed. Vein		-4.8		12.6		
JSB-116	Ankerite	Turbiditic Sed. Vein		-3.1		11.8		
JSB-149	Fe-Dolomite	Turbiditic Sed. Vein		-3.8		11.9		
JSB-150	Ankerite	Turbiditic Sed. Vein		-4.0		11.8		
JSB-164	Fe-Dolomite	Turbiditic Sed. Vein		-4.0		12.1		
JSB-165	Ankerite	Turbiditic Sed. Vein		-4.4		12.6		
JSB-166	Ankerite	Turbiditic Sed. Vein		-4.8		12.1		
JSB-102	Ankerite	Turbiditic Sediment		-6.7		11.4		
JSB-106	Ankerite	Turbiditic Sediment		-6.3		11.8		
JSB-113	Ankerite	Turbiditic Sediment		-4.3		12.2		
JSB-115	Ankerite	Turbiditic Sediment		-5.8		10.9		
JSB-135	Ankerite	Turbiditic Sediment		-3.9		14.1		
JSB-149	Fe-Dolomite	Turbiditic Sediment		-4.1		12.5		
JSB-150	Ankerite	Turbiditic Sediment		-4.7		12.2		
JSB-164	Fe-Dolomite	Turbiditic Sediment		-4.2		12.2		
JSB-166	Ankerite	Turbiditic Sediment		-4.8		12.4		
JSB-168	Fe-Dolomite	Turbiditic Sediment		-5.7		12.8		
JSB-195	Fe-Dolomite	Turbiditic Sediment		-4.3		12.7		
JSB-167	Ankerite	Graphitic Argillite Vein		-1.6		15.9		
JSB-007	Ankerite	Graphitic Argillite		-2.5		17.1		
JSB-008	Ankerite	Graphitic Argillite		-2.7		18.9		
JSB-069	Ankerite	Graphitic Argillite		-2.8		12.5		
JSB-137	Ankerite	Graphitic Argillite		-5.4		16.1		
JSB-185	Fe-Dolomite	Graphitic Argillite		-2.9		14.4		
JSB-189	Fe-Dolomite	Graphitic Argillite		-6.9		14.7		

### Appendix D. (Continued)

Sample	Mineralogy Based on XRD	Unit	$\delta^{13}\text{C PDB}, \text{‰}$		$\delta^{18}\text{O VSMOW}, \text{‰}$		$\delta^{13}\text{C PDB}, \text{‰}$		$\delta^{18}\text{O VSMOW}, \text{‰}$	
			Calcite	Ankerite	Calcite	Ankerite or Fe-Dolomite	Calcite	Ankerite or Fe-Dolomite	Ankerite or Fe-Dolomite	Ankerite or Fe-Dolomite
JSB-030	Calcite and Ankerite	Andesitic Dyke	-2.6		14.0		-2.0		13.2	
JSB-031	Fe-Dolomite	Andesitic Dyke					-2.9		12.0	
JSB-037	Fe-Dolomite	Andesitic Dyke					-3.3		11.8	
JSB-066	Ankerite	Andesitic Dyke					-2.7		12.6	
JSB-067	Calcite and Fe-Dolomite	Andesitic Dyke	-2.6		12.6		-2.0		12.7	
JSB-126 <sup>†</sup>	Calcite and Ankerite	St. Deformed Rock Vein	-1.9		15.0		-1.7		14.2	
JSB-171 <sup>†</sup>	Ankerite	St. Deformed Rock Vein					-3.0		15.7	
JSB-172 <sup>†</sup>	Ankerite	St. Deformed Rock Vein					-1.7		16.1	
JSB-003 <sup>†</sup>	Ankerite	Strongly Deformed Rock					-2.3		13.2	
JSB-006 <sup>†</sup>	Ankerite	Strongly Deformed Rock					-2.7		12.3	
JSB-047 <sup>†</sup>	Ankerite	Strongly Deformed Rock					-3.6		13.8	
JSB-054 <sup>†</sup>	Ankerite	Strongly Deformed Rock					-1.1		12.5	
JSB-126 <sup>†</sup>	Ankerite	Strongly Deformed Rock					-1.8		12.9	
JSB-127 <sup>†</sup>	Ankerite	Strongly Deformed Rock					-2.3		12.6	
JSB-156 <sup>†</sup>	Ankerite	Strongly Deformed Rock					-1.6		13.1	
JSB-180 <sup>†</sup>	Ankerite	Strongly Deformed Rock					-2.0		12.9	
JSB-194 <sup>†</sup>	Ankerite	Strongly Deformed Rock					-2.0		12.7	
JSB-208 <sup>†</sup>	Ankerite	Strongly Deformed Rock					-3.2		12.0	

### South Patch Occurrence

Sample	Mineralogy Based on XRD	Unit	$\delta^{13}\text{C PDB}, \text{‰}$		$\delta^{18}\text{O VSMOW}, \text{‰}$		$\delta^{13}\text{C PDB}, \text{‰}$		$\delta^{18}\text{O VSMOW}, \text{‰}$	
			Calcite	Ankerite	Calcite	Ankerite or Fe-Dolomite	Ankerite or Fe-Dolomite	Ankerite or Fe-Dolomite		
SPJS-008	Fe-Dolomite	Mineralized Veining					-2.1		12.7	
SPJS-011	Fe-Dolomite	Mineralized Veining					-3.8		14.7	
SPJS-012	Fe-Dolomite	Mineralized Veining					-2.1		12.1	
SPJS-013	Ankerite	Mineralized Veining					-2.4		11.6	
SPJS-018	Fe-Dolomite	Mineralized Veining					-2.1		12.1	



### Appendix D. (Continued)

Sample	Mineralogy Based on XRD	Unit	$\delta^{13}\text{C PDB, ‰}$		$\delta^{18}\text{O VSMOW, ‰}$		$\delta^{13}\text{C PDB, ‰}$		$\delta^{18}\text{O VSMOW, ‰}$	
			Calcite	Ankerite	Calcite	Ankerite or Fe-Dolomite	Ankerite or Fe-Dolomite	Ankerite or Fe-Dolomite		
SPJS-032	Calcite and Ankerite	Mineralized Veining	-3.1		14.9		-3.0		13.2	
SPJS-036	Ankerite	Mineralized Veining					-2.6		12.6	
SPJS-001	Calcite	Basalt	-2.5		11.4		-1.5		12.8	
SPJS-005	Calcite	Basalt	-1.6		12.0		-1.8		12.5	
SPJS-009	Ankerite	Basalt					-2.1		13.6	
SPJS-010	Ankerite	Basalt					-1.3		13.6	
SPJS-014	Fe-Dolomite	Basalt					-2.0		12.0	
SPJS-016	Ankerite	Basalt					-2.1		12.2	
SPJS-017	Ankerite	Basalt					-0.2		13.5	
SPJS-019	Calcite and Fe-Dolomite	Basalt	-2.4		11.8		-1.4		13.1	
SPJS-020	Ankerite	Basalt					-0.9		13.0	
SPJS-021	Fe-Dolomite	Basalt					-1.3		13.1	
SPJS-022	Ankerite	Basalt								
SPJS-023	Ankerite	Basalt								
SPJS-028	Calcite	Basalt	-2.7		12.3		-2.0		13.0	
SPJS-029	Calcite and Ankerite	Basalt	-2.3		13.9					
SPJS-030	Calcite and Fe-Dolomite	Basalt	-1.3		12.1		-2.2		11.8	
SPJS-037	Ankerite	Basalt								
SPJS-006	Ankerite	Gabbro					-3.4		12.4	
SPJS-027	Fe-Dolomite	Gabbro					-3.5		10.9	
SPJS-031	Calcite and Ankerite	Gabbro	-4.0		11.9		-4.1		11.2	
SPJS-033	Fe-Dolomite	Gabbro					-3.5		12.5	
SPJS-003	Fe-Dolomite	Carbonate Unit					0.2		19.8	

All samples identified on the basis of hand sample and thin section petrography

\* - Sample identification changed from field identification based on petrography and geochemistry

† - Sample identification changed from field identification based on XRF whole rock analysis, petrography, and geochemistry

‡ - Protolith impossible to determine due to intense deformation and hydrothermal alteration (Isotopically samples resemble basalt).

**Appendix E.** Oxygen isotope data for quartz separated from mineralized and barren veins within the Boston deposit and the South Patch occurrence and surrounding wallrock. All values reported relative to VSMOW and have a  $2\sigma$  error of  $\pm 0.2\%$ .

<b>Boston Deposit</b>		
<b>Sample</b>	<b>Unit</b>	<b><math>\delta^{18}\text{O}</math> VSMOW, ‰</b>
JSB-046	B2 Vein	14.6
JSB-056	B2 Vein	14.8
JSB-057	B2 Vein	14.7
JSB-058	B2 Vein	14.7
JSB-059	B2 Vein	14.9
JSB-012	B3 Vein	13.5
JSB-022	B3 Vein	13.6
JSB-032	B3 Vein	13.9
JSB-070	B3 Vein	12.8
JSB-075	B3 Vein	14.3
JSB-083	B4 Vein	14.8
JSB-085	B4 Vein	14.7
JSB-021	Flat Vein - B3 Zone	13.8
JSB-045	Flat Vein - B3 Zone	14.0
JSB-077	Flat Vein - Basalt	14.2
JSB-082	Flat Vein - B3 Zone	14.6
JSB-027	Basalt	15.3
JSB-043	Basalt	14.2
JSB-138*	Basalt	16.6
JSB-147†	Basalt	15.6
JSB-177	Basalt	15.6
JSB-179	Basalt	15.8
JSB-026	Basalt	15.9
JSB-175	Basalt	15.6
JSB-028	Gabbro	10.2
JSB-029	Gabbro	13.4
JSB-041†	Gabbro	10.6
JSB-051*	Gabbro	11.8
JSB-071	Gabbro	12.2
JSB-072	Gabbro	12.7
JSB-106	Sediment	13.3
JSB-116	Sediment	14.2
JSB-150	Sediment	14.6
JSB-164	Sediment	14.3

<b>Appendix E (continued)</b>		
<b>Boston Deposit</b>		
<b>Sample</b>	<b>Unit</b>	<b><math>\delta^{18}\text{O}</math> VSMOW, ‰</b>
JSB-007	Sediment (Graphitic)	15.6
JSB-137	Sediment (Graphitic)	15.8
JSB-140	Sediment (Graphitic)	16.4
JSB-174	Sediment (Graphitic)	14.1
JSB-004‡	Strongly Deformed Rock	12.9
JSB-126‡	Strongly Deformed Rock	14.8
<b>South Patch Occurrence</b>		
<b>Sample</b>	<b>Unit</b>	<b><math>\delta^{18}\text{O}</math> VSMOW, ‰</b>
SPJS-008	Mineralized Veining	14.6
SPJS-011	Mineralized Veining	14.3
SPJS-013	Mineralized Veining	14.5
SPJS-018	Mineralized Veining	10.2

All samples identified on the basis of hand sample and thin section petrography

\* - Sample identification changed from field identification based on petrography and geochemistry

† - Sample identification changed from field identification based on XRF whole rock analysis, petrography and geochemistry

‡ - Protolith impossible to determine due to intense deformation and hydrothermal alteration (Isotopically samples resemble basalt)

**Appendix F.** Sulphur isotope data for pyrite separated from the sulphidation halo adjacent to mineralized and barren veins and from vuggs and bands within turbiditic and graphitic sediments associated with the Boston deposit. All values reported relative to CDT and are accurate to within 0.3‰.

<b>Sample</b>	<b>Unit</b>	<b>Occurrence</b>	<b><math>\delta^{34}\text{S}</math> CDT</b>
JSB-046	B2 Zone	Sulphide Halo (Vein)	2.1
JSB-056	B2 Zone	Sulphide Halo (Vein)	2.7
JSB-076	B2 Zone	Sulphide Halo (Vein)	2.6
JSB-079	B2 Zone	Sulphide Halo (Vein)	3.0
JSB-012	B3 Zone	Sulphide Halo (Vein)	3.1
JSB-023	B3 Zone	Sulphide Halo (Vein)	3.5
JSB-033	B3 Zone	Sulphide Halo (Vein)	2.4
JSB-085	B4 Zone	Sulphide Halo (Vein)	2.5
JSB-179	Basalt	Sulphide Halo (Vein)	3.4
JSB-074	Gabbro	Sulphide Halo (Vein)	2.2
JSB-104	Gabbro	Sulphide Halo (Vein)	2.2
JSB-150	Turbiditic Sediment	Sulphide Halo (Vein)	2.2
JSB-162	Graphitic Sediment	Sulphide Halo (Vein)	2.5
JSB-126	Strongly Altered Rock	Sulphide Halo (Vein)	1.6
JSB-106	Turbiditic Sediment	Pyrite Vuggs	0.3
JSB-135	Turbiditic Sediment	Pyrite Vuggs	0.9
JSB-007	Graphitic Sediment	Pyrite Bands or Clots	4.7
JSB-008	Graphitic Sediment	Pyrite Bands or Clots	4.4
JSB-134	Graphitic Sediment	Pyrite Bands or Clots	3.4
JSB-137	Graphitic Sediment	Pyrite Bands or Clots	4.4

**Appendix G.** Carbon isotope data for graphite separated from graphitic sediment associated with the Boston deposit. All values are reported relative to PDB and are accurate to within 0.2‰.

<b>Boston Deposit</b>		
<b>Sample</b>	<b>Unit</b>	<b><math>\delta^{13}\text{C}</math> PDB</b>
JSB-134	Graphitic Sediment	-28.8
JSB-137	Graphitic Sediment	-29.0
JSB-140	Graphitic Sediment	-27.6
JSB-145	Graphitic Sediment	-26.6
JSB-162	Graphitic Sediment	-25.6
JSB-185	Graphitic Sediment	-25.0

**Average = -27.1**  
**Standard Deviation =  $\pm 1.7$**